TOR VERGATA
UNIVERSITÀ DEGLI STUDI DI ROMA

PhD in Biochemistry and Molecular Biology

XXXVIII Cycle

Deciphering p63-governed transcriptional programs in bladder cancer: novel links to lipid metabolism and lncRNAs

Mariacristina Franzese Canonico

A.Y. 2025/2026

Tutor: Dr Artem Smirnov

Coordinator: Prof. Eleonora Candi

ABSTRACT (ENGLISH)

Urothelial carcinoma, the predominant histological subtype of bladder cancer (BLCA), is the most common malignancy of the urinary system. According to GLOBOCAN 2022 estimates, this tumor affects approximately 600.000 people each year and leads to the death of about a third of patients with advanced-stage tumors. The molecular and histological heterogeneity of this tumor represents a hard challenge for developing targeted and effective therapies. p63 is a transcription factor that plays a crucial role in epithelial development and differentiation. While it is frequently overexpressed in most epithelial tumors, acting as an oncogene, its expression in BLCA progressively decreases with tumor progression, and its loss is associated with a poor outcome in patients. However, the molecular mechanisms underlying the role of p63 in BLCA remain incompletely understood.

In this study, we investigated the transcriptional program driven by p63 in BLCA, integrating RNAseq, ChIPseq, ATACseq, proteomics, lipidomics and functional analyses. We found that p63 represses a transcriptional program associated with lipid metabolism in low-stage BLCA cells. Among the identified targets, we found that p63 binds a promoter region of the gene that encodes the monoacylglycerol lipase (MGLL), repressing its expression through epigenetic mechanisms involving chromatin accessibility and histone acetylation. Interestingly, functional studies revealed that MGLL promotes cell invasion, lipid metabolism reprogramming and mitochondrial respiration in high-stage BLCA cells. Furthermore, we identified the long non-coding RNA *LEADR* as a p63-direct transcriptional target and showed that the p63–*LEADR* axis represses interferon-related pathways. Collectively, our findings identify novel p63-dependent regulatory networks involved in BLCA progression and provide a robust multi-omics resource available for future investigations on p63 biology in this tumor.

ABSTRACT (ITALIANO)

Il carcinoma della vescica, istologicamente il tumore più diffuso fra i tumori della vescica, rappresenta la neoplasia più frequente del sistema urinario. Secondo le stime GLOBOCAN 2022, ogni anno vengono diagnosticati nel mondo circa 600.000 nuovi casi e in particolare i tumori in stadio avanzato sono associati ad una prognosi sfavorevole. La complessa eterogeneità istologica e molecolare di questo tumore rappresenta una delle principali sfide per lo sviluppo di terapie mirate ed efficaci. p63 è un fattore di trascrizione che svolge un ruolo fondamentale nello sviluppo e nel differenziamento epiteliale. Sebbene sia frequentemente sovraespresso nella maggior parte dei tumori epiteliali, agendo da oncogene, la sua espressione diminuisce progressivamente durante la progressione del carcinoma della vescica e la sua perdita è associata a una prognosi sfavorevole. Tuttavia, i meccanismi molecolari attraverso cui p63 contribuisce all'insorgenza e allo sviluppo di questo tumore non sono ancora completamente conosciuti.

In questo studio abbiamo caratterizzato il programma trascrizionale regolato da p63 nel carcinoma della vescica mediante l'integrazione di analisi di RNAseq, ChIPseq, ATACseq, proteomica, lipidomica e saggi funzionali. Abbiamo dimostrato che p63 reprime un programma trascrizionale associato al metabolismo lipidico in cellule derivanti da carcinoma della vescica di basso stadio. Fra i target identificati, abbiamo dimostrato che p63 si lega al promotore del gene che codifica per la monoacilglicerol lipasi (MGLL*)*, reprimendone l'espressione attraverso meccanismi epigenetici che coinvolgono l'accessibilità della cromatina e l'acetilazione degli istoni. I nostri studi funzionali hanno evidenziato che MGLL promuove l'invasione cellulare, il rimodellamento del metabolismo lipidico e la respirazione mitocondriale nelle cellule di carcinoma della vescica di stadio avanzato. Inoltre, abbiamo identificato il lnc-RNA *LEADR* come un target trascrizionale diretto di p63 e dimostrato che l'asse p63–*LEADR* reprime vie di segnalazione correlate all'interferone. Nel complesso, questo lavoro identifica nuovi programmi trascrizionali dipendenti da p63 coinvolti nella progressione del carcinoma della vescica e fornisce preziose risorse multi-omiche che saranno utili per futuri studi sulla biologia di p63 in questo tumore.

Summary

INTRODUCTION

1. Bladder cancer

1.1 Epidemiology, aetiology and clinical manifestations

Bladder cancer (BLCA) is the most common malignancy of the genitourinary tract, representing a clinical challenge due to its complex aetiology and high incidence, especially in men. In 2022, it ranks thirteenth in mortality rate, with 613,799 new cases - 76.7% in men and 23.3% in women (Bray et al., 2024). In a prospective study, it has been found that the primary neoplastic lesions appeared in patients older than 40 years. Generally, the risk of developing the tumor rises with age, with the median age at 65 years, and it is a rarity before age 40 (Ponnaboina et al., 2023). Cigarette smoking, electronic nicotine delivery and hydrocarbon exposure are the main risk factors for developing BLCA (Gaffney et al., 2023). Unfortunately, there is not a widely accepted BLCA screening program nowadays, probably because of the low incidence of aggressive disease and lack of an optimal screening tool. However, patients affected by aristolochic acid nephropathy were subjected to biannual cystoscopies for 10 years, and in half of them, BLCA is diagnosed (Zlotta et al., 2011). The main manifestations of the disease depend on the stage of the tumor, ranging from asymptomatic microhematuria, gross hematuria and irritative voiding symptoms (such as dysuria and frequency or urge incontinence), in low stage tumors, to abdominal pain, lower extremity edema due to the compression of iliac vessels, or flank pain resulting from the obstruction of the ureters, that appear in high stage tumors (Davis et al., 2012; Jakus et al., 2023). Overall, the clinical manifestations of BLCA are heterogeneous, but a prompt evaluation of the symptoms and the introduction of a screening program are essential for an early diagnosis and for reducing the progression to muscle-invasive stage.

1.2 Staging and clinical management

Urothelial carcinomas account for around 90% of BLCA cases and they are classified into non-muscle-invasive and muscle-invasive bladder cancers, respectively abbreviated as NMIBCs and MIBCs, while carcinoma in situ represents around 10% of NMIBCs. Tumor stage is determined by the spread and depth of bladder wall invasion of the mass (Figure I). Based on the updated European Association of Urology (EAU) guidelines, papillary tumors confined to the mucosa and tumors invading the lamina propria are classified

as stage Ta and T1, respectively, according to the TNM (Tumor – Nodes – Metastasis) classification system. Flat, high-grade tumors confined to the mucosa are classified as carcinoma in situ (Tis). From T2 stage, the tumors invade the muscle. Table 1 shows the TNM classification approved by Union International Contre le Cancer, updated in 2017 (Babjuk et al., 2022). At diagnosis, 70-75% of patients have NMIBC, 20-25% have MIBC, and 5% have metastatic disease. Even if most patients present a low stage tumor at the diagnosis, high grade NMIBCs often recur or progress, while low grade NMIBCs frequently recur, but progression is rare (Lopez-Beltran et al., 2024). Prognosis and clinical approach differ significantly depending on the stage of the tumor. Transurethral resection (TURBT) is the master diagnostic approach for BLCA. Often, for the NMIBC cases, it is also used as therapeutic approach to remove the mass, when the dimensions are small (Kim & Patel, 2020). The intravesical administration of Bacillus Calmette–Guérin (BCG) is the standard treatment for patients with NMIBC; this immunotherapy activates a complex of immune cells, including dendritic cells, macrophages, NK cells, and T lymphocytes, triggering the production of cytokines that fight against the tumor. However, some patients with high grade NMIBC do not respond to BCG treatment (S. Jiang & Redelman-Sidi, 2022). For these patients, a number of alternative treatments were developed in the last decade, such as nadofaragene firadenovec-vncg (Adstiladrin), the first gene therapy approved by Food and Drud Administration (FDA) in 2022 for patients with high grade NMIBC and carcinoma in situ (Colbert et al., 2025), nogapendekin alfa inbakicept-pmln (NAI) (Waheed et al., 2024) and intravesical gemcitabine and docetaxel (Gem/Doce) (Abou Chakra et al., 2024). Regarding MIBC, radical cystectomy is the standard approach, together the previous administration of gemcitabine and cisplatin as neoadjuvant chemotherapy, aiming to reduce tumor size and facilitate surgical resection. In addition, adjuvant chemotherapy, after cystectomy, is recommended for patients with high-risk features such as lymph node involvement (pN+) (McFerrin et al., 2020). Given the impact of radical cystectomy on quality of life, the trimodal therapy (TMT) is considered an alternative option aimed to preserve the bladder. It combines three components: TURBT, radiotherapy and radiosensitizing chemotherapy (e.g., cisplatin or mitomycin C with 5-fluorouracil) (Khalifa et al., 2022).

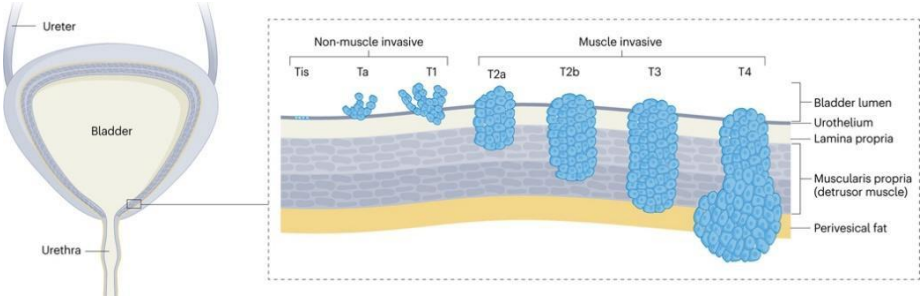

Figure I. Bladder cancer staging. Image from (Dyrskjøt et al., 2023).

T: Primary tumour	
Tx	Primary tumour cannot be assessed
T0	No evidence of primary tumour
Ta	Noninvasive papillary carcinoma
Tis	Carcinoma in situ: "flat tumour"
T1	Tumour invades subepithelial connective tissue
T2	Tumour invades muscle
T2a	Tumour invades superficial muscle (inner half)
T2b	Tumour invades deep muscle (outer half)
T3	Tumour invades perivesical tissue
T3a	Microscopic invasion
T3b	Macroscopic invasion (extravesical mass)
T4	Tumour invades any of the following: prostate stroma, seminal vesicles, uterus, vagina, pelvic wall, abdominal wall
T4a	Tumour invades prostate stroma, seminal vesicles, uterus or vagina
T4b	Tumour invades pelvic wall or abdominal wall
N: Regional lymph nodes	
Nx	Regional lymph nodes cannot be assessed
N0	No regional lymph node metastasis
N1	Metastasis in a single lymph node in the true pelvis (hypogastric, obturator, external iliac, or presacral)
N2	Metastasis in multiple regional lymph nodes in the true pelvis (hypogastric, obturator, external iliac, or presacral)
N3	Metastasis in common iliac lymph node(s)
M: Distant metastasis	
M0	No distant metastasis
M1a	Nonregional lymph nodes
M1b	Other distant metastases

Table I. 2017 TNM classification of urinary bladder cancer (Babjuk et al., 2022).

1.3 Molecular features of bladder cancer subtypes

NMIBC and MIBC have distinct molecular characteristics. In NMIBC, chromosome 9 deletions are found in about 50% of these tumors. These deletions include the *CDKN2A* locus (9p21), encoding p16 and p14ARF, which protect the cell from oncogenesis, promoting the RB and p53 pathways, respectively. Loss of the tumor suppressor *TSC1*, on chromosome 9, is associated with upregulated expression of mammalian target of rapamycin (mTOR) targets and, interestingly, mTOR has been implicated as a regulator of telomerase reverse transcriptase (TERT) gene transcription. In addition, extremely common in all tumor grades and stages (70–80%) are mutations in the promoter of *TERT* gene, which lead to an upregulated expression of this gene. Chromosomal translocations in *FGFR3* are found in most NMIBC cases and they result in fusion proteins acting as oncogenes. Activating mutations in *RAS* gene family members have also been found in NMIBC. Of note, these mutations and *FGFR3* mutations are mutually exclusive. At epigenetic level, common hypomethylations in non-CpG islands occur in NMIBC (Dyrskjøt et al., 2023). The 50% of BLCA patients show *TP53* mutation which results in a lower *TP53* mRNA expression level and it is associated with more advanced tumor stage and higher histologic grade. Mitomycin-C, doxorubicin and gemcitabine, were especially more sensitive to patients with the *TP53* mutation (Wu et al., 2019).

Even if it is more frequent in NMIBCs, *FGFR3* expression is upregulated in up to 40% of MIBCs. The activation of another *FGFR* family member, *FGFR1*, can induce epithelial-mesenchymal transition (EMT), promoting migratory and invasive properties, that could lead to metastasis. *RAS* mutations and mutational inactivation of *NOTCH* pathway genes contribute to MAPK pathway activation. Also, gain-of-function mutations of *ERBB2* and *ERBB3*, or amplification of *ERBB2* and *EGFR51* lead to activation of the RAS–MAPK and PI3K pathways, estimated to occur in about 70% of MIBCs. Loss of *PTEN* and *TSC1* has been found to contribute to AKT–mTOR activation. Finally, genome wide analysis has indicated a common widespread promoter hypermethylation in MIBCs (Dyrskjøt et al., 2023; Lopez-Beltran et al., 2024).

2. p63: a transcription factor belonging to the p53 family

2.1 Gene structure, transcripts and protein isoforms of p63

The transcription factor p63 belongs to the p53 tumor suppressor family. *TP63* gene encodes multiple protein isoforms with both transactivating and transcriptional repressor activities that can regulate a wide spectrum of target genes. *TP63* is located on chromosome 3q27–29 and contains 15 exons spread over about 220 kb; while the intron regions reach up to 100 kb in length. Two different promoters, one immediately preceding the first exon and a second lying in the third intron, give rise to TA- or ΔN-amino-termini of p63, respectively. TA isoforms possess an ammino-terminal transactivation domain, while ΔNp63 proteins lack this domain. Both transcripts can be alternatively spliced at the carboxy-terminus, leading to α, β, and γ isoforms. The different carboxy-termini isoforms also contribute to the diversity of p63 proteins; α, but not β and γ, isoform contains a sterile alpha-motif (SAM) domain that functions as a protein–protein interaction module and a transactivation inhibitory domain (TID) that can interact with the TA domain, limiting its transactivation capability. All p63 proteins possess a DNA-binding domain (DBD) and an oligomerization domain (OD) (Figure II) (Barbieri & Pietenpol, 2006). Given the high sequence and structural homology of the p53 and p63 DNA-binding domains, it was thought that the p63 proteins could bind to p53 consensus DNA-binding sites. However, more recent genome-wide and functional studies indicated that only a subset of canonical p53 targets are consistently regulated by p63 *in vivo* and demonstrated that ΔNp63 can have both a trans-activator and trans-repressor function on p53 in a context-dependent manner (Fischer et al., 2022; Gallant-Behm et al., 2012; McDade et al., 2014; Osterburg & Dötsch, 2022; Riege et al., 2020). In fact, Flores *et al.* showed that p53 and p63 cooperate to regulate DNA damage-induced apoptosis in mouse embryonic fibroblasts; they found that p53 binds target genes involved in cell cycle arrest, like *CDKN1A*, in the absence of p63, but was unable to interact with promoters of the pro-apoptotic genes *NOXA* and *BAX* (Flores et al., 2002). Another study reported that the cooperation between p53 and p63 is essential in maintaining the epithelial integrity, inducing *Perp* expression and promoting apoptosis (Ihrie et al., 2005). Woodstock *et al.* reviewed well the evidence that p53 and p63 can act both as competitors and collaborators: even if they share some transcriptional

targets, their genomic occupancy and regulatory outcomes are largely context-dependent and vary by isoform expression, chromatin state and co-factors (Woodstock et al., 2021). Furthermore, the function of ΔNp63α seems to be that of an organizer of an epithelial cell specific chromatin landscape rather than that of a classical transcription factor, interacting with the DNA as well as cooperating with other factors. For instance, the repressive activity of ΔNp63 could be associated with its capability to recruit co-repressors and chromatin modifiers, such as HDAC1 (Fierro et al., 2023).

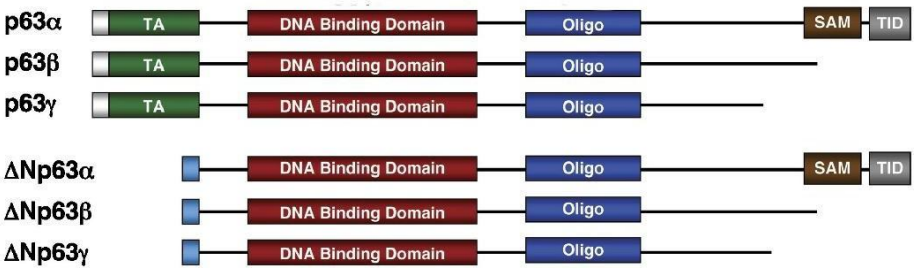

Figure II. *TP63* gene structure. Modified from (Barbieri & Pietenpol, 2006).

2.2 Biological role of p63 isoforms

Unlike p53, p63 is critical for the development of stratified epithelial tissues such as epidermis, breast and prostate. Animal models allowed to study the function of p63 *in vivo*. *p63* −/− mice have striking developmental defects, such as the complete lack of all stratified squamous epithelia and their derivatives, including epidermal appendages and mammary, lacrimal and salivary glands, leading to their death after birth. A mouse model exploring p63 function demonstrated that its expression in single-layered lung epithelium resulted in a shift to a stratified squamous epithelium, reinforcing the role of p63 in the development of stratified epithelia (Barbieri & Pietenpol, 2006). Notably, the selective genetic deletion of the ΔNp63 isoforms recapitulates the phenotype observed in the p63 global knock-out mice, strongly indicating that this is the main p63 isoform driving epithelial morphogenesis (Romano et al., 2012).

The observation that the ΔNp63α isoform is expressed predominantly in the proliferative, basal compartment of epithelia, and specifically in epidermal stem cells possessing the highest proliferative capability, suggest that p63 is critical for regenerative proliferation (Candi et al., 2008; Di Como et al., 2002). Supporting its role in promoting the viability and proliferative potential of epithelial progenitor cells, IGFBP-3, an antiproliferative, p53-inducible protein, has been found to be negatively regulated by ΔNp63 (Barbieri et al., 2005). Genome-wide approaches also confirmed the critical role of p63 in regulating keratinocytes proliferation and differentiation (Kouwenhoven et al., 2010). In addition, other studies unveiled that ΔNp63 recruits epigenetic modulators and chromatin remodelling factors, such as Brg1 and Satb1, to directly regulate numerous target genes involved in cell proliferation, differentiation and adhesion (Fessing et al., 2011; Mardaryev et al., 2014). If on the one hand, p63 supports cells proliferation, on the other hand, it drives the specification of squamous epithelia and the epithelial–mesenchymal interactions of these tissues, in fact *p63* deficient animals have defects in structures that require proper epithelial–mesenchymal interactions during their morphogenesis (Mills et al., 1999). Among the molecular mechanisms involved in terminal differentiation and proliferation in squamous epithelia, Notch/ΔNp63 crosstalk is particularly relevant. In the basal layer of epidermis, ΔNp63 inhibits the expression of p21WAF1/Cip1 and HES1, a NOTCH1 target gene, sustaining cell cycle progression and repressing late differentiation stages (Nguyen et al., 2006). On the other hand, ΔNp63 induces

the expression of JAG2, another Notch ligand, likely favouring the initial step of skin differentiation (Candi et al., 2007). Together these results suggest that the role of ΔNp63 is a balance between the maintenance of progenitor cells and the specification of epithelial lineage.

Lena *et al.* demonstrated that the C-terminal region of p63 is required to keep the TAp63 isoform inactive in oocytes; in fact, the replacement with a β-like C-terminus causes the constitutive activation of pro-apoptotic targets such as *Puma* and *Noxa*, leading to oocytes depletion and female infertility (Lena et al., 2021). Additionally, TAp63 is required for normal heart development and for cardiac differentiation of embryonic stem cells, acting via endodermal signals by regulating secreted cardiogenic factors such as Activin A and Angiomodulin (IGFBP7) (Rouleau et al., 2011). Finally, TAp63 has been implicated in supporting aerobic respiration and metabolic programs relevant for muscle function. In this case, it acts transcriptionally regulating the hexokinase II, suggesting that this p63 isoform could help meet the high energy demand of differentiating and mature myocytes (Viticchiè et al., 2015).

3. Paradoxical role of p63 in epithelial tumors: oncogene or tumor suppressor?

As *TP63* gene is a homologue of *TP53* and p63 proteins have similar biochemical characteristics to p53, the early hypothesis supposed that p63 was also a tumor suppressor, performing compensatory and redundant functions with respect to p53. However, the mutations found in these two genes are different: *TP53* is the most commonly mutated gene in human cancers, supporting its role as a crucial tumor suppressor, while *TP63* gene is very rarely mutated in human cancers or cancer cell lines. For instance, Loss Of Heterozygosity (LOH) at chromosome 17p13, where *TP53* resides, is a common event during tumorigenesis, allowing the elimination of a wild type *TP53* allele (L. C. Chen et al., 1991). In contrast, no LOH occurs at the *TP63* locus in cancer; rather, the 3q27–29 region containing the *TP63* gene is amplified and/or overexpressed in several human cancers (Massion et al., 2003).

3.1 p63 as an oncogene

As well as for its physiological role, mouse models have also been fundamental for studying the role of p63 in the tumor context. Its relevance during squamous cell carcinoma (SCC) initiation and progression has been elucidated by the skin-specific genetic ablation of *TP63* in a mouse model of chemical-induced skin carcinogenesis, that has induced a rapid and dramatic tumor regression (A. Yang et al., 1999); on the other hand, the induction of a moderate expression of ΔNp63 in the basal layer of stratified epithelia causes the development of spontaneous epidermal cysts that resemble cutaneous premalignant lesions (Devos et al., 2017). These results demonstrate the strong dependence of SCCs on high levels of p63 and that it favours the early steps of SCCs development, as we might expect, given its role in promoting cell proliferation. Supporting the oncogenic activity of p63, in head and neck squamous cell carcinoma (HNSCC) and lung SCC, genomic amplification of the *TP63* locus has been reported in up to 10% and 16% of the cases, respectively, and the overexpression of ΔNp63 is observed in the majority of invasive HNSCCs as well as in lung, skin and esophageal SCC (Cancer Genome Atlas Network, 2015; Pecorari et al., 2025a). RNA sequencing data indicated that the ΔNp63α is the mainly expressed isoform, suggesting that this is the major p63 isoform driving SCC tumorigenesis (Compagnone et al.,

2017; Rocco et al., 2006). In addition to p63 amplification and/or overexpression, other events support its oncogenic activity, promoting an immature and more proliferative basal-like phenotype. For example, SOX2 is frequently amplified in lung, esophageal and oral SCCs and physically interacts with ΔNp63 proteins, exhibiting overlapping genomic occupancy at many loci and enhancing the expression of pro-survival factors. Also, in normal conditions, the expression of the transcription factor IRF6 is sustained by the Notch signalling, contributing to the activation of growth/differentiation-related genes. On the other hand, IRF6 promotes the ΔNp63 protein degradation. In SCC, genetic events such as promoter methylation and gene mutation impair IRF6 activity, reflecting in a minor ΔNp63 proteins degradation. Another well-established example supporting the ΔNp63 oncogenic activity is represented by the downregulation of ASPP2, frequently observed in human HNSCC, that is associated with an increased p63 expression, as it represses ΔNp63 expression through a nuclear factor kappa-light-chain-enhancer of activated B cells (NF-κB)-dependent mechanism in normal conditions (Gatti et al., 2019). Other studies showed that ΔNp63α negatively regulates apoptosis, transcriptionally repressing pro-apoptotic *IGFBP-3* gene (Barbieri et al., 2005) and transactivating anti-apoptotic *Hsp70* gene (Wu et al., 2005).

3.2 p63 as a tumor suppressor

Mouse models have also revealed that loss of a p63 allele could enhance tumorigenesis. Different research groups demonstrated that a loss of p63 expression is associated with a high tumor incidence. Flores *et al.* found that $p53^{+/-}$ - $p63^{+/-}$ mice, compared with $p53^{+/-}$ mice, spontaneously developed SCC in several tissues (larynx, pharynx, cervix, and esophagus) with higher metastatic tendence than those in $p53^{+/-}$ mice (Flores et al., 2005). Guo *et al.* demonstrated that the heterozygosity of p63 significantly enhanced sarcoma development in p53-deficient mice (X. Guo et al., 2009). Again, other studies showed that human bladder carcinomas with low or lack p63 expression are associated with tumor progression and poor prognosis (Urist et al., 2002). Several studies show that the loss of ΔNp63 expression is associated with tumorigenesis and/or progression until metastasis, in a variety of epithelial cancers, such as urothelium, prostate, breast and cervix, indicating that ΔNp63 may possess anti-metastatic activities. Supporting this evidence, the ectopic expression of ΔNp63α significantly inhibited metastasis of malignant spindle

carcinoma D3S2 cells to the lungs (Adorno et al., 2009). Metastasis initiation is based on a dysregulation of cell adhesion, motility and migration. The reduction of ΔNp63 expression results in upregulation of proteins involved in cell adhesion, motility and migration, such as N-cadherin, L1 cell adhesion molecule (L1CAM), Periostin and Wnt-5a. Supporting the role of p63 as tumor suppressor, it has been found that ΔNp63 inhibits cell invasion upregulating inhibitor of differentiation-3 (Id-3), which consequently downregulate expression of matrix metallopeptidase 2 (MMP2) preventing the cleavage of components of the extracellular matrix (Y. Chen et al., 2018).

3.3 p63 involvement in epithelial-mesenchymal transition in cancer

Epithelial-mesenchymal transition is a process occurring during epithelial cancer progression, which provides cancer cells with a higher capacity of migration and invasion, as well as the ability to skip physical and immunological barriers and in addition it plays a role in drug resistance. Loss of E-cadherin and an increase of N-cadherin and vimentin are central manifestations of EMT. The main transcription factors that mediate the activation of this phenomenon are SNAIL, SLUG, TWIST and ZEB (Fernandez-Figueras & Puig, 2020). In cervical SCC, ΔNp63α attenuated tumor aggressiveness by suppressing miR-205/ZEB1-mediated EMT (Zhao et al., 2016). Similarly, ΔNp63 also inhibited the EMT expression patterns in prostate cancer, acting as a predictor of metastatic spreading (Tucci et al., 2012). On contrary, another study showed that ΔNp63 positively regulates MTSS1 expression in breast cancer, driving cell migration and invasion. This study suggests that the ΔNp63/MTSS1 axis represents a negative prognostic factor in three human breast tumor data sets (Giacobbe et al., 2016). However, the involvement of p63 in EMT in BLCA has been little studied until now, and the limited number of available studies report contradictory findings. One of these studies showed that ΔNp63α positively regulates the expression of miR-205 and consequently impedes the expression of ZEB1/2, inhibiting cell invasiveness. In addition, they found that ΔNp63α controls the expression of other EMT-related genes which probably are not directly or indirectly regulated via miR-205. Therefore, future studies should be necessary to identify the molecular mechanisms involved in these other EMT-related effects of ΔNp63α (Tran et al., 2013b). Another study showed opposite results, demonstrating that ΔNp63 promotes the EMT through the inhibition of *PTEN* expression and the consequently activation of AKT signalling which is known

to promote the EMT program (Tian et al., 2022). Given these contradictory results, other investigations will be necessary to better understand the role of p63 in EMT in this tumor type.

3.4 Prognostic value of p63 in bladder cancer

In literature, the prognostic value of p63 in BLCA is controversial, likely because of the molecular complexity of these tumors. Several studies show that p63 is overexpressed in NMIBCs, but its expression decreases in MIBCs, and a higher expression is associated to a favourable prognosis (Furlano et al., 2024; Koga et al., 2003; Steurer et al., 2021). As the TAp63 expression is very low and hard to detect, most of the works focus on ΔNp63. In a study conducted on 342 BLCA tissues, ΔNp63 transcripts levels were strongly and significantly overexpressed in low grade (LG) non-muscle-invasive bladder tumors compared to healthy urothelium or matched adjacent normal tissue. On contrary, downregulated ΔNp63 levels were observed in high grade (HG) NMIBCs and in MIBCs (T2-T4) compared to superficial (Ta-T1) tumors. The clinical significance of p63 in this tumor is supported by the survival analysis that confirmed the positive correlation between p63 expression and the favourable outcome in patients (Hedegaard et al., 2016; Papadimitriou et al., 2019). p63 upregulation in early stage of the tumor, in line with its oncogenic role in most epithelial tumors (Moses et al., 2019), accelerates papilloma formation and facilitates tumorigenesis, through the promotion of tumor cell proliferation and survival as well as the inhibition of senescence and apoptotic death (Compérat et al., 2007). However, on disease progression, ΔNp63 acts by assuming a tumor-suppressive and anti-metastatic behaviour. In fact, ΔNp63 has been found to inhibit EMT and therefore aggressive cancer cell phenotype (Barbieri et al., 2006). In summary, ΔNp63 expression acts as oncogene in early stage of BLCA, while it assumes a protective role in tumor progression and invasion, probably acting as tumor suppressor. However, to better understand the role of p63 in the transition from LG to HG BLCA, identifying the molecular pathways driven by this transcription factor will be necessary.

3.5 Correlation between p63 and other markers in bladder cancer

To date, several studies have investigated the correlation between p63 and other markers expression, in order to better stratify bladder tumors. A positive

correlation between E-cadherin and ΔNp63 expression, and a negative correlation between these two epithelial markers and mesenchymal markers such as Zeb-1, Zeb-2, and vimentin were found in BLCA (Choi et al., 2012). In addition, ΔNp63 expression was found to be positively correlated to β-catenin expression (which plays a crucial role in cell-cell adhesion as well as E-cadherin) and negatively correlated to uroplakin III expression (which is associated to terminal urothelial differentiation) and to FGFR3 (which is required for extended proliferation) (Koga et al., 2003; Sayan et al., 2010). Based on these observations, bladder tumors and BLCA cell lines can be clustered into "epithelial" and "mesenchymal" subsets, respectively. The loss of ΔNp63 expression in mesenchymal tumor subtype could be explained by the fact that it inhibits the EMT in early urothelial cancer cells through the regulation of cell adhesion, migration and motility genes (Tran et al., 2013a). These results are in line with another study showing that the loss of ΔNp63 was accompanied by a shift towards mesenchymal morphology and an increase in motility of squamous cell lines (Barbieri et al., 2006). However, some MIBCs retain the expression of ΔNp63, and these tumors display a significantly poor patient survival compared to those that lose p63 expression. This suggests that the molecular mechanisms driven by p63 in muscle invasion need to be further explored in future studies (Choi et al., 2012; Furlano et al., 2024). Until now, these results suggest that the MIBCs derived from basal cells retain p63 expression, while those derived from luminal cells lose p63 expression. Comparing the overall survival between NMIBCs and all MIBCs, p63 expression is lost in MIBCs and its loss is correlated with a worse prognosis. However, among the MIBCs, the restricted subset of basal cells-derived tumors, retaining p63 expression, lead to a worse prognosis compared to the luminal cells-derived tumors.

In summary, p63 status might contribute to better stratify the molecular subtypes of BLCA, but further research focusing on p63-targets and on p63 evaluation in combination with other factors and parameters, are needed to define the prognostic and predictive value of this transcription factor.

4. Lipid metabolism dysregulation in cancer

Lipid metabolism dysregulation is a well-recognized hallmark of malignant tumors and it represents the primary cause of chemoresistance. For this reason, shedding light on the molecular mechanisms underlying this metabolic dysregulation would allow the development of new therapies against cancers. This metabolic reprogramming consists of increased lipid uptake, storage and lipogenesis, promoting rapid tumor growth. Lipidic molecules are part of the structure of biological membranes and function as signalling molecules and energy source. Several studies demonstrated that a few key regulators of these pathways are often significantly upregulated in various human cancers and could represent potential therapeutic targets (Cheng et al., 2018). For instance, sterol regulatory element-binding proteins (SREBPs), a family of membrane-bound transcription factors in the endoplasmic reticulum, are upregulated in various cancers, leading to an increase in tumor growth through their pathways (Ettinger et al., 2004; D. Guo et al., 2009). Regarding the lipid uptake route, the blockage of the fatty acid receptor CD36 was found to have anti-metastatic effect in oral cancer xenograft models, while the EGFR/PI3K/Akt/SREBP-1 signalling plays an important role in tumor growth in glioblastoma (Pascual et al., 2017). Also, acyl-CoA acyltransferase 1 (ACAT1), the enzyme which converts cholesterol to cholesteryl esters for storage in lipid droplets, is highly expressed in glioblastomas and in cancer of the prostate and pancreas and its expression level correlates with poor patient survival. The inhibition of its activity (by genetic silencing or using specific inhibitors) effectively suppresses tumor growth in several cancer xenograft models (Geng et al., 2016; Ohmoto et al., 2015).

4.1 p63 involvement in lipid metabolism dysregulation in squamous cell carcinoma

p63 is a well-established master transcription factor in SCC, as its amplification in these tumors promotes tumorigenesis and progression (Y. Jiang et al., 2018; Y.-Y. Jiang et al., 2020). Mechanistically, p63 occupies and controls many *cis*-regulatory elements (especially enhancers and super-enhancers) and orchestrates gene regulatory program for cell-type-specific function. p63 was found to regulate the fatty acid metabolism pathway in different SCCs. Particularly, in oesophagus SCC (ESCC) it affects this

metabolic dysregulation through a feedback co-regulatory loop between itself, sterol regulatory element binding transcription factor 1 (SREBF1) and Kruppel like factor 5 (KLF5), co-activating the transcription of each other. Bioinformatic analyses based on public data showed that this co-regulatory loop also occurs in other cancer cell lines, such as MCF-7 and HepG2 (L.-Y. Li et al., 2021). However, no studies have explored the potential involvement of p63 in the dysregulation of lipid metabolism in BLCA until now.

4.2 Lipid metabolism dysregulation in bladder cancer

A number of studies performed in BLCA showed that lipid metabolism reprogramming occurs during tumor progression and represents a hard challenge at clinical level. With the advent of metabolomics, a large-scale study of lipids in tumors has been possible. In BLCA tissues higher levels of phospholipids and free fatty acids such as stearic acid and oleic acid were found compared to normal urothelium, while triglycerides levels were lower. In addition, the content of diacylglycerols increases with the tumor progression. The lipid metabolism reprogramming is based on a dysregulation of key regulators involved in this metabolism affecting the tumor micro-environment and driving immune suppression by regulating fatty acid synthesis, oxidation, and cholesterol metabolism (Liu et al., 2025). In fact, in BLCA cells, the upregulation of two enzymes, the fatty acid synthase (FASN) and the acetyl-CoA carboxylase, promotes the synthesis of fatty acids, available to synthesize immunosuppressive lipids (such as prostaglandin E2, PGE2), which suppress $CD8^+$ T cell function. Lipidomic analyses revealed that the level of PGE2 in metastatic BLCA tissues is higher than in normal tissues; inhibiting COX-2 (PGE2 synthase) can promote T cell infiltration again, restoring IFN-γ secretion (Fu et al., 2021). Also, a dysregulation of cholesterol homeostasis in cancer cells is involved in tumor progression. In BLCA, the level of 25-hydroxycholesterol, a product of cholesterol oxidation, is elevated and it can promote the proliferation of cancer cells and EMT (C. Wang et al., 2020). By bioinformatic analysis, Yuan-Yuan Yang *et al.* found novel 6-gene signature associated with lipid metabolism which could predict the outcome of patients with BLCA. However, this study lacks experimental results *in vivo* and *in vitro* (Y.-Y. Yang et al., 2022). Other more recent investigations in BLCA have found a dysregulation of other factors involved in lipid metabolism. The E3 ubiquitin ligase RNF112 was found to be downregulated in MIBCs, reducing the ubiquitin-mediated degradation of c-

Myc. This study revealed that the transcription factor c-Myc promotes the ATP citrate lyase (ACLY) transcription, leading to an increase in cell proliferation, migration and lipid synthesis (Xiong et al., 2025). The low-density lipoprotein receptor-related protein 8 (LRP8), which contributes to control the cholesterol and lipid uptake in cells, it has been found upregulated in several cancers including BLCA, where it inhibits apoptosis and reduces cisplatin sensitivity in cancer cells. However, this study did not elucidate the specific mechanism by which LRP8 exerts these functions, and it was performed only *in vitro*. Despite this evidence, no therapeutic targets directed at lipid metabolism is applied in clinic to date. Nevertheless, FASN remains the most attractive therapeutic target, with the TVB-3166 inhibitor (denifanstat) which can reverse the gemcitabine-resistant *in vitro* and *in vivo* (Zhou et al., 2024).

4.3 Contribution of MGLL in lipid metabolism dysregulation in cancer

The monoacylglycerol lipase (MGLL) is an important enzyme involved in lipid metabolism converting triglycerides into free fatty acids and cholesterol. Together with FASN, they are upregulated in many types of tumors and are highly correlated with tumor migration and invasion and with a poor patient survival (Nomura et al., 2010). Both enzymes promote synthesis of the free fatty acids providing raw materials for synthetizing cell membrane phospholipids, acting as signal molecules and supplying energy to the cell. The cellular metabolic process that involves FASN and MGLL is shown in Figure III. At physiological level, MGLL acts on the endogenous cannabinoid system catalysing the hydrolysis of 2-arachidonylglycerol (2-AG) in the central nervous system and plays a key role in pain and perception (Cao et al., 2013). MGLL is upregulated in many types of cancer, including melanoma, ovarian cancer, and breast cancer where it promotes cell proliferation. Its expression in hepatocellular carcinoma (HCC) is higher than in para-carcinoma tissues, and it promotes HCC invasion and metastasis through the NF-kB pathway, leading to a poor prognosis (Zhu et al., 2016). Recently, in pancreatic adenocarcinoma (PAAD) has been observed that MGLL is significantly overexpressed compared to normal tissue and its high expression is associated with a poor patient prognosis. Li *et al.* found that MGLL promotes cell proliferation, migration, and invasion in a PAAD cell line, likely via the P-AKT/AKT pathway. However, this study is limited to a single cell line (W. Li et al., 2025). Two studies showed that MGLL has oncogenic properties in uveal melanoma (UM), promoting macrophage M2 polarization,

that contribute to the evolution of the tumor and fosters proliferation, metastasis and fatty acids accumulation in the cells (Tan et al., 2023; Y. Xu et al., 2024). Despite the strong evidence regarding the oncogenic properties attributed to MGLL, some studies showed a tumor-suppressive behaviour for MGLL. In fact, in human colorectal cancer its expression is lost or decreased. Its overexpression can inhibit the colony formation of tumor cells, playing a negative regulatory role in the PI3K/AKT signal pathway (Sun et al., 2013). Another example of MGLL as tumor suppressor is reported by Yang *et al.* who found the KLF4-MGLL axis to be essential to suppress HCC cell migration, in fact both these proteins are decreased in tumor. At molecular level, they found that the lipase is a direct target of KLF4 (X. Yang et al., 2018). This double face of MGLL needs to be deeper investigated, as it seems to be tumor dependent. However, the role of MGLL in BLCA has been poorly studied until now.

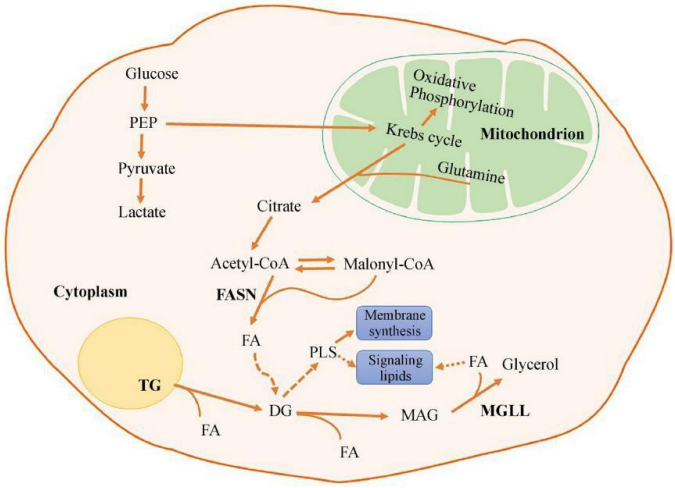

Figure III. MGLL localization in lipid metabolism. Image from (Zhang et al., 2021).

5. lncRNAs in cancer

In recent years, non-coding RNAs (ncRNAs) have emerged as key regulators of numerous biological processes, including cell differentiation, proliferation and metabolism (Agostini et al., 2022; Mancini et al., 2023). Over 120.000 ncRNAs have been annotated but the complex network of ncRNAs is still under intensive investigation. ncRNAs can be localised both in cytoplasm and nucleus and can regulate a variety of cellular pathways including chromatin remodelling and gene expression (Nemeth et al., 2024).

Long non-coding RNA (lncRNA), a class of ncRNA, characterized by their length that exceeds 200 nucleotides, have introduced new levels in regulating gene expression. In the last decades, it has been found that aberrant expression of a number of lncRNAs play a pivotal role in processes ranging from tumor progression to therapy resistance. Some lncRNAs act as oncogenes promoting cancer cell proliferation and migration/invasion, others act as tumor suppressors inhibiting these processes and promoting cancer cell death. Overall, the alterations in lncRNAs expression in cancer alter cell proliferation and apoptosis, leading to genomic instability, metabolic reprogramming and evasion of immune surveillance. Also, these alterations are involved in metastasis and tumor angiogenesis, as well as in therapy resistance (Nadhan & Dhanasekaran, 2021). Just to give some examples: the lncRNA XIST interacts with the polycomb repressive complex 2 (PRC2) complex to induce repressive H3K27-trimethylation on the promoter of *p21* gene, leading to uncontrolled cell proliferation (T. Xu et al., 2017). Similarly, the lncRNA NEAT1 represses the expression of Wnt regulators, such as *ICAT, GSK3B* and *Axin2*, facilitating β-catenin nuclear transport and promoting glioblastoma progression (Q. Chen et al., 2018). We recently found that the lncRNA *LEADR* is among the top ncRNAs downregulated in muscle-invasive cell lines. Its expression is positively regulated by the transcription factor p63. We showed that *LEADR* could dampen the hyperactivation of genes stimulated by the interferon, suggesting an anti-tumoral role as it could increase the sensitivity of BLCA cells to interferon signalling (Barnaba et al., 2025). Other ncRNAs were found upregulated in BLCA, for instance the urothelial carcinoma associated 1 (UCA1) which increases chemoresistance by regulating Wnt signaling (X.-S. Wang et al., 2006) and ZEB2-AS1 which promotes BLCA cell proliferation and inhibits apoptosis through miR-27b (X.-S. Wang et al., 2006). Altogether these results suggest a potential application of lncRNAs as therapeutic targets in cancer.

OBJECTIVES OF THE RESEARCH

Thanks to the recent advances in early detection of bladder tumors, successful management of NMIBCs is possible. On the other hand, the aggressive MIBCs are life-threatening and challenging to cure still today. Therefore, discovering key molecular pathways involved in BLCA progression is critical for developing new personalized targeted therapies. Several studies have established that p63 expression tends to decrease in advanced MIBCs, correlating to a worse prognosis. However, the molecular mechanisms underlying the role of p63 in BLCA remain incompletely understood. Therefore, the overall aim of this research was to characterize the transcriptional networks regulated by p63 in BLCA and to investigate their contribution to tumor progression.

Specifically, the objectives of this study were:

- **To generate an integrated multi-omics resource of p63-regulated pathways in BLCA**
- **To identify direct transcriptional targets of p63**
- **To investigate the molecular mechanisms by which p63 regulates the identified targets**
- **To assess the impact of the identified targets on tumor progression**

RESULTS

1. p63 expression level decreases in advanced BLCA, wherease high p63 expression is associated with a favourable prognosis

By integrating public data from GEPIA2 and Our World in Data across 5 epithelial tumors characterized by high *TP63* expression and elevated mortality per year, we found that BLCA was the only tumor type in which *TP63* expression was significantly associated with patient survival. Moreover, we observed that only this tumor type, among those analysed, showed a significant stage-dependent decline in the expression of *TP63* (Table 1). The loss of p63 expression in high-stage bladder tumors has been previously reported (Furlano et al., 2024; Steurer et al., 2021). Therefore, we further validated these observations in TCGA BLCA cohort, which showed a marked reduction in *TP63* expression in high-stage bladder tumors compared to low-stage tumors (Figure 1A) and a significant favourable correlation between its expression and patient prognosis (Figure 1B). To confirm this trend at protein level, we performed p63 immunohistochemical staining on a tissue microarray (TMA) composed of non-muscle-invasive and muscle-invasive tumors. The histological score (H-score) was evaluated as shown in the representative images corresponding to different p63 expression levels. TMA confirmed a substantial reduction of p63 expression in most invasive tumors compared to those non-invasive (Figure 1C). p63 expression trend was also confirmed in BLCA-derived organoids provided by Dr Giovanni Blandino (IFO-IRCSS, Rome) (Figure 1D).

Cancer type	*TP63* expression (TPM)	Death per year (Worldwide)	Survival (P-val)	High stage vs Low stage (P-val)
Bladder cancer	29	228,734	**0.033**	**0.001**
Lung cancer	123	2,040,000	0.054	0.197
Cervical carcinoma	58	280,479	0.182	0.179
Head and neck cancer	149	508,571	0.561	0.707
Esophageal carcinoma	46	498,067	0.946	0.009

Table 1. Correlation between *TP63* expression and patient survival, and its expression trend in epithelial tumors progression.

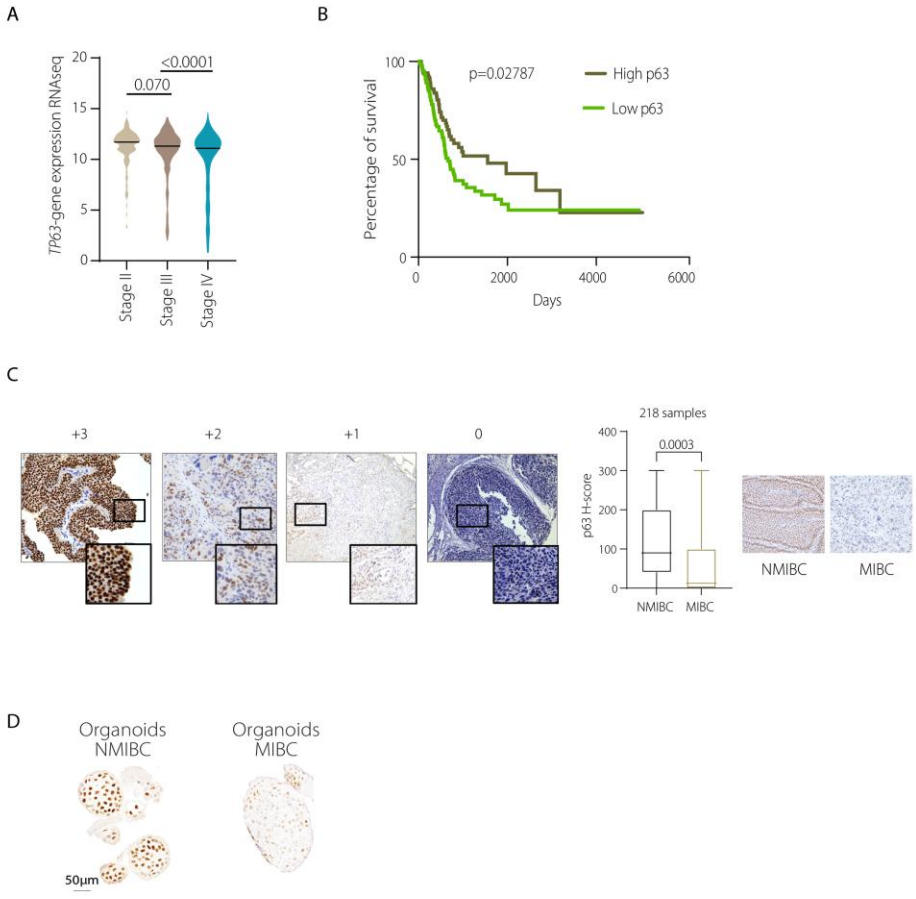

Figure 1. p63 expression in BLCA stages and its correlation with patient prognosis. **(A)** Bioinformatic analysis in BLCA TCGA cohort showing a significant decrease of *TP63* expression in high-stage tumors compared to low-stage tumors. p by ordinary one-way ANOVA. **(B)** Survival analysis in TCGA BLCA cohort showing a favourable prognosis in patients with high *TP63* expression. p by Log-rank (Mantel-Cox) test. **(C)** (left) Representative images of different p63 expression levels corresponding to assigned H-score. (right) TMA analysis of 217 BLCA samples (27 non-invasive tumors and 90 invasive tumors) stained for p63 by immunohistochemistry. p by unpaired t test. **(D)** p63 immunohistochemical staining of BLCA-derived organoids.

2. ΔNp63α isoform is the most expressed in low-stage BLCA cell lines

To investigate the role of p63 in BLCA evolution, we set a panel of BLCA cell lines, reflecting tumor progression. By applying the Celligner algorithm, we mapped all TCGA patients and the available cancer cell lines together, according to their transcriptional profiles. We then isolated only bladder tumors and BLCA cell lines. This transcriptomic classification enabled the identification and selection of urothelial-like (epithelial-like) and fibroblast-like cell lines and tumors. As expected, we found that the urothelial-like tumors and cell lines had high levels of p63, while the fibroblast-like tumors and cell lines had low/absent levels of p63. Therefore, we chose 5 BLCA cell lines (RT4, RT112, 5637, T24 and TCCSUP) with decreasing p63 expression level, which reflect BLCA progression from non-muscle-invasive tumors (low-stage cell lines) to those more invasive (high-stage cell lines) (Figure 2A). We assessed the p63 mRNA expression level by RT-qPCR, by using a pair of primers recognizing TAp63 isoform and another pair of primers recognizing ΔNp63 isoform. We found that only ΔNp63 isoform was expressed in low-stage cell lines, while the TAp63 expression was not detectable. We did not detect any p63 isoform in high-stage cell lines. At protein level, by western Blot, we detected a predominant band of approximately 80 kDa in low-stage cell lines, using an antibody recognizing all p63 isoforms (Figure 2B). The molecular weight of this band corresponds to that of ΔN isoform, suggesting that it was the predominantly expressed isoform in low-stage cell lines. However, an additional weaker band migrating approximately 10–20 kDa below the predominant band was also detected. To further confirm that the predominant identified band represented the ΔN isoform, we silenced p63 in low-stage RT4 cells by using a siRNA either against all p63 isoforms and specifically against ΔNp63. At RNA level, by using a pair of primers against all p63 isoforms, and at protein level, by using an antibody against all p63 isoforms, we found the same decrease in p63 expression both in cells depleted for all p63 isoforms and in cells depleted specifically for ΔNp63 (Figure 2C). Notably, also the lower band was reduced following p63 silencing using both siRNAs, indicating that it represents another p63 protein isoform. Based on its lower molecular weight, this band may correspond to a shorter C-terminal p63 isoform, potentially p63β. To characterize the p63 C-terminus, we performed the p63-silencing in RT4 cells by using a siRNA targeting all p63 isoforms. Evaluating protein expression by

using either a p63pan antibody or an antibody specifically recognizing the α C-terminal domain, we found a comparable expression patterns with both antibodies in control cells, as well as a similar reduction following p63-silencing (Figure 2D). These results indicate that the ΔNp63α isoform represents the predominant p63 isoform expressed in RT4 cells and that another lower-molecular-weight isoform was expressed. However, further investigations will be necessary to determine its identity.

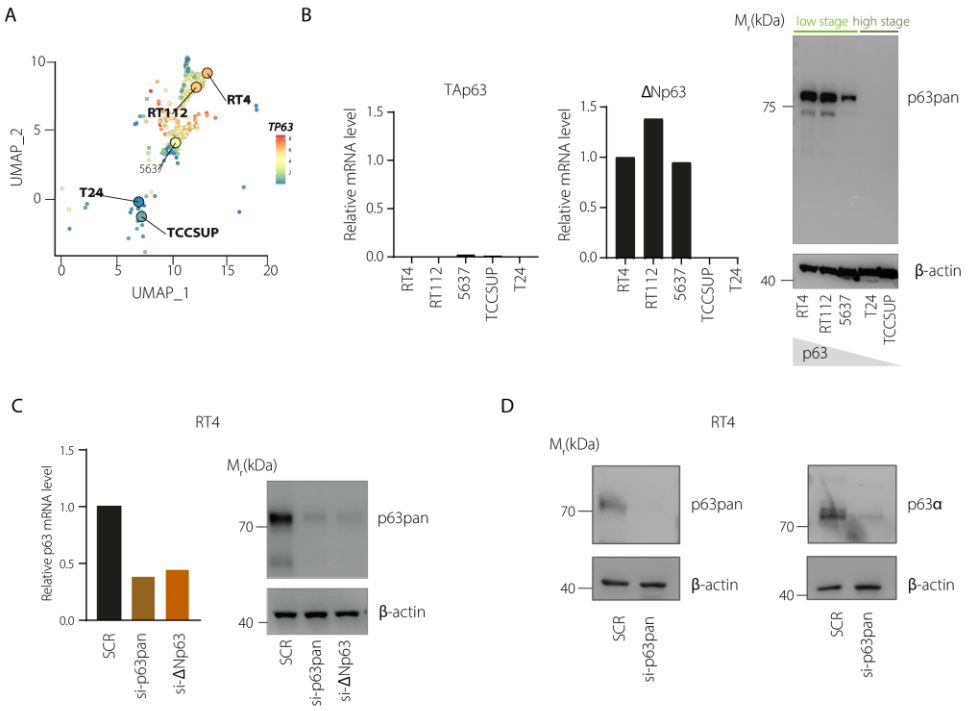

Figure 2. BLCA cell lines selection and p63 isoforms characterization. (A) UMAP showing BLCA tumors and BLCA cell lines created by Celligner algorithm. In evidence are shown the selected cell lines. **(B)** (left) RT-qPCR showing mRNA levels of TAp63 and ΔNp63 in BLCA cell lines, n=1. (right) Western Blot showing p63 expression level in BLCA cell lines by using an anti-p63pan, n=3. **(C)** (left) RT-qPCR showing mRNA p63 levels in p63-depleted RT4 cells by using a siRNA either against all p63 isoforms and ΔNp63. (right) Western Blot showing p63 expression in RT4 cells depleted for all p63 isoforms and in RT4 cells depleted for ΔNp63 by using an anti-p63pan, n=1. **(D)** Western Blots showing total p63 isoforms expression and p63α-specific expression in RT4 cells following p63 silencing using a siRNA against all p63 isoforms, n=1.

3. p63 controls the expression of genes associated with cell cycle and lipid metabolism

To explore the transcriptional program driven by p63 in BLCA, we silenced this transcription factor by a siRNA recognizing all its isoforms in the three low-stage BLCA cell lines and performed the RNA sequencing (RNAseq). By comparing p63-depleted cells with control cells we identified the differentially expressed genes. The volcano plots show the p63-significantly regulated genes (adj $p<0.05$) with a $|log2FC|= 0.5$ (Figure 3A). The enrichment pathways analysis showed that the downregulated genes (activated by p63) in common between RT4 and RT112, the two cell lines with the highest and similar p63 expression level, are involved in cell cycle regulation, as expected since the role of p63 in regulating cell cycle is well-known (Y. Li et al., 2023). However, in 5637 cells this transcription factor seems to not promote the cell cycle (Figure 3B). Consistent with our transcriptomic analysis, our preliminary results showed that p63 depletion by RNA interference in RT4 and RT112 cells induced a reduction of cell proliferation, assessed by performing a growth curve analysis in IncuCyte system. However, this preliminary experiment did not show a reduction in the proliferation of 5637 cells (Figure 3C). We further confirmed this result in RT4 cells by depleting p63 by using two distinct siRNAs against all its isoforms and performing the EdU assay which showed a dramatic reduction of S phase in p63-depleted cells compared to control cells (Figure 3D, left). In parallel, we found a marked reduction in the expression of the master proliferation marker Ki-67, by immunofluorescence staining (Figure 3D, right). However, these analyses are based on a single biological replicate and require further validation in additional independent experiments. On the other hand, among the upregulated genes (repressed by p63) in common between RT4 and RT112 cell lines, surprisingly, we found a significant enrichment of lipid metabolism pathway. Notably, in 5637 cells we did not find an enrichment of lipid metabolism among the upregulated genes (Figure 3E). These results suggest that p63 acts differentially in the transition from NMIBC to MIBC. However, p63 involvement in controlling lipid metabolism in BLCA has not been explored until now. Together our results suggest that p63 plays a major role in sustaining cell proliferation and inhibiting lipid metabolism in low-stage cell lines expressing high p63 levels. However, its regulatory activity appears to be attenuated in 5637 cells, expressing lower p63 levels, indicating that p63-dependent transcriptional

programs are progressively lost during tumor progression.

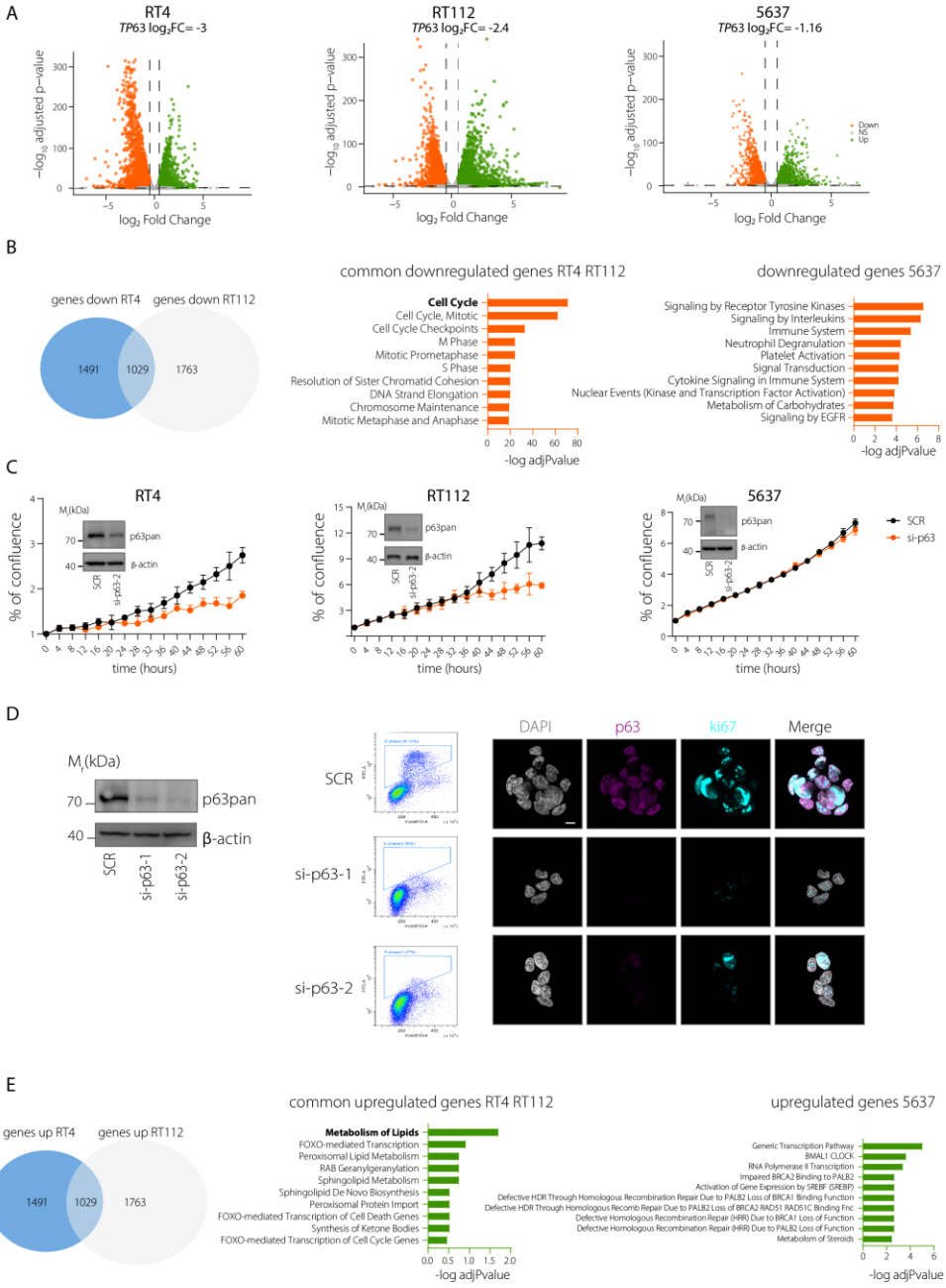
A
RT4
TP63 log2FC= -3
RT112
TP63 log2FC= -2.4
5637
TP63 log2FC= -1.16
−log10 adjusted p−value
log2 Fold Change
Down
NS
Up
B
genes down RT4
genes down RT112
1491
1029
1763
common downregulated genes RT4 RT112
Cell Cycle
Cell Cycle, Mitotic
Cell Cycle Checkpoints
M Phase
Mitotic Prometaphase
S Phase
Resolution of Sister Chromatid Cohesion
DNA Strand Elongation
Chromosome Maintenance
Mitotic Metaphase and Anaphase
-log adjPvalue
downregulated genes 5637
Signaling by Receptor Tyrosine Kinases
Signaling by Interleukins
Immune System
Neutrophil Degranulation
Platelet Activation
Signal Transduction
Cytokine Signaling in Immune System
Nuclear Events (Kinase and Transcription Factor Activation)
Metabolism of Carbohydrates
Signaling by EGFR
-log adjPvalue
C
RT4
RT112
5637
Mr(kDa)
70
40
p63pan
β-actin
SCR
si-p63-2
% of confluence
time (hours)
SCR
si-p63
D
Mr(kDa)
70
40
p63pan
β-actin
SCR
si-p63-1
si-p63-2
DAPI
p63
ki67
Merge
SCR
si-p63-1
si-p63-2
E
genes up RT4
genes up RT112
1491
1029
1763
common upregulated genes RT4 RT112
Metabolism of Lipids
FOXO-mediated Transcription
Peroxisomal Lipid Metabolism
RAB Geranylgeranylation
Sphingolipid Metabolism
Sphingolipid De Novo Biosynthesis
Peroxisomal Protein Import
FOXO-mediated Transcription of Cell Death Genes
Synthesis of Ketone Bodies
FOXO-mediated Transcription of Cell Cycle Genes
-log adjPvalue
upregulated genes 5637
Generic Transcription Pathway
BMAL1 CLOCK
RNA Polymerase II Transcription
Impaired BRCA2 Binding to PALB2
Activation of Gene Expression by SREBF (SREBP)
Defective HDR Through Homologous Recombination Repair Due to PALB2 Loss of BRCA1 Binding Function
Defective HDR Through Homologous Recomb Repair Due to PALB2 Loss of BRCA2 RAD51 RAD51C Binding Fnc
Defective Homologous Recombination Repair (HRR) Due to BRCA1 Loss of Function
Defective Homologous Recombination Repair (HRR) Due to PALB2 Loss of Function
Metabolism of Steroids
-log adjPvalue

Figure 3. Transcriptional programs driven by p63 in low-stage BLCA cell lines. (A) Volcano plots showing the differential gene expression (DGE) analyses in RT4, RT112 and 5637 cell lines, comparing p63-depleted cells vs control cells. In orange are shown the p63-activated genes (downregulated genes) and in green the p63-repressed genes (upregulated genes). Thresholds: adj $p<0.05$; $|\log_2 FC|= 0.5$; n=3. **(B)** (left) Venn diagram showing the common downregulated genes in RT4 and RT112 cells. (right) Enrichment pathways analyses performed by Reactome. **(C)** Western Blot assessing p63 depletion and cell proliferation assay performed in IncuCyte system in low-stage BLCA cell lines, by comparing control cells with p63-depleted cells, n=1. **(D)** (left) Western Blot assessing p63-depletion in RT4 cells by using two siRNAs. (center) Flow cytometric analysis showing the cell cycle distribution of RT4 cells after p63 silencing, assessed by EdU incorporation, n=1. (right) Immunofluorescence staining showing p63 and Ki-67 expression in p63-depleted RT4 cells, n=1. Scale bar= 10 μm **(E)** (left) Venn diagram showing the common upregulated genes in RT4 and RT112 cells. (right) Enrichment pathways analyses performed by Reactome.

4. p63 and MGLL are inversely correlated in BLCA

To confirm our findings in patients, we first performed the differential gene expression analysis (DGE) between tumors with high and low p63 expression, which is showed as a volcano plot, putting in evidence the significantly differentially expressed genes (adj $p<0.05$) with a $|\log_2 FC|= 0.5$ (Figure 4A). Then, we intersected all p63-regulated genes in RT4 cells, which is the cell line with the highest p63 expression, and in bladder tumors and extrapolated only the common down- and upregulated genes (Figure 4B). By performing the enrichment pathways analysis, among the upregulated genes, we confirmed an enrichment in lipid metabolism, consistent with the results obtained *in vitro* (Figure 4C). Therefore, we performed a correlation analysis between *TP63* and lipid metabolism related-genes expression in TCGA BLCA cohort and we found that *MGLL* gene (encoding the monoacylglycerol lipase) was the most inversely related to *TP63* expression (Figure 4D). Consistently, at protein level, both in our panel of cell lines (by western Blot) (Figure 4E) and in histological sample comprising non-muscle-invasive and muscle-invasive parts (by immunohistochemistry), we confirmed the inverse expression of p63 and MGLL (Figure 4F). As preliminary investigation, to understand whether p63 is directly involved in regulating MGLL expression, we first silenced the transcription factor in RT4 cells by using two independent siRNAs recognizing all p63 isoforms and in RT112 cells by using one siRNA recognizing all p63 isoforms and observed a significant increase in MGLL expression both at RNA and protein level, by RT-qPCR and western Blot, respectively (Figure 4G). Together, these results suggest the p63 regulates the expression of this enzyme.

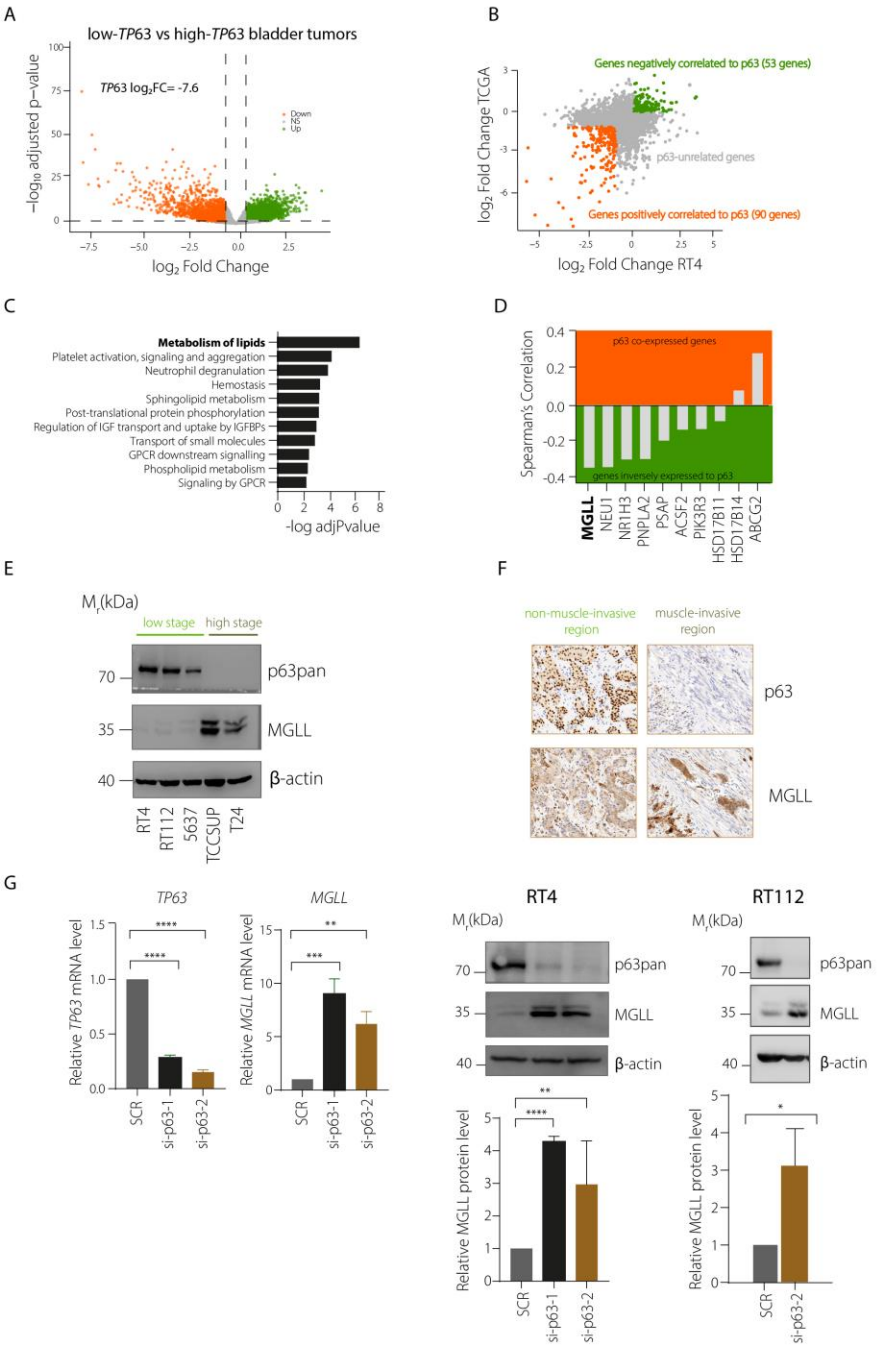
A
low-TP63 vs high-TP63 bladder tumors
TP63 log2FC= -7.6
Down
NS
Up
−log10 adjusted p−value
log2 Fold Change
B
Genes negatively correlated to p63 (53 genes)
p63-unrelated genes
Genes positively correlated to p63 (90 genes)
log2 Fold Change TCGA
log2 Fold Change RT4
C
Metabolism of lipids
Platelet activation, signaling and aggregation
Neutrophil degranulation
Hemostasis
Sphingolipid metabolism
Post-translational protein phosphorylation
Regulation of IGF transport and uptake by IGFBPs
Transport of small molecules
GPCR downstream signalling
Phospholipid metabolism
Signaling by GPCR
-log adjPvalue
D
p63 co-expressed genes
genes inversely expressed to p63
Spearman's Correlation
MGLL
NEU1
NR1H3
PNPLA2
PSAP
ACSF2
PIK3R3
HSD17B11
HSD17B14
ABCG2
E
Mr(kDa)
low stage
high stage
p63pan
MGLL
β-actin
RT4
RT112
5637
TCCSUP
T24
F
non-muscle-invasive region
muscle-invasive region
p63
MGLL
G
TP63
MGLL
Relative TP63 mRNA level
Relative MGLL mRNA level
SCR
si-p63-1
si-p63-2
RT4
RT112
Relative MGLL protein level

Figure 4. Correlation between p63 and MGLL expression. **(A)** Volcano plot showing the differentially expressed genes in low-p63 tumors vs high-p63 tumors. Thresholds: adj $p<0.05$; $|\log_2 FC|= 0.5$ **(B)** Intersection of p63-regulated genes in RT4 cells and in bladder tumors. In evidence, the common downregulated genes (in orange) and the common upregulated genes (in green). **(C)** Enrichment pathways analysis performed by Reactome among the upregulated genes in common. **(D)** Spearman's correlation between *TP63* and lipid metabolism-related genes expression, performed in TCGA BLCA cohort. In orange part are shown the positively p63-correlated genes; in green part are shown the negatively p63-correlated genes. **(E)** Western Blot showing p63 and MGLL expression levels in our panel of BLCA cell lines, n=3. **(F)** Immunohistochemical staining showing p63 and MGLL expression in non-muscle-invasive and muscle-invasive regions of the tumor. A representative sample is shown. **(G)** (left) RT-qPCR showing the increase of MGLL expression after p63 silencing by using two siRNAs in RT4 cells, n=3. p by one-way ANOVA (**** $p< 0.001$). (right) Western Blots showing the increase of MGLL expression after p63 silencing by using two siRNAs in RT4 cells and one siRNA in RT112 cells, n=3. Densitometric quantification of the corresponding western Blot is shown below. p by one-way ANOVA (**** $p< 0.001$) for RT4 cells. p by Unpaired t test (**** $p< 0.001$) for RT112 cells.

5. p63 inhibits MGLL expression in BLCA at epigenetic level

5.1 p63 regulates chromatin accessibility on MGLL gene

To identify the genes directly bound by p63, we performed the p63 chromatin immunoprecipitation followed by sequencing (ChIPseq) in RT4, RT112 and 5637 cells, by using an antibody that recognizes all p63 isoforms. The success of the experiments was demonstrated by the significant enrichment of the canonical p63 binding motifs (Figure 5A). The intersection between the genes repressed by p63 (identified through the RNAseq following p63 depletion) and the genes bound by p63 (identified through the p63 ChIPseq) in RT4 cells, and the subsequent enrichment pathways analysis, confirmed that p63 regulated by binding some lipid metabolism-related genes (Figure 5B). Among these, we found a common peak in a promoter region of *MGLL* gene in all three low-stage cell lines. However, in 5637 cells the peak was lower, consistent with the lower abundance of p63 in these cells (Figure 5C, top).

At this point, to investigate the molecular mechanism by which p63 regulates MGLL expression, we silenced it in RT4 cells by using a siRNA and performed the Assay for Transposase-Accessible Chromatin using sequencing (ATACseq), which uses the hyperactive Tn5 transposase. By comparing p63-depleted cells with control cells, we observed an increased chromatin accessibility in the same promoter region of *MGLL* gene identified by ChIPseq, upon p63 silencing (Figure 5C, bottom), suggesting that p63 binding contributes to maintain the closed chromatin at this locus. These findings suggested that p63 regulates *MGLL* transcription by binding a promoter region of this gene and shaping chromatin organization.

5.2 p63 contributes to the repression of MGLL expression recruiting HDAC1/2

To characterize the p63 interactome in BLCA cells, we isolated nuclei from RT4 cells, performed p63 immunoprecipitation and subsequently carried out mass spectrometry analysis to identify p63-associated proteins. Western Blot analysis confirmed the efficiency of p63 immunoprecipitation, while IgG control sample did not show any specific binding (Figure 6A). MaxQuant analysis, which allowed peptide identification, protein assembly, protein

quantification and LFQ normalization was performed. Integration of two biological replicates revealed a strong enrichment of nuclear proteins in p63-immunoprecipitated samples compared with IgG control samples, although several cytoplasmic proteins were also detected. Among the identified interactors, we detected several well-known epigenetic regulators, including HDAC1/2, DNMT1, WDR5, CHD family members, and RUVBL1/2, consistent with the observation that p63 regulates MGLL expression by shaping chromatin accessibility (Figure 6B). To investigate whether the interaction between p63 and DNMT1 could effectively induce the methylation of the identified promoter region of *MGLL* gene, we performed the DNA methylation analysis by using the Illumina HumanMethylation450K array. We did not identify any significantly differentially methylated CpG probes within this region among the TCGA BLCA patients, indicating that variations in MGLL expression are unlikely to be driven by DNA methylation of the regions covered by the array (Figure 6C). Therefore, we next investigated whether the interaction between p63 and HDAC1/2 at the identified promoter region of *MGLL* gene could effectively cause the deacetylation of this region. To this end, we compared publicly available H3K27ac ChIPseq experiments (GSE213533) in RT4 cells, with high p63 expression, and in T24 cells, which lack p63 expression. We found that the *MGLL* promoter region was specifically deacetylated in RT4 cells, while it was strongly acetylated in T24 cells, supporting a role for p63 in regulating chromatin acetylation at this locus (Figure 6D). Collectively, these results suggest that p63-HDAC1/2 interaction contributes to the repression of MGLL expression in BLCA.

A

Rank	Motif	Name	P-value	log P-pvalue	
1		p53(p53)/mES-cMyc-ChIP-Seq(GSE1 1431)/Homer	1e-584	-1.346e+03	RT4
2		RORg(NR)/Liver -Rorc-ChIP-Seq(GSE101 115)/Homer	1e-520	-1.198e+03	
3		p53(p53)/Saos-p53-ChIP-Seq(GSE15780)/Homer	1e-411	-9.480e+02	
1		p53(p53)/mES-cMyc-ChIP-Seq(GSE1 1431)/Homer	1e-1044	-2.405e+03	RT112
2		RORg(NR)/Liver -Rorc-ChIP-Seq(GSE101 115)/Homer	1e-721	-1.660e+03	
3		Foxa3(Forkhead)/Liver -Foxa3-ChIP-Seq(GSE77670)/Homer	1e-589	-1.357e+03	
1		p73(p53)/Trachea-p73-ChIP-Seq(PRJNA310161)/Homer	1e-343	-7.921e+02	5637
2		p53(p53)/Saos-p53-ChIP-Seq(GSE15780)/Homer	1e-339	-7.816e+02	
3		p53(p53)/Saos-p53-ChIP-Seq/Homer	1e-339	-7.816e+02	
4		p63(p53)/Keratinocyte-p63-ChIP-Seq(GSE1761 1)/Homer	1e-277	-6.386e+02	

B

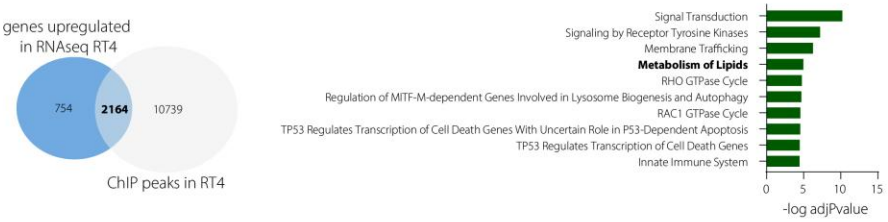

C

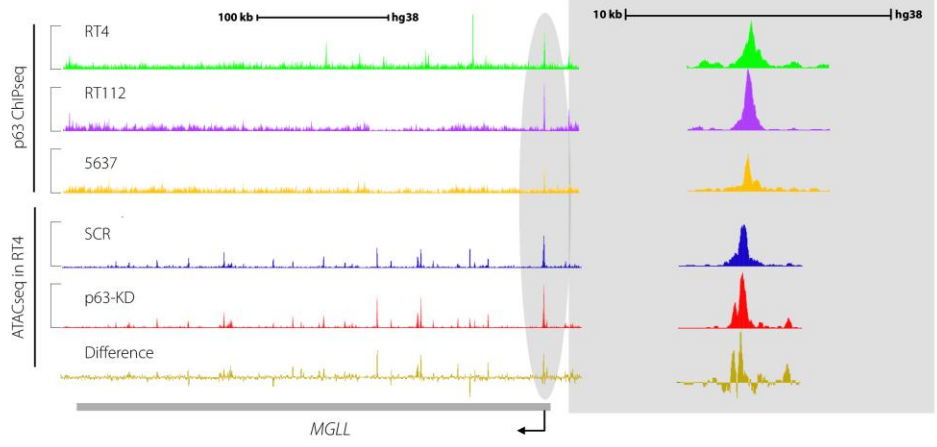

Figure 5. p63 represses MGLL transcription shaping chromatin organization. (A) p63-binding motifs enrichment from p63 ChIPseq experiments in RT4, RT112 and 5637 cells. **(B)** (left) Venn diagram showing the intersection between the upregulated genes in p63-depleted RT4 cells identified by RNAseq and p63 ChIPseq peaks in the same cell lines. (right) Enrichment pathways analysis of p63-bound and regulated genes in RT4 cells, performed by Reactome. **(C)** (top) p63 ChIPseq signal in RT4, RT112 and 5637 cells, n=1. (bottom) ATACseq signal in RT4 cells, n=1. The "difference" represents the signal of the p63-KD subtracted of the signal of the SCR. In grey are shown the zooms of the peak of interest.

A

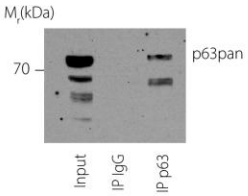

B

GENE NAME	FUNCTION	LOG_2 LFQ INTENSITY
TP63	Transcription factor	9.03
HDAC1/2	Histone deacetylase	6.6
DNMT1	DNA methyltransferase	5.6
WDR5	COMPASS/MLL chromatin complex	7.1
RUVBL1	Chromatin remodeling ATPase	6.475
RUVBL2	Chromatin remodeling ATPase	6.8
CHD4	Chromatin remodeler (NuRD complex)	6.7

C

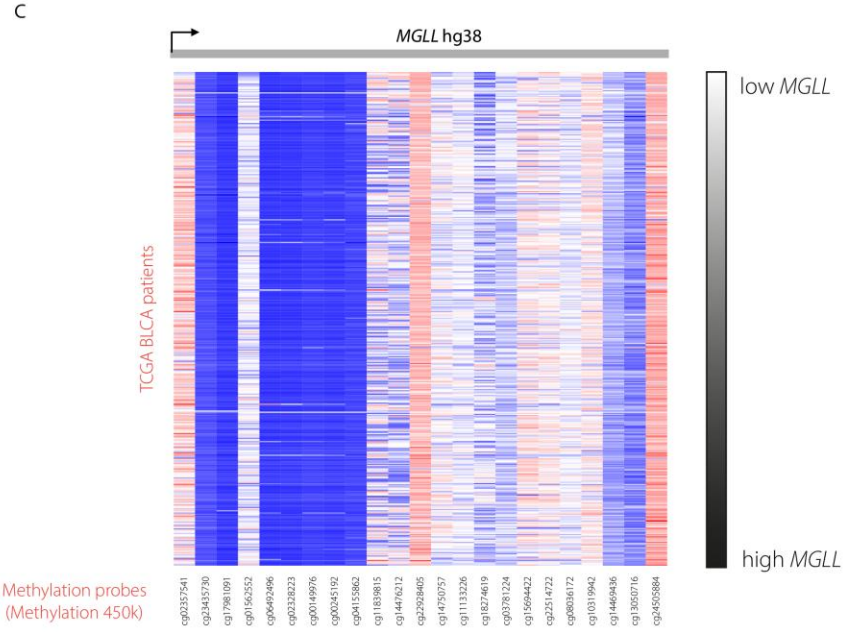

D

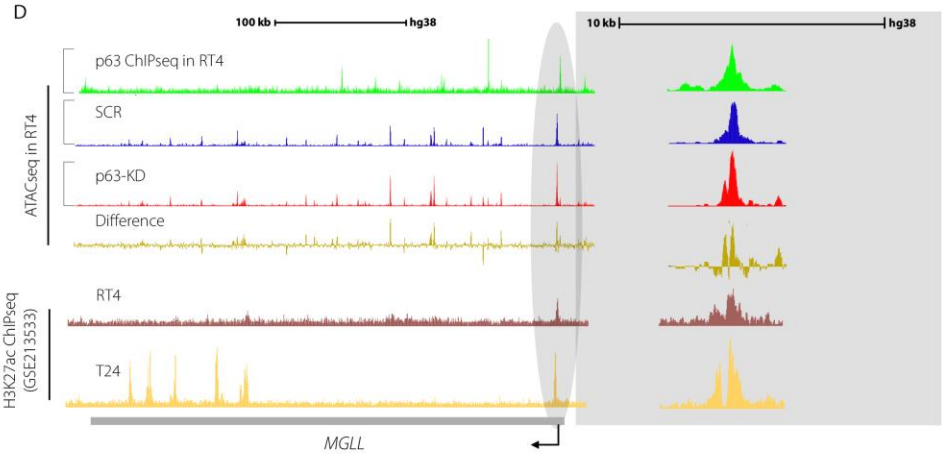

Figure 6. p63-HDAC1/2 interaction promotes the deacetylation on the promoter region of *MGLL* gene. (A) Western Blot confirming the success of p63 immunoprecipitation. Input and IgG samples are used as positive and negative control, respectively, n=2. **(B)** Representative nuclear proteins identified in the p63 immunoprecipitated samples followed by MaxQuant analysis in RT4 cells. **(C)** DNA methylation analysis on promoter region of *MGLL* gene, performed by using the Illumina HumanMethylation450K array in TCGA BLCA patients. **(D)** p63 ChIPseq and ATACseq signals as in Figure 5C, on top; publicly available H3K27ac ChIPseq signals in RT4 and T24 cells (GSE213533), on bottom.

6. MGLL expression promotes glycerophospholipids metabolism and inhibits sphingolipids metabolism in high-stage BLCA

To investigate the functional consequences of MGLL expression on lipid metabolism, we explored the MGLL-dependent lipid content in the high-stage BLCA cell lines (T24 and TCCSUP). To this end, we silenced MGLL by using a siRNA (n=4) (Figure 7A) and lipid extract was analysed by performing mass spectrometry-based non-targeted lipidomic, at Helmholtz Munich facility (Germany). Three hundred and three (303) annotated lipids were identified in both cell lines. Among them, 101 were differentially expressed, considering a $|\log_2 FC|$ 0.5, in MGLL-depleted T24 cells compared to control cells (88 up- and 13 downregulated). Similarly, 110 lipids were differentially expressed in MGLL-depleted TCCSUP cells compared to control cells (59 up- and 51 downregulated) (Figure 7B). Lipid pathways enrichment analysis, performed by LIPEA (Lipid Pathway Enrichment Analysis), revealed that MGLL mainly promotes glycerophospholipids metabolism and inhibits sphingolipids signalling/metabolism pathways in both cell lines (Figure 7C). We then extended our analysis to the TCGA BLCA cohort to assess the correlation between MGLL expression and genes involved in glycerophospholipid (KEGG hsa00564) and sphingolipid metabolism/signalling (KEGG hsa00600). This approach revealed that MGLL expression was positively correlated with a number of genes involved in glycerophospholipids metabolism and negatively correlated with a number of genes involved in sphingolipids metabolism (Figure 7D). These findings provide independent patients-derived data and *in vitro*-derived data supporting that MGLL contributes to lipid metabolic reprogramming in aggressive BLCA through the regulation of glycerophospholipids and sphingolipids homeostasis.

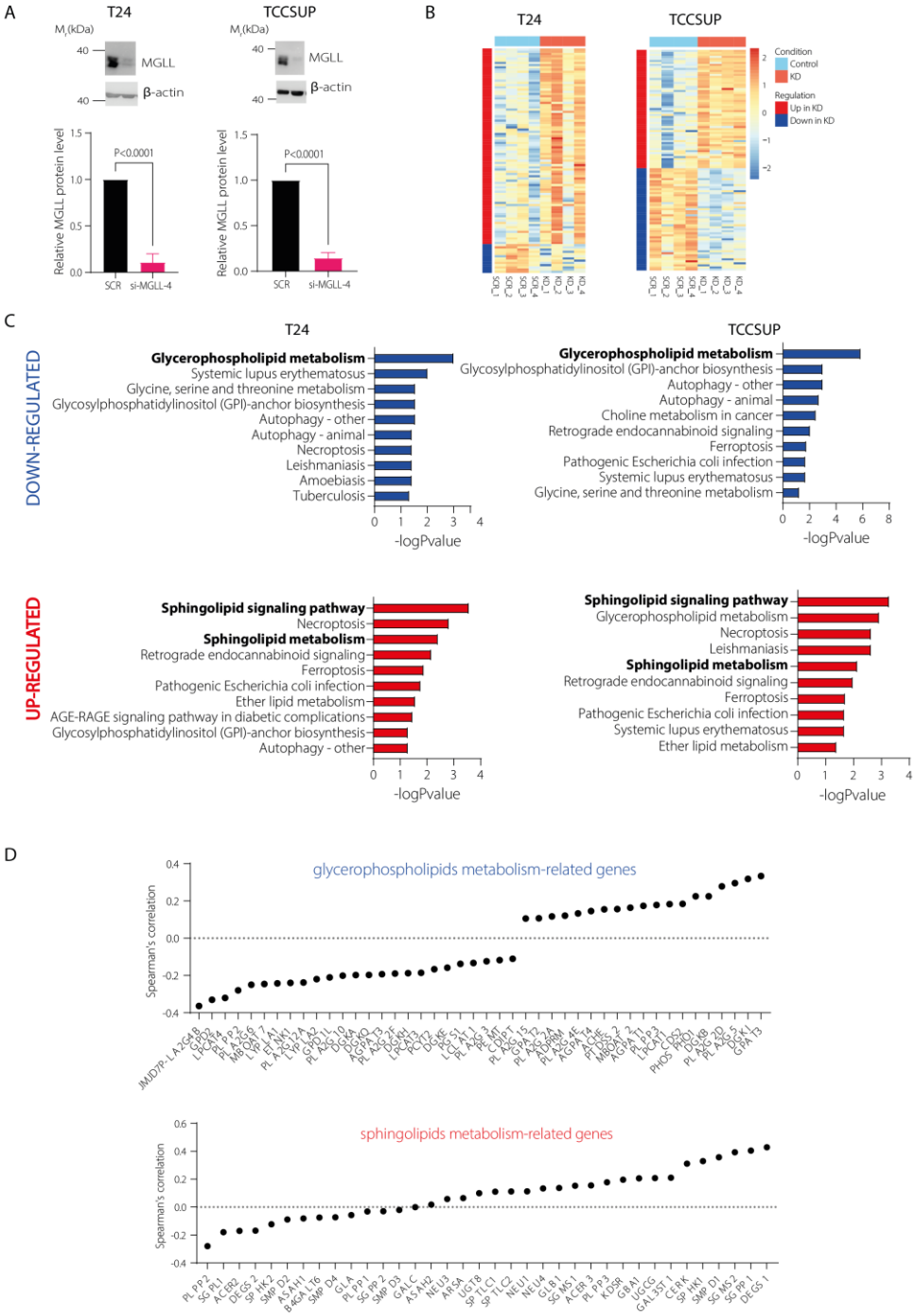
A
T24
TCCSUP
Mr(kDa)
40
MGLL
β-actin
Relative MGLL protein level
P<0.0001
SCR
si-MGLL-4
B
T24
TCCSUP
Condition
Control
KD
Regulation
Up in KD
Down in KD
C
DOWN-REGULATED
UP-REGULATED
Glycerophospholipid metabolism
Systemic lupus erythematosus
Glycine, serine and threonine metabolism
Glycosylphosphatidylinositol (GPI)-anchor biosynthesis
Autophagy - other
Autophagy - animal
Necroptosis
Leishmaniasis
Amoebiasis
Tuberculosis
Choline metabolism in cancer
Retrograde endocannabinoid signaling
Ferroptosis
Pathogenic Escherichia coli infection
Sphingolipid signaling pathway
Sphingolipid metabolism
AGE-RAGE signaling pathway in diabetic complications
Ether lipid metabolism
-logPvalue
D
glycerophospholipids metabolism-related genes
sphingolipids metabolism-related genes
Spearman's correlation

Figure 7. MGLL-dependent lipid metabolism in high-stage BLCA. (A) Western Blots showing MGLL silencing in T24 and TCCSUP cells, n=4. Densitometric quantification of the corresponding western Blot is shown below. p by Unpaired t test (**** p< 0.001). **(B)** Heatmaps showing differentially expressed lipid species in MGLL-depleted cells vs control cells, n=1. Thresholds: $|log_2FC|= 0.5$ **(C)** Lipid pathways enrichment analyses performed by LIPEA tool. **(D)** Spearman's correlation in TCGA BLCA cohort between *MGLL* expression and the expression of genes belonging KEGG pathways (glycerophospholipids metabolism hsa00564 and sphingolipids metabolism hsa00600).

7. MGLL expression promotes cell invasion without affecting cell proliferation and migration

Since MGLL affects glycerophospholipids metabolism, which is involved in cellular membranes building (Fu et al., 2021), and given its well-established oncogenic role in several cancer types (Nomura et al., 2010), we first investigated whether the expression of this lipase affected the most aggressive features of BLCA cells. To this end, we silenced MGLL in our two high-stage cell lines (T24 and TCCSUP), by using 4 distinct siRNAs. We found that its expression did not affect cell proliferation, assessed by IncuCyte growth curve analysis (Figure 8A, on top). Similarly, IncuCyte wound-healing assays also revealed that MGLL did not affect cell migration (Figure 8A, on bottom). The consistent phenotype observed with 4 independent siRNAs reduced the probability that these results were caused by off-target effects. Based on these experiments, two independent siRNAs were selected for subsequent invasion assays, as they showed robust MGLL silencing and were representative of the phenotype observed with the full siRNAs panel. Following MGLL depletion in T24 and TCCSUP cell lines, by using the two selected siRNAs, we performed the invasion assay in Matrigel-coated chambers and observed a marked reduction in the invasive ability of MGLL-depleted cells compared to control cells. Although there was a clear trend in the reduction of cell invasion in MGLL-depleted cells, the observed difference did not reach statistical significance (Figure 8B). Possibly, the relatively high variability of the assay may have contributed to the lack of statistical significance. Therefore, this observation requires further validation in additional independent experiments. Nevertheless, these findings indicated that the activity of this enzyme could promote the invasive phenotype of aggressive BLCA cells.

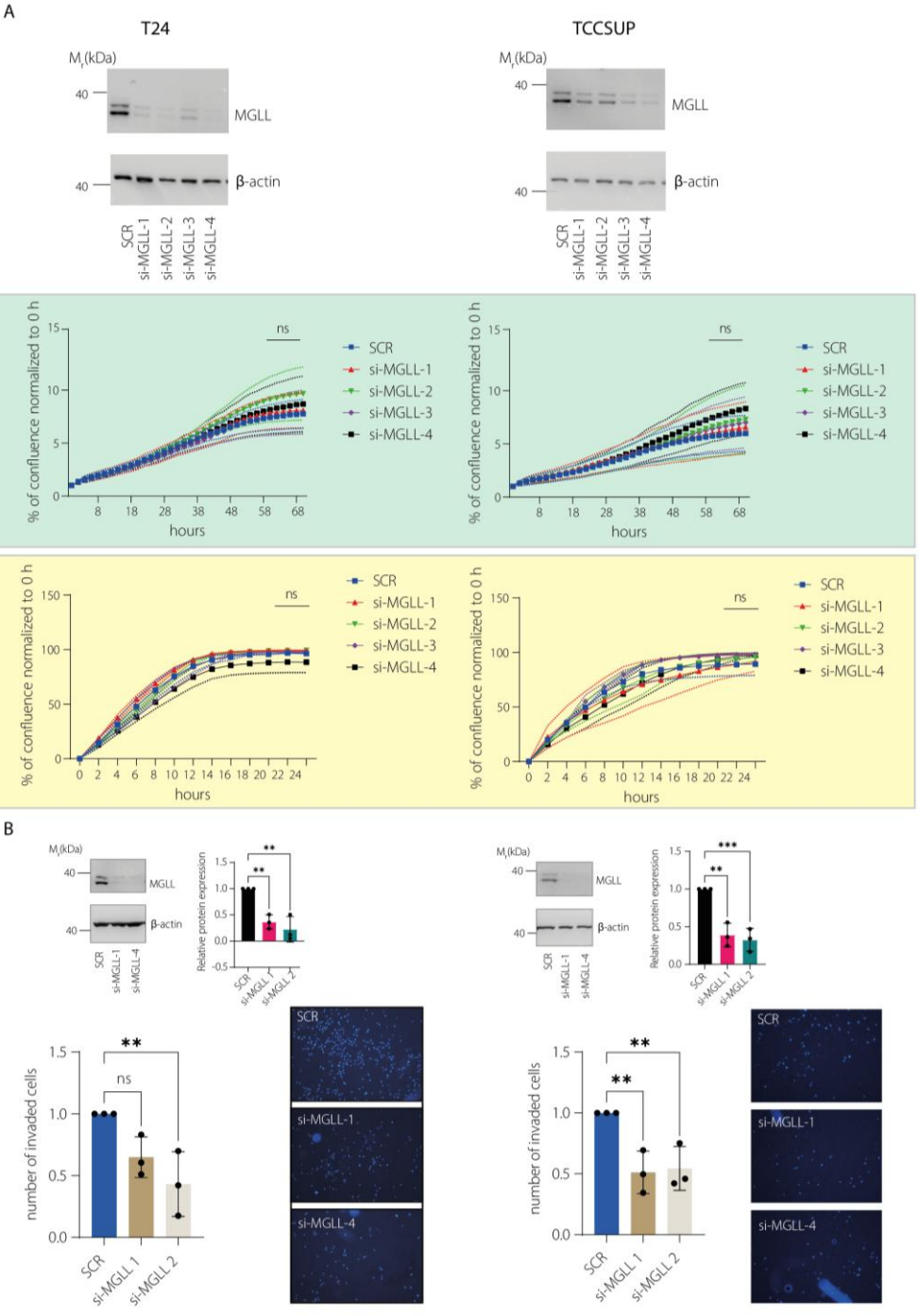
A
T24
TCCSUP
Mr(kDa)
40
MGLL
β-actin
SCR
si-MGLL-1
si-MGLL-2
si-MGLL-3
si-MGLL-4
% of confluence normalized to 0 h
hours
ns
B
Relative protein expression
number of invaded cells
**
***

Figure 8. MGLL effect on cell proliferation, migration and invasion. (A) (top) Representative western Blots showing the success of MGLL silencing by using 4 independent siRNAs in T24 and TCCSUP cell lines. (bottom) Growth curve analyses showing cell proliferation (in green) and cell migration (in yellow) performed in IncuCyte system, n=3. p by two-way ANOVA multiple comparisons. **(B)** (top) Representative western Blots showing the success of MGLL silencing by using 2 selected siRNAs, n=3. Densitometric quantification of the corresponding western Blot is shown. p by one-way ANOVA (**** $p < 0.001$). (bottom) Box plots showing the number of invaded cells per well. Five fields per well were acquired. One representative field of each experimental condition is shown. n=3, p by one-way ANOVA.

8. MGLL contributes to mitochondrial respiration in high-stage BLCA cells

To investigate the bioenergetic effect of MGLL in high-stage BLCA cells (T24 and TCCSUP), we silenced MGLL by using two independent siRNAs (Figure 9A). We then inhibited the electron transport chain (ETC) by using Oligomycin and Rotenone/Antimycin A and subsequently measured the oxygen consumption rate (OCR) with a Seahorse XF analyzer. Analysis of individual respiratory parameters revealed a marked reduction in both basal respiration and ATP-linked respiration in MGLL-depleted cells compared to control cells (Figure 9B). In parallel, to further assess mitochondrial status, we stained the cells with MitoTracker Red CMXRos, a dye that selectively accumulates in polarized mitochondria in a membrane potential-dependent manner. Quantification of CMXRos-positive mitochondrial structures did not show marked changes following MGLL depletion (Figure 9C). Overall, these findings indicate that MGLL sustains mitochondrial respiratory activity in high-stage BLCA cells, without altering mitochondrial function. However, as these analyses are based on a low number of biological replicates, these findings require further validation in additional independent experiments.

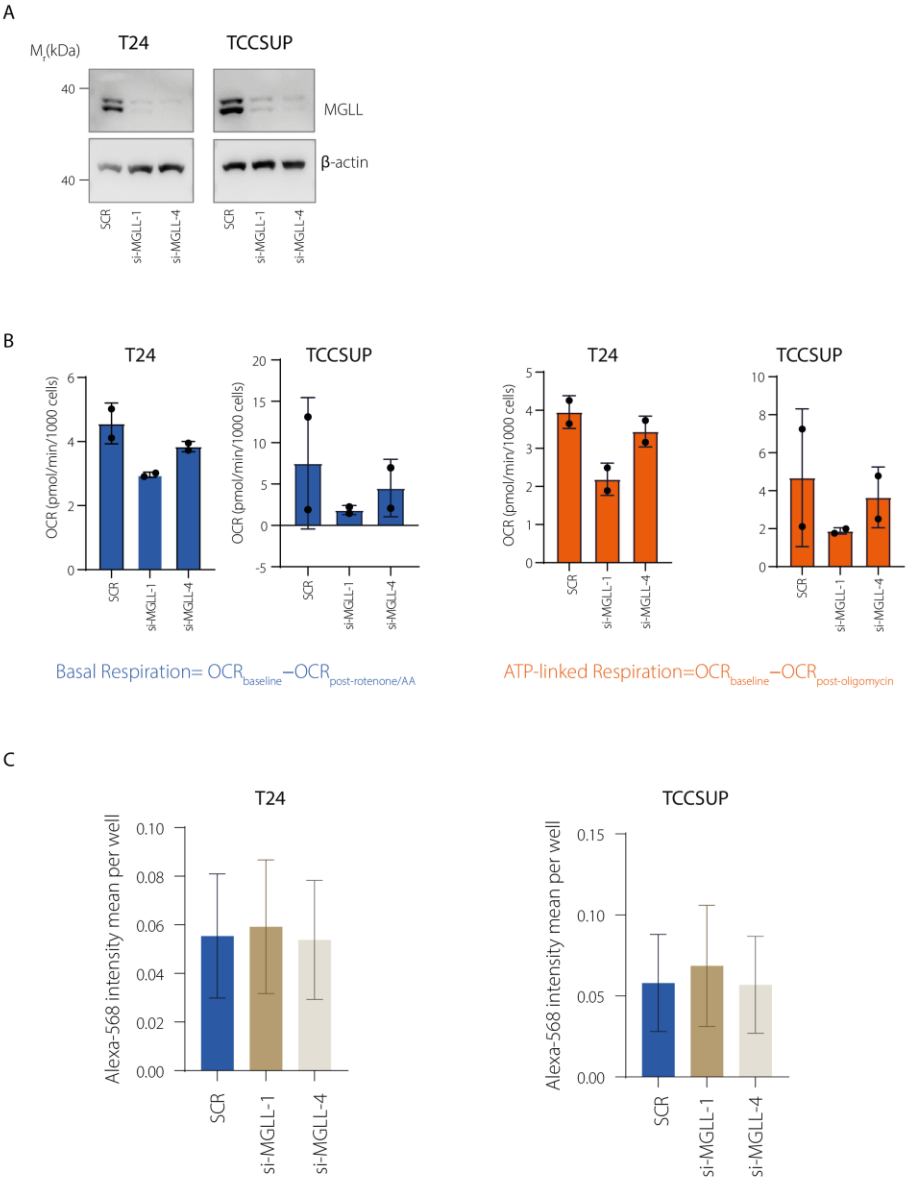
A
M,(kDa)
T24
TCCSUP
40
40
MGLL
β-actin
SCR
si-MGLL-1
si-MGLL-4
B
T24
TCCSUP
OCR (pmol/min/1000 cells)
Basal Respiration= OCR baseline –OCR post-rotenone/AA
ATP-linked Respiration=OCR baseline –OCR post-oligomycin
C
Alexa-568 intensity mean per well

Figure 9. Contribution of MGLL to mitochondrial respiration. (A) Western Blots showing MGLL silencing in high-stage cell lines by using two independent siRNAs, n=2. **(B)** Box plots showing the difference in basal respiration and ATP-linked respiration comparing control cells with MGLL-depleted cells. Data are shown as mean ± SD of 3 measurements for each condition, n=2. **(C)** Box plots showing the intensity of MitoTracker Red CMXRos, n=1. Analysis was performed by Harmony software (Revvity).

9. p63 contributes to a hybrid-EMT in BLCA

9.1 p63 directly regulates Slug expression in epithelial BLCA cells

To investigate the role of p63 in EMT in BLCA, we first classified BLCA cell lines into epithelial-like and mesenchymal-like groups according to their expression of the canonical epithelial and mesenchymal markers *CDH1* (E-cadherin) and *CDH2* (N-cadherin), respectively (Figure 10A). By performing DGE analysis by using public transcriptomic data (DepMap), we identified mesenchymal- and epithelial-specific genes (Figure 10B). We found that the significantly ($p<0.05$) differentially expressed genes were enriched to be significantly bound by p63 according to public libraries of ChIPseq performed in several tissues and cell lines (ENCODE and ChEA Consensus TFs from ChIP-X), confirming a role for p63 in this process (Figure 10C). To evaluate the functional role of p63 in EMT, we silenced this transcription factor by a siRNA against all p63 isoforms in the epithelial-like cell line with the highest p63 expression (RT4). Our preliminary results revealed that p63 depletion did not affect cell migration, assessed by wound-healing IncuCyte assay (Figure 10D). Additionally, we found that p63 silencing in RT4 and RT112 cell lines did not affect E-cadherin expression (Figure 10E). Together, these results suggested that p63 alone is not sufficient to induce EMT in our context. However, combining our transcriptomic and gene occupancy analyses in RT4 cells, we found that p63 directly regulated the expression of 3 common genes involved in EMT. Among these, we found that *SNAI2* gene (encoding Slug) showed the strongest positive correlation with *TP63* (Figure 10F). This positive correlation was also confirmed at protein level in RT4 and RT112 cells (Figure 10G) and in TCGA BLCA cohort (Figure 10H). To investigate the molecular mechanism by which p63 regulated Slug expression, we interrogated p63 ChIPseq experiment in RT4 cells which showed several peaks in a putative enhancer region of *SNAI2* locus. ATACseq demonstrated a marked reduction of the chromatin accessibility in the region of these peaks following p63 silencing, indicating that p63 promotes Slug expression through epigenetic regulation (Figure 10I). Consistently, by interrogating two publicly available H3K27ac ChIPseq experiments carried out in RT4 and T24 cell lines, we found high levels of histone acetylation in this enhancer region only in RT4 cells, but not in T24 cells. Although Slug is known to cooperate with the transcription factor Snail to repress epithelial genes such as E-cadherin and promote EMT (Medici et al., 2008; Y. Wang et al., 2013), Snail was not expressed in RT4 cells (Figure 10E), and in addition p63-

Slug axis did not inhibit the expression of E- cadherin in our model (Figure 10E). Collectively, these results suggest that p63 promotes the expression of Slug without inducing a complete EMT program in low-stage BLCA cells.

1.1 p63 regulates the expression of the atypical cadherin Fat2

Consistent with previous report (Dang et al., 2016), which demonstrated that ΔNp63α induces the expression of Fat2 (an atypical cadherin) and Slug to promote tumor invasion in HNSCC, our p63 ChIPseq showed that p63 bound *FAT2* gene in RT4 cells, while ATACseq demonstrated a reduction of the chromatin accessibility in this region following p63 silencing (Figure 11A). Supporting a role for p63 in regulating *FAT2* transcription at epigenetic level, we found high levels of histone acetylation in this region only in RT4 cells, but not in T24 cells (data from GSE213533) (Figure 11A). As preliminary investigation, we silenced p63 in RT4 cells by using two independent siRNAs targeting all p63 isoforms and cultured the cells as 3D spheroids. We found that p63-depleted cells appeared less compact than control cells, suggesting an initial loss of cell adhesion (Figure 11B). Together, our results suggest that p63 promotes a hybrid pre-EMT state in epithelial BLCA cells by simultaneously promoting Fat2 expression, which inhibits EMT, and Slug expression, which is associated with EMT program.

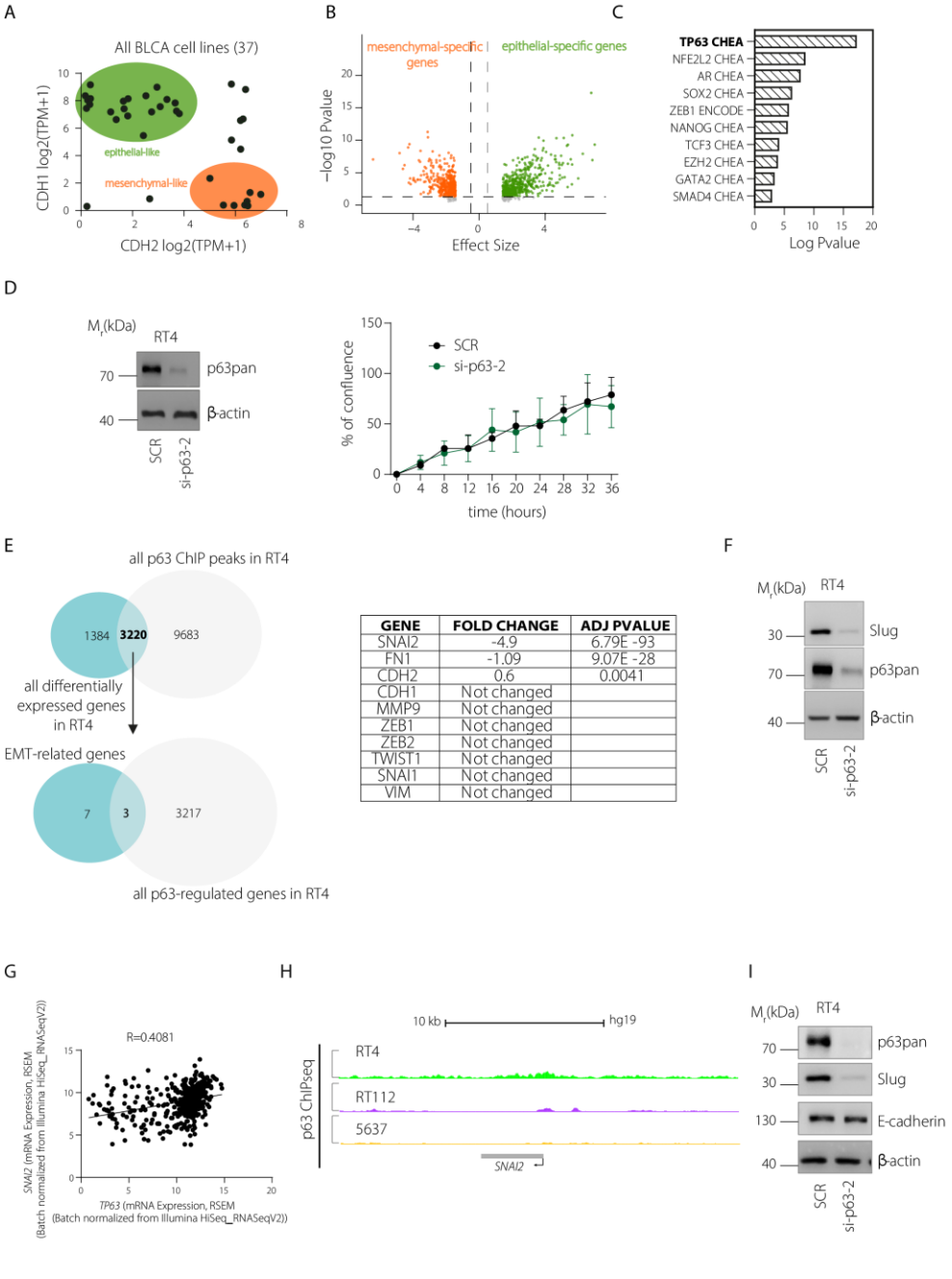

GENE	FOLD CHANGE	ADJ PVALUE
SNAI2	-4.9	6.79E -93
FN1	-1.09	9.07E -28
CDH2	0.6	0.0041
CDH1	Not changed	
MMP9	Not changed	
ZEB1	Not changed	
ZEB2	Not changed	
TWIST1	Not changed	
SNAI1	Not changed	
VIM	Not changed	

Figure 10. p63-Slug axis does not affect E-cadherin expression. (A) Dot plot showing *CDH1* and *CDH2* expression levels in all BLCA cell lines. **(B)** Volcano plot showing the DGE analysis, performed by DepMap, between epithelial-like and mesenchymal-like BLCA cell lines. Thresholds: $p<0.05$; Effect size= 0.5 **(C)** Transcription factors enrichment analysis of the differentially expressed genes in (B), performed using the ChEA 2022 database. **(D)** (left) Western Blot showing p63 knock-down in RT4 cells. An anti-p63pan was used. (right) Growth curve analysis performed in IncuCyte system comparing control cells and p63-depleted cells, n=1. **(E)** Western Blot showing E-cadherin expression after p63 silencing in RT4 and RT112 cells, n=1. **(F)** (left) Intersection between all p63-regulated genes (from RNAseq following p63 silencing) and p63-bound genes (from p63 ChIPseq) in RT4 cells. The p63-regulated genes by binding were intersected with a list of 10 genes canonically involved in EMT. (right) *TP63* correlation with the 10 genes involved in EMT (from the RNAseq in RT4 cells). **(G)** (left) Western Blot showing p63 and Slug correlation in RT4 cells, n=3. Densitometric quantification of the corresponding western Blot is shown on the left. p by Unpaired t test (**** $p< 0.001$). (right) Western Blot showing p63 and Slug correlation in RT112 cells, n=1. **(H)** *TP63* and *SNAI2* correlation in BLCA TCGA cohort. **(I)** p63 ChIPseq signal in RT4 cells, n=1; ATACseq signal following p63 silencing in RT4 cells, n=1; H3K27ac in RT4 and T24 cell lines from GSE213533 study. The *SNAI2* locus is shown.

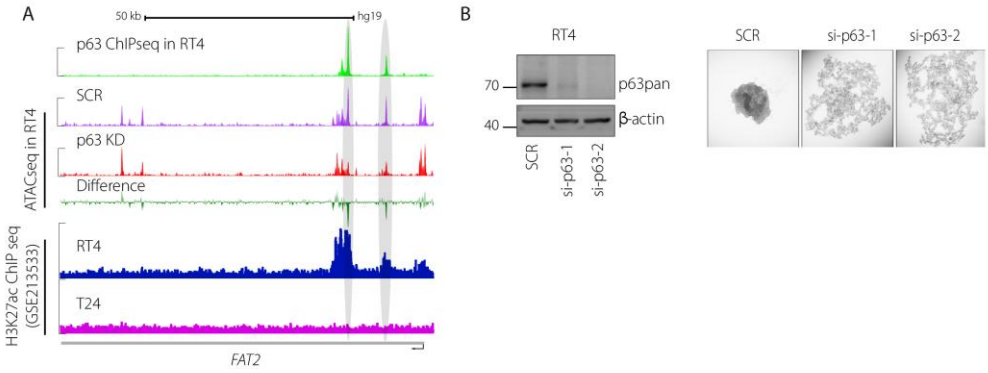

Figure 11. p63 regulation on *FAT2* gene and p63 silencing effect on 3D cell growth. (A) p63 ChIPseq signal in RT4 cells, n=1; ATACseq signal following p63 silencing in RT4 cells, n=1; H3K27ac in RT4 and T24 cell lines from GSE213533 study. The *FAT2* locus is shown. **(B)** (left) Western Blot showing p63 know-down performed by using two distinct siRNAs in RT4 cells. An anti-p63pan was used. (right) Spheroids derived from control and p63-depleted RT4 cells, n=1.

2. p63–*LEADR* axis regulates the expression of interferon-stimulated genes in BLCA

2.1 p63 directly regulates LEADR transcription through chromatin remodelling

To investigate the transcriptional regulation of long non-coding RNAs (lncRNAs) by p63 in BLCA cells, we analysed the significantly differentially expressed lncRNAs identified by RNAseq following p63 depletion in RT4 cells. Among these, we identified *LEADR*, a transcript of *MIR205HG* gene, as the most non-coding RNA downregulated in p63-depleted cells, indicating that its transcription is activated by p63 (Figure 12A). By immunofluorescence and fluorescence in situ hybridization (FISH) we confirmed the positive correlation between p63 and *LEADR* transcript in our panel of BLCA cell lines (Figure 12B). Consistently, we confirmed the positive correlation between *TP63* and *MIR205HG* expression in TCGA BLCA patients (Figure 12C) and we found that *MIR205HG* expression decreases in advanced BLCA (Figure 12D). To understand whether p63 regulated *LEADR* expression, we silenced p63 by using a set of siRNAs either against all p63 isoforms or specifically ΔNp63 isoform and we found that all the siRNAs led to a dramatic decrease of *LEADR* expression in low-stage RT4 cells (Figure 12E). To investigate the molecular mechanism by which p63 regulates *LEADR* expression, we interrogated p63 ChIPseq in RT4 cells and we found that the *MIR205HG* locus had three enhancer regions, highlighted as Enhancer 1 (intronic +2.3 kb region), Enhancer 2 (intergenic -13 kb region) and Enhancer 3 (intergenic −17 kb region), bound by p63. ATACseq after p63 silencing in RT4 cells showed a marked reduction of chromatin accessibility at all three enhancers in p63-depleted cells compared to control cells, suggesting that p63 regulated *MIR205HG* expression by shaping chromatin organization. Consistently with our results, two publicly available H3K27ac ChIPseq experiments carried out in RT4 and T24 cell lines showed that the high levels of histone acetylation within all the three enhancer sites were reduced at enhancer 1 and partially at enhancer 2 regions, whereas enhancer 3 retained acetylation in T24 cells (Figure 12F). Collectively, we demonstrated that p63 controls the epigenetic state of the *MIR205HG* locus.

2.2 LEADR represses interferon-stimulated genes expression and is associated with immune cell infiltration

We next sought to investigate the role of *LEADR* transcript in low-stage BLCA cells. Therefore, we performed the knock-down of *LEADR* spliced transcript using a specific siRNA which does not affect *MIR205*-generating unspliced RNA as described before (Profumo et al., 2019) and carried out the RNAseq (Figure 13A). We identified 312 *LEADR*-activated and 235 *LEADR*-repressed genes. Reactome gene set enrichment analysis (GSEA) revealed that *LEADR*-repressed genes were strongly associated with interferon signalling, homology directed repair and replication stress (Figure 13B). To answer the question whether interferon pathway was affected by *LEADR* depletion, we identified some interferon-stimulated genes (ISGs), such as transcription factors from STAT and IRF families and downstream targets, for instance, IFITs (Figure 13C), and we assessed if their expression at protein level changed in *LEADR*-depleted cells. We observed a significant increase in IRF7 and IRF9 protein levels in *LEADR*-depleted cells (Figure 13D). Notably, IRF7 and IRF9 levels were dramatically increased in the two high-stage cell lines T24 and TCCSUP compared to low-stage RT4 and RT112 cells (Figure 13E). These findings indicated that *LEADR* restrains the expression of some ISGs in low-stage BLCA cells .

Given the central role of interferon signalling in tumor immune responses, we next investigated whether *MIR205HG/LEADR* expression was associated with the immune-cell composition of bladder tumors. To address this question, we used distinct deconvolution methods available through TIMER2.0 tool. We found that tumors with high levels of *MIR205HG* were enriched for $CD4^+$ T cells and NK cells; on contrary, tumors with low levels of *MIR205HG* were characterized by a higher proportion of M2 macrophages (Figure 13F). Importantly, by integrating data from BLCA TCGA and TIMER2.0, we found that $CD4^+$ T cell abundance was not significantly associated with tumor stage in BLCA TCGA cohort (Figure 13G). In summary, our results suggested that p63-*LEADR* axis represses the expression of ISGs and that tumors with high *LEADR* expression are associated with increased $CD4^+$ T cell infiltration, independently of tumor stage.

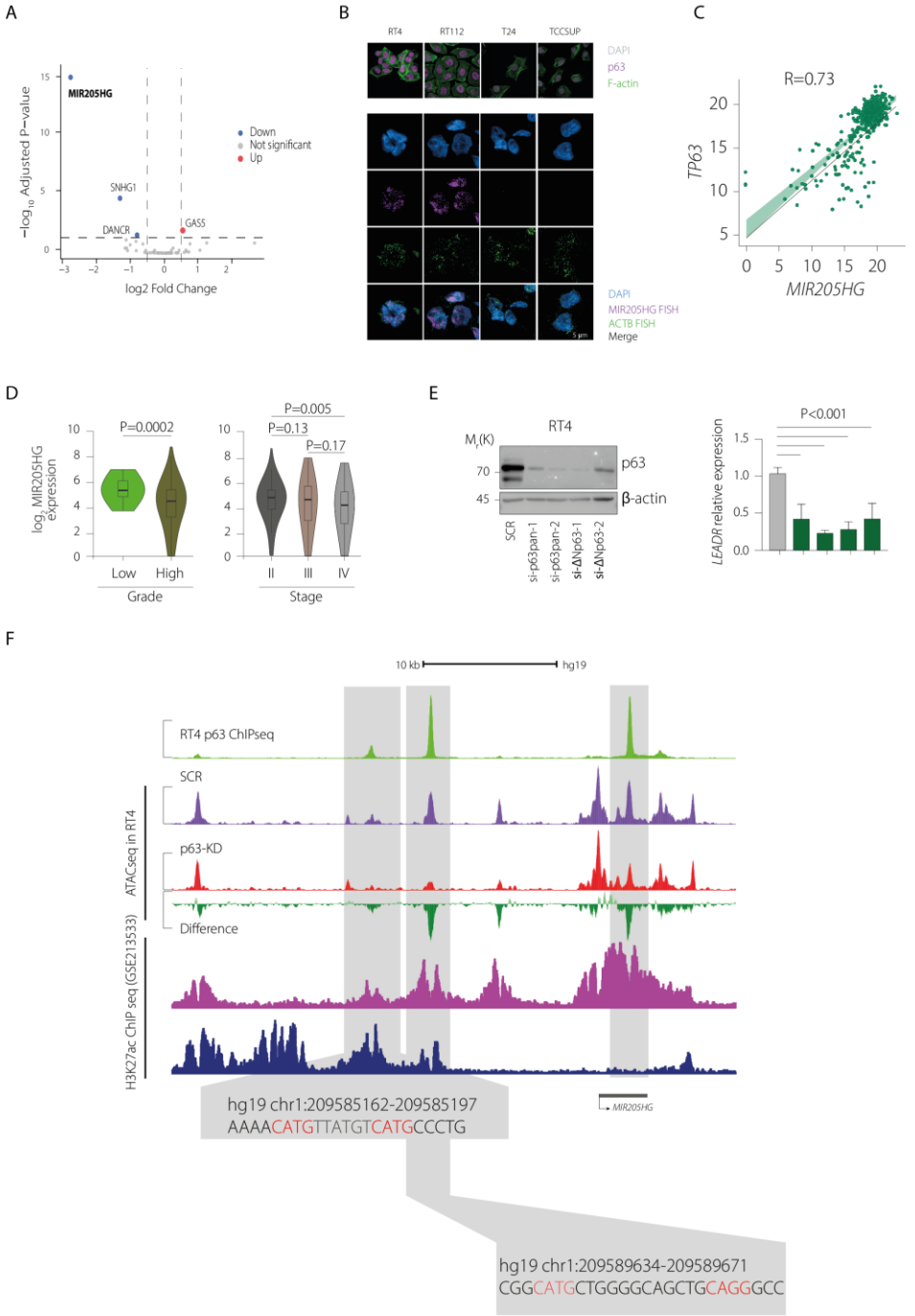
A
MIR205HG
SNHG1
DANCR
GAS5
Down
Not significant
Up
−log10 Adjusted P−value
log2 Fold Change
B
RT4
RT112
T24
TCCSUP
DAPI
p63
F-actin
DAPI
MIR205HG FISH
ACTB FISH
Merge
C
R=0.73
TP63
MIR205HG
D
log2 MIR205HG expression
P=0.0002
Low
High
Grade
P=0.005
P=0.13
P=0.17
II
III
IV
Stage
E
RT4
M,(K)
70
45
p63
β-actin
SCR
si-p63pan-1
si-p63pan-2
si-ΔNp63-1
si-ΔNp63-2
P<0.001
LEADR relative expression
F
10 kb
hg19
RT4 p63 ChIPseq
SCR
p63-KD
Difference
ATACseq in RT4
H3K27ac ChIP seq (GSE213533)
MIR205HG
hg19 chr1:209585162-209585197
AAAACATGTTATGTCATGCCCTG
hg19 chr1:209589634-209589671
CGGCATGCTGGGGCAGCTGCAGGGCC

Figure 12. p63 regulates *LEADR* transcription in low-stage BLCA cells. (A) Volcano plot showing differential expression of ncRNAs in p63-depleted RT4 cells vs control cells. Thresholds: $p<0.05$; $|\log_2 FC|= 0.5$; n=3. **(B)** (top) Immunofluorescence images showing p63 expression levels in BLCA cell lines. (bottom) FISH showing *LEADR* localization and expression levels in BLCA cell lines. *ACTB* was used as control. n=1 **(C)** Correlation analysis between *TP63* and *MIR205HG* expression in TCGA BLCA cohort. **(D)** Violino plots showing $\log_2$ *MIR205HG* expression in TCGA BLCA samples based on the grade and stage. p by Kolmogorov-Smirnov ("grade") or one-way ANOVA ("stage") tests. **(E)** (left) Western Blot confirming the efficiency of knock-down of p63 by using distinct siRNAs against *TP63* in RT4 cells. RT-qPCR showing *LEADR* transcript expression levels after p63 depletion in RT4 cells, n=4. p by one-way ANOVA (right) Western Blot confirming the efficiency of knock-down of p63 by using a siRNAs against *TP63* in RT112 cells. RT-qPCR showing *LEADR* transcript expression levels after p63 depletion in RT112 cells, n=1. **(F)** p63 ChIPseq signal in RT4 cells, n=1; ATACseq signal following p63 depletion in RT4 cells, n=1; H3K27ac ChIPseq from the GSE213533 study. The *MIR205HG* locus is shown. The three regions with putative enhancer activity are highlighted in grey. The predicted p63 binding motifs are shown below.

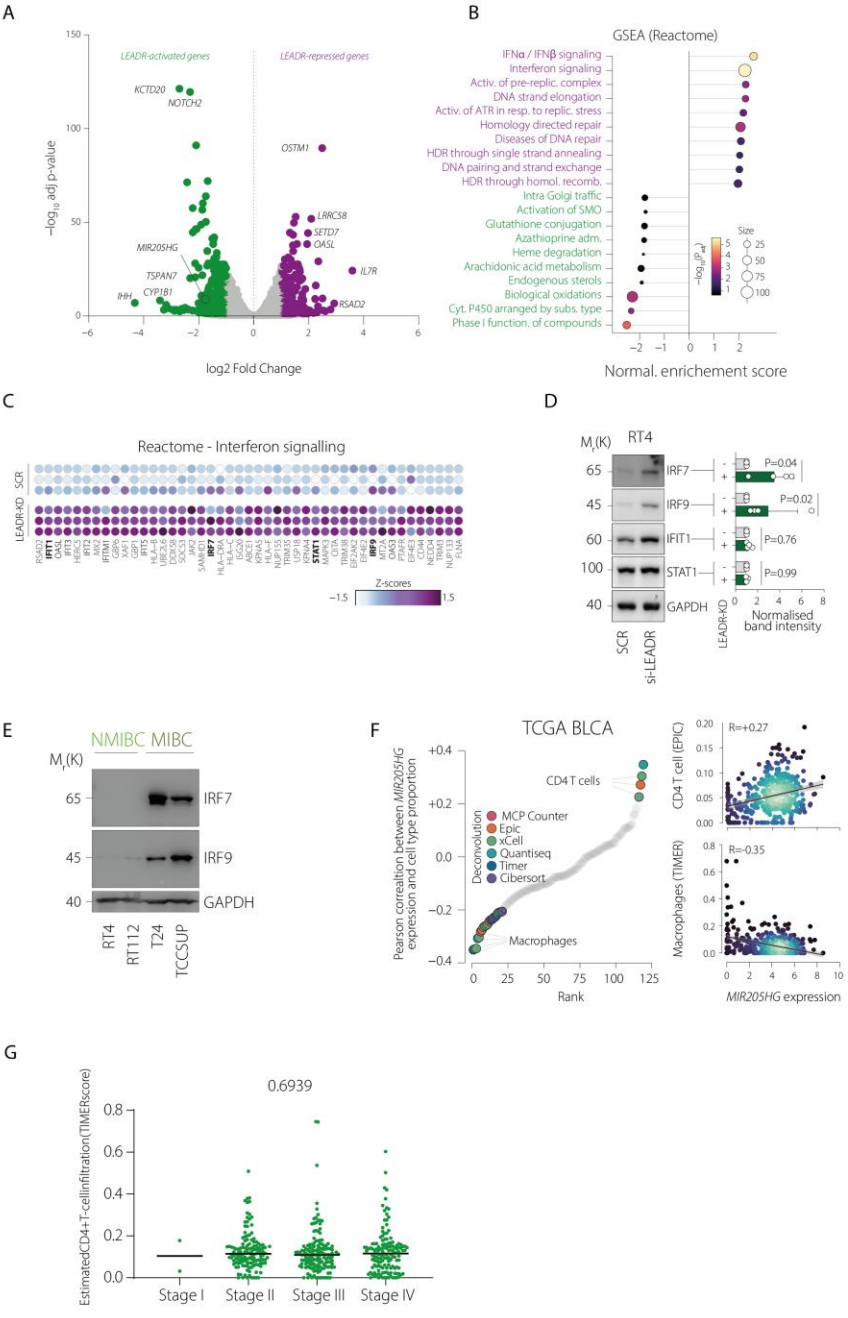
A
LEADR-activated genes
LEADR-repressed genes
KCTD20
NOTCH2
OSTM1
LRRC58
SETD7
OASL
MIR205HG
TSPAN7
IL7R
IHH
CYP1B1
RSAD2
−log10 adj p-value
log2 Fold Change
B
GSEA (Reactome)
IFNα / IFNβ signaling
Interferon signaling
Activ. of pre-replic. complex
DNA strand elongation
Activ. of ATR in resp. to replic. stress
Homology directed repair
Diseases of DNA repair
HDR through single strand annealing
DNA pairing and strand exchange
HDR through homol. recomb.
Intra Golgi traffic
Activation of SMO
Glutathione conjugation
Azathioprine adm.
Heme degradation
Arachidonic acid metabolism
Endogenous sterols
Biological oxidations
Cyt. P450 arranged by subs. type
Phase I function. of compounds
Size
Normal. enrichement score
C
Reactome - Interferon signalling
SCR
LEADR-KD
Z-scores
D
Mr(K)
RT4
65
45
60
100
40
IRF7
IRF9
IFIT1
STAT1
GAPDH
P=0.04
P=0.02
P=0.76
P=0.99
Normalised band intensity
SCR
si-LEADR
E
NMIBC MIBC
Mr(K)
65
45
40
IRF7
IRF9
GAPDH
RT4
RT112
T24
TCCSUP
F
TCGA BLCA
Pearson correlation between MIR205HG expression and cell type proportion
Deconvolution
MCP Counter
Epic
xCell
Quantiseq
Timer
Cibersort
CD4 T cells
Macrophages
Rank
R=+0.27
CD4 T cell (EPIC)
R=−0.35
Macrophages (TIMER)
MIR205HG expression
G
0.6939
EstimatedCD4+T-cellinfiltration(TIMERscore)
Stage I
Stage II
Stage III
Stage IV

Figure 13. Functional effect of LEADR on BLCA. (A) Volcano plots showing the differential gene expression (DGE) analyses in RT4, comparing *LEADR*-depleted cells vs control cells. In orange are shown the p63-activated genes (downregulated genes) and in green the p63-repressed genes (upregulated genes). Thresholds: adj $p<0.05$; $|\log_2 FC|= 1$; n=3. **(B)** Enrichment pathways analysis of modulated genes from (G) performed by Reactome. **(C)** Heatmap showing expression Z-scores of genes from the "Interferon signalling" pathway. **(D)** (left) Western Blot showing the expression of IRF7, IRF9, IFIT1, and STAT1 in *LEADR*-depleted RT4 cells compared to control cells. (right) Densitometry analysis of the same samples. Values shown are fold enrichment over scramble normalized over GAPDH intensity for each protein, n = 4. p by two-way ANOVA. **(E)** Western Blot showing the expression levels of IRF7 and IRF9 in the panel of BLCA cell lines, n=1. **(F)** (left) Dot plot showing Pearson correlation between *MIR205HG* expression and predicted proportion of infiltrating cells in TCGA BLCA samples based on publicly available deconvolution algorithms. (right) Dot plots showing expression of *MIR205HG* and predicted proportion of either $CD4^+$ T cells or macrophages in TCGA BLCA. **(G)** Scatter plot showing $CD4^+$ T cell infiltration across tumor stages. Each dot represents individual BLCA patient and horizontal lines indicate the median. p by Kruskal–Wallis test.

DISCUSSION

Despite recent advances in the clinical management of superficial bladder tumors, the treatment of the muscle-invasive tumors remains challenging and associated with a worse prognosis (Lopez-Beltran et al., 2024). Therefore, biomedical research aims to identify the molecular mechanisms driving the transition from non-muscle-invasive to muscle-invasive disease. Although several molecular alterations driving BLCA progression have been identified (Dyrskjøt et al., 2023; Lopez-Beltran et al., 2024; Wu et al., 2019), the molecular mechanisms underlying this transition remain unclear. In this study we investigated the transcriptional program governed by p63, a transcription factor emerged as a critical regulator of most epithelial cancers, exerting either oncogenic or tumor suppressive functions. Our findings revealed novel pathways linking p63 to lipid metabolism and to non-coding RNA-mediated signalling in this tumor type, providing new insights into the molecular mechanisms underlying BLCA progression.

In line with previous reports (Furlano et al., 2024; Steurer et al., 2021; Urist et al., 2002), our findings confirmed that *TP63* expression progressively decreases during BLCA progression and that high *TP63* expression is associated with a more favourable clinical outcome. Notably, among several epithelial cancers characterized by high *TP63* expression, BLCA appeared the only one which showed a significant stage-dependent decline in *TP63* expression and a significant association with patient survival. These findings suggest that its progressive loss may contribute to disease progression. Since the p63 function is highly isoform-dependent, we first characterized p63 isoforms in our panel of BLCA cell lines (reflecting tumor progression), founding that ΔNp63α represents the predominant p63 isoform expressed in low-stage BLCA cell lines. This isoform is indeed widely recognized as a master regulator of epithelial stemness and differentiation (Y. Li et al., 2023; McDade et al., 2014; Pokorná et al., 2021). However, by western Blot analysis and using an anti-p63pan antibody, we detected a weaker band in low-stage cell lines that, based on its molecular weight, may correspond to a shorter C-terminal p63 isoform, potentially p63β. Although the biological significance of this isoform in BLCA is currently unknown, accumulating evidence suggest that p63 C-terminal isoforms can exert distinct functions. Lena *et al.*, demonstrated that the replacement of p63α with p63β, through the deletion of exon 13 in mice, results in an increased transcriptional activation of p63 target genes, leading to profound defects in epithelial development (Lena et al., 2025). Therefore, further studies will be required to determine the identity of

the lower-molecular-weight band detected in low-stage BLCA cells and to elucidate its potential contribution to BLCA biology.

Our transcriptomic and functional analyses revealed that p63 positively regulates the expression of genes involved in cell-cycle progression and cell proliferation. Indeed, our preliminary results showed that p63 silencing in p63-high cell lines resulted in reduced proliferation, assessed by EdU incorporation and Ki-67 expression, supporting previous evidence demonstrating that ΔNp63α promotes self-renewal and proliferative capacity in epithelial stem cells and squamous tumors (Antonini et al., 2006; Y. Li et al., 2023; Truong et al., 2006). Consistent with our results, ΔNp63α has been found to regulate the expression of several genes involved in cell-cycle progression and cell proliferation, including *CCND1*, *CDK1* and the chromatin remodeler *HELLS* (Keyes et al., 2011; Truong et al., 2006). Moreover, Pecorari *et al.*, showed that p63/ZNF148/*CCND1* regulatory axis sustains tumor cell proliferation in HNSCC (Pecorari et al., 2025b). Despite its role in supporting cell proliferation, p63 expression was associated with favourable prognosis in patients. This apparent paradox probably reflects the dual nature of p63 function in BLCA: while it promotes cell proliferation, it simultaneously suppresses transcriptional programs associated with tumor progression. Surprisingly, our transcriptomic analyses revealed lipid metabolism as a major pathway negatively regulated by p63, suggesting a previously unrecognized role for this transcription factor in lipid metabolism reprogramming in this tumor. This is consistent with our hypothesis that p63 suppresses aggressive features of BLCA, as the promotion of lipid metabolism in cancer is associate in supporting membrane biosynthesis, energy production, redox balance and metastatic dissemination (Fu et al., 2021; Liu et al., 2025; Pascual et al., 2017).

Among the lipid metabolism-related genes identified from our analyses, *MGLL* gene, which encodes for monoacylglycerol lipase, a key enzyme involved in the hydrolysis of monoacylglycerols generating free fatty acids and cholesterol, emerged as the most compelling candidate (W. Li et al., 2025; Nomura et al., 2010; Tan et al., 2023). However, its role in BLCA is largely unexplored. Our work first demonstrated that MGLL expression was inversely correlated with p63 expression in TCGA BLCA cohort and in high-stage cell lines. Second, by the intersection of our transcriptomic and gene occupancy data, we showed that p63 physically binds a promoter region of *MGLL* gene, regulating its transcription. ATACseq analysis revealed an increased

chromatin accessibility at the *MGLL* promoter region following p63 depletion in high-p63 cells, suggesting that p63 regulates MGLL expression at epigenetic level. Indeed, proteomic analyses in high-p63 cells, following p63 immunoprecipitation, identified several chromatin regulators including HDAC1/2, DNMT1, WDR5, CHD family members and RUVBL1/2. Interrogating publicly available H3K27ac ChIPseq data, we found a reduction in acetylation of the *MGLL* promoter in high-p63 cells compared with p63-lack cells, consistent with our hypothesis that the interaction between p63 and HDAC1/2 inhibits chromatin accessibility on this genomic region. Collectively, our findings suggest a model in which p63 recruits chromatin-organization complexes to maintain a repressive chromatin configuration at the *MGLL* locus. This mechanism is in line with the role of ΔNp63α as a chromatin organizer, responsible to coordinate large-scale transcriptional programs through epigenetic regulation (Keyes et al., 2011; Qu et al., 2019).

To investigate the biological consequences of MGLL expression, non-targeted lipidomic analysis following MGLL depletion in high-stage cells, showed profound alterations in lipid composition. Specifically, MGLL promoted glycerophospholipid metabolism while inhibited sphingolipid signalling/metabolism. While glycerophospholipids represent essential structural components of cellular membranes and are frequently associated with tumor growth and metastatic potential (Fu et al., 2021), several sphingolipids are often involved in stress responses, apoptosis and growth suppression (Hannun & Obeid, 2018). Given the crucial structural role of glycerophospholipids in cellular membranes and therefore in tumor growth, we assessed the effect of this enzyme on cell proliferation, migration and invasion. We found that MGLL depletion did not significantly affect cell proliferation or migration, but markedly reduced cell invasion. The selective impact of MGLL on cell invasion could represent a mechanism through which the loss of p63 contributes to the transition toward a more aggressive phenotype. Deeper investigations of the functional impact of MGLL in BLCA revealed that MGLL depletion in high-stage BLCA cell lines reduced basal respiration and ATP-linked respiration, whereas MitoTracker staining did not reveal marked changes in mitochondrial activity. These findings suggest that the reduced respiratory activity under MGLL-depletion could result from a decreased availability of lipids required for the β-oxidation rather than from impaired mitochondrial activity. This interpretation is consistent with the emerging role of fatty acid oxidation in supporting cancer cell survival, metabolic flexibility and adaptation to stressful microenvironmental

conditions (Rodríguez-Enríquez et al., 2015). However, these preliminary findings require further confirmation in independent experiments.

Previous reports have shown conflicting conclusions regarding the role of p63 in EMT in BLCA. While Tran *et al.* proposed that ΔNp63α inhibits EMT through miR-205-dependent mechanisms (Tran et al., 2013b), others suggested pro-invasive functions for ΔNp63α in specific contexts (Tian et al., 2022). Our preliminary results showed that p63 does not affect cell migration and E-cadherin expression, suggesting that it is not involved in EMT. However, further analyses showed that p63 simultaneously promotes the expression of Slug, a canonical EMT-associated transcription factor, and Fat2, an atypical cadherin previously implicated in maintaining epithelial behavior. Previous study showed that the transcription factor Slug cooperates with the transcription factor Snail to promote the expression of EMT-related genes (Medici et al., 2008; Y. Wang et al., 2013), however Snail is not expressed in cell line in which we performed the transcriptomic analysis. This last result could explain the reason why p63-Slug axis does not inhibit E-cadherin expression. Together, our data suggest that p63 could preserve epithelial identity while preparing cells for the subsequent phenotypic transition, sustaining a hybrid-EMT state. This mechanism may be particularly relevant during early stages of tumor progression, where cellular plasticity rather than complete EMT may facilitate adaptation to changing microenvironmental conditions (Aggarwal et al., 2021; Bornes et al., 2021).

Finally, our work identifies the lncRNA *LEADR* (Long Epithelial Alu-interacting Differentiation-related RNA), encoded by the *MIR205HG* locus, as the most strongly downregulated ncRNAs following p63 depletion in RT4 cells, exhibiting a robust positive correlation with *TP63* expression in both our panel of cell lines and TCGA BLCA patients. Mechanistically, we found that p63 directly regulates chromatin accessibility in an enhancer region of the *MIR205HG* locus, demonstrating *LEADR* as a *bona fide* p63 transcriptional target. Although *LEADR* has previously been implicated in the regulation of epithelial differentiation and epithelial gene expression programs in prostate cancer (Profumo et al., 2019), its role in BLCA has not been investigated until now. Our findings reveal a previously unrecognized function of *LEADR* in repressing interferon-related transcriptional programs. Indeed, its depletion in RT4 cells resulted in the activation of several interferon-responsive genes, including IRF7, IRF9 and members of the IFIT family, suggesting its contribution in dampening the interferon signalling in low-stage BLCA cells. Interferon signalling plays a context-dependent role in cancer, exerting both

anti-tumor and pro-tumor functions (Benci et al., 2016; Parker et al., 2016). Interestingly, a recent study demonstrated that low-grade BLCA cell lines are sensitive to IFNα treatment, which induces the expression of interferon-stimulated genes (ISGs) and promotes tumor cell death, while high-grade BLCA cell lines exhibit resistance to IFNα because of the constitutive ISGs activation (Chhipa et al., 2024; Green et al., 2021). This observation is consistent with the elevated levels of IRF7 and IRF9 that we detected in the high-stage cell lines, which potentially promote the acquisition of resistance mechanisms. Together, these data suggest the possibility that *LEADR* prevents the chronic activation of ISGs that have been associated with tumor progression and therapeutic resistance (Benci et al., 2016). Given the crucial role of interferon signalling in anti-tumor immunity, we further investigated the relationship between *MIR205HG* expression and immune cell infiltration. Computational deconvolution analyses revealed that tumors with higher *MIR205HG* expression exhibited an enrichment of $CD4^+$ T cells and NK cells, while tumors with lower *MIR205HG* expression exhibited an enrichment of M2 macrophages. Supporting the positive association between p63–*LEADR* and $CD4^+$ T cell infiltration, we found that $CD4^+$ T cell abundance is not significantly associated with bladder tumor stage. Although these observations require experimental validations, they support a model in which the p63–*LEADR* axis contributes to the establishment of a more favourable immune microenvironment, attenuating aberrant interferon signalling.

Although MGLL and *LEADR* regulate apparently distinct biological processes, they *may* represent two complementary downstream effectors by which p63 preserves the epithelial state of BLCA cells. On the one hand, p63 represses MGLL limiting lipid metabolic reprogramming and invasive behaviour, on the other hand it modulates immune-related pathways by regulating *LEADR* expression. Previous evidence indicates that alterations of lipid metabolism in tumor cells can modulate paracrine signalling and influence immune-cell infiltration (Offer et al., 2019). Based on these evidence, MGLL-dependent lipid remodelling may potentially contribute to the immune contexture associated with the p63–*LEADR* axis. Nevertheless, our study does not demonstrate a direct functional interaction between MGLL and *LEADR*, and this hypothesis will require future dedicated experimental investigation.

Despite these significant findings obtained, our study presents a few limitations that should be addressed. First, p63 silencing or knock-out induces the arrest of cell proliferation, limiting the study of downstream

molecular and functional effects. Second, all experiments were performed *in vitro*, and thus validation in appropriate *in vivo* models will be necessary to confirm the biological and clinical relevance of our findings. Another important limitation concerns the mechanistic characterization of MGLL. Indeed, although MGLL silencing demonstrated to have impacted functional consequences, further studies will be necessary to better explain the molecular mechanism by which it exerts its oncogenic role. In particular, the pathways linking MGLL-dependent lipid metabolic reprogramming to the acquisition of invasive properties remain to be clarified. Finally, the association between *LEADR* expression and immune-cell infiltration remains based on computational deconvolution of bulk transcriptomic data, therefore future mechanistic validation will be necessary to establish a direct role for *LEADR* transcript in $CD4^+$ T cells recruitment.

Taking together, our study provides a comprehensive characterization of the transcriptional program driven by p63 in BLCA with a focus on previously unrecognized links between p63, lipid metabolism and lncRNA-mediated signalling, expanding our understanding of p63 biology in urothelial carcinoma and providing several promising directions for future research.

EXPERIMETAL PROCEDURES

i. Cell cultures

Established human bladder cancer cell lines were purchased from American Type Culture Collection (ATCC) and Cell Lines Service (CLS). RT4 cells (ATCC; HTB-2) and T24 cells (ATCC; HTB-4) were cultured in McCoy′s medium (Gibco), RT112 cells (CLS; 300324) and 5637 cells (ATCC; HTB-9) were cultured in RPMI medium (Gibco), TCCSUP (ATCC; HTB-5) cells were grown in Minimum essential medium (Eagle). Three-dimensional (3D) RT4-derived spheroids were generated through the hanging-drop method. Briefly, cell suspensions were prepared in complete culture medium and droplets containing 10.000 cells were dispensed onto the inner surface of a Petri dish lid. The lid was then inverted over the dish containing sterile 1X PBS to maintain humidity during the incubation. All the media were supplemented with heat-inactivated 10 % Fetal Bovine Serum (Invitrogen) and penicillin/streptomycin (100 µg/mL, Gibco). Cells and spheroids were maintained at 37 °C and 5 % CO_2 humidified atmosphere and monitored by bright-field microscopy regularly. Cells were routinely checked for possible mycoplasma contamination through MycoAlert Mycoplasma Detection Kit (Lonza).

ii. RNA interference (RNAi)

Gene silencing was achieved using RNAi to transiently reduce expression of the gene of interest. Cells were seeded, at different density based on the cell line, in a mix with specific siRNAs, Optimem medium (Thermo Fisher Scientific) and Lipofectamine-RNAiMAX reagent (Thermo Fisher Scientific) according to the manufacturer's protocol, for 48 h. A control siRNA (scr, mission siRNA universal negative control #1 SIC001, Sigma) with no homology to any known human mRNA was used as a negative control. The target sequences of siRNAs used in the study are the following:

si-p63-pan-1: GGAUGAACCGCCGUCCAAU

si-p63-pan-2: CAGGUUGGCACUGAAUUCA

si-ΔNp63-1: GAAGAAAGGACAGCAGCAUUG

si-ΔNp63-2: ACAAUGCCCAGACUCAAUUUU

si-MGLL-1: CUGGACCUACCUUAAUGGUUA

si-MGLL-2: AAGACAGAGGUCGACAUUUAU

si-MGLL-3: UCAGAGCUUGAUGCUACUGUA

si-MGLL-4: CAACUCCGUCUUCCAUGAAAU

si-LEADR: AACUGGGUGCUUUAUAUAGGA

iii. RNA isolation, reverse transcription and RT-qPCR

Total RNA was isolated from cells by using RNeasy Mini Kit (QIAGEN, Hilden, Germany) with DNase I digestion (QIAGEN, Hilden, Germany) according to the manufacturer's protocol. RNA yield and A260/280 ratio were measured with a NanoDrop 1000 spectrophotometer (Thermo Fisher Scientific Inc., Waltham, MA, USA). cDNA was synthesized using SensiFast cDNA Syntesis Kit with oligo-dT and random hexamer primers (Bioline). Real-time qPCR was performed using the PowerUp SYBR Green Master Mix (AppliedBiosystems), in an QuantStudio™ 5 Real-Time PCR System (Applied Biosystems) with the following termic profile: one cycle at 95 °C for 20'', 40 cycles at 95 °C for 3'' and 60 °C for 20''. GAPDH was used as housekeeping gene for data normalization. Relative expression was calculated by using the $2^{-\Delta\Delta Ct}$ method. The primers used in the study are the following:

qPCR primers	
p63-pan For	ACCTGGAAAACAATGCCCAGA
p63-pan Rev	ACGAGGAGCCGTTCTGAATC
TAp63 For	TCAGAAGATGGTGCGACAAAC
TAp63 Rev	GTTCAGGAGCCCCAGGTTCG
ΔNp63 For	ACCTGGAAAACAATGCCCAGA
ΔNp63 Rev	ACGAGGAGCCGTTCTGAATC
MGLL For	GGCATGGTACTCATTTCGCCTC
MGLL Rev	GTTTGGCAGCACAAGGTTGAGC
LEADR For	GAGACATCTGGAGTGTGCGT
LEADR Rev	TAAGGTTCCCATCTGCGGTG
GAPDH For	GTCTCCTCTGACTTCAACAGCG
GAPDH Rev	ACCACCCTGTTGCTGTAGCCAA

iv. RNA sequencing analysis

Total RNA was isolated as described before. The amount and integrity of the extracted RNA were assessed by Agilent TapeStation instrument (Agilent Technologies, CA). Total or poly(A)-enriched RNA sequencing were performed in paired-end mode with a read length of 150 bp using the Illumina NovaSeq 6000 (Illumina, CA) with a coverage of 100 M reads. Library preparation and sequencing were performed by Novogene. Sequencing reads were aligned to the human reference genome (hg19 or hg38 as indicated) and signal tracks were visualized using the UCSC Genome Browser. The reproducibility of biological replicates was assessed by Principal component analysis (PCA). Differential gene expression analysis was performed using DESeq2 through iDEP web platform.

v. Immunoblotting

For total protein extraction, cells were lysed in RIPA lysis buffer (50 mM Tris-HCl pH 8.0, 150 mM NaCl, 1 % NP40, 0.5 % Na-deoxycholate, 0.1 % SDS + protease and phosphatase inhibitors) for 10 min on ice and then centrifuged for 10 min to remove any debris. Proteins were denatured and negatively charged with Laemmli buffer and then boiled at 95 °C for 5 min. Proteins were loaded onto SDS-PAGE for separation and transferred onto polyvinylidendifluoride membranes. Membranes were blocked for 1 h in 5 % milk and incubated overnight with shaking at +4 °C with the following primary antibodies: anti-p63pan (Cell Signaling #39692), anti-ΔNp63 (Cell Signaling #67825), anti-p63α (Cell Signaling #4892), anti-MGLL (Santa Cruz #398942), anti-Slug (Cell Signaling #9585), anti-E-cadherin (Cell Signaling #14472), anti-IRF7 (Cell Signaling #13014), anti-IRF9 (Cell Signaling #76684), anti-IFIT1 (Cell Signaling #14769), anti-STAT1 (Cell Signaling #14994), anti-β-actin clone AC-15 (Sigma A-5441). After three washes with 1X PBS-Tween20, membranes were incubated with the secondary antibodies conjugated to horseradish peroxidase (Goat Anti-Mouse HRP Conjugate BIO-RAD 170-5047, dilution: 1:10.000; Goat Anti-Rabbit IgG (H+L)-HRP Conjugate BIO-RAD 170-6515, dilution: 1:10.000) for 1 h at room temperature. Immunoreactivity was detected by immunodetection system (Alliance Q9 Advanced; Uvitec) with Luminol Reagent (Western Lightning Plus, Revvity). Spectra™ Multicolor Broad Range Protein Ladder (Thermo Scientific™ 26634) was used to determine the protein molecular

weight. Samples normalization was performed adjusting the volume of samples loaded on SDS/PAGE based on housekeeping protein detection. Densitometric analyses were performed using ImageJ software.

i. Flow cytometric analysis following EdU incorporation

After appropriate treatments, EdU was added to the culture medium at a final concentration of 10 µM for 4 h. Then, the culture medium was collected, and cells were harvested by trypsinization. Cells were washed once with 3 mL of 1 % BSA in PBS and the pellet was resuspended in 100 µL Clik-IT fixative for 15 min at room temperature. Samples preparation was subsequently performed according to the manufacturer's instructions provided with the Click-iT™ EdU Flow Cytometry assay kit (Invitrogen #C1042). Samples were acquired on a CytoFLEX (Beckman Coulter) and analysed using CytExpert.

ii. Chromatin immunoprecipitation followed by sequencing (ChIP)

To perform ChIP experiments, we used a modified version of the ChIPmentation CeMM v1.14 (September 2016) protocol (Schmidl et al., 2015). Cells were detached and cross-linked with methanol-free 1% formaldehyde (ThermoFisher) for 10 min at room temperature. The formaldehyde was quenched by addition of freshly prepared 125 mM glycine (Sigma) and incubating for 10 min. After washing twice with 1X PBS complemented with protease inhibitor 1X and PMSF 1 mM, cell pellet was resuspended in 130 µL 1 % SDS sonication buffer (10 mM Tris pH8.0, 1 % SDS, 2 mM EDTA) with protease inhibitors and incubated for 30 min on ice. The fragmentation was performed by sonication (Covaris M220) to obtain DNA fragments of 200-500 nt of length. Size of the sheared chromatin was determined by TapeStation instrument (Agilent Technologies, CA). Five µL of sonicated chromatin was used to check the fragments size, running samples on TapeStation (kit D1000 high sensitivity). Then, 175 µL of Equilibration Buffer were added to 125 µL of chromatin to reduce the % of SDS (1:1.5). Then, 1.2 mL RIPA-LS + 1X protease inhibitors + PMSF 1 mM was added. The antibody was added to the chromatin and placed in a shaker at 4 °C overnight. The following antibody was used: anti-p63 (Cell Signaling #39692). The day after, the Dynalbeads Protein A (Invitrogen #10001D) were added to the complex for immunoprecipitation for at least 2 h at 4 °C. The beads were washed as described in the original protocol. The

immunoprecipitated chromatin was eluted in elution buffer with proteinase K for de-crosslinking and incubated at 55 °C for 1 h and then at 65 °C for overnight. DNA was purified by DNA Purification Buffers and Spin Columns (Cell Signaling, #14209). The genomic quantification was normalized to the input sample. The sequencing was performed by Novogene. ChIPseq data were analysed using the Galaxy platform. Sequencing reads were aligned to the human reference genome (hg19 or hg38 as indicated) using Bowtie2. Peak calling was performed using MACS2. Following peak calling, the genomic regions corresponding to the identified ChIPseq peaks were submitted to the Genomic Regions Enrichment of Annotations Tool (GREAT) for region-to-gene association. Genome-wide coverage tracks were generated from the aligned reads using the deepTools bamCoverage function. Signal coverage was normalized according to the effective genome size of the corresponding human genome assembly, and the signal tracks were exported as BigWig file. The resulting signal profiles were visualized using the UCSC Genome Browser.

iii. Assay for Transposase-Accessible Chromatin using Sequencing (ATACseq)

Assay for Transposase-Accessible Chromatin using sequencing was performed following the protocol described by Buenrostro *et al.* (Buenrostro et al., 2015). Briefly, 48 h after knock-down, cells were harvested and nuclei were isolated by cell lysis. Fifty thousand cells were used for each reaction. Purified nuclei were then subjected to transposition using the hyperactive Tn5 transposase, which simultaneously fragments accessible chromatin regions and inserts sequencing adapters into the generated DNA fragments. Then, DNA was purified, PCR-amplified and subjected to next-generation sequencing. Sequencing data were subsequently processed and analysed to identify genomic regions displaying differential chromatin accessibility between experimental conditions. The sequencing was performed at IFO-IRCSS, Rome.

iv. Interactome analysis and mass spectrometry

Nuclear protein extraction was performed by Nuclear Complex Co-IP Kit (Activ Motif #54001) according to the manufacturer's instructions. Briefly, 5 mg of nuclear proteins were incubated with 500 ng of primary antibody or control IgG overnight at 4°C. Then, 50 µL of Protein A Sepharose beads were

added and incubated with the protein-antibody complex at 4°C for 45 min. The protein-antibody-beads complexes were then pelleted by centrifugation and the supernatant was discarded. The beads were washed four times with IP wash buffer to remove non-specifically bound proteins. Bound proteins were eluted by incubating the beads with 50 µL of elution buffer (NH4OH 0.5 M + EDTA 0.5 mM) for 5 min at room temperature. The supernatant was collected and a second elution step was performed as before with an additional 50 µL of elution buffer. One tenth of eluate was used to assess the efficiency of immunoprecipitation by western blot analysis. The remaining sample was subjected to mass spectrometry analysis at the INMI Lazzaro Spallanzani (Rome). MaxQuant software was used for peptide identification, protein assembly, label-free quantification (LFQ) and normalization.

i. Lipidomic analysis

After appropriate treatments, adherent cells were washed twice with pre-warmed 1X PBS (37 °C). Then, cells were covered with 2 mL of the pre-cooled 80% (v/v) methanol and collected by scraping. Samples were stored at -80°C until their processing. Lipid identification and quantification were subsequently performed by mass spectrometry-based lipidomic analysis at Helmholtz Munich facility (Germany).

ii. Proliferation, migration and invasion assays

Five thousand cells were seeded onto 96 well plates 24 h after knock-down and allowed to attach. The cell growth was assessed in an automated cell counter IncuCyte (Sartorius) using 10X objective and acquiring the images every 2 h for 3 days.

Thirty thousand cells were seeded onto 96 well plate (Sartorius) 24 h after knock-down and allowed to attach. The day after, mechanical scratch was practiced and the wound closure was assessed in an automated cell counter IncuCyte (Sartorius) using 10X objective and acquiring the images every 2 h for 24 h.

Seventy-two hours after knock-down, cells were seeded into 6-well Corning® BioCoat™ Matrigel® Invasion Chamber (#CLS354481). After 16 h of incubation, non-invading cells were removed from the upper surface of the membrane by scrubbing, using a cotton swab. Then, invading-cells were fixed

with a solution of 4 % formaldehyde added to both the insert and the lower well for 10 min at room temperature. Following fixation, the invading cells were washed once with 1X PBS and permeabilized/stained with a solution containing Triton-X100 0.25 % and DAPI (1:1000 dilution) for 15 min. The images were acquired using a fluorescence microscope. Five fields per well were acquired using a fluorescence microscope, and the total number of cells was manually counted using ImageJ.

iii. Seahorse assay

Forty-eight hours after knock-down, cells were seeded on Agilent Seahorse XF Pro M Cell Culture Microplates and allowed to adhere overnight. On the day of the assay, cells were washed with Seahorse XF assay medium (EMEM) and equilibrated in a non-CO_2 incubator according to the manufacturer's instructions. During the assay, oligomycin was injected to a final concentration of 1.5 µM to inhibit ATP synthase, followed by rotenone/antimycin A at a final concentration of 0.5 µM to inhibit complexes I and III of the electron transport chain, respectively. Oxygen consumption rate (OCR) was measured using the Seahorse XF Analyzer (Agilent Technologies). Data analysis was performed using Seahorse Wave software (Agilent Technologies). After Seahorse assay, cells were stained with Hoechst 33342 (Invitrogen #62249) and fluorescent images of each well were acquired using a Cytation imaging system (BioTek). Cell nuclei were counted and OCR values were normalized to cell number.

i. Immunofluorescence staining

Cells were grown in flat bottom 96-well PhenoPlates (Revvity) or on glass slides and then fixed in 4 % formaldehyde in 1X PBS for 10 min. Samples were washed twice for 5 min in 1X PBS. Cells were permeabilized in 0.25 % Triton X-100 for 10 min. Five percent goat serum in 1X PBS was used to block the samples for 1 h. Cells were incubated with primary antibodies diluted in 5 % goat serum overnight at 4 °C. The wells or glass slides were washed 3 times for 5 min in 1X PBS before the incubation with 1 µg/mL DAPI (Sigma #11190301) and secondary antibodies for 1 h. The wells or glass slides was washed 3 times for 5 min in 1X PBS. The images were acquired by Operetta high content imaging system (Revvity) in confocal mode or Stellaris confocal microscope. The following antibodies were used: anti-p63 (Cell Signaling #39692S, 1:200), anti-Ki-67 (Sigma #P-6834, 1;200), anti-mouse Alexa Fluor

647 (Invitrogen #A-21235, 1:1000), anti-rabbit Alexa Fluor 488 (Invitrogen #A-11034, 1:1000), Phalloidin (Invitrogen #A-12380, 1:400).

ii. Immunohistochemical staining

Tissue microarrays were purchased from TissueArray.com. Histological samples were provided by Prof. Alessandro Mauriello from Policlinico of Tor Vergata, Rome. Organoids slides were provided by Dr Giovnni Blandino from IFO-IRCSS, Rome. Immunohistochemistry was carried out using an automated staining system BOND III (Leica). For p63 and MGLL staining, 20 min antigen retrieval in Solution 2 was performed. Following antibodies were used: anti-p63 at 1:200 dilution (Cell Signaling #39692) and anti-MGLL (Santa Cruz #398942). Slides images were acquired on a MIDI 3DHistech scanner. H-score was assigned as follow: 0=absent, 1=weak, 2=medium and 3=strong).

i. RNA-FISH on cell lines

RNA-FISH was performed as described in the protocol ViewRNA Tissue Fluorescence Assay (Invitrogen). Cells were fixed in 4 % formaldehyde for 10 min and permeabilised in 70 % ethanol for 1 h at 4 °C. RNA FISH probe was diluted in hybridization buffer 1:40, added to cells and then incubated for 2 h at 40 °C. Cells were washed twice for 10 min in Wash Buffer. RNA probes (diluted 1:25) were labelled with specific fluorophores (AlexaFluor-546 for *ACTB*; AlexaFluor-647 for *MIR205HG*) and incubated at 40 °C for 30 min. Finally, a counterstain was performed with 1 μg/mL DAPI (Sigma). Cells were washed two times with 1X PBS and analysed on the high content imaging system Operetta (Revvity).

ii. Bioinformatic analyses

Cell line transcriptome data and TCGA data were downloaded from DepMap and UCSC Xena Browser. Other analysis on TCGA was performed by cBioPortal and UCSC Xena Browser. Pathways enrichment was performed by by emplying Reactome library through enrichR platform or GSEA. Volcano plots and heatmaps were generated using ggplot2 and pheatmap packages. Published ChIP seq data on H3K27ac were obtained from GSE213533. ChIPseq signal tracks and peaks were visualised in UCSC Genome Browser. DNA methylation analysis was performed by MethSurv

and UCSC Xena Browser. Immune cell infiltration analyses were performed by using TIMER 2.0 (Tumor Immune Estimation Resource 2.0) by interrogating TCGA BLCA transcriptomic data.

iii. Statistical analyses

All statistical analyses were performed by GraphPad Prism 9 and are indicated in the corresponding figure legends. Overall, statistical significance between two groups was assessed using unpaired Student's t-test. For comparisons involving more than two groups, one-way or two-way ANOVA was applied. Correlation analyses were performed using Spearman's rank correlation coefficient. Survival analyses were carried out using Kaplan–Meier curves and log-rank tests. For all experiments, p values < 0.05 were considered statistically significant.

References

Abou Chakra, M., McElree, I. M., Packiam, V. T., Mott, S. L., & O'Donnell, M. A. (2024). Early experience with sequential intravesical gemcitabine and docetaxel for micropapillary variant non-muscle invasive bladder cancer. *Urologic Oncology*, *42*(9), 289.e13-289.e21. https://doi.org/10.1016/j.urolonc.2024.05.006

Adorno, M., Cordenonsi, M., Montagner, M., Dupont, S., Wong, C., Hann, B., Solari, A., Bobisse, S., Rondina, M. B., Guzzardo, V., Parenti, A. R., Rosato, A., Bicciato, S., Balmain, A., & Piccolo, S. (2009). A Mutant-p53/Smad complex opposes p63 to empower TGFbeta-induced metastasis. *Cell*, *137*(1), 87–98. https://doi.org/10.1016/j.cell.2009.01.039

Aggarwal, V., Montoya, C. A., Donnenberg, V. S., & Sant, S. (2021). Interplay between tumor microenvironment and partial EMT as the driver of tumor progression. *IScience*, *24*(2), 102113. https://doi.org/10.1016/j.isci.2021.102113

Agostini, M., Mancini, M., & Candi, E. (2022). Long non-coding RNAs affecting cell metabolism in cancer. *Biology Direct*, *17*(1), 26. https://doi.org/10.1186/s13062-022-00341-x

Antonini, D., Rossi, B., Han, R., Minichiello, A., Di Palma, T., Corrado, M., Banfi, S., Zannini, M., Brissette, J. L., & Missero, C. (2006). An autoregulatory loop directs the tissue-specific expression of p63 through a long-range evolutionarily conserved enhancer. *Molecular and Cellular Biology*, *26*(8), 3308–3318. https://doi.org/10.1128/MCB.26.8.3308-3318.2006

Babjuk, M., Burger, M., Capoun, O., Cohen, D., Compérat, E. M., Dominguez Escrig, J. L., Gontero, P., Liedberg, F., Masson-Lecomte, A., Mostafid, A. H., Palou, J., van Rhijn, B. W. G., Rouprêt, M., Shariat, S. F., Seisen, T., Soukup, V., & Sylvester, R. J. (2022). European Association of Urology Guidelines on Non–muscle-invasive Bladder Cancer (Ta, T1, and Carcinoma in Situ). *European Urology*, *81*(1), 75–94. https://doi.org/10.1016/j.eururo.2021.08.010

Barbieri, C. E., Perez, C. A., Johnson, K. N., Ely, K. A., Billheimer, D., & Pietenpol, J. A. (2005). IGFBP-3 Is a Direct Target of Transcriptional Regulation by ΔNp63α in Squamous Epithelium. *Cancer Research*, *65*(6),

2314–2320. https://doi.org/10.1158/0008-5472.CAN-04-3449

Barbieri, C. E., & Pietenpol, J. A. (2006). p63 and epithelial biology. *Experimental Cell Research*, *312*(6), 695–706. https://doi.org/10.1016/j.yexcr.2005.11.028

Barbieri, C. E., Tang, L. J., Brown, K. A., & Pietenpol, J. A. (2006). Loss of p63 Leads to Increased Cell Migration and Up-regulation of Genes Involved in Invasion and Metastasis. *Cancer Research*, *66*(15), 7589–7597. https://doi.org/10.1158/0008-5472.CAN-06-2020

Barnaba, D., Franzese Canonico, M., Helmer-Citterich, M., Gandellini, P., Melino, G., Smirnov, A., & Candi, E. (2025). LEADR, a p63 target, dampens interferon signalling in bladder cancer. *Cell Death Discovery*, *11*(1), 264. https://doi.org/10.1038/s41420-025-02546-1

Benci, J. L., Xu, B., Qiu, Y., Wu, T. J., Dada, H., Twyman-Saint Victor, C., Cucolo, L., Lee, D. S. M., Pauken, K. E., Huang, A. C., Gangadhar, T. C., Amaravadi, R. K., Schuchter, L. M., Feldman, M. D., Ishwaran, H., Vonderheide, R. H., Maity, A., Wherry, E. J., & Minn, A. J. (2016). Tumor Interferon Signaling Regulates a Multigenic Resistance Program to Immune Checkpoint Blockade. *Cell*, *167*(6), 1540-1554.e12. https://doi.org/10.1016/j.cell.2016.11.022

Bornes, L., Belthier, G., & van Rheenen, J. (2021). Epithelial-to-Mesenchymal Transition in the Light of Plasticity and Hybrid E/M States. *Journal of Clinical Medicine*, *10*(11). https://doi.org/10.3390/jcm10112403

Bray, F., Laversanne, M., Sung, H., Ferlay, J., Siegel, R. L., Soerjomataram, I., & Jemal, A. (2024). Global cancer statistics 2022: GLOBOCAN estimates of incidence and mortality worldwide for 36 cancers in 185 countries. *CA: A Cancer Journal for Clinicians*, *74*(3), 229–263. https://doi.org/10.3322/caac.21834

Buenrostro, J. D., Wu, B., Chang, H. Y., & Greenleaf, W. J. (2015). ATAC-seq: A Method for Assaying Chromatin Accessibility Genome-Wide. *Current Protocols in Molecular Biology*, *109*, 21.29.1-21.29.9. https://doi.org/10.1002/0471142727.mb2129s109

Cancer Genome Atlas Network. (2015). Comprehensive genomic characterization

of head and neck squamous cell carcinomas. *Nature*, *517*(7536), 576–582. https://doi.org/10.1038/nature14129

Candi, E., Cipollone, R., Rivetti di Val Cervo, P., Gonfloni, S., Melino, G., & Knight, R. (2008). p63 in epithelial development. *Cellular and Molecular Life Sciences : CMLS*, *65*(20), 3126–3133. https://doi.org/10.1007/s00018-008-8119-x

Candi, E., Rufini, A., Terrinoni, A., Giamboi-Miraglia, A., Lena, A. M., Mantovani, R., Knight, R., & Melino, G. (2007). DeltaNp63 regulates thymic development through enhanced expression of FgfR2 and Jag2. *Proceedings of the National Academy of Sciences of the United States of America*, *104*(29), 11999–12004. https://doi.org/10.1073/pnas.0703458104

Cao, Z., Mulvihill, M. M., Mukhopadhyay, P., Xu, H., Erdélyi, K., Hao, E., Holovac, E., Haskó, G., Cravatt, B. F., Nomura, D. K., & Pacher, P. (2013). Monoacylglycerol lipase controls endocannabinoid and eicosanoid signaling and hepatic injury in mice. *Gastroenterology*, *144*(4), 808-817.e15. https://doi.org/10.1053/j.gastro.2012.12.028

Chen, L. C., Neubauer, A., Kurisu, W., Waldman, F. M., Ljung, B. M., Goodson, W., Goldman, E. S., Moore, D., Balazs, M., & Liu, E. (1991). Loss of heterozygosity on the short arm of chromosome 17 is associated with high proliferative capacity and DNA aneuploidy in primary human breast cancer. *Proceedings of the National Academy of Sciences of the United States of America*, *88*(9), 3847–3851. https://doi.org/10.1073/pnas.88.9.3847

Chen, Q., Cai, J., Wang, Q., Wang, Y., Liu, M., Yang, J., Zhou, J., Kang, C., Li, M., & Jiang, C. (2018). Long Noncoding RNA *NEAT1* , Regulated by the EGFR Pathway, Contributes to Glioblastoma Progression Through the WNT/ **β** -Catenin Pathway by Scaffolding EZH2. *Clinical Cancer Research*, *24*(3), 684–695. https://doi.org/10.1158/1078-0432.CCR-17-0605

Chen, Y., Peng, Y., Fan, S., Li, Y., Xiao, Z.-X., & Li, C. (2018). A double dealing tale of p63: an oncogene or a tumor suppressor. *Cellular and Molecular Life Sciences : CMLS*, *75*(6), 965–973. https://doi.org/10.1007/s00018-017-2666-y

Cheng, C., Geng, F., Cheng, X., & Guo, D. (2018). Lipid metabolism

reprogramming and its potential targets in cancer. *Cancer Communications*, *38*(1). https://doi.org/10.1186/s40880-018-0301-4

Chhipa, A. S., Boscaro, V., Gallicchio, M., & Patel, S. (2024). The curious case of type I interferon signaling in cancer. *Biochimica et Biophysica Acta (BBA) - Reviews on Cancer*, *1879*(6), 189204. https://doi.org/10.1016/j.bbcan.2024.189204

Choi, W., Shah, J. B., Tran, M., Svatek, R., Marquis, L., Lee, I.-L., Yu, D., Adam, L., Wen, S., Shen, Y., Dinney, C., McConkey, D. J., & Siefker-Radtke, A. (2012). p63 Expression Defines a Lethal Colbert, L., Jia, Y., Sharma, A., Hu, J., Xu, Z., Suzman, D. L., Das, A., Bross, P., Kluetz, P. G., & Fashoyin-Aje, L. A. (2025). FDA Approval Summary: Nadofaragene Firadenovec-vncg for Bacillus Calmette-Guérin-Unresponsive Non-Muscle-Invasive Bladder Cancer. *Clinical Cancer Research : An Official Journal of the American Association for Cancer Research*, *31*(7), 1182–1185. https://doi.org/10.1158/1078-0432.CCR-24-2812

Compagnone, M., Gatti, V., Presutti, D., Ruberti, G., Fierro, C., Markert, E. K., Vousden, K. H., Zhou, H., Mauriello, A., Anemone, L., Bongiorno Borbone, L., Melino, G., & Peschiaroli, A. (2017). ΔNp63-mediated regulation of hyaluronic acid metabolism and signaling supports HNSCC tumorigenesis. *Proceedings of the National Academy of Sciences of the United States of America*, *114*(50), 13254–13259. https://doi.org/10.1073/pnas.1711777114

Compérat, E., Bièche, I., Dargère, D., Ferlicot, S., Laurendeau, I., Benoît, G., Vieillefond, A., Verret, C., Vidaud, M., Capron, F., Bedossa, P., & Paradis, V. (2007). p63 Gene Expression Study and Early Bladder Carcinogenesis. *Urology*, *70*(3), 459–462. https://doi.org/10.1016/j.urology.2007.04.030

Dang, T. T., Westcott, J. M., Maine, E. A., Kanchwala, M., Xing, C., & Pearson, G. W. (2016). ΔNp63α induces the expression of FAT2 and Slug to promote tumor invasion. *Oncotarget*, *7*(19), 28592–28611. https://doi.org/10.18632/oncotarget.8696

Davis, R., Jones, J. S., Barocas, D. A., Castle, E. P., Lang, E. K., Leveillee, R. J., Messing, E. M., Miller, S. D., Peterson, A. C., Turk, T. M. T., Weitzel, W., & American Urological Association. (2012). Diagnosis,

evaluation and follow-up of asymptomatic microhematuria (AMH) in adults: AUA guideline. *The Journal of Urology*, *188*(6 Suppl), 2473–2481. https://doi.org/10.1016/j.juro.2012.09.078

Devos, M., Gilbert, B., Denecker, G., Leurs, K., Mc Guire, C., Lemeire, K., Hochepied, T., Vuylsteke, M., Lambert, J., Van Den Broecke, C., Libbrecht, L., Haigh, J., Berx, G., Lippens, S., Vandenabeele, P., & Declercq, W. (2017). Elevated ΔNp63α Levels Facilitate Epidermal and Biliary Oncogenic Transformation. *The Journal of Investigative Dermatology*, *137*(2), 494–505. https://doi.org/10.1016/j.jid.2016.09.026

Di Como, C. J., Urist, M. J., Babayan, I., Drobnjak, M., Hedvat, C. V, Teruya-Feldstein, J., Pohar, K., Hoos, A., & Cordon-Cardo, C. (2002). p63 expression profiles in human normal and tumor tissues. *Clinical Cancer Research : An Official Journal of the American Association for Cancer Research*, *8*(2), 494–501.

Dyrskjøt, L., Hansel, D. E., Efstathiou, J. A., Knowles, M. A., Galsky, M. D., Teoh, J., & Theodorescu, D. (2023). Bladder cancer. *Nature Reviews. Disease Primers*, *9*(1), 58. https://doi.org/10.1038/s41572-023-00468-9

Ettinger, S. L., Sobel, R., Whitmore, T. G., Akbari, M., Bradley, D. R., Gleave, M. E., & Nelson, C. C. (2004). Dysregulation of sterol response element-binding proteins and downstream effectors in prostate cancer during progression to androgen independence. *Cancer Research*, *64*(6), 2212–2221. https://doi.org/10.1158/0008-5472.can-2148-2

Fernandez-Figueras, M.-T., & Puig, L. (2020). The Role of Epithelial-to-Mesenchymal Transition in Cutaneous Squamous Cell Carcinoma : Epithelial-to-Mesenchymal Transition in Cutaneous SCC. *Current Treatment Options in Oncology*, *21*(6), 47. https://doi.org/10.1007/s11864-020-00735-x

Fessing, M. Y., Mardaryev, A. N., Gdula, M. R., Sharov, A. A., Sharova, T. Y., Rapisarda, V., Gordon, K. B., Smorodchenko, A. D., Poterlowicz, K., Ferone, G., Kohwi, Y., Missero, C., Kohwi-Shigematsu, T., & Botchkarev, V. A. (2011). p63 regulates Satb1 to control tissue-specific chromatin remodeling during development of the epidermis. *The Journal of Cell Biology*, *194*(6), 825–839.

https://doi.org/10.1083/jcb.201101148

Fierro, C., Gatti, V., La Banca, V., De Domenico, S., Scalera, S., Corleone, G., Fanciulli, M., De Nicola, F., Mauriello, A., Montanaro, M., Calin, G. A., Melino, G., & Peschiaroli, A. (2023). The long non-coding RNA NEAT1 is a ΔNp63 target gene modulating epidermal differentiation. *Nature Communications*, *14*(1), 3795. https://doi.org/10.1038/s41467-023-39011-5

Fischer, M., Schwarz, R., Riege, K., DeCaprio, J. A., & Hoffmann, S. (2022). TargetGeneReg 2.0: a comprehensive web-atlas for p53, p63, and cell cycle-dependent gene regulation. *NAR Cancer*, *4*(1). https://doi.org/10.1093/narcan/zcac009

Flores, E. R., Sengupta, S., Miller, J. B., Newman, J. J., Bronson, R., Crowley, D., Yang, A., McKeon, F., & Jacks, T. (2005). Tumor predisposition in mice mutant for p63 and p73: evidence for broader tumor suppressor functions for the p53 family. *Cancer Cell*, *7*(4), 363–373. https://doi.org/10.1016/j.ccr.2005.02.019

Flores, E. R., Tsai, K. Y., Crowley, D., Sengupta, S., Yang, A., McKeon, F., & Jacks, T. (2002). p63 and p73 are required for p53-dependent apoptosis in response to DNA damage. *Nature*, *416*(6880), 560–564. https://doi.org/10.1038/416560a

Fu, Y., Zou, T., Shen, X., Nelson, P. J., Li, J., Wu, C., Yang, J., Zheng, Y., Bruns, C., Zhao, Y., Qin, L., & Dong, Q. (2021). Lipid metabolism in cancer progression and therapeutic strategies. *MedComm*, *2*(1), 27–59. https://doi.org/10.1002/mco2.27

Furlano, K., Plage, H., Hofbauer, S., Weinberger, S., Ralla, B., Fendler, A., Roßner, F., Schallenberg, S., Elezkurtaj, S., Kluth, M., Lennartz, M., Blessin, N. C., Marx, A. H., Samtleben, H., Fisch, M., Rink, M., Slojewski, M., Kaczmarek, K., Ecke, T., … Zecha, H. (2024). Reduced p63 expression is linked to unfavourable prognosis in muscle-invasive urothelial carcinoma of the bladder. *BJUI Compass*, *5*(11), 1195–1203. https://doi.org/10.1002/bco2.431

Gaffney, C. D., Katims, A., D'Souza, N., Bjurlin, M. A., & Matulewicz, R. S. (2023). Bladder Cancer Carcinogens: Opportunities for Risk Reduction. *European Urology Focus*, *9*(4), 575–578. https://doi.org/10.1016/j.euf.2023.03.017

Gallant-Behm, C. L., Ramsey, M. R., Bensard, C. L., Nojek, I., Tran, J., Liu, M., Ellisen, L. W., & Espinosa, J. M. (2012). ΔNp63α represses anti-proliferative genes via H2A.Z deposition. *Genes & Development*, *26*(20), 2325–2336. https://doi.org/10.1101/gad.198069.112

Gatti, V., Fierro, C., Annicchiarico-Petruzzelli, M., Melino, G., & Peschiaroli, A. (2019). ΔNp63 in squamous cell carcinoma: defining the oncogenic routes affecting epigenetic landscape and tumour microenvironment. *Molecular Oncology*, *13*(5), 981–1001. https://doi.org/10.1002/1878-0261.12473

Geng, F., Cheng, X., Wu, X., Yoo, J. Y., Cheng, C., Guo, J. Y., Mo, X., Ru, P., Hurwitz, B., Kim, S.-H., Otero, J., Puduvalli, V., Lefai, E., Ma, J., Nakano, I., Horbinski, C., Kaur, B., Chakravarti, A., & Guo, D. (2016). Inhibition of SOAT1 Suppresses Glioblastoma Growth via Blocking SREBP-1-Mediated Lipogenesis. *Clinical Cancer Research : An Official Journal of the American Association for Cancer Research*, *22*(21), 5337–5348. https://doi.org/10.1158/1078-0432.CCR-15-2973

Giacobbe, A., Compagnone, M., Bongiorno-Borbone, L., Antonov, A., Markert, E. K., Zhou, J. H., Annicchiarico-Petruzzelli, M., Melino, G., & Peschiaroli, A. (2016). p63 controls cell migration and invasion by transcriptional regulation of MTSS1. *Oncogene*, *35*(12), 1602–1608. https://doi.org/10.1038/onc.2015.230

Green, J. L., Osterhout, R. E., Klova, A. L., Merkwirth, C., McDonnell, S. R. P., Zavareh, R. B., Fuchs, B. C., Kamal, A., & Jakobsen, J. S. (2021). Molecular characterization of type I IFN-induced cytotoxicity in bladder cancer cells reveals biomarkers of resistance. *Molecular Therapy - Oncolytics*, *23*, 547–559. https://doi.org/10.1016/j.omto.2021.11.006

Guo, D., Prins, R. M., Dang, J., Kuga, D., Iwanami, A., Soto, H., Lin, K. Y., Huang, T. T., Akhavan, D., Hock, M. B., Zhu, S., Kofman, A. A., Bensinger, S. J., Yong, W. H., Vinters, H. V, Horvath, S., Watson, A. D., Kuhn, J. G., Robins, H. I., … Mischel, P. S. (2009). EGFR signaling through an Akt-SREBP-1-dependent, rapamycin-resistant pathway sensitizes glioblastomas to antilipogenic therapy. *Science Signaling*, *2*(101), ra82. https://doi.org/10.1126/scisignal.2000446

Guo, X., Keyes, W. M., Papazoglu, C., Zuber, J., Li, W., Lowe, S. W., Vogel, H., & Mills, A. A. (2009). TAp63 induces senescence and suppresses tumorigenesis in vivo. *Nature Cell Biology*, *11*(12), 1451–1457. https://doi.org/10.1038/ncb1988

Hannun, Y. A., & Obeid, L. M. (2018). Sphingolipids and their metabolism in physiology and disease. *Nature Reviews. Molecular Cell Biology*, *19*(3), 175–191. https://doi.org/10.1038/nrm.2017.107

Hedegaard, J., Lamy, P., Nordentoft, I., Algaba, F., Høyer, S., Ulhøi, B. P., Vang, S., Reinert, T., Hermann, G. G., Mogensen, K., Thomsen, M. B. H., Nielsen, M. M., Marquez, M., Segersten, U., Aine, M., Höglund, M., Birkenkamp-Demtröder, K., Fristrup, N., Borre, M., … Dyrskjøt, L. (2016). Comprehensive Transcriptional Analysis of Early-Stage Urothelial Carcinoma. *Cancer Cell*, *30*(1), 27–42. https://doi.org/10.1016/j.ccell.2016.05.004

Ihrie, R. A., Marques, M. R., Nguyen, B. T., Horner, J. S., Papazoglu, C., Bronson, R. T., Mills, A. A., & Attardi, L. D. (2005). Perp Is a p63-Regulated Gene Essential for Epithelial Integrity. *Cell*, *120*(6), 843–856. https://doi.org/10.1016/j.cell.2005.01.008

Jakus, D., Šolić, I., Jurić, I., Borovac, J. A., & Šitum, M. (2023). The Impact of the Initial Clinical Presentation of Bladder Cancer on Histopathological and Morphological Tumor Characteristics. *Journal of Clinical Medicine*, *12*(13). https://doi.org/10.3390/jcm12134259

Jiang, S., & Redelman-Sidi, G. (2022). BCG in Bladder Cancer *Immunotherapy*. *Cancers*, *14*(13). https://doi.org/10.3390/cancers14133073

Jiang, Y., Jiang, Y.-Y., Xie, J.-J., Mayakonda, A., Hazawa, M., Chen, L., Xiao, J.-F., Li, C.-Q., Huang, M.-L., Ding, L.-W., Sun, Q.-Y., Xu, L., Kanojia, D., Jeitany, M., Deng, J.-W., Liao, L.-D., Soukiasian, H. J., Berman, B. P., Hao, J.-J., … Koeffler, H. P. (2018). Co-activation of super-enhancer-driven CCAT1 by TP63 and SOX2 promotes squamous cancer progression. *Nature Communications*, *9*(1), 3619. https://doi.org/10.1038/s41467-018-06081-9

Jiang, Y.-Y., Jiang, Y., Li, C.-Q., Zhang, Y., Dakle, P., Kaur, H., Deng,

J.-W., Lin, R. Y.-T., Han, L., Xie, J.-J., Yan, Y., Doan, N., Zheng, Y., Mayakonda, A., Hazawa, M., Xu, L., Li, Y., Aswad, L., Jeitany, M., … Koeffler, H. P. (2020). TP63, SOX2, and KLF5 Establish a Core Regulatory Circuitry That Controls Epigenetic and Transcription Patterns in Esophageal Squamous Cell Carcinoma Cell Lines. *Gastroenterology*, *159*(4), 1311-1327.e19. https://doi.org/10.1053/j.gastro.2020.06.050

Keyes, W. M., Pecoraro, M., Aranda, V., Vernersson-Lindahl, E., Li, W., Vogel, H., Guo, X., Garcia, E. L., Michurina, T. V, Enikolopov, G., Muthuswamy, S. K., & Mills, A. A. (2011). ΔNp63α is an oncogene that targets chromatin remodeler Lsh to drive skin stem cell proliferation and tumorigenesis. *Cell Stem Cell*, *8*(2), 164–176. https://doi.org/10.1016/j.stem.2010.12.009

Khalifa, J., Roumiguié, M., Pouessel, D., & Sargos, P. (2022). [Bladder-sparing trimodal therapy for muscle invasive bladder cancer]. *Cancer Radiotherapie : Journal de La Societe Francaise de Radiotherapie Oncologique*, *26*(6–7), 771–778. https://doi.org/10.1016/j.canrad.2022.06.009

Kim, L. H. C., & Patel, M. I. (2020). Transurethral resection of bladder tumour (TURBT). *Translational Andrology and Urology*, *9*(6), 3056–3072. https://doi.org/10.21037/tau.2019.09.38

Koga, F., Kawakami, S., Fujii, Y., Saito, K., Ohtsuka, Y., Iwai, A., Ando, N., Takizawa, T., Kageyama, Y., & Kihara, K. (2003). Impaired p63 expression associates with poor prognosis and uroplakin III expression in invasive urothelial carcinoma of the bladder. *Clinical Cancer Research : An Official Journal of the American Association for Cancer Research*, *9*(15), 5501–5507.

Kouwenhoven, E. N., van Heeringen, S. J., Tena, J. J., Oti, M., Dutilh, B. E., Alonso, M. E., de la Calle-Mustienes, E., Smeenk, L., Rinne, T., Parsaulian, L., Bolat, E., Jurgelenaite, R., Huynen, M. A., Hoischen, A., Veltman, J. A., Brunner, H. G., Roscioli, T., Oates, E., Wilson, M., … Zhou, H. (2010). Genome-wide profiling of p63 DNA-binding sites identifies an element that regulates gene expression during limb development in the 7q21 SHFM1 locus. *PLoS Genetics*, *6*(8), e1001065. https://doi.org/10.1371/journal.pgen.1001065

Lena, A. M., Rossi, V., Osterburg, S., Smirnov, A., Osterburg, C., Tuppi, M., Cappello, A., Amelio, I., Dötsch, V., De Felici, M., Klinger, F. G., Annicchiarico-Petruzzelli, M., Valensise, H., Melino, G., & Candi, E. (2021). The p63 C-terminus is essential for murine oocyte integrity. *Nature Communications*, *12*(1), 383. https://doi.org/10.1038/s41467-020-20669-0

Lena, A. M., Smirnov, A., Mancini, M., Montanaro, M., Ciccosanti, F., Foti, V., Nardacci, R., Fimia, G. M., Mavilio, M., Federici, M., Mauriello, A., Piacentini, M., Melino, G., & Candi, E. (2025). Deletion of p63 exon 13 in mice reveals C-terminal isoform–specific functions in epithelial development. *Proceedings of the National Academy of Sciences*, *122*(29). https://doi.org/10.1073/pnas.2503866122

Li, L.-Y., Yang, Q., Jiang, Y.-Y., Yang, W., Jiang, Y., Li, X., Hazawa, M., Zhou, B., Huang, G.-W., Xu, X.-E., Gery, S., Zhang, Y., Ding, L.-W., Ho, A. S., Zumsteg, Z. S., Wang, M.-R., Fullwood, M. J., Freedland, S. J., Meltzer, S. J., … Lin, D.-C. (2021). Interplay and cooperation between SREBF1 and master transcription factors regulate lipid metabolism and tumor-promoting pathways in squamous cancer. *Nature Communications*, *12*(1), 4362. https://doi.org/10.1038/s41467-021-24656-x

Li, W., Qian, J., Yang, H., Wu, J., Wang, Z., He, C., & Li, G. (2025). MGLL Promotes Pancreatic Cancer Progression and Invasion: Potential Therapeutic Inhibition by Melatonin. *Annals of Clinical and Laboratory Science*, *55*(1), 10–18.

Li, Y., Giovannini, S., Wang, T., Fang, J., Li, P., Shao, C., Wang, Y., TOR centre, Shi, Y., Candi, E., Melino, G., & Bernassola, F. (2023). p63: a crucial player in epithelial stemness regulation. *Oncogene*, *42*(46), 3371–3384. https://doi.org/10.1038/s41388-023-02859-4

Liu, F., Li, K., & Zhu, Q. (2025). Targeting Metabolic Reprogramming in Bladder Cancer Immunotherapy: A Precision Medicine Approach. *Biomedicines*, *13*(5). https://doi.org/10.3390/biomedicines13051145

Lopez-Beltran, A., Cookson, M. S., Guercio, B. J., & Cheng, L. (2024). Advances in diagnosis and treatment of bladder cancer. *BMJ (Clinical Research Ed.)*, *384*, e076743.

https://doi.org/10.1136/bmj-2023-076743

Mancini, M., Sergio, S., Cappello, A., Farkas, T., Bernassola, F., Scarponi, C., Albanesi, C., Melino, G., & Candi, E. (2023). Involvement of transcribed lncRNA uc.291 in hyperproliferative skin disorders. *Biology Direct*, *18*(1), 82. https://doi.org/10.1186/s13062-023-00435-0

Mardaryev, A. N., Gdula, M. R., Yarker, J. L., Emelianov, V. U., Poterlowicz, K., Sharov, A. A., Sharova, T. Y., Scarpa, J. A., Joffe, B., Solovei, I., Chambon, P., Botchkarev, V. A., & Fessing, M. Y. (2014). p63 and Brg1 control developmentally regulated higher-order chromatin remodelling at the epidermal differentiation complex locus in epidermal progenitor cells. *Development (Cambridge, England)*, *141*(1), 101–111. https://doi.org/10.1242/dev.103200

Massion, P. P., Taflan, P. M., Jamshedur Rahman, S. M., Yildiz, P., Shyr, Y., Edgerton, M. E., Westfall, M. D., Roberts, J. R., Pietenpol, J. A., Carbone, D. P., & Gonzalez, A. L. (2003). Significance of p63 amplification and overexpression in lung cancer development and prognosis. *Cancer Research*, *63*(21), 7113–7121.

McDade, S. S., Patel, D., Moran, M., Campbell, J., Fenwick, K., Kozarewa, I., Orr, N. J., Lord, C. J., Ashworth, A. A., & McCance, D. J. (2014). Genome-wide characterization reveals complex interplay between TP53 and TP63 in response to genotoxic stress. *Nucleic Acids Research*, *42*(10), 6270–6285. https://doi.org/10.1093/nar/gku299

McFerrin, C., Davaro, F., May, A., Raza, S., Siddiqui, S., & Hamilton, Z. (2020). Trends in utilization of neoadjuvant and adjuvant chemotherapy for muscle invasive bladder cancer. *Investigative and Clinical Urology*, *61*(6), 565–572. https://doi.org/10.4111/icu.20200132

Medici, D., Hay, E. D., & Olsen, B. R. (2008). Snail and Slug promote epithelial-mesenchymal transition through beta-catenin-T-cell factor-4-dependent expression of transforming growth factor-beta3. *Molecular Biology of the Cell*, *19*(11), 4875–4887. https://doi.org/10.1091/mbc.e08-05-0506

Mills, A. A., Zheng, B., Wang, X. J., Vogel, H., Roop, D. R., & Bradley, A. (1999). p63 is a p53 homologue required for limb and epidermal

morphogenesis. *Nature*, *398*(6729), 708–713. https://doi.org/10.1038/19531

Moses, M. A., George, A. L., Sakakibara, N., Mahmood, K., Ponnamperuma, R. M., King, K. E., & Weinberg, W. C. (2019). Molecular Mechanisms of p63-Mediated Squamous Cancer Pathogenesis. *International Journal of Molecular Sciences*, *20*(14). https://doi.org/10.3390/ijms20143590

Nadhan, R., & Dhanasekaran, D. N. (2021). Decoding the Oncogenic Signals from the Long Non-Coding RNAs. *Onco*, *1*(2), 176–206. https://doi.org/10.3390/onco1020014

Nemeth, K., Bayraktar, R., Ferracin, M., & Calin, G. A. (2024). Non-coding RNAs in disease: from mechanisms to therapeutics. *Nature Reviews. Genetics*, *25*(3), 211–232. https://doi.org/10.1038/s41576-023-00662-1

Nguyen, B.-C., Lefort, K., Mandinova, A., Antonini, D., Devgan, V., Della Gatta, G., Koster, M. I., Zhang, Z., Wang, J., Tommasi di Vignano, A., Kitajewski, J., Chiorino, G., Roop, D. R., Missero, C., & Dotto, G. P. (2006). Cross-regulation between Notch and p63 in keratinocyte commitment to differentiation. *Genes & Development*, *20*(8), 1028–1042. https://doi.org/10.1101/gad.1406006

Nomura, D. K., Long, J. Z., Niessen, S., Hoover, H. S., Ng, S.-W., & Cravatt, B. F. (2010). Monoacylglycerol lipase regulates a fatty acid network that promotes cancer pathogenesis. *Cell*, *140*(1), 49–61. https://doi.org/10.1016/j.cell.2009.11.027

Ohmoto, T., Nishitsuji, K., Yoshitani, N., Mizuguchi, M., Yanagisawa, Y., Saito, H., & Sakashita, N. (2015). K604, a specific acyl-CoA:cholesterol acyltransferase 1 inhibitor, suppresses proliferation of U251-MG glioblastoma cells. *Molecular Medicine Reports*, *12*(4), 6037–6042. https://doi.org/10.3892/mmr.2015.4200

Osterburg, C., & Dötsch, V. (2022). Structural diversity of p63 and p73 isoforms. *Cell Death and Differentiation*, *29*(5), 921–937. https://doi.org/10.1038/s41418-022-00975-4

Papadimitriou, M.-A., Avgeris, M., Levis, P. K., Tokas, T., Stravodimos, K., & Scorilas, A. (2019). ΔNp63 transcript loss in bladder cancer constitutes an independent molecular predictor of TaT1 patients post-

treatment relapse and progression. *Journal of Cancer Research and Clinical Oncology*, *145*(12), 3075–3087. https://doi.org/10.1007/s00432-019-03028-5

Parker, B. S., Rautela, J., & Hertzog, P. J. (2016). Antitumour actions of interferons: implications for cancer therapy. *Nature Reviews Cancer*, *16*(3), 131–144. https://doi.org/10.1038/nrc.2016.14

Pascual, G., Avgustinova, A., Mejetta, S., Martín, M., Castellanos, A., Attolini, C. S.-O., Berenguer, A., Prats, N., Toll, A., Hueto, J. A., Bescós, C., Di Croce, L., & Benitah, S. A. (2017). Targeting metastasis-initiating cells through the fatty acid receptor CD36. *Nature*, *541*(7635), 41–45. https://doi.org/10.1038/nature20791

Pecorari, R., Mancini, M., Smirnov, A., Corleone, G., Novelli, F., Lena, A. M., Franzese Canonico, M., Montanaro, M., Cappello, A., Sacconi, A., Misso, G., Falco, M., Tammaro, C., Ciccosanti, F., Piacentini, M., Scimeca, M., Caraglia, M., Blandino, G., Mauriello, A., … Candi, E. (2025a). p63 and ZNF148 cooperate to regulate head and neck squamous cell carcinoma. *Proceedings of the National Academy of Sciences of the United States of America*, *122*(28), e2500579122. https://doi.org/10.1073/pnas.2500579122

Pokorná, Z., Vysloužil, J., Hrabal, V., Vojtěšek, B., & Coates, P. J. (2021). The foggy world(s) of p63 isoform regulation in normal cells and cancer. *The Journal of Pathology*, *254*(4), 454–473. https://doi.org/10.1002/path.5656

Ponnaboina, D. M., Perumandal, S., & I, S. (2023). Correlation of HER2 With p53 and p63 in Urothelial Bladder Carcinoma. *Cureus*, *15*(4), e38018. https://doi.org/10.7759/cureus.38018

Profumo, V., Forte, B., Percio, S., Rotundo, F., Doldi, V., Ferrari, E., Fenderico, N., Dugo, M., Romagnoli, D., Benelli, M., Valdagni, R., Dolfini, D., Zaffaroni, N., & Gandellini, P. (2019). LEADeR role of miR-205 host gene as long noncoding RNA in prostate basal cell differentiation. *Nature Communications*, *10*(1), 307. https://doi.org/10.1038/s41467-018-08153-2

Qu, J., Yi, G., & Zhou, H. (2019). p63 cooperates with CTCF to modulate chromatin architecture in skin keratinocytes. *Epigenetics &*

Chromatin, *12*(1), 31. https://doi.org/10.1186/s13072-019-0280-y

Riege, K., Kretzmer, H., Sahm, A., McDade, S. S., Hoffmann, S., & Fischer, M. (2020). *Dissecting the DNA binding landscape and gene regulatory network of p63 and p53*. https://doi.org/10.1101/2020.06.11.145540

Rocco, J. W., Leong, C.-O., Kuperwasser, N., DeYoung, M. P., & Ellisen, L. W. (2006). p63 mediates survival in squamous cell carcinoma by suppression of p73-dependent apoptosis. *Cancer Cell*, *9*(1), 45–56. https://doi.org/10.1016/j.ccr.2005.12.013

Rodríguez-Enríquez, S., Hernández-Esquivel, L., Marín-Hernández, A., El Hafidi, M., Gallardo-Pérez, J. C., Hernández-Reséndiz, I., Rodríguez-Zavala, J. S., Pacheco-Velázquez, S. C., & Moreno-Sánchez, R. (2015). Mitochondrial free fatty acid β-oxidation supports oxidative phosphorylation and proliferation in cancer cells. *The International Journal of Biochemistry & Cell Biology*, *65*, 209–221. https://doi.org/10.1016/j.biocel.2015.06.010

Romano, R.-A., Smalley, K., Magraw, C., Serna, V. A., Kurita, T., Raghavan, S., & Sinha, S. (2012). ΔNp63 knockout mice reveal its indispensable role as a master regulator of epithelial development and differentiation. *Development (Cambridge, England)*, *139*(4), 772–782. https://doi.org/10.1242/dev.071191

Rouleau, M., Medawar, A., Hamon, L., Shivtiel, S., Wolchinsky, Z., Zhou, H., De Rosa, L., Candi, E., de la Forest Divonne, S., Mikkola, M. L., van Bokhoven, H., Missero, C., Melino, G., Pucéat, M., & Aberdam, D. (2011). TAp63 Is Important for Cardiac Differentiation of Embryonic Stem Cells and Heart Development. *Stem Cells*, *29*(11), 1672–1683. https://doi.org/10.1002/stem.723

Sayan, A. E., D'Angelo, B., Sayan, B. S., Tucci, P., Cimini, A., Cerù, M. P., Knight, R. A., & Melino, G. (2010). p73 and p63 regulate the expression of fibroblast growth factor receptor 3. *Biochemical and Biophysical Research Communications*, *394*(3), 824–828. https://doi.org/10.1016/j.bbrc.2010.03.084

Schmidl, C., Rendeiro, A. F., Sheffield, N. C., & Bock, C. (2015). ChIPmentation: fast, robust, low-input ChIP-seq for histones and transcription factors. *Nature Methods*, *12*(10), 963–965.

https://doi.org/10.1038/nmeth.3542

Steurer, S., Riemann, C., Büscheck, F., Luebke, A. M., Kluth, M., Hube-Magg, C., Hinsch, A., Höflmayer, D., Weidemann, S., Fraune, C., Möller, K., Menz, A., Fisch, M., Rink, M., Bernreuther, C., Lebok, P., Clauditz, T. S., Sauter, G., Uhlig, R.,… Marx, A. H. (2021). p63 expression in human tumors and normal tissues: a tissue microarray study on 10,200 tumors. *Biomarker Research*, *9*(1), 7. https://doi.org/10.1186/s40364-021-00260-5

Sun, H., Jiang, L., Luo, X., Jin, W., He, Q., An, J., Lui, K., Shi, J., Rong, R., Su, W., Lucchesi, C., Liu, Y., Sheikh, M. S., & Huang, Y. (2013). Potential tumor-suppressive role of monoglyceride lipase in human colorectal cancer. *Oncogene*, *32*(2), 234–241. https://doi.org/10.1038/onc.2012.34

Tan, Y., Pan, J., Deng, Z., Chen, T., Xia, J., Liu, Z., Zou, C., & Qin, B. (2023). Monoacylglycerol lipase regulates macrophage polarization and cancer progression in uveal melanoma and pan-cancer. *Frontiers in Immunology*, *14*. https://doi.org/10.3389/fimmu.2023.1161960

Tian, Y.-H., He, Y.-F., Tan, J.-S., Jiang, Y., Xu, Q., & Cheng, H.-L. (2022). The DeltaN p63 Promotes EMT and Metastasis in Bladder Cancer by the PTEN/AKT Signalling Pathway. *Evidence-Based Complementary and Alternative Medicine : ECAM*, *2022*, 9566055. https://doi.org/10.1155/2022/9566055

Tran, M. N., Choi, W., Wszolek, M. F., Navai, N., Lee, I.-L. C., Nitti, G., Wen, S., Flores, E. R., Siefker-Radtke, A., Czerniak, B., Dinney, C., Barton, M., & McConkey, D. J. (2013a). The p63 Protein Isoform ΔNp63α Inhibits Epithelial-Mesenchymal Transition in Human Bladder Cancer Cells. *Journal of Biological Chemistry*, *288*(5), 3275–3288. https://doi.org/10.1074/jbc.M112.408104

Tran, M. N., Choi, W., Wszolek, M. F., Navai, N., Lee, I.-L. C., Nitti, G., Wen, S., Flores, E. R., Siefker-Radtke, A., Czerniak, B., Dinney, C., Barton, M., & McConkey, D. J. (2013b). The p63 protein isoform ΔNp63α inhibits epithelial-mesenchymal transition in human bladder cancer cells: role of MIR-205. The Journal of Biological Chemistry, 288(5), 3275–3288. https://doi.org/10.1074/jbc.M112.408104

Truong, A. B., Kretz, M., Ridky, T. W., Kimmel, R., & Khavari, P. A.

(2006). p63 regulates proliferation and differentiation of developmentally mature keratinocytes. *Genes & Development*, *20*(22), 3185–3197. https://doi.org/10.1101/gad.1463206

Tucci, P., Agostini, M., Grespi, F., Markert, E. K., Terrinoni, A., Vousden, K. H., Muller, P. A. J., Dötsch, V., Kehrloesser, S., Sayan, B. S., Giaccone, G., Lowe, S. W., Takahashi, N., Vandenabeele, P., Knight, R. A., Levine, A. J., & Melino, G. (2012). Loss of p63 and its microRNA-205 target results in enhanced cell migration and metastasis in prostate cancer. *Proceedings of the National Academy of Sciences of the United States of America*, *109*(38), 15312–15317. https://doi.org/10.1073/pnas.1110977109

Urist, M. J., Di Como, C. J., Lu, M.-L., Charytonowicz, E., Verbel, D., Crum, C. P., Ince, T. A., McKeon, F. D., & Cordon-Cardo, C. (2002). Loss of p63 expression is associated with tumor progression in bladder cancer. *The American Journal of Pathology*, *161*(4), 1199–1206. https://doi.org/10.1016/S0002-9440(10)64396-9

Viticchiè, G., Agostini, M., Lena, A. M., Mancini, M., Zhou, H., Zolla, L., Dinsdale, D., Saintigny, G., Melino, G., & Candi, E. (2015). p63 supports aerobic respiration through hexokinase II. *Proceedings of the National Academy of Sciences*, *112*(37), 11577–11582. https://doi.org/10.1073/pnas.1508871112

Waheed, A., Gul, M. H., Wardak, A. B., Raja, H. A. A., & Hussaini, H. (2024). Nogapendekin alfa inbakicept-PMLN: first approval milestone for BCG-unresponsive noninvasive bladder cancer: editorial. *Annals of Medicine and Surgery (2012)*, *86*(11), 6386–6388. https://doi.org/10.1097/MS9.0000000000002591

Wang, C., He, H., & Fang, W. (2020). Oncogenic roles of the cholesterol metabolite 25-hydroxycholesterol in bladder cancer. *Oncology Letters*, *19*(6), 3671–3676. https://doi.org/10.3892/ol.2020.11475

Wang, X.-S., Zhang, Z., Wang, H.-C., Cai, J.-L., Xu, Q.-W., Li, M.-Q., Chen, Y.-C., Qian, X.-P., Lu, T.-J., Yu, L.-Z., Zhang, Y., Xin, D.- Q., Na, Y.-Q., & Chen, W.-F. (2006). Rapid identification of UCA1 as a very sensitive and specific unique marker for human bladder carcinoma. *Clinical Cancer Research : An Official Journal of the American Association for Cancer Research*, *12*(16), 4851–4858. https://doi.org/10.1158/1078-0432.CCR-06-0134

Wang, Y., Shi, J., Chai, K., Ying, X., & Zhou, B. P. (2013). The Role of Snail in EMT and Tumorigenesis. *Current Cancer Drug Targets*, *13*(9), 963–972. https://doi.org/10.2174/15680096113136660102

Woodstock, D. L., Sammons, M. A., & Fischer, M. (2021). p63 and p53: Collaborative Partners or Dueling Rivals? *Frontiers in Cell and Developmental Biology*, *9*, 701986. https://doi.org/10.3389/fcell.2021.701986

Wu, G., Osada, M., Guo, Z., Fomenkov, A., Begum, S., Zhao, M., Upadhyay, S., Xing, M., Wu, F., Moon, C., Westra, W. H., Koch, W. M., Mantovani, R., Califano, J. A., Ratovitski, E., Sidransky, D., & Trink, B. (2005). ΔNp63α Up-Regulates the *Hsp70* Gene in Human Cancer. *Cancer Research*, *65*(3), 758–766. https://doi.org/10.1158/0008-5472.758.65.3

Wu, G., Wang, F., Li, K., Li, S., Zhao, C., Fan, C., & Wang, J. (2019). Significance of TP53 mutation in bladder cancer disease progression and drug selection. *PeerJ*, *7*, e8261. https://doi.org/10.7717/peerj.8261

Xiong, K., Chen, S., Xu, H., Tu, S., Weng, H., Wang, Y., Li, M., Yu, J., Qian, K., Ju, L., Zhang, Y., Xiao, Y., Wang, X., & Wang, G. (2025). RNF112 Facilitates Ubiquitin-Mediated Degradation of c-Myc, Suppressing Proliferation, Migration and Lipid Synthesis in Bladder Cancer. *Advanced Science (Weinheim, Baden-Wurttemberg, Germany)*, *12*(20), e2408311. https://doi.org/10.1002/advs.202408311

Xu, T., Jiang, W., Fan, L., Gao, Q., & Li, G. (2017). Upregulation of long noncoding RNA Xist promotes proliferation of osteosarcoma by epigenetic silencing of P21. *Oncotarget*, *8*(60), 101406–101417. https://doi.org/10.18632/oncotarget.20738

Xu, Y., Zhong, J., Liu, Z., & Li, D. (2024). The role of monoglyceride lipase gene in promoting proliferation, metastasis, and free fatty acid accumulation in uveal melanoma cells. *Human Cell*, *37*(6), 1719–1733. https://doi.org/10.1007/s13577-024-01120-8

Yang, A., Schweitzer, R., Sun, D., Kaghad, M., Walker, N., Bronson, R. T., Tabin, C., Sharpe, A., Caput, D., Crum, C., & McKeon, F. (1999). p63 is essential for regenerative proliferation in limb, craniofacial and epithelial development. *Nature*, *398*(6729), 714–718.

https://doi.org/10.1038/19539

Yang, X., Zhang, D., Liu, S., Li, X., Hu, W., & Han, C. (2018). KLF4 suppresses the migration of hepatocellular carcinoma by transcriptionally upregulating monoglyceride lipase. *American Journal of Cancer Research*, *8*(6), 1019–1029.

Yang, Y.-Y., Hong, S.-Y., Xun, Y., Liu, C.-Q., Sun, J.-X., Xu, J.-Z., Xu, M.-Y., An, Y., He, D., Xia, Q.-D., & Wang, S.-G. (2022). Characterization of the Lipid Metabolism in Bladder Cancer to Guide Clinical Therapy. *Journal of Oncology*, *2022*, 1–12. https://doi.org/10.1155/2022/7679652

Zhang, J., Song, Y., Shi, Q., & Fu, L. (2021). Research progress on FASN and MGLL in the regulation of abnormal lipid metabolism and the relationship between tumor invasion and metastasis. *Frontiers of Medicine*, *15*(5), 649–656. https://doi.org/10.1007/s11684-021-0830-0

Zhao, W., Wang, H., Han, X., Ma, J., Zhou, Y., Chen, Z., Zhou, H., Xu, H., Sun, Z., Kong, B., & Fang, H. (2016). ΔNp63α attenuates tumor aggressiveness by suppressing miR-205/ZEB1-mediated epithelial-mesenchymal transition in cervical squamous cell carcinoma. *Tumour Biology : The Journal of the International Society for Oncodevelopmental Biology and Medicine*, *37*(8), 10621–10632. https://doi.org/10.1007/s13277-016-4921-5

Zhou, L., Du, K., Dai, Y., Zeng, Y., Luo, Y., Ren, M., Pan, W., Liu, Y., Zhang, L., Zhu, R., Feng, D., Tian, F., & Gu, C. (2024). Metabolic reprogramming based on RNA sequencing of gemcitabine-resistant cells reveals the FASN gene as a therapeutic for bladder cancer. *Journal of Translational Medicine*, *22*(1), 55. https://doi.org/10.1186/s12967-024-04867-8

Zhu, W., Zhao, Y., Zhou, J., Wang, X., Pan, Q., Zhang, N., Wang, L., Wang, M., Zhan, D., Liu, Z., He, X., Ma, D., Liu, S., & Wang, L. (2016). Monoacylglycerol lipase promotes progression of hepatocellular carcinoma via NF-κB-mediated epithelial-mesenchymal transition. *Journal of Hematology & Oncology*, *9*(1), 127. https://doi.org/10.1186/s13045-016-0361-3

Zlotta, A. R., Roumeguere, T., Kuk, C., Alkhateeb, S., Rorive, S., Lemy, A.,

van der Kwast, T. H., Fleshner, N. E., Jewett, M. A. S., Finelli, A., Schulman, C., Lotan, Y., Shariat, S. F., & Nortier, J. (2011). Select screening in a specific high-risk population of patients suggests a stage migration toward detection of non-muscle-invasive bladder cancer. *European Urology*, *59*(6), 1026–1031. https://doi.org/10.1016/j.eururo.2011.03.027

Mariacristina Franzese Canonico

Rome, Italy
e-mail address: mariacristina.franzesecanonico@students.uniroma2.eu
mariacristina.franzese@gmail.com
ORCID: 0009-0003-0096-0503

CURRENT POSITION **PhD candidate in biochemistry and molecular biology (end of PhD: April 2026)**

ACCADEMIC TITLE Master's degree in medical veterinary and pharmaceutical biotechnologies

SCIENTIFIC INTERESTS Study of p63 in bladder cancer progression
Study of p63 in skin cancer

RESEARCH EXPERIENCE

May 2023 – April 2026	**PhD student in Biochemistry and Molecular Biology** Department of Experimental Medicine at University of Rome Tor Vergata (Italy) Professor Eleonora Candi Dr Artem Smirnov, PhD
July 2021 – April 2023	**Research fellow in the "5000@genomi@VdA" project** CMP^3 VdA, Aosta (Italy) Professor Stefano Gustincich, Istituto Italiano di Tecnologia (IIT), Genova (Italy)
November 2020	**Qualification to practice the profession of biologist** University of Salento (Italy)
July 2019 – June 2020	**Experimental thesis in Biochemistry and Molecular Biology** Department of Food and Drug Sciences at University of Parma (Italy) Professor Barbara Campanini Thesis title: "Recombinant expression of the MGL-VIP fusion protein targeting human cancer cells".
Sep 2016 – Dec 2016	**Curricular internship in Biochemistry and Molecular Biology** Department of Biology, Ecology and Earth Sciences at University of Calabria (Italy) Professor Cesare Indiveri Professor Mariafrancesca Scalise

EDUCATION

July 2020	**Master's degree in Medical Veterinary and Pharmaceutical Biotechnologies**, with final mark 110/110 cum laude – University of Parma (Italy)
July 2017	**Bachelor's degree in Biological Science and Technologies**, with final mark 93/110 – University of Calabria (Italy)

OTHER EXPERIENCES

Research period abroad, at University of Bath, UK (from November 2025 to February 2026)
Tutor: Dr Maria Victoria Niklison Chirou
Research topic: study of lipid metabolism in bladder cancer

Delivered practical training to medical biotechnologies students as part of their curricular internship (June 2024)

EDITORIAL ACTIVITIES:

Reviewer of scientific papers from 2023. Journals: Discover Oncology - Frontiers in molecular biosciences – Gene, chromosomes and cancer – Biology Direct

LANGUAGES

Mother tongue: Italian
Other language: English (level: B2)

INFORMATIC SKILLS

- EIPASS certification:
  - Word, Excel and PowerPoint: advanced level
  - Access: intermediate level
- GraphPad
- Illustrator
- Bioinformatic tools (e.g. Genome Browser, cBioPortal for Cancer Genomics, DepMap)
- RNAseq and ChIPseq analyses

LABORATORY TECHNIQUES

- RNA purification, qPCR, RT-PCR
- ChIP-seq, RNA-seq and ATAC-seq
- Electrophoresis
- Plasmid DNA purification and molecular cloning
- Purification of proteins via affinity chromatography (IMAC), western Blot, SDS-PAGE
- Bacterial cultures, human cells cultures, transformation of bacteria, transfection of human cells and gene silencing
- Co-immunoprecipitation of proteins
- Immunofluorescence and immunohistochemistry
- Confocal microscopy (advanced systems: Leica Microsystem STELLARIS, Operetta)
- Preparation and analysis of samples by FACS
- Seahorse assays
- Proliferation and migration assay (Incucyte)
- Nanopore Sequencing, Illumina Sequencing, Sanger sequencing

CONGRESS PARTECIPATION:

ORAL PRESENTATIONS:

NGS approach used to uncover the transcriptional program of p63 in bladder cancer. *Novogene symposium – From sequencing to discovery, Rome, Italy, March 2026.*

Uncovering the transcriptional program of p63 in bladder cancer. *13th Tuscany Retreat on Cancer Research and Apoptosis, Tuscany, Italy, August 2025.*

POSTER PRESENTATION

Mariacristina Franzese Canonico, Maurizio Fanciulli, Alessandro Mauriello, Gerry Melino, Artem Smirnov, Eleonora Candi. **Exploring p63-targets involved in bladder cancer evolution.** *Impact of environmental pollution on complex diseases, Rome, Italy, October 2025.*

Mariacristina Franzese Canonico, Maurizio Fanciulli, Alessandro Mauriello, Gerry Melino, Artem Smirnov, Eleonora Candi. **Uncovering the transcriptional program of p63 in bladder cancer.** *13th Tuscany Retreat on Cancer Research and Apoptosis, Tuscany, Italy, August 2025.*

Mariacristina Franzese Canonico, Maurizio Fanciulli, Alessandro Mauriello, Gerry Melino, Artem Smirnov, Eleonora Candi. **The transcriptional factor p63 represses bladder cancer aggressiveness.** *The international p53/p63/p73 isoforms workshop in cancer and ageing, Dundee, UK, Giugno 2025.*

Mariacristina Franzese Canonico, Artem Smirnov, Maurizio Fanciulli, Alessandro Mauriello, Gerry Melino, Eleonora Candi. **The interplay between the transcriptional factor p63 and lipase MGLL affects bladder cancer progression.** *The 48th FEBS Congress, Milan, Italy, July 2024.*

PUBLISHED ABSTRACTS

R. Belardi, S. Velocci, M. Baldetti, M. Franzese Canonico, M. Pieri, L. Diluvio, M. Minieri, A. Smirnov, E. Campione, S. Bernardini, A. Terrinoni. **Identification of a novel AAGAB mutation in a family affected by punctate palmoplantar keratoderma: clinical, histological, and molecular characterization.** *57° Congresso Nazionale SIBioC, Firenze, Italia 2025.* ***Biochimica clinica, volume 49 · suppl. 2 · 2025, abstract nr EP057.***

Artem Smirnov, Mariacristina Franzese Canonico, Damiano Barnaba, Maurizio Fanciulli, Gerry Melino, Alessandro Mauriello, Eleonora Candi. **Epigenetic regulation of bladder cancer progression by the transcription factor p63.** *Epigenetics & Chromatin 2024 CSHL Meeting, Cold Spring Harbor, NY, USA.* ***Cold Spring Harbor Laboratory Meetings Abstracts Collection.***

Artem Smirnov, Mariacristina Franzese Canonico, Damiano Barnaba, Maurizio Fanciulli, Alessandro Mauriello, Gerry Melino, Eleonora Candi. **p63 represses metabolic pathways in aggressive bladder cancer.** *American Association for Cancer Research Annual Meeting 2025, Chicago, IL.* ***Cancer Res 2025;85(8_Suppl_1): Abstract nr 4040.***

Mariacristina Franzese Canonico, Artem Smirnov, Maurizio Fanciulli, Alessandro Mauriello, Gerry Melino, Eleonora Candi. **The interplay between the transcriptional factor p63 and lipase MGLL affects bladder cancer progression.** *The 48th FEBS Congress, Milano, Italia 2024.* ***Posters, FEBS Open Bio***, 14: 055. doi:10.1002/2211-5463.13837, P-26-055.

PUBLICATIONS

Spirito G, Trova S, Treves G, Farmanli K, Canonico MF, Fant A, Marangoni S, Furia F, Charrance D, Locci N, Gottardo S, Groppo F, Perseghin V, Toscano M, Bibbò E, Dontin SD, Cargnelutti C, Colliard M, Rosina A, Beoni AM, Bérard C, Coppe A, Serravalle P, Landuzzi F, Musacchia F, Amoroso A, Sanges R, Cavalli A, Vecchi M, Obino L, Gustincich S. **New insights into neurodevelopmental disorders by whole genome sequencing of 100 families from Italy.** NPJ Genom Med. 2026 Feb 2;11(1):11. doi: 10.1038/s41525-025-00547-8. PMID: 41629344

Pecorari R, Mancini M, Smirnov A, Corleone G, Novelli F, Lena AM, Franzese Canonico M, Montanaro M, Cappello A, Sacconi A, Misso G, Falco M, Tammaro C, Ciccosanti F, Piacentini M, Scimeca M, Caraglia M, Blandino G, Mauriello A, Fanciulli M, Melino G, Candi E. **p63 and ZNF148 cooperate to regulate head and neck squamous cell carcinoma.** Proc Natl Acad Sci U S A. 2025 Jul 15;122(28):e2500579122. doi: 10.1073/pnas.2500579122. Epub 2025 Jul 7.PMID: 40623191

Barnaba D*, Franzese Canonico M*, Helmer-Citterich M, Gandellini P, Melino G, Smirnov A, Candi E. **LEADR, a p63 target, dampens interferon signalling in bladder cancer.** Cell Death Discov. 2025 Jun 3;11(1):264. doi: 10.1038/s41420-025-02546-1. PMID: 40461454; PMCID: PMC12134291 ***contributed equally**

Riccardo Belardi, Laura Diluvio, Mariacristina Franzese Canonico, Silvia Velocci, Matteo Baldetti, Artem Smirnov, Eleonora Candi, Marilena Minieri, Elena Campione, Giusella Maria Francesca Moscato, Sergio Bernardini and Alessandro Terrinoni. **Toward Precision Medicine in PPPK1: Characterization of a Novel AAGAB Mutation and Phenotypic Extension.** Submitted.

AWARDS AND FELLOWSHIPS

EACR Travel Fellowship, *Sept 2025*, sustaining my research period at University of Bath.

Company of Biologists Travelling Fellowship, *Sept 2025*, sustaining my research period at University of Bath.

Second award best poster at "The international p53/p63/p73 isoforms workshop in cancer and ageing" Dundee, UK, June 2025.

PARTICIPATION IN FUNDED RESEARCH PROJECTS:

Research team member from 15/02/2025 to 15/03/2026
Project title: **AI-assisted identification of p63 targetome in skin cancer**
Principal Investigator: Dr Artem Smirnov, PhD
Funding: 9.800 € (RSA funding University of Rome Tor Vergata)
Role: cell culture, preparation samples for RNA seq, ChIP seq and validation by RT-qPCR.

MEMBERSHIPS:

Member, EACR (August 2025-April 2026)
Member, SIC (August 2025-present)
Member, SIB (November 2023-November 2024)

I authorize the processing of my personal data in my CV in accordance with the current laws.

Rome, 09/06/2026 Mariacristina Franzese Canonico

List of Publications

Spirito, G., Trova, S., Treves, G., Farmanli, K., **Canonico, M. F.**, Fant, A., Marangoni, S., Furia, F., Charrance, D., Locci, N., Gottardo, S., Groppo, F., Perseghin, V., Toscano, M., Bibbò, E., Dontin, S. D., Cargnelutti, C., Colliard, M., Rosina, A., Beoni AM, Bérard C, Coppe A, Serravalle P, Landuzzi F, Musacchia F, Amoroso A, Sanges R, Cavalli A, Vecchi M, Obino L, Gustincich S. (2026). **New insights into neurodevelopmental disorders by whole genome sequencing of 100 families from Italy.** Npj Genomic Medicine, 11(1), 11. https://doi.org/10.1038/s41525-025-00547-8

Pecorari, R., Mancini, M., Smirnov, A., Corleone, G., Novelli, F., Lena, A. M., **Franzese Canonico, M.**, Montanaro, M., Cappello, A., Sacconi, A., Misso, G., Falco, M., Tammaro, C., Ciccosanti, F., Piacentini, M., Scimeca, M., Caraglia, M., Blandino, G., Mauriello, A., Fanciulli M, Melino G, Candi E. (2025). **p63 and ZNF148 cooperate to regulate head and neck squamous cell carcinoma.** Proceedings of the National Academy of Sciences, 122(28). https://doi.org/10.1073/pnas.2500579122

Barnaba, D.*, **Franzese Canonico, M.***, Helmer-Citterich, M., Gandellini, P., Melino, G., Smirnov, A., & Candi, E. (2025). **LEADR, a p63 target, dampens interferon signalling in bladder cancer.** Cell Death Discovery, 11(1), 264. https://doi.org/10.1038/s41420-025-02546-1 ***co-primo autore**

Riccardo Belardi, Laura Diluvio, **Mariacristina Franzese Canonico**, Silvia Velocci, Matteo Baldetti, Artem Smirnov, Eleonora Candi, Marilena Minieri, Elena Campione, Giusella Maria Francesca Moscato, Sergio Bernardini and Alessandro Terrinoni. **Toward Precision Medicine in PPPK1: Characterization of a Novel AAGAB Mutation and Phenotypic Extension.** Submitted.

npj | genomic medicine

Article

Published in partnership with CEGMR, King Abdulaziz University

https://doi.org/10.1038/s41525-025-00547-8

New insights into neurodevelopmental disorders by whole genome sequencing of 100 families from Italy

Giovanni Spirito[1,2,13], Sara Trova[1,2,13], Gaia Treves[1,2], Khudayar Farmanli[2], Mariacristina Franzese Canonico[1], Agata Fant[1], Stefano Marangoni[3,4], Federica Furia[3,4], Debora Charrance[3,4], Nicola Locci[1], Sara Gottardo[1], Francesca Groppo[1], Vittoria Perseghin[1,2], Martina Toscano[1,2], Erika Bibbò[1], Serena Donetti Dontin[5], Cecilia Cargnelutti[5], Mélody Colliard[5], Alessandro Rosina[5], Anna Maria Beoni[6], Cristina Bérard[6], Alessandro Coppe[3,4], Paolo Serravalle[7], Fabio Landuzzi[3,4], Francesco Musacchia[1,2,8], Antonio Amoroso[1,2,9], Remo Sanges[8,10], Andrea Cavalli[3,4,11,12], Manuela Vecchi[1,2] ✉, Laure Obino[5] ✉ & Stefano Gustincich[1,2,8] ✉

Neurodevelopmental disorders (NDDs) have a strong but largely unexplained genetic basis. Moreover, the genetic architecture of these complex disorders in under-represented communities is poorly studied. We analyzed 110 probands from 100 families (for a total of 298 individuals), using whole genome sequencing (WGS) to identify genetic contributors to NDDs. This study is part of the '5000genomi@VdA' project characterizing Valle d'Aosta (Italy) genomic landscape in health and disease. Probands were stratified into three diagnostic categories: ASD (autism spectrum disorder without intellectual disability), ID (intellectual disability without ASD), and ASD-ID (autism spectrum disorder with comorbid intellectual disability). Following the ACMG guidelines, we identified 32 likely phenotype-causing variants in known NDD-associated genes in 26.4% of the probands. We observed a diagnostic yield gradient, lowest in ASD, intermediate in ASD-ID, and highest in ID. We also identified 42 variants of uncertain significance, 14 of which were located in genes not previously linked to NDDs but relevant to neurodevelopment, and may thus represent new NDD candidate genes. Furthermore, we used Evo 2, an evolutionary constraint-based model, to refine variant interpretation and identify VUS with pathogenic-like signatures. These findings highlight the utility of WGS in exploring the genetic heterogeneity within stratified NDD clinical groups.

Neurodevelopmental disorders (NDDs) encompass a diverse group of conditions that affect the development of the central nervous system (CNS), leading to a wide range of cognitive, motor, and behavioral impairments[1,2]. Among them, Autism Spectrum Disorder (ASD) and Intellectual Disability (ID) are the most prevalent, posing significant challenges for affected individuals, their families, and healthcare systems worldwide[3].

Although highly heritable[4–8], with estimates reaching 80-90% for ASD based on twin and sibling studies[9–11], the genetic basis of many NDDs remains incompletely understood[1,2], complicating diagnosis and treatment.

The global prevalence of ASD and ID is estimated to be approximately 1%[1]. In Italy, a nationwide study has recently reported a prevalence of 13.4 ASD cases per 1000 children aged 7-9 years[12], consistent across northern, central, and southern regions. However, a precise mapping of the prevalence of ASD/ID in each region of the country is still missing, and the genetic architecture of these complex disorders in the different areas and under-represented small populations is poorly studied.

Over the past decade, next-generation sequencing (NGS) has transformed the study of NDD genetics[13]. Whole Exome Sequencing (WES) is the most cost-effective method to identify Single-Nucleotide Variants (SNVs) and small insertions and deletions (Indels) of clinical relevance[14–17]. However, the majority of diagnosed individuals, approximately 70%, remain unsolved[18–20], partly because WES lacks the capability to reliably detect structural variants (SV), copy-number variants (CNV), and non-coding alterations. On the other hand, whole genome sequencing (WGS), though more expensive and computationally demanding, is a comprehensive technology able to identify a broader spectrum of genomic variants

A full list of affiliations appears at the end of the paper. ✉ e-mail: manuela.vecchi@iit.it; lobino@ausl.vda.it; stefano.gustincich@iit.it

that may be missed by conventional methods[13,21,22]. Indeed, recent studies indicate that WGS can enhance diagnostic yield by at least 8% compared to WES[18]. Importantly, multiple studies underline the importance of intronic SVs[23,24], CNVs[25–27], Mobile Elements Insertions (MEI)[28,29], and Tandem-Repeat Expansions[30,31] in NDDs.

Currently, high-throughput sequencing of large cohorts of NDD families has led to the discovery of thousands of genes involved in both the pathogenesis or susceptibility of these disorders[13,32–34]. Several NDD-related genes are strongly associated with specific phenotypes[32,35], while others are involved in broader neurodevelopmental processes and are not strictly tied to specific clinical presentations[34]. This latter group, although not immediately adopted for diagnostic utility, may offer insights into the fundamental mechanisms of neurodevelopment and the genetic basis of NDDs[36,37]. Overall, reconstructing the genetic architecture of NDDs is challenging due to their complexity and heterogeneity.

In this study, we sequenced and analyzed whole genomes of 110 probands affected by NDDs (100 families) and their parents (298 individuals in total). We stratified probands in three main clinical categories: ASD (autism spectrum disorder without intellectual disability, 40 cases), ID (intellectual disability without ASD, 27 cases), and ASD-ID (autism spectrum disorder with comorbid intellectual disability and/or severe language impairment, 43 cases). Our investigation examined SNVs, indels, SVs, CNVs, and MEIs, providing a comprehensive view of the genetic landscape underlying these heterogeneous conditions.

This investigation is part of the broader '5000genomi@VdA' research initiative, supported by the Valle d'Aosta regional government, which aims to elucidate the genomic architecture of this population. Our objective is to achieve deep molecular profiling of affected families subdivided into three main clinical groups by identifying both clinically relevant variants in established disease-causing genes and novel candidate genes implicated in NDDs, thereby contributing to the expansion of scientific knowledge and promoting the development of personalized therapeutic strategies for these complex disorders.

Results

The study cohort

We recruited 110 probands diagnosed with neurodevelopmental phenotypes comprising ASD, ID, or both (78 males and 32 females) from 100 families (298 individuals in total) (Table 1; Supplementary Data 1 and Table S1). Among the 110 probands, 90 were from simplex families, while 20 belonged to multiplex families (including one pair of dizygotic twins). For 10 probands, only one parent genome was available for sequencing, and for 2 probands, parental genomes could not be sequenced.

We stratified the probands into three main clinical groups: 40 with ASD alone, 27 with ID, and 43 with mixed ASD-ID (Supplementary Data 1 and Table S1). Although we did not observe significant differences in age at diagnosis between male and female probands, we found that probands in the ASD group were, on average, diagnosed at an older age than those in the other two groups (Supplementary Data 1 and Table S1). This likely reflects the predominance of high-functioning cases (67.5%, 27 out of 40) in the ASD group, who are typically diagnosed later in life. Among the ten multiplex families with two probands each, four pairs were assigned to different experimental groups due to marked differences in their clinical phenotypes. Of the remaining six pairs assigned to the same group, two exhibited mild but notable phenotypic differences (Supplementary Data 1 and Table S1). Our cohort did not include unaffected siblings. In 18 families, one or both parents, although not formally diagnosed with an NDD, exhibited behavioral or cognitive traits potentially relevant to the NDD spectrum (Supplementary Data 1 and Table S1). As expected, all parent-proband and sibling-sibling pairs displayed a kinship coefficient of approximately 0.25 (Supplementary Data 1 and Table S2). All mother-father pairs were confirmed to be unrelated (kinship coefficient around 0); with the exception of parents of family NED052, the father (NED052_F) and the mother (NED052_M), who showed a kinship coefficient of 0.03 (Supplementary Data 1 and Table S2), suggestive of potential fourth-degree relatedness. It is important to note that populations with a history of genetic drift, founder effects, or inbreeding, may exhibit slightly elevated background levels of relatedness, which could influence kinship estimates. We performed WGS on all 298 participants, achieving an average coverage of 38X. Detailed quality metrics for *fastq* files and alignment files are provided in Tables S3-S5.

Table 1 | Overview of individuals enrolled in the study

	Probands (n)	Parents (n)	Proband age at enrollment mean (± stdev)
Demographic composition			
Total	110	188	12.3 (±7)
Male	78 (71%)	91 (49%)	11.9 (±6.1)
Female	32 (29%)	97 (51%)	13.3 (±8.8)
Diagnostic group			
ASD	40 (36.5%)	na	16.5 (±6.8)
ID	27 (24.5%)	na	10.8 (±5.3)
ASD-ID	43 (39%)	na	9.5 (±6.2)

Overview of short variants and structural variants identified in the cohort

We performed short variant calling (SNVs and indels) across the cohort of 298 individuals (comprising probands and parents) using the NVIDIA Clara™ Parabricks® pipeline (version 3.8) (Fig. 1). This analysis identified a total of 26,176,852 unique variants (21,745,848 SNVs and 4,431,004 indels) (Fig. 2a,b). The variants were then prioritized according to a procedure outlined in the Methods section, with the objective of identifying a subset of potentially causative variants present in the probands that correlate with their phenotypes. After filtering, we identified a total of 3703 short variants across the 110 probands (Supplementary Data 1 and Table S6). Of these, 3334 were heterozygous and inherited from one parent, 148 were heterozygous but could not be definitively classified as de novo or inherited (due to the unavailability of one parental genome) and are thus referred to as "putative de novo" variants, 37 were confirmed as de novo, 33 were X-linked (found in hemizygosity in male probands and inherited maternally) and 5 were homozygous and inherited from both parents. We were unable to clearly determine the segregation pattern for approximately 2.3% of the identified variants (85 variants out of 3703).

Filtered variants were then manually curated to prioritize those that most likely contribute to the probands phenotype. The most significant findings are detailed below (Tables 2–4).

We performed SVs discovery on WGS data using both CNVkit[38], designed to detect copy number variants (CNVs), and a custom SV-discovery pipeline adapted from Vialle et al. [39,40] (see Methods). This pipeline integrates the results of multiple bioinformatics tools (Manta, Melt, CNVnator, BreakDancer, Lumpy), to identify deletions, duplications, insertions, and mobile element insertions (Fig. 1 and Methods). Using CNVkit, we initially identified 20,664 CNVs (8809 deletions and 11,855 duplications) (Fig. 2c), while our custom SV-discovery pipeline detected 94,082 SVs, including 50,576 deletions, 8105 duplications, 23,515 insertions and 11,886 MEI (Fig. 2d). Following variant calling, we applied frequency filters to retain only rare events (<1% in gnomAD, CCDG, and the 1000 Genomes Project) located within genes relevant to neurodevelopment. After filtering, 241 CNVs (95 deletions and 146 duplications) and 114 SVs (70 deletions, 44 duplications, 43 insertions, and 25 MEIs) were retained for downstream analyses (Supplementary Data 1 and Table S7-S10). We prioritized de novo and hemizygous SVs in genes with high dosage-sensitivity (pHaplo ≥ 0.55 for deletions; pTriplo ≥ 0.68 for duplications) or pLI (Probability of Loss-of-Function Intolerance) > 0.9 for insertions and MEIs. We also evaluated CNVs affecting genes with lower dosage-sensitivity scores. We believe that the inclusion of potentially suggestive variants from genes below the canonical dosage-sensitivity thresholds may provide

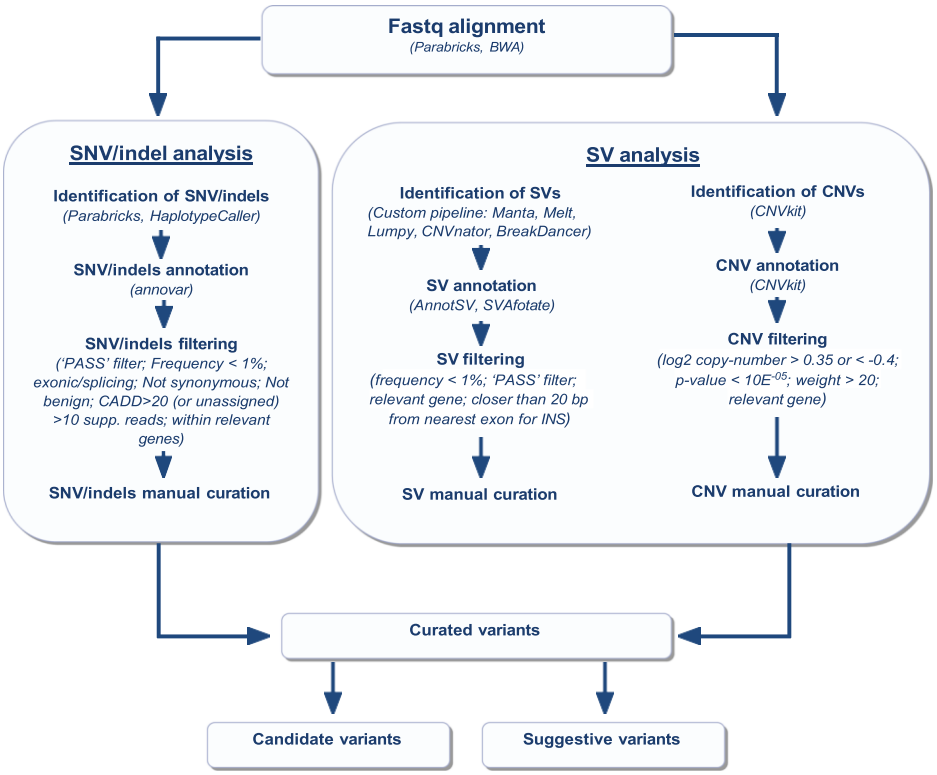

Fig. 1 | Overview of the methods used for variant discovery and prioritization. Created in microsoft powerpoint.

valuable insights into complex cases, particularly highlighting genes previously understudied in the context of NDD susceptibility. To assess the likelihood of false positives and evaluate the genotypes and segregation patterns, we manually inspected visualizations generated using CNVkit[38] and SamPlot[41] (Figure S1a-u). SVs present in more than ten families, and thus relatively frequent, were excluded as potential contributors to the phenotypes. The most relevant SVs are described in the following sections. Furthermore, to investigate the presence of two potentially gene-damaging variants in different alleles of the same recessive gene, we screened all families to identify probands who inherited at least one filtered SV and one filtered short variant on different alleles, each contributed by a different parent. We identified six probands with both a filtered CNV and a filtered short variant affecting the same gene. However, only one of these variant combinations was considered clinically relevant in the context of NDD phenotype, as discussed in the following sections (Table 3).

Identification of clinically relevant variants in the NDD cohort

Following variant filtering and manual curation, as detailed in the Methods section, we identified 74 variants of potential relevance in 53 probands (Supplementary Data 1 and Table S11). Among these, 60 were classified as "candidate variants" (47 SNVs/indels and 13 CNVs) located in known NDD-related genes, and 14 were classified as "suggestive variants" (4 SNVs/indels and 9 CNVs) found in genes not yet strongly associated with NDDs but implicated in neurodevelopmental processes based on literature or experimental evidence. Of the 60 candidate variants, 32 (found in 29 probands) were classified as pathogenic/likely pathogenic (P/LP) or warm/hot variants of uncertain significance (VUS), contributing to an overall diagnostic yield of 26.4%.

To further investigate the biological relevance of the affected genes, we examined the 44 unique genes harboring candidate and suggestive SNVs/indels using denovo-db ssc[42], a curated database compiling de novo variants from large ASD sequencing studies such as the Simons Simplex Collection (SSC). For each variant in our dataset, we assessed three levels of correspondence: (i) *Exact variant match*: whether the same variant was reported as de novo in an ASD proband; (ii) Gene-levelmatch: whether otherde novo variants in the same gene were reported in ASD individuals; (iii) Exon-level match: whether de novo variants from ASD cohorts occurred in the same exon, possibly indicating mutational hotspots or shared functional domains (Supplementary Data 1 and Table S12). Among the 44 genes, 33 were present in denovo-db; three of our variants occurred in the same exon as the de novo variants reported in denovo-db ssc, although no exact variant matches were found (Supplementary Data 1 and Table S12). Finally, 52 of the 74 variants (50 candidate and 2 suggestive) affected at least one SFARI gene (Supplementary Data 1 and Table S12).

Then, we further investigated both candidate and suggestive variants within each of the three clinical groups.

Analysis of genomic variants within the ASD group

We analyzed genomic variants from WGS data of probands in the ASD group (40 cases). These subjects were diagnosed with ASD, did not exhibit clinical phenotypes of ID, and displayed no or less pronounced language impairments compared to those within the ASD-ID group. Importantly, 27 out of 40 probands in this cohort present high-functioning ASD. The genetic architecture of high-functioning autism is complex and may involve both highly and moderately penetrant variants[17,43,44]. For the interpretation of manually curated genomic variants in WGS, we considered that even variants with moderate penetrance, as suggested by in-silico predictions, may be relevant to milder phenotypic presentations. Accordingly, we report several variants with likely moderate penetrance that may contribute to the ASD phenotype (Table 2).

Two rare variants were identified in *SRCAP* (OMIM * 611421) in proband NED016_P, who presented with mild cognitive deficits, behavioral disorder, modest phonological disorder, language and intersubjectivity difficulties, and selective eating habits. The family also reports that the older sister has epilepsy, migraine, psychiatric disorders, and eating disorders; the younger sister presents with a language disorder. Additionally, the father received a diagnosis of ADHD in adulthood. *SRCAP* encodes the core catalytic component of the multiprotein chromatin-remodeling *SRCAP* complex[45]. One variant is a rare splice-acceptor SNV inherited from the mother

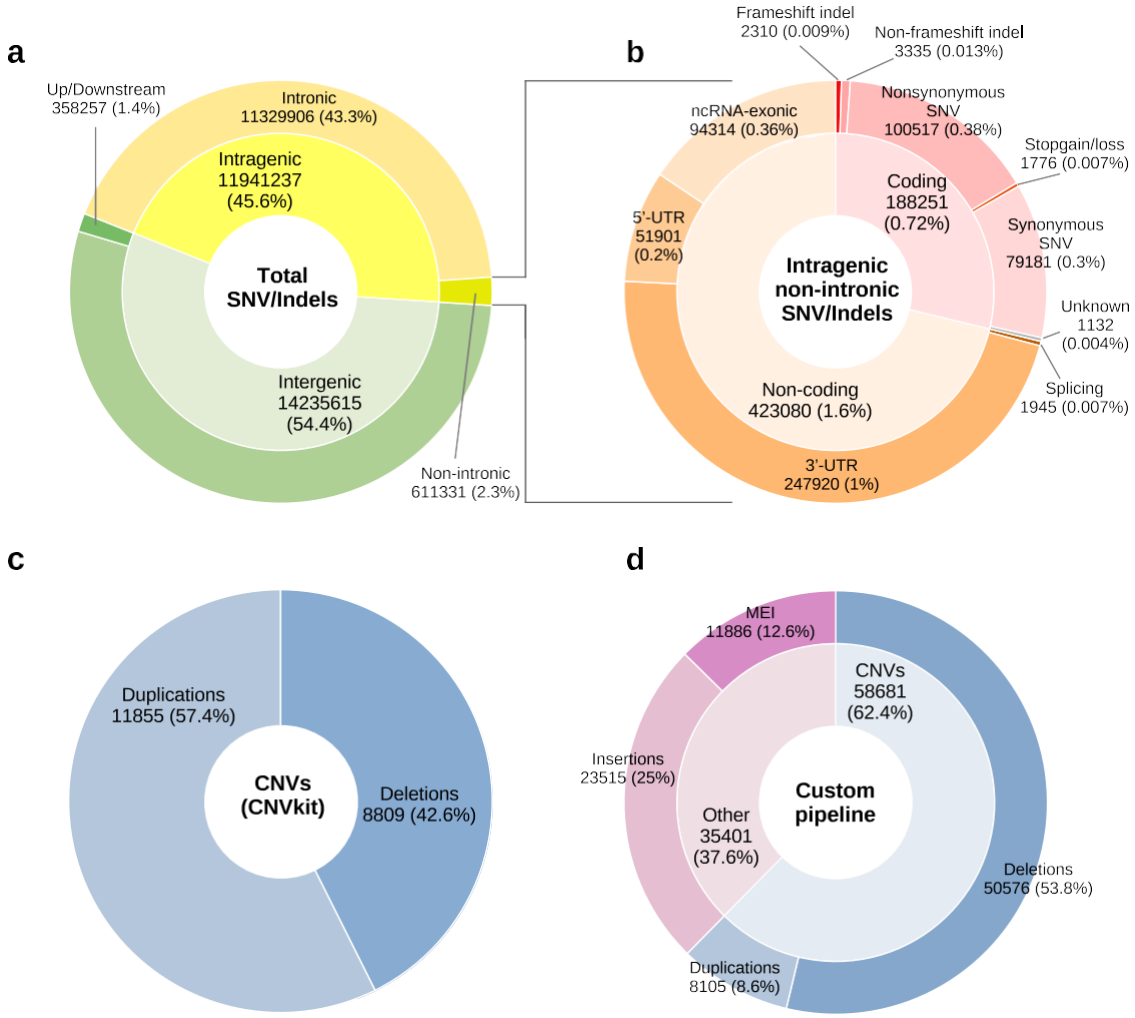

Fig. 2 | Summary of genomic variants identified in study participants; a, b percentages of short variants categories are related to the total number of short variants identified, short variants identified with Parabricks were filtered using the following criteria: marked as "PASS," supported by more than 10 reads, and containing a single genotype. a total genomic short variants, b intergenic non-intronic short variants; c percentages and counts of CNVs detected related to the total number of CNVs identified with CNVkit, CNVs were filtered for a $\log_2$ copy-number ratio > 0.35 or <−0.4, a p-value < 1×10^{-5}; d percentages and counts of SVs detected with our custom SV pipeline related to the total number of SVs identified, SVs identified using the custom pipeline were filtered to include only those marked as "PASS". Created with R (ggplot2 package).

(NM_006662.3:c.6729+9dup(p.?)), previously classified in ClinVar as a VUS, but predicted as likely pathogenic by in-silico tools (Franklin and AlphaMissense). The second one is an unannotated *missense* SNV inherited from the father (NM_006662.2:c.2494G > A(p.Val832Ile)), classified as a VUS, but located in a highly conserved region (GERP++_RS = 5.36) and predicted to be likely pathogenic (AlphaMissense). *SRCAP* is associated with the Floating-Harbor syndrome (OMIM #136140), a language and behavioral disorder, with an autosomal dominant inheritance, and LoF *SRCAP* variants have been found in ASD[46]. The presence of two different variants in the same gene within the family could potentially suggest variable expressivity among family members.

A particularly noteworthy case involved a de novo 660 kbp microdeletion at 1p36.32 (NC_000001.11:g.2538784_3205123del), affecting *MMEL*, *PRDM16*, and *ACTR2*, in a proband with ASD (NED007_P1, Table 5). While classical deletions within the 1p36.31/1p36.32 region are associated with a spectrum of neurodevelopmental conditions, including developmental delay, macrocephaly, brain anomalies, and dysmorphic features[47], these outcomes are mostly attributed to the deletion of the gene *NFIA*. However, this CNV does not overlap *NFIA*, and it occurs in a proband with high-functioning ASD and without any of the distinctive clinical features of the 1p36.31/1p36.32 deletion syndrome[48]. This microdeletion has also been recently found by Bacchelli et al. and overlaps *PRDM16*, whose Loss-of-function variants have mostly been associated with cardiomyopathy (OMIM#615373)[49]. However, several recent works suggest a crucial role of *PRDM16* in neurodevelopment[50–54].

A 275 Kbp microdeletion at 16q24.3 (NC_000016.10:g.89640587_89914558del) was inherited from the mother in the family NED082 and overlaps several genes, including dosage-sensitive *CDK10* (OMIM *603464), *CHMP1A* (OMIM *164010), and *FANCA* (OMIM *607139). 16q24.3 microdeletion syndrome is a recently identified disorder associated with variable developmental delay, distinctive facial features, seizures, and ASD. However, the clinical features of 16q24.3 microdeletion syndrome are primarily attributed to haploinsufficiency of the *ANKRD11* (OMIM *611192) gene, which is not involved in the deletion identified in the proband. Nevertheless, de novo variants in the *CHMP1A* gene have been associated with autism[32]. Furthermore, in silico pathogenicity prediction based on ACMG criteria classifies the variant as pathogenic. Notably, the mother, although lacking a formal ASD diagnosis, exhibits ASD-like behavioural traits. It would therefore be advisable to investigate the mother's phenotype to determine whether the identified variant could be pathogenic but characterized by incomplete penetrance or variable expressivity, a

https://doi.org/10.1038/s41525-025-00547-8

Table 2 | Candidate and suggestive variants in probands affected by ASD

Proband	Variant	Variant Type	Candidate gene	Segregation	ACMG Class	ClinVar	Sex
Candidate							
NED012_P	NM_017635.5:c.2347C > T(p.Arg783Ter)	Nonsense SNV	*KMT5B*	de novo	P (PVS1, PS6, PS2, PM2)	LP	M
NED092_P	NM_152296.5:c.1790G > A(p.Arg597His)	Missense SNV	*ATP1A3*	de novo	P (PM2, PS2, PP3, PM5, PP2, PP5); AM = LP	VUS	F
NED016_P	NM_006662.3:c.6729+9dup(p.?)	Splicing indel (ins)	*SRCAP*	Inherited (M)	LP (PVS1, PM2)	VUS	M
NED016_P	NM_006662.2:c.2494 G > A(p.Val832Ile)	Missense SNV	*SRCAP*	Inherited (F)	VUS warm (PM2, PP3); AM = LP	-	M
NED045_P	NC_000015.10:g.22579193_23125407del	Deletion	*NIPA1, NIPA2, TUBGCP5, CYFIP1 (pH = 0.1;0.4;0.2;0.84)*	Inherited (F)	P (1)	-	F
NED007_P1	NC_000001.11:g.2538784_3205123del	Deletion	*MMEL1, PRDM16, ACTR2 (pH = 0.37;0.99;0.96)*	de novo	LP (0.9)	-	M
NED082_P	NC_000016.10:g.89640587_89914558del	Deletion	*CDK10, CHMP1A, FANCA*	Inherited (M)	P (1)	-	M
NED060_P	NC_000015.10:g.31714997_32155815dup	Duplication	*CHRNA7, OTUD7A (pT = 0.58;0.3)*	Inherited (M)	VUS (0.3)	-	M
NED065_P	NM_013275.6:c.-145 + 32621_-60+2372del(p.?)	Deletion	*ANKRD11*	Inherited (M)	VUS (0.3)	-	M
NED086_P	NM_001374828.1:c.588_589insAGCAGCAGCAGCAGCAGCAGCAAC(p.Phe196_Gln197insSerSerSerSerSerSerSerAsn)	Indel (ins)	*ARID1B*	de novo	VUS (PM2, PM4, PM6, BP4)	VUS	M
NED092_P	NM_152641.4:c.3197C > T(p.Pro1066Leu)	Missense SNV	*ARID2*	de novo	VUS (PM2); AM = LP	-	F
NED055_P	NM_004187.5:c.3506C > G(p.Ser1169Trp)	Missense SNV	*KDM5C*	X-linked	VUS (PM2, PP2); AM = LB	-	M
NED020_P2	NM_001368397.1:c.3598 T > C(p.Ser1200Pro)	Missense SNV	*FRMPD4*	X-linked	VUS (PM2, BS2); AM = LB	-	M
NED049_P1	NM_000240.4:c.608G > A(p.Gly203Asp)	Missense SNV	*MAOA*	X-linked	VUS (PM2, PP3, BS2); AM = LP	-	M
NED024_P	NM_001128840.3:c.5935C > T(p.Arg1979Trp)	Missense SNV	*CACNA1D*	Putative de novo	VUS (PM2, BP4); AM = LB	VUS	M
NED024_P	NM_205861.3:c.356G > A(p.Arg119Gln)	Missense SNV	*DHDDS*	Putative de novo	VUS (PM2, PP2, BP1); AM = VUS	VUS	M
NED047_P	NM_006734.4:c.5807C > T(p.Thr1936Ile)	Missense SNV	*HIVEP2*	Putative de novo	VUS (PM2, PP2); AM = LP	-	F
NED082_P	NM_014516.4:c.1069G > A(p.Ala357Thr)	Missense SNV	*CNOT3*	Putative de novo	VUS (PM2, PP2, BP4); AM = LB	-	M
NED082_P	NM_005639.3:c.1228G > A(p.Val410Ile)	Missense SNV	*SYT1*	Inherited (M)	VUS (PM2, PP2, BP4); AM = LB	-	M
NED094_P	NM_001348716.2:c.3431G > A(p.Arg1144His)		*KDM6B*	Inherited (M)		VUS	M

Table 2 (continued) | Candidate and suggestive variants in probands affected by ASD

Proband	Variant	Variant Type	Candidate gene	Segregation	ACMG Class	ClinVar	Sex
		Missense SNV			VUS (PM2); AM = VUS		
Suggestive							
NED039_P	NM_002860.4:c.2054T > C(p.Ile685Thr)	Missense SNV	*ALDH18A1*	de novo	VUS (PM2, PP3); AM = LB	VUS	M
NED015_P	NM_001370165.1:c.1655A > C(p.Lys552Thr)	Missense SNV	*SYTL4*	X-linked	VUS (PM2, PP3); AM = LP	-	M
NED020_P1 NED020_P2	NC_000019.10:g.49288833_49294972del	Deletion	*SLC6A16*	Inherited (M)	VUS (0)	-	M

SNV/MNV/indels highlighted in bold are unannotated in public databases (GnomAD and ClinVar). Classification of variants according to the ACMG guidelines was performed with Franklin, except in the case of indels, where VarSome was used (*P* pathogenic, *LP* likely pathogenic, *VUS* variant of unknown significance, *LB* likely benign); pathogenicity score for CNVs was calculated with Franklin (<-0.99 = benign, <-0.9 = likely benign, >0.9 < 0.9 = VUS, >0.9 = likely pathogenic, >0.99 = pathogenic); *fs* frameshift, *no-fs* non-frameshift. *pH* pHaplo score, *pT* pTriplo score, *AM* Alpha Missense prediction, *S* SpliceAI score.
SNV single nucleotide variant, *MNV* multi nucleotide variant.

plausible scenario considering that the proband presents with a high-functioning form of autism, in which genetic contributions may sometimes be subclinical or manifest to a lesser extent in carriers.

We also detected a 6 Kbp deletion affecting the last five C-terminus exons of *SLC6A16* (NC_000019.10:g.49288833_49294972del) (OMIM *607972), which was found in both probands and their mother in family NED020. All three individuals share a similar ASD phenotype. While *SLC6A16* is not well characterized, it is expressed in the choroid plexus and may play a role in neuronal function[45], consistent with its predicted neurotransmitter symporter activities (Supplementary Data 1 and Table S13).

Lastly, we identified two noteworthy single-nucleotide variants of uncertain significance (VUS) in genes not previously implicated in ASD. The first is a de novo VUS in *ALDH18A1* (NM_002860.4:c.2054T > C(p.Ile685Thr)) (OMIM *138250) detected in proband NED039_P. Although this gene, a member of the aldehyde dehydrogenase family, has not been directly associated with ASD, alterations in aldehyde metabolism and toxicity have been implicated in ASD[55]. The second variant is a VUS in *SYTL4* (NM_001370165.1:c.1655A > C(p.Lys552Thr)), which encodes a synaptotagmin-like protein that interacts with Rab GTPases and plays a role in intracellular membrane trafficking[45]. Notably, a likely deleterious missense variant in *SYTL4* was recently reported in an individual with ASD[56].

In summary, our WGS analysis of 40 probands within the ASD group identified seven pathogenic variants in six probands and sixteen variants of uncertain significance in fifteen probands (Table 2). Among the latter, three occurred in genes not yet strongly associated with ASD. Notably, seven of the detected variants would likely have been missed by exome sequencing, including two CNVs that were not detected by CGH-array analysis. Importantly, 15% (6/40) of the probands in this ASD cohort displayed a disease-causing variant.

These findings highlight a diverse landscape of genetic variation, often of moderate or uncertain penetrance, that may underlie ASD phenotypes in the absence of intellectual disability.

Analysis of genomic variants within the ID group

We aimed to detect both high-penetrance variants in known ID-causing genes and variants within less characterized genes, which could influence the severity or specific characteristics of the observed phenotypes. Ten out of fourteen pathogenic or likely pathogenic variants were either de novo or X-linked (hemizygous in a male proband) (Table 3).

The remaining four variants were inherited. For instance, in proband NED026_P, we identified a pathogenic nonsense variant in *PHIP* (NM_017934.7:c.487C > T(p.Arg163Ter)) (OMIM * *612870*) inherited from the mother. *PHIP* haploinsufficiency is known to cause a syndrome characterized by behavioral disturbances, intellectual disability, obesity or overweight, and dysmorphic features (OMIM#617991). Consistently, this proband presented with a Sotos-like phenotype, including mild ID, ADHD, and oppositional defiant disorder (ODD), mirroring the clinical features observed in his mother (Supplementary Data 1 and Table S1).

In proband NED034_P, we found a 1.8 Mbp 15q13.2-q13.3 deletion inherited from the mother (NC_000015.10:g.30581193_32433579del) (Table 3). Heterozygous 15q13.3 microdeletions are associated with a wide range of neurodevelopmental conditions, with approximately 75% of these deletions inherited in an autosomal dominant manner. Notably, both the proband's mother and sister (not enrolled in the study) exhibit a pathological EEG, which could suggest that this CNV contributes to the proband's phenotype.

In proband NED081_P, we found a combination of two likely pathogenic variants in the *TRAPPC9* (OMIM*611966) gene, one inherited from each parent (NM_001160372.4:c.1439_1440del(p.Ser480CysfsTer71), NM_001160372.4:c.1135-8243_1768+2574del(p.?)). Biallelic deleterious variants in *TRAPPC9* cause a recently described condition associated with non-syndromic intellectual disability and microcephaly (OMIM#613192)[35] observed only in a limited number of cases to date (n = 48 as of 2020), and our case contributes additional allelic and phenotypic information[57]. Notably, one variant is a CNV and the other is an indel, making whole

https://doi.org/10.1038/s41525-025-00547-8

Table 3 | Candidate and suggestive variants in probands affected by ID

Proband		Variant type	Candiate genes	Segregation	ACMG class	ClinVar	Sex
Candidate							
NED003_P	NM_031263.4:c.1326_1343del(p.Asp442_Gln448delinsGlu)	Indel (del)	*HNRNPK*	de novo	LP (PM1, PM2, PM4)	-	M
NED028_P	NM_001830.4:c.995T > C(p.Leu332Pro)	Missense SNV	*CLCN4*	de novo	LP (PP2, PP3, PM2, PS2); AM = LP	-	M
NED038_P	NM_182641.4:c.2597_2600del(p.Lys866ArgfsTer16)	Indel (del, fs)	*BPTF*	de novo	P (PVS1, PS2, PM2)	-	M
NED044_P	NM_018896.5:c.1174G > A(p.Val392Met)	Missense SNV	*CACNA1G*	de novo	VUS (PM2, PP2, PP3); AM = LP	-	M
NED088_P	NM_002971.6:c.1084G > T(p.Glu362Ter)	Nonsense SNV	*SATB1*	de novo	P (PVS1, PS2, PM2)	-	M
NED073_P	NM_013275.6:c.1381_1384del(p.Glu461GlnfsTer48)	Indel (del, fs)	*ANKRD11*	de novo	P (PVS1, PP5, PM2)	LP/P	F
NED025_P	NC_000017.11:g.16751634_20572953dup	Duplication	*RAI1* (pT = 0.38)	de novo	P (1)	-	M
NED083_P	NC_000001.11:g.146169841_148577763del	Deletion	*CHD1L*, *BLC9*, *GJA8* (pH = 0.04, -, 0.2)	de novo	P (1)	-	M
NED083_P	NM_000531.6:c.264A > T(p.Lys88Asn)	Missense SNV	*OTC*	X-linked	LP (PM1, PM2, PP2, PS1, PP3); AM = LP	LP/P	M
NED026_P	NM_017934.7:c.487C > T(p.Arg163Ter)	Nonsense SNV	*PHIP*	Inherited (M)	P (PM2, PVS1, PS4)	-	M
NED034_P	NC_000015.10:g.30581193_32433579del	Deletion	FAN1, KLF13, CHRNA7 (pH = 0.5, 0.24, 0.26)	Inherited (M)	P (1)	-	M
NED036_P	NM_153252.5:c.3601A > G(p.Arg1201Gly)	Missense SNV	*BRWD3*	X-linked	LP (PM2, PP2, PP3, PM6); AM = LP	-	M
NED081_P	NM_001160372.4:c.1439_1440del(p.Ser480CysfsTer71)	Indel (del, fs)	*TRAPPC9*	Inherited (F)	LP (PVS1, PM2)	-	M
NED081_P	NM_001160372.4:c.1135-8243_1768+2574del(p.?)	Deletion	*TRAPPC9*	Inherited (M)	LP (0.9)	-	M
NED073_P	NC_000015.10:g.20019885_23284457dup	Duplication	*NIPA1*, *NIPA2*, *TUBGCP5*, *CYFIP1* (pT = 0.5, 0.4, 0.2, 0.84)	Inherited (F)	VUS (−0.21)	-	F
NED052_P1	NM_001330078.2:c.253C > T(p.Arg85Cys)	Missense SNV	*NRXN1*	Inherited (M/P)	VUS (BP1,PM2); AM = LB	VUS	M
NED052_P1	NM_153252.5:c.4945A > G(p.Arg1649Gly)	Missense SNV	*BRWD3*	X-linked	VUS (PM2); AM = LB	-	M
NED003_P	NM_001008537.3:c.2720A > C(p.Glu907Ala)	Missense SNV	*NEXMIF*	X-linked	VUS (PM2,BP4); AM = LB	VUS	M
Suggestive							
NED003_P	NM_017514.5:c.4703C > G(p.Thr1568Arg)	Missense SNV	*PLXNA3*	X-linked	VUS (PM2); AM = LB	-	M

SNV/MNV/indels highlighted in bold are unannotated in public databases (GnomAD and ClinVar). Classification of variants according to the ACMG guidelines was performed with Franklin, except in the case of indels, where VarSome was used (*P* pathogenic, *LP* likely pathogenic, *VUS* variant of unknown significance, *LB* likely benign); pathogenicity score for CNVs was calculated with Franklin (<−0.99 = benign, <−0.9 = likely benign, >0.9 < 0.9 = VUS, >0.9 = likely pathogenic, >0.99 = pathogenic); *fs* frameshift, *no-fs* non-frameshift. *pH* pHaplo score, *pT* pTriplo score, *AM* Alpha Missense prediction, *S* SpliceAI score.
SNV single nucleotide variant, *MNV* multi nucleotide variant.

https://doi.org/10.1038/s41525-025-00547-8

Table 4 | Candidate and suggestive variants in probands affected by ASD-ID

Proband		Variant type	Candidate gene	Segregation	ACMG class	ClinVar	Sex
Candidate							
NED005_P	NM_001134407.3:c.1123-1G > A(p.?)	Splicing SNV	*GRIN2A*	de novo	P (PVS1, PP5, PM2); S = 0.99 (splice acceptor)	P	M
NED063_P	NM_001348323.3:c.2359_2360insA(p.Pro787HisfsTer9)	Indel (ins)	*TRIP12*	de novo	P (PVS1, PS2, PM2)	-	M
NED031_P	NM_001348323.3:c.1483C > T(p.Gln495Ter)	Nonsense SNV	*TRIP12*	de novo	P (PVS1, PS2, PM2)	-	M
NED078_P	NM_001374828.1:c.625C > T(p.Gln209Ter)	Nonsense SNV	*ARID1B*	de novo	P (PVS1, PS2, PM2)	-	M
NED018_P	NM_001190274.2:c.2681C > T(p.Thr894Ile)	Missense SNV	*FBXO11*	de novo	LP (PS2, PM2, PM6, PP2, PP3); AM = LP	-	M
NED101_P	NM_005629.4:c.1006_1008del(p.Asn336del)	Indel (del)	*SLC6A8*	de novo	P (PS2, PP5, PP3, PM2)	P	M
NED077_P	NM_014225.6:c.1375C > T(p.Arg459Cys)	Missense SNV	*PPP2R1A*	de novo	LP (PS2, PM2, PP2); AM = LP	-	M
NED001_P	NC_000022.11:g.18751100_21330400del	Deletion	*TBX1*, *COMT*, *DGCR8*, *HIRA*, *CRKL* (pH = 0.8;0.27;0.8;0.9;0.7)	de novo	P (1)	-	F
NED080_P	NM_013450.4:c.349C > T(p.Arg117Ter)	Nonsense SNV	*BAZ2B*	Inherited (M)	LP (PVS1, PM2)	-	M
NED067_P	NM_001848.3:c.1138G > A(p.Gly380Arg)	Missense SNV	*COL6A1*	de novo	LP (PM2, PS2, PP3, PP5); AM = LP	LP	M
NED029_P	NC_000007.14:g.152335080_153117170dup	Duplication	*KMT2C*	Inherited (M)	VUS (0.3)	-	M
NED075_P1	NC_000015.10:g.20000921_23357453dup	Duplication	*NIPA1*, *NIPA2*, *TUBGCP5*, *CYFIP1* (pT = 0.53;0.4;0.39;0.88)	Inherited (M)	VUS (-0.62)	-	M
NED080_P	NM_004380.3:c.2558T > G(p.Leu853Arg)	Missense SNV	*CREBBP*	Inherited (M)	VUS (PM2, PP2); AM = LB	-	M
NED080_P	NM_018896.5:c.205C > T(p.Arg69Cys)	Missense SNV	*CACNA1G*	Inherited (M)	VUS (PM2, PP2); AM = VUS	-	M
NED080_P	NM_006245.4:c.1735G > A(p.Val579Met)	Missense SNV	*PPP2R5D*	Inherited (M)	VUS (PM2, PP2, BP4); AM = LP	-	M
NED037_P1	NM_004187.5:c.3561C > G(p.Ile1187Met)	Missense SNV	*KDM5C*	X-linked	VUS (PM2, PM6, PP2); AM = LB	-	M
NED018_P	NM_001543.5:c.2284 G > A(p.Glu762Lys)	Missense SNV	*NDST1*	Inherited (M)	VUS (PM2, PM6); AM = LB	-	M
NED018_P	NM_001543.5:c.2558 G > A(p.Arg853Gln)	Missense SNV	*NDST1*	Inherited (F)	VUS (PM2); AM = LB	VUS	M
NED067_P	NM_020987.5:c.10042A > G(p.Lys3348Glu)	Missense SNV	*ANK3*	Inherited (F)	VUS (PM2, BP4); AM = LB	VUS	F
NED067_P	NM_020987.5:c.11090C > G(p.Ser3697Cys)	Missense SNV	*ANK3*	Inherited (M)	VUS (PM2, BP4); AM = LB	VUS	F
NED023_P	NM_004615.4:c.149T > C(p.Leu50Pro)	Missense SNV	*TSPAN7*	X-linked	VUS warm (PM2, PP3); AM = LP	-	M
NED040_P	NM_001256789.3:c.3609G > C(p.Gln1203His)	Missense SNV	*CACNA1F*	X-linked	VUS (PM2, PP3); AM = LP	-	M
Suggestive							
NED007_P2	NM_001388419.1:c.5327C > T(p.Pro1776Leu)	Missense SNV	*KALRN*	de novo	LP (PM2, PS2, PP3, PP2); AM = LP	-	F
NED059_P	NM_002533.4:c.2182G > T(p.Asp728Tyr)	Missense SNV	*NVL*	de novo	LP (PM2, PP3); AM = LP	-	F
NED029_P	NC_000005.10:g.151891111_151989703dup	Duplication	*GLRA1*	Inherited (F)	VUS (0.3)	-	M
NED029_P	NM_002517.4:c.522+1355_688+1210del(p.?)	Duplication	*NPAS1*	Inherited (F)	VUS (0.3)	-	M
NED029_P	NM_015480.3:c.160+1729_160+5410del(p.?)	Deletion	*NECTIN3*	Inherited (F)	VUS (−0.6)	-	M
NED074_P	NC_000022.11:g.21956425_22222810dup	Duplication	*TOP3B*	Inherited (F)	VUS (−0.35)	-	F
NED074_P	NC_000017.11:g.19340574_20369135del	Deletion	*AKAP10*	Inherited (F)	VUS (0.75)	-	F
NED041_P	NC_000002.12:g.130702734_131311349del	Deletion	*ARHGEF4*	Inherited (M)	VUS (0.65)	-	M
NED051a_P	NC_000009.12:g.152201_384463dup	Duplication	*CBWD1*, *DOCK8* (pT = 0.2; 0.1)	Inherited (F)	VUS (−0.06)	-	M

SNV/MNV/indels highlighted in bold are unannotated in public databases (GnomAD and ClinVar). Classification of variants according to the ACMG guidelines was performed with Franklin, except in the case of indels, where VarSome was used (*P* pathogenic, *LP* likely pathogenic, *VUS* variant of unknown significance, *LB* likely benign); pathogenicity score for CNVs was calculated with Franklin (<−0.99 = benign, <−0.9 = likely benign, >0.9 < 0.9 = VUS, >0.9 = likely pathogenic, >0.99 = pathogenic); *fs* frameshift, *no-fs* non-frameshift. *pH* pHaplo score, *pT* pTriplo score, *AM* Alpha Missense prediction, *S* SpliceAI score.
SNV single nucleotide variant, *MNV* multi nucleotide variant.

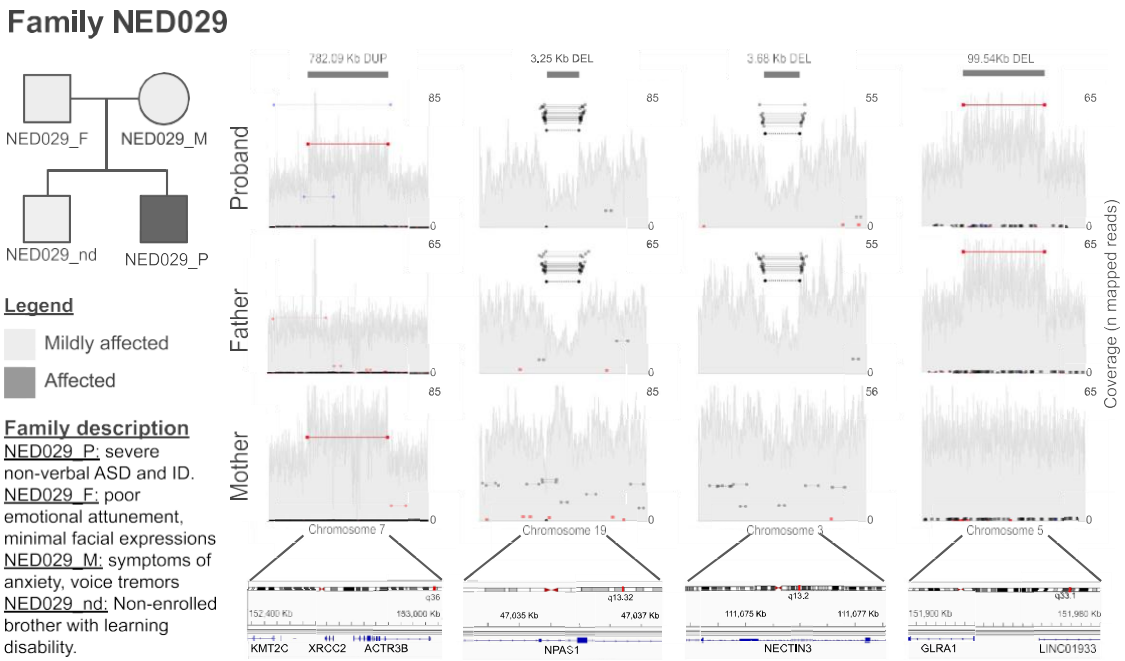

Fig. 3 | Family structure and CNVs identified in the members of family NED029. Created with Samplot and Microsoft Powerpoint.

genome sequencing the only approach capable of simultaneously identifying both variants within a single analysis.

Overall, upon manual evaluation of the filtered short variants and SVs, we identified eighteen "candidate" and one "suggestive" variants in thirteen out of twenty-seven probands affected by ID (Table 3). Importantly, WGS allowed us to identify disease-causing variants (deleterious "candidate variants") in approximately 44.4% (12/27) of the probands in this ID cohort.

Analysis of genomic variants within the ASD-ID group

The cohort included 43 probands with mid- to low-functioning ASD, typically presenting a complex phenotype involving ID or language impairment (Supplementary Data 1 and Table S1). Among these, several cases illustrated the contribution of inherited variation to complex phenotypes, highlighting the importance of family-based analyses.

Family NED029 exemplifies the value of trio-based WGS. The proband, diagnosed with ASD and ID (Supplementary Data 1 and Table S1), inherited multiple CNVs from both parents (each exhibiting NDD-like traits):: (i) a 780 kbp maternally inherited duplication overlapping the first two exons of *KMT2C* (OMIM*606833) (NC_000007.14:g.152335080_153117170dup) and the whole gene of *XRCC2* (OMIM*600375) and *ACTR3B*; (ii) a 100 kbp paternally inherited duplication of exons 1 and 2 of *GLRA1* (OMIM*138491) (NC_000005.10:g.151891111_151989703dup); (iii) a 3 Kbp paternal deletion overlapping the exon 5 of *NPAS1* (OMIM*603346) (NM_002517.4:c.522+1355_688+1210del(p.?)); and (iv) a 3.7 kbp paternal deletion affecting exon 2 of the transcript ENST00000481766.1 of *NECTIN3* (OMIM*607147) (NM_015480.3:c.160+1729_160+5410del(p.?)). Although neither parent nor the proband's brother (who was not enrolled in the study) has a formal NDD diagnosis, all present notable behavioural traits. Loss-Of-Function (LoF) variants in *KMT2C* have been associated with autosomal dominant Kleefestra syndrome type-2 (OMIM#617768)[58], and a partial copy-number gain of this gene has been reported in a child with ASD, poor growth, speech, and developmental delay[59]. *GLRA1* encodes a glycine receptor subunit involved in inhibitory neurotransmission; deleterious variants cause hyperekplexia[60]; and mutant mice exhibit exaggerated startle responses[61] (Supplementary Data 1 and Table S13). *NPAS1* encodes for a transcription factor with a potential role in neurodevelopment[62] (Supplementary Data 1 and Table S13), and *NECTIN3* functions in neuronal adhesion, with knockout models showing altered behavior[63] (Supplementary Data 1 and Table S13). This complex variant landscape may explain the proband's phenotype and offers insights into the genetic liability in the parents. (Fig. 3).

In NED080_P, the mother shares ASD traits, ID, and severe obesity with the proband. We identified a maternally inherited likely pathogenic variant in *BAZ2B* (OMIM*605683) gene (NM_013450.4:c.349C > T(p.Arg117Ter)), a recently proposed ASD/ID gene[64], which is also downregulated in adipose tissue of individuals with obesity[65].

We also identified a likely pathogenic de novo SNV in *COL6A1* (OMIM*120220) (NM_001848.3:c.1138G > A(p.Gly380Arg)) in proband NED067_P. Although this gene has not been previously implicated in ASD, *COL6A1* knockout mice display marked behavioral abnormalities[66]. Furthermore, the motor impairment component characterizing the probands phenotype is consistent with disorders associated with this gene, including Bethlem myopathy (OMIM#158810) and Ullrich congenital muscular dystrophy (OMIM#254090). In addition, we detected two VUS in *KALRN* (NM_001388419.1:c.5327C > T(p.Pro1776Leu)) and *NVL* (NM_002533.4:c.2182G > T(p.Asp728Tyr)), both of which are involved in neurodevelopmental regulation[67,68] (Supplementary Data 1 and Table S13).

Overall, in the ASD-ID group, we identified 22 "candidate" causative variants in eleven probands (approximately 25.6%, 11/43) and nine "suggestive"" variants in six probands (Table 4).

WGS reveals a higher diagnostic yield in the ID group

To evaluate whether the three diagnostic groups differed in their predicted diagnostic yield, we performed a chi-squared test, which revealed a statistically significant difference between groups ($\chi^2 = 6.002$, df = 2, $p = 0.049$), suggesting that the likelihood of identifying deleterious 'candidate' variants is not evenly distributed across clinical subtypes. Notably, individuals with isolated ID showed a higher diagnostic rate compared to those with ASD or combined ASD-ID phenotypes.

We also performed pairwise comparisons between groups using Fisher's exact test. The difference between the ID and ASD-ID groups did not reach statistical significance ($p = 0.1223$), although there was a trend toward a higher diagnostic rate in the ID group. This lack of statistical significance may be attributable to the limited cohort size. No significant difference was found between the ASD and ASD-ID groups ($p = 0.4318$). In contrast, individuals with ID showed a significantly higher diagnostic yield compared to those with ASD-only ($p = 0.0263$).

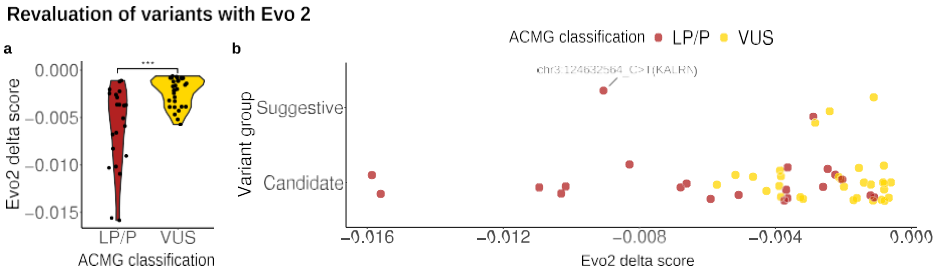

Fig. 4 | Re-evaluation of variants using Evo 2. a Distribution of Evo 2 delta scores for variants previously classified as pathogenic/likely pathogenic (P/LP) or of uncertain significance (VUS) according to ACMG guidelines (***p-value < 0.001); b Distribution of Evo 2 delta scores for variants classified in this study as candidate or suggestive. Created with R (ggplot2 package).

These results suggest that individuals with isolated ID may have a higher likelihood of receiving a molecular diagnosis through whole genome sequencing than those with ASD or combined phenotypes ASD-ID, although the limited sample size warrants cautious interpretation.

Evo 2 analysis highlights potentially deleterious VUS variants

We applied the Evo 2[69] algorithm to score all short variants (SNVs and Indels) described in the previous sections (Tables 2-4; Supplementary Data 1 and Table S14). In parallel, we analyzed 17,054 ClinVar variants to compare the distribution of Evo 2 scores for our variants with those of variants having well-defined clinical interpretations in the same genes (Supplementary Data 1 and Table S15; Supplementary File 1 and Fig. S1).

Pathogenic or likely pathogenic (P/LP) variants in NDD probands showed significantly lower Evo 2 delta scores (p-value < 0.001) than VUS (Fig. 4a), supporting the potential of Evo 2 delta scores as predictors of variant deleteriousness in NDDs.

Interestingly, eight candidate VUS displayed Evo 2 delta scores comparable to those of ClinVar entries annotated as P/LP in the same genes (Supplementary Data 1 and Tables S14 and S15; Supplementary File 1 and Fig. S1). These include: NM_004380.3:c.2558T > G (p.Leu853Arg) in *CREBBP* (proband NED080_P), NM_001368397.1:c.3598T > C (p.Ser1200Pro) in *FRMPD4* (proband NED020_P2), NM_006734.4:c.5807C > T (p.Thr1936Ile) in *HIVEP2* (proband NED047_P), NM_004187.5:c.3506C > G (p.Ser1169Trp) in *KDM5C* (proband NED055_P), NM_000240.4:c.608G > A (p.Gly203Asp) in *MAOA* (proband NED049_P1), NM_001008537.3:c.2720A > C (p.Glu907Ala) in *NEXMIF* (proband NED003), NM_001374828.1:c.588_589insAGCAGCAGCAGCAGCAGCAGCAAC (p.Phe196_Gln197insSerSerSerSerSerSerSerAsn) in *ARID1B* (proband NED082_P), and NM_152641.4:c.3197C > T (p.Pro1066Leu) in *ARID2* (proband NED092_P). In particular, variants within *HIVEP2*, *MAOA*, and *ARID2* were also classified as LP by the AlphaMissense algorithm, suggesting that they may warrant re-evaluation as ACMG criterion and be considered as C4 candidates, potentially contributing to an increased diagnostic yield.

Furthermore, all five suggestive SNV/indels described (Tables 2-4) showed lower delta scores than most ClinVar VUS in the corresponding genes (Supplementary Data 1 and Table S14), supporting their potential functional relevance. Among these, the de novo variant in *KALRN* NM_001388419.1:c.5327C > T(p.Pro1776Leu) (proband NED007_P2) is particularly noteworthy. This variant not only displays a delta score lower than all ClinVar VUS in *KALRN* but also lower than most P/LP variants described in our study (Fig. 4b), and it is classified as LP by Alphamissense. The variant was identified in a proband with ASD with severe motor impairment and difficulties in handling objects, mild ID, language delay, motor and verbal stereotypies, mild selective eating, and epileptic episodes. The *KALRN* gene (OMIM *604605) encodes a multidomain guanine nucleotide exchange factor (GEF) for Rho family GTP-binding proteins and has been proposed to play a crucial role in synaptic regulation[68,70,71]. Homozygous variants in *KALRN* have been reported as causative of intellectual disability[72], while alterations in *KALRN* have also been implicated in schizophrenia[73] and epilepsy[74] in experimental models. The extent to which this gene influences NDD phenotypes, and whether it does so via a dominant or recessive inheritance pattern, remains a matter of debate. Nevertheless, taken together, these observations provide strong support for *KALRN* as a promising novel candidate gene for ASD.

Secondary findings

Whole genome sequencing enables the detection of pathogenic variants not directly associated with NDDs but falling within the list of 84 genes recommended for clinical reporting by the American Society of Human Genetics[75]. Variants in these genes are associated with diseases for which preventive measures, surveillance, or treatments are available, thus representing actionable findings that may significantly improve health outcomes. These variants are commonly referred to as "*secondary findings*". In our cohort, we identified three clinically relevant secondary findings: (i). A pathogenic hemizygous variant in *OTC* gene (NM_000531.6:c.264 A), in proband NED083_P, inherited from the mother. This variant is associated with ornithine transcarbamylase deficiency (OTCD, OMIM#311250), an X-linked recessive metabolic disorder that can lead to hyperammonemia and neurological complications. As previously discussed, the proband also exhibits ID and carries a likely pathogenic CNV at 1q21.1, suggesting a complex genetic background.; (ii). a heterozygous pathogenic variant in *MYBPC3* (NM_000256.3:c.2459G > A), identified in the mother of NED093_P. This variant is associated with hypertrophic cardiomyopathy, an autosomal dominant cardiac condition characterized by variable expressivity and risk of sudden cardiac death[35]; (iii). a heterozygous pathogenic variant in *BRCA2* (NM_000059.4:c.9117G > A) found in the mother of NED054_P. *BRCA2* deleterious variants confer an increased risk for hereditary breast and ovarian cancer syndromes, following an autosomal dominant inheritance[35]. This finding has important implications for cancer screening and familial risk assessment.

These cases exemplify the potential of WGS to uncover medically actionable information beyond the primary diagnostic intent, underscoring the utility of genomic approaches in precision medicine.

Independent validation of relevant variants

We aimed to validate the most relevant genomic variants identified through WGS using independent methods in order to exclude potential artefacts arising from alignment or variant calling errors.

Of the 55 SNVs and indels identified through WGS and classified in our study as candidate, suggestive or secondary findings, we were not able to design appropriate primers in 4 cases, primarily due to the presence of repetitive elements, high GC content, or other sequence complexities at the *locus* that interfered with efficient primer binding or PCR amplification (Supplementary Data 1 and Table S16). Overall, the validation rate was 100%, supporting the reliability of NGS-based variant detection and consistent with reported validation rates in literature (91.29%-100%, depending on variant calling quality)[76].

To assess the reliability of our CNV calls, we conducted a visual validation of all 21 CNVs classified as candidate or suggestive by manually inspecting read-depth plots generated with CNVkit and Samplot, which enable the visualization of sequencing coverage across the genomic regions encompassing the predicted CNVs (Supplementary File 1 and Fig. S2a-u). Among these 21 CNVs, 13 were successfully validated using independent

methods (Supplementary Data 1 and Table S16). Specifically, nine had previously been identified through array Comparative Genomic Hybridization (CGH-array), and our analysis of WGS data confirmed their presence in the probands and enabled us to assess their segregation in the parents (Supplementary File 1 and Fig. S2a-u). Four CNVs were successfully validated using a PCR-based method specifically designed for the corresponding *loci*. The remaining eight CNVs could not be validated through the available approaches. In two cases, PCR validation was attempted but failed due to non-functional primers, likely because of the high content of repetitive sequences in the targeted regions. Five CNVs are currently scheduled for PCR validation and remain unconfirmed. Another CNV could not be assessed via CGH-array because the analysis was not performed on the proband. Given that the array platform employed probes spaced 40-60 Kbp apart, we hypothesize that CNVs smaller than approximately 200 Kbp may fall below the resolution of the assay. Nevertheless, four CNVs, although relatively large in size (greater than 230 Kbp), were not reported in the CGH-array results. Nonetheless, the absence of these specific CNVs in the CGH-array data is difficult to fully interpret, particularly because visual inspection of the sequencing read-depth plots provides clear evidence supporting their presence (Supplementary File 1 and Fig. S2a-u). Overall, these data indicate that whole genome sequencing may be more accurate than CGH-array for the identification of CNVs, although further validation is needed to confirm this across different CNV lengths.

Discussion

We present a comprehensive WGS analysis to investigate rare genomic variants that contribute to NDDs, with a focus on ASD and ID. Our study cohort consisted of 100 families, including 110 probands affected by NDDs. The probands exhibited a broad range of NDD phenotypes, from severe ASD with profound cognitive impairment to high-functioning ASD with mild presentations. The inclusion of individuals with milder phenotypes is particularly valuable, as these cases are often underdiagnosed and under-represented in genomic studies. Analyzing these cases may help clarify the genetic contribution to these forms of ASD. Although most families included two healthy parents, 18 families had at least one parent with NDD-like traits, which was considered in the interpretation of segregation and variant effects.

Through an integrative approach, we identified damaging de novo and inherited variants across different classes, including SNVs, indels, SVs, INSs, and MEI, which helped expand the allelic spectrum and elucidate diverse inheritance patterns across NDD-associated and candidate genes. While no INS or MEI of clinical significance was observed, multiple SNVs, indels, and SVs emerged as promising candidates for further analysis.

In total, we identified 32 potentially phenotype-causing variants in 27 out of 110 probands (26.4%), comprising 23 short variants and 9 SVs. Additionally, we report 41 variants of uncertain significance (VUS) we deemed worthy of further investigation (29 short variants, 12 SVs). No relevant variants were detected in approximately 52% of the probands (57/110).

We identified 24 likely pathogenic single-gene variants in 20 genes previously associated to NDDs, including *TRAPPC9*, *HNRNPK, CLCN4, BPTF, CACNA1G, SATB1, ANKRD11, OTC, PHIP, BRWD3, GRIN2A, TRIP12, ARID1B, PPP2R1A, FBXO11, SLC6A8, TSPAN7, KMT5B, ATP1A3, BAZ2B, COL6A1*, and *SRCAP*. We also detected three de novo protein-altering SNVs in *KALRN, NVL*, and *ALDH18A1*, genes not currently recognized as high-confidence ASD-ID *loci*. These probands were all affected by ASD with different degrees of severity, suggesting these genes warrant further functional exploration.

Two VUS were identified in *PLXNA3 and SYTL4*, and seven SVs of unknown significance affecting *GLRA1, NPAS1, NECTIN3, TOP3B, AKAP10, SLC6A16*, and *ARHGEF4*, none of which are well established in NDD etiology.

25 VUS were identified in 22 known NDD-causative genes, including *NRXN1, BRWD3, NEXMIF, CREBBP, CACNA1G, PPP2R5D, KDM5C, NDST1, ANK3, CACNA1F, ARID1B, ARID2, KDM5C, FRMPD4, MAOA, CACNA1D, DHDDS, HIVEP2, CNOT3, ANKRD11, SYT1*, and *KDM6B*. In addition, 12 large CNVs were found in 9 recurrent NDD-associated *loci*: 17p11.2, 1q21.1, 15q13.2-q13.3, 22q11.2, 1p36.32, 15q11.2, 9q24.3, 7q36.1/7q36.2, and 16q24.3.

The clinical significance of variants followed ACMG guidelines[77], resulting in 12 variants classified as likely pathogenic and 17 as pathogenic in known NDD genes (Tables 2-4); although the remaining three variants were classified as VUS by in silico analyses, we nonetheless included them as potential phenotype-modifying candidates following a rigorous critical evaluation. Overall, we estimate a diagnostic rate of 26.4%, consistent with previous WGS-based studies[18,19]. Notably, 11 of the 32 phenotype-causing variants would have been missed by WES due to their genomic localization in non-coding regions, and one likely pathogenic CNV was not detected by CGH-array, supporting an estimated ~10% increase in diagnostic yield when using WGS compared to WES.

Reported diagnostic yields for genome/exome sequencing in NDDs vary widely by cohort composition, ascertainment, and analytic strategy. Meta-analyses estimate yields around 31-36%, with higher rates in consanguineous or deeply phenotyped cohorts. Our lower yield (26.4%) likely reflects the heterogeneity of our cohort of non-consanguineous families, which includes many high-functioning ASD cases with potentially stronger polygenic contributions[44], and its modest sample size, which increases variability.

In addition, following a detailed re-evaluation of VUS in collaboration with the referring clinicians, taking into account family history and phenotypic data, we anticipate that some of these variants may ultimately be reclassified as likely pathogenic (class 4). Consequently, the reported diagnostic yield may represent a conservative (downward) estimate.

Furthermore, re-evaluation of variants using Evo 2[69] indicated that eight VUS might be reconsidered as likely pathogenic, potentially leading to an increase, though modest, diagnostic yield. The observation that several VUS displayed Evo 2 delta scores comparable to those of ClinVar P/LP variants in the same genes suggests that evolutionary modeling approaches can refine the prioritization of variants in NDD cohorts. These findings are consistent with recent evidence supporting the use of large-scale language models trained on genomic sequences to capture functional constraints beyond conventional conservation metrics[78]. Moreover, the algorithm contributed supportive evidence for the deleterious effect of a de novo suggestive variant in *KARLN*, highlighting it as a potential candidate gene for NDDs despite the current lack of a well established association. Importantly, Evo 2 is also expected to be highly valuable for evaluating the potential clinical relevance of non-coding variants, an area that remains particularly challenging in genetic diagnostics. While our study focused on coding variants that alter protein function, WGS provides access to the non-coding genome, harboring regulatory elements such as enhancers, silencers, insulators, and transcription factor binding sites. Disruption of such regulatory elements may significantly impact gene expression and contribute to disease pathogenesis[23]. We speculate that non-coding variants may account for a subset of unsolved cases and plan to implement genome-wide regulatory variant annotation. Although Evo 2 has not yet undergone full peer-reviewed, our preliminary results suggest it may meaningfully refine variant interpretation.

Interestingly, we observed a stepwise increase in diagnostic yield, from the lowest in ASD, to intermediate in ASD-ID, and the highest in ID. This aligns with prior studies[79] and may reflect the more severe and clearly delineated phenotypes typically observed in the ID group, which are more often attributable to rare, highly penetrant variants. In contrast, the ASD-only subgroup includes several high-functioning individuals whose phenotypes are more likely influenced by polygenic and environmental factors[44,80], reducing the likelihood of identifying a single causative variant. When considering the ASD-ID group, no significant difference was detected relative to ASD-only, suggesting broadly comparable rates of monogenic diagnoses between these two subgroups. At the same time, the absence of statistical significance may simply reflect the limited sample sizes available for subgroup analyses.

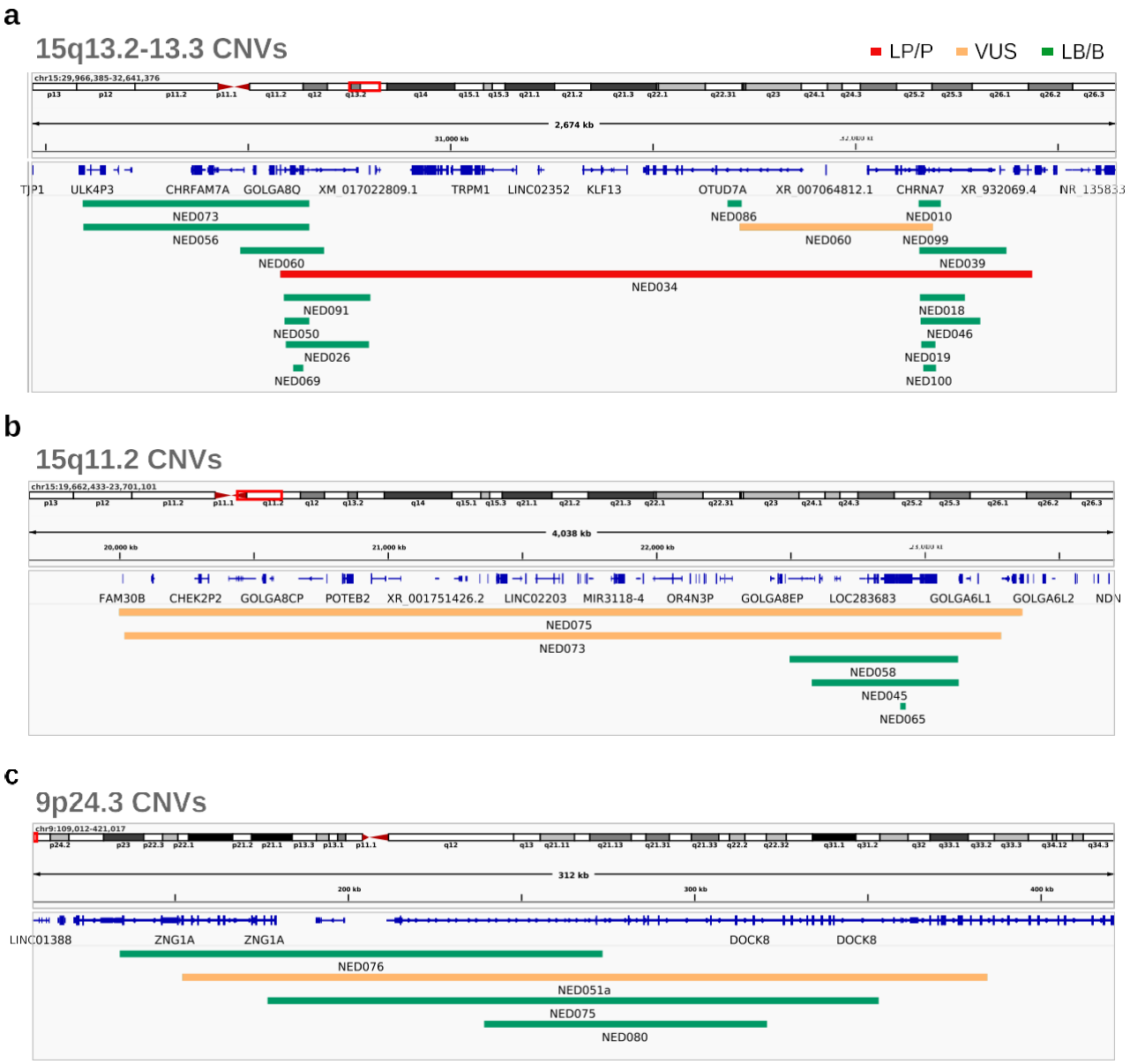

Fig. 5 | Potentially phenotype-relevant recurrent CNVs identified in multiple analyzed individuals. a CNVs found in locus 15q13.2-13.3; b CNVs found in locus 15q11.2; c CNVs found in locus 9p24.3. B/LB benign/likely benign, VUS variant of unknown significance, LP/P likely pathogenic/pathogenic. Created with IGV (Integrative Genomic Viewer) and LibreOffice Draw.

Table 5 | Number of probands affected by potentially pathogenic (P/LP/hot-warm VUS) candidate variants identified in the three experimental groups

Group	Positive	Negative	Total analysed	Yield
ASD	6	34	40	15%
ID	12	15	27	44.4%
ASD-ID	11	32	43	25.6%
Total probands	29	81	110	26.4%

We also assessed CNVs known for incomplete penetrance and variable expressivity, such as those affecting 15q13.2-q13.3, 15q11.2, and 9p24.3 (Fig. 5a-c and Table 5). Notably, all CNVs mapping into chr15 in probands were inherited from the opposite sex parent (father to female proband or mother to male proband). This is intriguing given that these CNVs are located in the immediate upstream and downstream loci from the canonical imprinted region on chromosome 15q11-13 (Table 6 and Fig. 5b).

We identified four 9p24.3 duplications partially overlapping *DOCK8*,a gene previously implicated in learning disabilities and behavioral disturbances, with cases of incomplete penetrance[81,82] (Table 5 and Fig. 5c). The largest duplication was detected in a male proband with ASD-ID (NED051a_P) and his father, while the other three were detected in fathers not transmitting the variant. One carrier father (NED076_F) reported a learning disability, suggesting incomplete penetrance and phenotypic variability (Supplementary Data 1 and Table S1). While the interpretation of these observations is uncertain, these results may help improve the understanding of the impact of partial *DOCK8* duplications in NDDs.

It is important to note that the results presented in this work represent a subset of data from a larger research initiative, "5000genomi@VdA," which involves the WGS of approximately 5000 individuals from the Valle d'Aosta region. This broader dataset, which includes a substantial proportion of healthy individuals from the same genetic background as the NDD cohort, provides an opportunity to refine our analyses and

Table 6 | Potentially phenotype-relevant recurrent CNVs identified in multiple analyzed individuals

Locus	Genomic coordinates	Carriers	CNV type
9p24.3	chr9:239418-320947	NED080_F	DUP
9p24.3	chr9:134189-273546	NED076_F	DUP
9p24.3	chr9:176849-356023	NED075_F	DUP
9p24.3	chr9:152201-384463	NED051a_P, NED051a_F	DUP
15q11.2	chr15:22477726-23280665	NED073_P, NED073_F	DUP
15q11.2	chr15:21043650-23357453	NED075_P, NED075_M	DUP
15q11.2	chr15:22571606-23125407	NED045_P, NED045_F	DEL
15q11.2	chr15:22553589-23122562	NED058_F	DEL
15q13.3	chr15:31714997-32155815	NED060_P, NED060_M	DUP
15q13.2-q13.3	chr15:30581192-32233551	NED034_P, NED034_M	DEL

interpretation of the variants identified in this study in the future. By integrating the NDD cohort with this larger population reference, we plan to investigate the potential contribution of common coding and noncoding variants that may not be captured by conventional diagnostic pipelines and to enhance the detection of structural variants and complex rearrangements through population-based calibration.

Although not related to the initial clinical indication for this NDD cohort, the large amount of data generated by WGS enabled the identification of a few secondary findings. In this study, we also outline a procedure for their effective communication to study participants, which is relevant for implementing preventive healthcare strategies and treatments.

Collectively, these results support WGS as a superior diagnostic tool compared to WES or other targeted approaches, given its ability to detect diverse and complex variant types. A key limitation of our study is the relatively small cohort size, which restricts power for novel gene discovery. Nevertheless, we believe that the family-based design and the analysis of an under-represented population provide valuable insights into the genetic architecture of NDDs and establish a foundation for future research and validation.

Methods

Study cohort

Participants were enrolled in a prospective monocentric observational study, entitled "*Neurodevgenomics*," designed to investigate the genomic alterations in families with ASD and/or ID resident in Valle d'Aosta. Pediatric and adult patients (age ratio 1-42 years old, male-to-female ratio 2.5:1) (Supplementary Data 1 and Table S1) and their parents were recruited through the SDD Pediatric Neuropsychiatry of Beauregard Hospital and SC Psichiatry of Umberto Parini Regional Hospital, Aosta, Italy, in the period between May 2022 and November 2024. Blood or saliva samples were collected from probands, their parents, and affected siblings, totalling 298 individuals (Supplementary Data 1 and Table S1). The study cohort included 100 families, encompassing 110 probands diagnosed with ASD or ID or both. Probands with severe language impairment were included in the ASD-ID group, as formal assessment of intellectual functioning was not feasible due to the limitations imposed by their language deficits.

The *Neurodevgenomics* study protocol was approved by the Institutional Review Board (IRB) of the Umberto Parini Regional Hospital in Aosta during the review meeting held on March 24, 2022, as documented in the official report (Protocol No. *CE PROTOCOLLO.I.0029523.05-04-2022*). Written informed consent was obtained from all the subjects involved or from their Legally Authorized Representatives, including consent for publication of anonymized genetic and clinical details. Investigations were conducted in accordance with the ethical standards as outlined in the Declaration of Helsinki.

Clinical assessment and proband stratification

Clinical diagnosis followed DSM-5 criteria[83] and was conducted by a multidisciplinary team. Evaluations included standardized tools to measure cognitive and developmental levels (Wechsler Scales, Griffiths Scales, PEP-3, Leiter-R) and adaptive behavior (Vineland Adaptive Behavior Scale, VABS; Adaptive Behavior Assessment System, ABAS-2)[84,85]. For suspected ASD cases, diagnostic and severity assessments were conducted using the Autism Diagnostic Observation Schedule, Second Edition (ADOS-2)[86]. IQ scores were categorized into five levels (severe, moderate, mild, borderline, normal) to ensure consistency across various measurement tools.

Whole genome sequencing

Genomic DNA (gDNA) was extracted from peripheral blood of all participants, except for two individuals NED014_F and NED032_F for whom gDNA was extracted from saliva. Short-read whole genome sequencing (srWGS) of gDNA was conducted on an Illumina NovaSeq 6000 platform (Illumina Inc., CA, USA) to produce paired 151 base-pair reads. The library preparation and sequencing of gDNA utilized barcode adapters. Specifically, 350 ng of gDNA was prepared using the Illumina DNA PCR-Free Prep, Tagmentation library preparation kit (Cat number 20041795), and IDT® for Illumina® DNA/RNA Unique Dual Indexes Set A and B, Tagmentation (96 Indexes, Cat numbers 20027213 and 20027214). The library preparation was carried out with a T100 Thermal Cycler instrument (Bio-Rad) and standard laboratory equipment. Library quantification was performed with KAPA qPCR Library Quantification Kit (Roche, Cat number 0 7960140001). Libraries were pooled by volume, adjusted for the index correction factor according to Illumina's instructions to ensure balanced sample coverage across each run. An average sequencing depth of approximately 38X was achieved for all samples (Supplementary Data 1 and Table S3-S5).

Validation of SNVs and SVs

SNVs and Indels were validated with Sanger sequencing. For each variant, DNA amplification was performed under different conditions depending on product length and melting temperatures of the designed primers (see Supplementary Data 1 and Table S16). The Sanger sequencing was performed using the SeqStudio Genetic Analyzer (ThermoFisher Scientific, CA, USA) according to the manufacturer's specification. Negative controls confirmed the absence of amplification inhibitors. DNA quality and quantity were assessed before genotyping. Primers were designed using Primer-BLAST from NCBI[87] and synthesized by Sigma-Aldrich (USA). To validate SVs via PCR amplification, forward and reverse primers were designed to flank the breakpoints of deletions or duplications, ensuring specificity by avoiding regions prone to non-specific annealing. Owing to the unique configuration of the variants, PCR products were observed exclusively in carrier individuals. Information for the validated variants and primer sequences is presented in Supplementary Data 1 and Table S16.

CGH-array had been previously performed on blood-derived samples for all probands, except for NED034_P, at Medical Genetics Unit, Molinette Hospital, Turin, Italy. CGH-array analysis was performed using the AGILENT SurePrint G3 60 K platform, which uses genome-wide probes with an average spacing of 60 Kbp. The identification of a deletion or duplication

requires a significant deviation from the normal value in at least 3 adjacent probes. The CytoGenomics 5.2 software was used to analyze the data.

Kinship analysis

We assessed the kinship of all families using Plink[88] (v1.90b6.21) and KING[89] (v2.2.6) on quality-filtered short variants detected with HaplotypeCaller (Parabricks). Results of the kinship analysis are available in Supplementary Data 1 and Table S2.

List of neurodevelopmentally-relevant genes

Evaluating the genomic causes of NDDs is challenging. In addition to well-established NDD genes, many genes are not yet recognized as definitive NDD genes but may still significantly contribute to the neurodevelopmental phenotypes. To address this issue, we compiled a comprehensive list that includes: (i) genes present in the SFARI (Simons Foundation Autism Research Initiative) database (January 2024 release)[32]; (ii) genes with high brain expression, defined as those genes with average log2 RPKM > 4.5 in the BrainSpan database (http://www.brainspan.org) (the top 18%)[90]; (iii) genes of the KEGG pathways[91] (https://www.genome.jp/kegg) selected for their possible relevance with ASD (including Nervous system, Genetic Information Processing, and Replication and repair); (iv) genes associated to neurodevelopmental phenotypes according to OMIM[35]. However, the role of some genes in NDDs may be supported only by recent evidence. We therefore aimed to ensure that potentially relevant genes were not overlooked in our analysis. To achieve this, we conducted an initial analysis of genomic variants across all annotated human protein-coding genes, with a particular focus on de novo and X-linked variants. All genomic variants described in this work have been found within genes included in this updated list (available in Supplementary Data 1 and Table S17).

Identification and prioritization of short variants

We used the NVIDIA Clara™ Parabricks® pipeline (version 3.8) with BWA-mem to map raw sequencing reads to the reference genome (hg38). We then performed germline short variant calling (SNVs and indels) with the NVIDIA Clara™ Parabricks® germline pipeline (3.8 version) with GATK HaplotypeCaller[92]. Called variants were filtered in order to retain only variants labeled as "PASS". Filtered variants were annotated using Annovar (databases updated to 04/01/2024).

We then filtered total variants in order to only retain variants with the following characteristics: (1) present in less than 0.5% of the population (GnomAD v4[93]), in less than 5 times in heterozigosys, and less than 3 times in homozigosys in the internal cohort (composed of 298 individuals); (2) annotated as "exonic" or "splicing"; (3) not synonymous; (4) not annotated as "Benign" or "Likely Benign" by InterVar[94] or ClinVar[95]; (5) associated with a CADD_phred score[96] above 20 (or unassigned); (6) present in the proband and supported by at least 10 reads in at least one member of the family, including the proband; (7) identified within a gene included in a curated list of 4264 genes of interest in the context of neurodevelopment (Supplementary Data 1 and Table S17). The application of these filters resulted in ~37 variants per family, which we refer to as 'filtered variants'. Additionally we assigned one of the following inheritance patterns to each filtered variant: inherited (when present in heterozygosity in a parent and a proband); de novo (variants present only in the proband); recessive (variants present in homozygosity in the proband and in heterozygosity in both parents); X-linked variants (variants present in hemizygosity in male probands and in heterozygosity in the mother); "composite recessive" variants (instances where more than at least one variant per parent is inherited in the same gene in the proband) and '*unknown*' when we were not able to clearly identify the inheritance pattern. We manually evaluated filtered variants employing the following criteria: (1) relevance of the gene in the context of the probands phenotype (assessed using databases OMIM/ORPHANET and literature review); (2) genes inheritance mode (when specified by OMIM); (3) ACMG guidelines (especially in the case of known disease-causing genes, by using the computational tools InteVar, VarSome and Franklin), moreover, we considered the AlphaMissense score[97] when evaluating *missense* variants; (4) protein domain overlapping the variant (assessed with UniProt); (5) overall damaging potential of the variant (CADD_phred score); (6) evolutionary conservation of the genomic locus (GERP++_RS score[98]); family structure (especially when one or both parents present a similar phenotype compared to the proband).

We performed manual curation to identify gene-damaging variants within known NDD-causing genes, which we define as candidate variants. We also identified potentially deleterious variants in genes not clearly associated with a specific phenotype but for which evidence suggests involvement in neurodevelopment; these are defined as "suggestive variants". All missense candidates and suggestive variants were also classified as either LB, VUS, or LP with Alphamissense[97].

Identification and prioritization of structural variants

Upon mapping raw sequencing reads to the reference genome (hg38) with NVIDIA Clara™ Parabricks® pipeline (version 3.8), we used two methods to detect structural variants: a custom pipeline comprising multiple SV-caller bioinformatics tools (adapted from Vialle et al. [39,40]) to identify CNVs (deletions and duplications) smaller than 500 kb, insertions (INS), and mobile element insertions (MEI); and CNVkit (v0.9.9) to detect larger CNVs. The pipeline adapted from Vialle et al. [39]. uses four tools to call CNVs (Manta[99] (v1.6.0), CNVnator[100] (v0.3.3), BreakDancer[101] (v1.4.5), and Lumpy[102] (v0.2.13)) and reports only CNVs identified by at least two of these four tools. Additionally, this pipeline calls insertions with Manta[99] and non-reference mobile element insertions with Melt[103].

We run CNVkit batch analysis to detect CNVs against a reference genome constructed with 10 genomes from healthy individuals, with "*hmm-germline*" segmentation method and "*wgs*" seq-method. We filtered identified CNVs to discard signals from background noise or non-germline CNVs (log2 copy-number> 0.35 or< −0.4, p-value < $10E^{-05}$, weight > 20). Moreover, we merged the genomic coordinates of CNVs of the same type (deletions or duplications) closer than 50 Kbp to each other.

Both in the case of variants called with CNVkit and with the SV pipeline adapted from Vialle et al., we merged the variants relative to the members of each family using SURVIVOR to generate family-level multi-sample VCF files. These files were then annotated with SVAFotate and AnnotSV (v3.2.3). We selected only rare variants (frequency < 0.01) overlapping exons of neurodevelopmentally-relevant genes (Supplementary Data 1 and Table S17) that were identified in at least one family member. We also filtered out all CNVs present in more than 10% of enrolled families. In the case of INS and MEI, we retained only variants found at less than 20 bp from one exon of a neurodevelopment-related gene. All filtered CNVs were subjected to manual curation. We generated and visually inspected family-level plots generated with the CNVkit scatterplot utility in the case of variants called with CNVkit, and with SamPlot46 in the case of structural variants identified with our custom pipeline. This allowed us to estimate the likelihood of false positives, verify variant inheritance within trios, and identify variants that might not have been formally called in all family members despite being present. Following validation of variant authenticity, the pathogenic potential of CNVs we deemed worthy of further investigation was evaluated according to ACMG guidelines using Franklin (Genoox) and VarSome.

Evaluation of genomic variants

To identify potentially phenotype-causing variants, we mainly focused on de novo, *X-linked*, and homozygous variants. Analysis of de novo SNVs/SVs variants was performed only for complete trios (89 out of 100 families); we took into account the genotype reported by HaplotypeCaller for short variants, by Melt for MEI, and by Manta for INS. We assessed the genotype of CNVs manually by inspecting plots produced with CNVkit and SamPlot.

However, we manually evaluated inherited variants as well, especially in the cases where one or both parents presented phenotypic traits similar to the ones observed in the proband. We divided variants of potential interest into two main categories: candidate and suggestive variants.

Candidate variants are variants affecting genes that are known to be involved in a neurodevelopmental phenotype that matches the proband's

phenotype, following a specific inheritance pattern observed in the variant. Candidate variants can be classified as either pathogenic (P), likely pathogenic (LP), variants of uncertain significance (VUS), or as VUS with strong supporting evidence (referred to as "warm/hot" VUS) according to the ACMG guidelines. The diagnostic yield in this study was driven exclusively by candidate variants classified as P, LP, or hot/warm VUS. Suggestive variants are those classified as VUS or P/LP according to ACMG guidelines, located in genes not yet strongly associated with NDDs but reported in recent literature as potentially relevant to human neurodevelopment.

Variant evaluation with Evo 2

To provide additional evidence supporting the variants identified in this study, we applied Evo 2[69], a recently developed machine learning-based prioritization framework that integrates measures of evolutionary constraint, gene-level intolerance, and variant pathogenicity scores to refine variant classification.

For each short variant described in the previous paragraphs (Tables 2-4), we computed the Delta likelihood scores using the Evo 2 7B model in a zero-shot setting. For each variant, its genomic position was located on the corresponding chromosome, and an 8000 bp window centered around that position was used to extract the variant and reference sequence pairs. For SNVs, the variant nucleotide replaced the reference nucleotide at the center of the variant sequence. For deletions, the deleted segment was removed after the given position, and the 8000 bp window was extended into the neighboring regions to maintain the total sequence length (8000 bp). For insertions, the inserted nucleotides were added after the specified position, and an equivalent number of nucleotides were removed from the end of the variant sequence to keep the length consistent. In addition to the original variant and reference sequences, their reverse complements were also used to calculate log-likelihoods. The original sequence and its reverse complement log-likelihood scores were averaged to obtain the final log-likelihood values for both variant and reference sequences. The Delta likelihood scores were then computed by subtracting the reference log-likelihoods from the corresponding variant log-likelihoods.

To contextualize these findings, we performed the same analysis on variants annotated in the ClinVar database. Specifically, for each gene harboring a candidate or suggestive variant in our dataset (Tables 2-4; Supplementary Data 1 and Table S15), we retrieved all ClinVar entries classified as *pathogenic* or *likely pathogenic*, together with a randomly downsampled subset of *variants of uncertain significance* (VUS) and *benign/likely benign* (B/LB) variants. For genes with more than 450 annotated variants, B/LB and VUS variants were pruned to a total of 450 variants per gene (Supplementary Data 1 - Table S15).

ClinVar annotations were harmonized into three major categories: (i) *Pathogenic/likely pathogenic* (including "Pathogenic," "Likely pathogenic," and "Pathogenic/Likely pathogenic"); (ii) *Benign/likely benign* (including "Benign," "Likely benign," and "Benign/Likely benign"); and (iii) *Uncertain significance* (including "Uncertain significance" and "Conflicting interpretation of pathogenicity"). In total, 17,054 ClinVar variants (8255 Uncertain_significance; 6045 Benign/Likely_benign; 2754 Pathogenic/Likely_pathogenic) were analyzed using the Evo2 framework (Supplementary Data 1 and Table S15).

We then visualized the distribution of Evo 2 delta scores across these ClinVar categories and overlaid a dotted line indicating the distribution of delta scores for the variants identified in our study (Supplementary Data 1 and Tables S14 and S15), allowing direct comparison of our findings with known variant classifications in the same genes.

Secondary findings

Although not directly related to the primary aim of our study, WGS analysis of this NDD cohort enabled the identification of several secondary findings associated with other clinically relevant and actionable conditions. We define as *secondary findings* variants classified as pathogenic or likely pathogenic by ClinVar, InterVar, or both. Variants were considered only if found in heterozygous state in an autosomal dominant gene, or in homozygous or hemizygous state in a recessive gene. The analysis was restricted to the 84 genes recommended by the American College of Medical Genetics and Genomics (ACMG) for clinical reporting[75].

As part of the informed consent process designed for this study, participants were offered the option to receive information about any clinically relevant secondary findings. In accordance with ethical guidelines and data protection regulations, only those who explicitly opted in are contacted regarding individual results and informed about the need for further molecular analyses. Only secondary findings that strictly adhere to the reporting criteria outlined by the American College of Medical Genetics and Genomics (ACMG) are disclosed. For these participants, a second blood sample is collected, and diagnostic validation of the identified variant is conducted using standard clinical procedures. A formal report is then prepared, and individuals are referred for genetic counselling. A clinical geneticist will then disclose and explain the validated secondary findings to the participants or their legal guardians.

Data availability

The data supporting the results of this study are available on request from the corresponding author. The data are not publicly available due to privacy or ethical restrictions.

Received: 23 July 2025; Accepted: 23 December 2025;
Published online: 02 February 2026

References

1. Morris-Rosendahl, D. J. & Crocq, M.-A. Neurodevelopmental disorders-the history and future of a diagnostic concept. *Dialogues Clin. Neurosci.* 22, 65–72 (2020).
2. Thapar, A., Cooper, M. & Rutter, M. Neurodevelopmental disorders. *Lancet Psychiatry* 4, 339–346 (2017).
3. Straub, L. et al. Neurodevelopmental disorders among publicly or privately insured children in the United States. *JAMA Psychiatry* 79, 232–242 (2022).
4. Gidziela, A. et al. A meta-analysis of genetic effects associated with neurodevelopmental disorders and co-occurring conditions. *Nat. Hum. Behav.* 7, 642–656 (2023).
5. Alonso-Gonzalez, A., Rodriguez-Fontenla, C. & Carracedo, A. De novo Mutations (DNMs) in Autism Spectrum Disorder (ASD): pathway and network analysis. *Front. Genet.* 9, 406 (2018).
6. Fu, J. M. et al. Rare coding variation provides insight into the genetic architecture and phenotypic context of autism. *Nat. Genet.* 54, 1320–1331 (2022).
7. Luo, W., Zhang, C., Jiang, Y.-H. & Brouwer, C. R. Systematic reconstruction of autism biology from massive genetic mutation profiles. *Sci. Adv.* 4, e1701799 (2018).
8. Ramaswami, G. & Geschwind, D. H. Genetics of autism spectrum disorder. *Handb. Clin. Neurol.* 147, 321–329 (2018).
9. van Dongen, J., Slagboom, P. E., Draisma, H. H. M., Martin, N. G. & Boomsma, D. I. The continuing value of twin studies in the omics era. *Nat. Rev. Genet.* 13, 640–653 (2012).
10. Sullivan, P. F., Daly, M. J. & O'Donovan, M. Genetic architectures of psychiatric disorders: the emerging picture and its implications. *Nat. Rev. Genet.* 13, 537–551 (2012).
11. Lundström, S. et al. Autism spectrum disorders and autistic like traits: similar etiology in the extreme end and the normal variation. *Arch. Gen. Psychiatry* 69, 46–52 (2012).
12. Scattoni, M. L. et al. Autism spectrum disorder prevalence in Italy: a nationwide study promoted by the Ministry of Health. *Child Adolesc. Psychiatry Ment. Health* 17, 125 (2023).
13. Sanders, S. J. Next-generation sequencing in autism spectrum disorder. *Cold Spring Harb. Perspect. Med.* 9, a026872 (2019).
14. Codina-Solà, M. et al. Integrated analysis of whole-exome sequencing and transcriptome profiling in males with autism spectrum disorders. *Mol. Autism* 6, 21 (2015).

15. Feliciano, P. et al. Exome sequencing of 457 autism families recruited online provides evidence for autism risk genes. *npj Genomic Med.* 4, 19 (2019).
16. Sanders, S. J. et al. De novo mutations revealed by whole-exome sequencing are strongly associated with autism. *Nature* 485, 237–241 (2012).
17. Satterstrom, F. K. et al. Large-scale exome sequencing study implicates both developmental and functional changes in the neurobiology of autism. *Cell* 180, 568–584.e23 (2020).
18. Álvarez-Mora, M. I. et al. Diagnostic yield of next-generation sequencing in 87 families with neurodevelopmental disorders. *Orphanet J. Rare Dis.* 17, 60 (2022).
19. Nurchis, M. C. et al. Whole genome sequencing diagnostic yield for paediatric patients with suspected genetic disorders: systematic review, meta-analysis, and GRADE assessment. *Arch. Public Health Arch. Belg. Santé Publique* 81, 93 (2023).
20. Palmer, E. E. et al. Diagnostic yield of whole genome sequencing after nondiagnostic exome sequencing or gene panel in developmental and epileptic encephalopathies. *Neurology* 96, e1770–e1782 (2021).
21. Viggiano, M. et al. Genomic analysis of 116 autism families strengthens known risk genes and highlights promising candidates. *NPJ Genomic Med.* 9, 21 (2024).
22. Bagger, F. O. et al. Whole genome sequencing in clinical practice. *BMC Med. Genomics* 17, 39 (2024).
23. D'haene, E. & Vergult, S. Interpreting the impact of noncoding structural variation in neurodevelopmental disorders. *Genet. Med. Off. J. Am. Coll. Med. Genet.* 23, 34–46 (2021).
24. Alibutud, R. et al. Structural Variations Contribute to the Genetic Etiology of Autism Spectrum Disorder and Language Impairments. *Int. J. Mol. Sci.* 24, 13248 (2023).
25. Pinto, D. et al. Functional impact of global rare copy number variation in autism spectrum disorders. *Nature* 466, 368–372 (2010).
26. Moreno-De-Luca, D. et al. Using large clinical data sets to infer pathogenicity for rare copy number variants in autism cohorts. *Mol. Psychiatry* 18, 1090–1095 (2013).
27. Zarrei, M. et al. A large data resource of genomic copy number variation across neurodevelopmental disorders. *npj Genomic Med.* 4, 26 (2019).
28. Torene, R. I. et al. Mobile element insertion detection in 89,874 clinical exomes. *Genet. Med. Off. J. Am. Coll. Med. Genet.* 22, 974–978 (2020).
29. Demidov, G. et al. Detection of mobile elements insertions for routine clinical diagnostics in targeted sequencing data. *Mol. Genet. Genomic Med.* 9, e1807 (2021).
30. Trost, B. et al. Genome-wide detection of tandem DNA repeats that are expanded in autism. *Nature* 586, 80–86 (2020).
31. Mitra, I. et al. Patterns of de novo tandem repeat mutations and their role in autism. *Nature* 589, 246–250 (2021).
32. Abrahams, B. S. et al. SFARI Gene 2.0: a community-driven knowledgebase for the autism spectrum disorders (ASDs). *Mol. Autism* 4, 36 (2013).
33. Martin, A. R. et al. PanelApp crowdsources expert knowledge to establish consensus diagnostic gene panels. *Nat. Genet.* 51, 1560–1565 (2019).
34. Leblond, C. S. et al. Operative list of genes associated with autism and neurodevelopmental disorders based on database review. *Mol. Cell. Neurosci.* 113, 103623 (2021).
35. Amberger, J. S., Bocchini, C. A., Schiettecatte, F., Scott, A. F. & Hamosh, A. OMIM.org: Online Mendelian Inheritance in Man (OMIM®), an online catalog of human genes and genetic disorders. *Nucleic Acids Res.* 43, D789–D798 (2015).
36. Greene, D. et al. Mutations in the U4 snRNA gene RNU4-2 cause one of the most prevalent monogenic neurodevelopmental disorders. *Nat. Med.* https://doi.org/10.1038/s41591-024-03085-5 (2024).
37. Moyses-Oliveira, M., Yadav, R., Erdin, S. & Talkowski, M. E. New gene discoveries highlight functional convergence in autism and related neurodevelopmental disorders. *Curr. Opin. Genet. Dev.* 65, 195–206 (2020).
38. Talevich, E., Shain, A. H., Botton, T. & Bastian, B. C. CNVkit: genome-wide copy number detection and visualization from targeted DNA sequencing. *PLoSComput. Biol.* 12, e1004873 (2016).
39. Vialle, R. A., de Paiva Lopes, K., Bennett, D. A., Crary, J. F. & Raj, T. Integrating whole-genome sequencing with multi-omic data reveals the impact of structural variants on gene regulation in the human brain. *Nat. Neurosci.* 25, 504–514 (2022).
40. Marangoni, S. et al. GeNePi: a GPU-enhanced next generation bioinformatics pipeline for whole genome sequencing analysis. *bioRxiv* https://doi.org/10.1101/2025.01.30.635645 (2025).
41. Belyeu, J. R. et al. Samplot: a platform for structural variant visual validation and automated filtering. *Genome Biol.* 22, 161 (2021).
42. Turner, T. N. et al. denovo-db: a compendium of human de novo variants. *Nucleic Acids Res.* 45, D804–D811 (2017).
43. Cirnigliaro, M. et al. The contributions of rare inherited and polygenic risk to ASD in multiplex families. *Proc. Natl. Acad. Sci. USA.* 120, e2215632120 (2023).
44. Alvarez-Mora, M. I. et al. Comprehensive molecular testing in patients with high functioning autism spectrum disorder. *Mutat. Res.* 784–785, 46–52 (2016).
45. Stelzer, G. et al. The genecards suite: from gene data mining to disease genome sequence analyses. *Curr. Protoc. Bioinforma.* 54, 1.30.1–1.30.33 (2016).
46. Iossifov, I. et al. The contribution of de novo coding mutations to autism spectrum disorder. *Nature* 515, 216–221 (2014).
47. Bayat, A., Kirchhoff, M., Madsen, C. G., Roos, L. & Kreiborg, S. Familial craniofacial abnormality and polymicrogyria associated with a microdeletion affecting the NFIA gene. *Clin. Dysmorphol.* 26, 148–153 (2017).
48. Bacchelli, E. et al. An integrated analysis of rare CNV and exome variation in Autism Spectrum Disorder using the Infinium PsychArray. *Abstr. Sci. Rep.* 10, 3198 (2020).
49. Arndt, A-K. et al. Fine Mapping of the 1p36 Deletion Syndrome Identifies Mutation of PRDM16 as a Cause of Cardiomyopathy. *Am. J. Hum. Genet.* 93, 67–77 (2013).
50. Baizabal, J-M. et al. The Epigenetic State of PRDM16-Regulated Enhancers in Radial GliaControls Cortical Neuron Position. *Neuron* 98, 945–962.e8 (2018).
51. He, L., Jones, J., He, W., Bjork, B. C., Wen, J. & Dai, Q. PRDM16 regulates a temporal transcriptional program to promote progression of cortical neural progenitors. *Development* 148, dev194670 (2021).
52. Inoue, M. et al. Prdm16 is crucial for progression of the multipolar phase during neural differentiation of the developing neocortex ABSTRACT Development. *Development* 144, 385–399 (2017).
53. Shimada, I. S., Acar, M., Burgess, R. J., Zhao, Z. & Morrison, S. J. Prdm16 is required for the maintenance of neural stem cells in the postnatal forebrain and their differentiation into ependymal cells. *Genes Dev.* 31, 1134–1146 (2017).
54. Su, L., Lei, X., Ma, H., Feng, C., Jiang, J. & Jiao, J. PRDM16 orchestrates angiogenesis via neural differentiation in the developing brain. *Cell Death Differ.* 27, 2313–2329 (2020).
55. Jurnak, F. The Pivotal Role of Aldehyde Toxicity in Autism Spectrum Disorder: The Therapeutic Potential of Micronutrient Supplementation. *Nutr. Metab. Insights* 8, 57–77 (2016).
56. Rafi, S. K., Fernández-Jaén, A., Álvarez, S., Nadeau, O. W. & Butler, G. High Functioning Autism with Missense Mutations in Synaptotagmin-Like Protein 4 (SYTL4) and Transmembrane Protein 187 (TMEM187) Genes: SYTL4- Protein Modeling Protein-Protein Interaction Expression Profiling and MicroRNA Studies. *Int. J. Mol. Sci.* 20, 3358 (2019).

57. Wilton, K. M., Gunderson, L. B., Hasadsri, L., Wood, C. P. & Schimmenti, L. A. Profound intellectual disability caused by homozygous TRAPPC9 pathogenic variant in a man from Malta. *Mol. Genet. Genomic Med.* 8, e1211 (2020).
58. Siano, M. A. et al. De novo mutation in KMT2C manifesting as Kleefstra syndrome 2: case report and literature review. *Pediatr. Rep.* 14, 131–139 (2022).
59. Gaur, R. et al. P629: a novel 198 kb partial duplication in KMT2C: report of a patient with features of Kleefstra syndrome-2 and adrenal ganglioneuroblastoma. *Genet. Med. Open* 2, 101535 (2024).
60. Ferraroli, E. et al. Hereditary hyperekplexia: a new family and a systematic review of GLRA1 gene-related phenotypes. *Pediatr. Neurol.* 132, 45–49 (2022).
61. Schaefer, N. et al. Anxiety and startle phenotypes in Glrb spastic and Glra1 spasmodic mouse mutants. *Front. Mol. Neurosci.* 13, 152 (2020).
62. Stanco, A. et al. NPAS1 represses the generation of specific subtypes of cortical interneurons. *Neuron* 84, 940–953 (2014).
63. Wang, H.-L. et al. Prefrontal nectin3 reduction mediates adolescent stress-induced deficits of social memory, spatial working memory, and dendritic structure in mice. *Neurosci. Bull.* 36, 860–874 (2020).
64. Scott, T. M. et al. BAZ2B haploinsufficiency as a cause of developmental delay, intellectual disability, and autism spectrum disorder. *Hum. Mutat.* 41, 921–925 (2020).
65. Pettersson, M. et al. Copy number variants are enriched in individuals with early-onset obesity and highlight novel pathogenic pathways. *J. Clin. Endocrinol. Metab.* 102, 3029–3039 (2017).
66. Gregorio, I., Mereu, M. & Contarini, G. Collagen VI deficiency causes behavioral abnormalities and cortical dopaminergic dysfunction. *Dis. Model Mech.* 15, dmm049481 (2022).
67. Wang, M. et al. The NVL gene confers risk for both major depressive disorder and schizophrenia in the Han Chinese population. *Prog. Neuropsychopharmacol. Biol. Psychiatry* 62, 7–13 (2015).
68. Parnell, E. et al. A developmental delay linked missense mutation in Kalirin-7 disrupts protein function and neuronal morphology. *Front. Mol. Neurosci.* 15, 994513 (2022).
69. Brixi, G. et al. Genome modeling and design across all domains of life with Evo 2. *bioRxiv* https://doi.org/10.1101/2025.02.18.638918 (2025).
70. Parnell, E. et al. KALRN: a central regulator of synaptic function and synaptopathies. *Gene.* 768, 145306 (2021).
71. Leblond, C. S. et al. Both rare and common genetic variants contribute to autism in the Faroe Islands. *npj Genomic Med.* 4, 1 (2019).
72. Makrythanasis, P. et al. Exome sequencing discloses KALRN homozygous variant as likely cause of intellectual disability and short stature in a consanguineous pedigree. *Hum. Genomics* 10, 26 (2016).
73. Russell, T. A. et al. A schizophrenia-linked KALRN coding variant alters neuron morphology, protein function, and transcript stability. *Biol. Psychiatry* 83, 499–508 (2018).
74. Chen, L. et al. Kalirin is involved in epileptogenesis by modulating the activity of the Rac1 signaling pathway. *J. Chem. Neuroanat.* 131, 102289 (2023).
75. Lee, K. et al. ACMG SF v3.3 list for reporting of secondary findings in clinical exome and genome sequencing: a policy statement of the American College of Medical Genetics and Genomics (ACMG). *Genet. Med. Off. J. Am. Coll. Med. Genet.* 27, 101454 (2025).
76. Kopernik, A. et al. Sanger validation of WGS variants. *Sci. Rep.* 15, 3621 (2025).
77. Richards, S. et al. Standards and guidelines for the interpretation of sequence variants: a joint consensus recommendation of the American College of Medical Genetics and Genomics and the Association for Molecular Pathology. *Genet. Med. Off. J. Am. Coll. Med. Genet.* 17, 405–424 (2015).
78. Karollus, A. et al. Species-aware DNA language models capture regulatory elements and their evolution. *Genome Biol.* 25, 83 (2024).
79. Neuens, S. et al. Diagnostic yield of clinical exome sequencing in 868 children with neurodevelopmental disorders. *Eur. J. Med. Genet.* 76, 105030 (2025).
80. Gupta, M. & Chaudhary, R. Diagnostic challenges of high-functioning autism spectrum disorder in females. *Cureus* 13, e13006 (2021).
81. Krgovic, D., Kokalj Vokac, N., Zagorac, A. & Gregoric Kumperscak, H. Rare structural variants in the DOCK8 gene identified in a cohort of 439 patients with neurodevelopmental disorders. *Sci. Rep.* 8, 9449 (2018).
82. Benítez-Burraco, A., Fernández-Urquiza, M. & Jiménez-Romero, M. S. Language impairment with a partial duplication of DOCK8. *Mol. Syndromol.* 11, 243–263 (2020).
83. American Psychiatric Association. Diagnostic and statistical manual of mental disorders (5th ed., text rev.). https://doi.org/10.1176/appi.books.9780890425787 (2022).
84. Harrison, P. L. & Oakland, T. Adaptive behavior assessment system: Third Edition. in *Encyclopedia of Clinical Neuropsychology* (eds Kreutzer, J. S., DeLuca, J. & Caplan, B.) 57–60 (Springer International Publishing, 2018).
85. Sparrow, S. S., & Cicchetti, D. V. *The Vineland Adaptive Behavior Scales.* In *Major Psychological Assessment Instruments,* (ed Newmark C. S.) Vol. 2 199–231 (1989).
86. Mccrimmon, A. & Rostad, K. Test review: autism diagnostic observation schedule, Second Edition (ADOS-2) manual (Part II): Toddler Module. *J. Psychoeduc. Assess.* 32, 88–92 (2013).
87. Ye, J. et al. Primer-BLAST: a tool to design target-specific primers for polymerase chain reaction. *BMC Bioinforma.* 13, 134 (2012).
88. Purcell, S. et al. PLINK: a tool set for whole-genome association and population-based linkage analyses. *Am. J. Hum. Genet.* 81, 559–575 (2007).
89. Manichaikul, A. et al. Robust relationship inference in genome-wide association studies. *Bioinforma. Oxf. Engl.* 26, 2867–2873 (2010).
90. Miller, J. A. et al. Transcriptional landscape of the prenatal human brain. *Nature* 508, 199–206 (2014).
91. Kanehisa, M., Furumichi, M., Tanabe, M., Sato, Y. & Morishima, K. KEGG: new perspectives on genomes, pathways, diseases and drugs. *Nucleic Acids Res.* 45, D353–D361 (2017).
92. Van der Auwera, G. A. et al. From FastQ data to high confidence variant calls: the Genome Analysis Toolkit best practices pipeline. *Curr. Protoc. Bioinforma.* 43, 11.10.1–11.10.33 (2013).
93. Gudmundsson, S. et al. Variant interpretation using population databases: Lessons from gnomAD. *Hum. Mutat.* https://doi.org/10.1002/humu.24309 (2021).
94. Li, Q. & Wang, K. InterVar: clinical interpretation of genetic variants by the 2015 ACMG-AMP guidelines. *Am. J. Hum. Genet.* 100, 267–280 (2017).
95. Landrum, M. J. et al. ClinVar: public archive of relationships among sequence variation and human phenotype. *Nucleic Acids Res.* 42, D980–D985 (2014).
96. Rentzsch, P., Schubach, M., Shendure, J. & Kircher, M. CADD-Splice-improving genome-wide variant effect prediction using deep learning-derived splice scores. *Genome Med.* 13, 31 (2021).
97. Cheng, J. et al. Accurate proteome-wide missense variant effect prediction with AlphaMissense. *Science* 381, eadg7492 (2023).
98. Davydov, E. V. et al. Identifying a high fraction of the human genome to be under selective constraint using GERP++. *PLoSComput. Biol.* 6, e1001025 (2010).
99. Chen, X. et al. Manta: rapid detection of structural variants and indels for germline and cancer sequencing applications. *Bioinforma. Oxf. Engl.* 32, 1220–1222 (2016).
100. Abyzov, A., Urban, A. E., Snyder, M. & Gerstein, M. CNVnator: an approach to discover, genotype, and characterize typical and

atypical CNVs from family and population genome sequencing. *Genome Res.* 21, 974–984 (2011).
101. Fan, X., Abbott, T. E., Larson, D. & Chen, K. BreakDancer: identification of genomic structural variation from paired-end read mapping. *Curr. Protoc. Bioinforma.* 45, 1–11 (2014).
102. Layer, R. M., Chiang, C., Quinlan, A. R. & Hall, I. M. LUMPY: a probabilistic framework for structural variant discovery. *Genome Biol.* 15, 1–19 (2014).
103. Gardner, E. J. et al. The Mobile Element Locator Tool (MELT): population-scale mobile element discovery and biology. https://doi.org/10.1101/gr.218032.116 (2017).

Acknowledgements

We thank individuals and families who participated in this study and donated their samples for research. We are indebted to the research nurses of the "5000genomi@VdA" project, Laura Gregoratto and Andrea Cheraz, for biological sample collection and for providing support in the management of participants in the Neurodevgenomics study. We are grateful to the technical IT support (in particular, Mathieu Clement), the project manager Alessandra Gastaldi, Arianna De Arcangelis for regulatory documents, and all the administrative staff of CMP3VdA, Aosta. Special thanks to Emilie Jacquemod and Eva Ferri (IIT). We are also indebted to all the partners of the project 5000genomi@Vda. This work was funded by the Project 5000genomi@VdA, co-founded by "Fondo Europeo di Sviluppo Regionale (FESR CUPB68H19005520007) to SG and AC; ST, MV, FL, ACo, VP, EB, FG, SGo, and MT were supported by "Fondo Europeo di Sviluppo Regionale (FESR CUPB68H19005520007); GS, GT, MFC, NL, AF, FF, DC, and SM were recipient of a fellowship from Programma Investimenti per la crescita e l'occupazione 2014/20" (European Social Fund, ESF CUP B65F19001200009), and GS, GT, AF, FF, DC, and KF continued their activity with a fellowship from Programma Regionale Fondo sociale europeo Plus 2021/2027 (European Social Fund, ESF CUP J51B24000170002). The authors acknowledge support from the project "National Centre for HPC, Big Data and Quantum Computing" (CN00000013 - Spoke 8).

Author contributions

Conceptualization: S.G., L.O., A.C., A.A., M.V., and G.S. Methodology: S.T. supervised sequencing activity; V.P., E.B., F.G., S.Go., M.T., M.F.C., N.L., and G.T. extracted DNA and performed sequencing. Software: S.M., A.F., F.F., D.C., F.M., F.L., A.Co., implemented the S.V. pipeline; K.F. performed the Evo 2 analysis. Formal analysis: G.S. performed bioinformatic and variant prioritization analyses. Data curation: S.T., L.O., P.S., S.D.D., G.S., M.V., A.A., and R.S. Validation: S.T., M.F.C., N.L., and G.T. Resources: L.O., M.V., and S.T. Investigation: G.S., R.S., A.A., M.V., and L.O. Writing, reviewing, and editing: G.S., S.G., S.T., M.V., and L.O. Supervision: M.V., L.O., and S.G. Funding acquisition: S.G. and A.C. All authors read and approved the final manuscript.

Competing interests

All authors declare no financial or non-financial competing interests.

Additional information

Supplementary information The online version contains supplementary material available at https://doi.org/10.1038/s41525-025-00547-8.

Correspondence and requests for materials should be addressed to Manuela Vecchi, Laure Obino or Stefano Gustincich.

Reprints and permissions information is available at http://www.nature.com/reprints

Publisher's note Springer Nature remains neutral with regard to jurisdictional claims in published maps and institutional affiliations.

[1]Non-coding RNAs and RNA-based therapeutics, Italian Institute of Technology, CMP3VdA, Aosta, Italy. [2]Center for Clinical and Computational Genomics, Non-coding RNAs and RNA-based therapeutics, Fondazione Istituto Italiano di Tecnologia (IIT), Aosta, Italy. [3]Computational and Chemical Biology, Italian Institute of Technology, CMP3VdA, Aosta, Italy. [4]Center for Clinical and Computational Genomics, Computational and Chemical Biology, Fondazione Istituto Italiano di Tecnologia (IIT), Aosta, Italy. [5]Pediatric Neuropsychiatry, Healthcare agency of the Aosta Valley, Beauregard Hospital, Aosta, Italy. [6]Psychiatry, Healthcare agency of the Aosta Valley, Aosta, Italy. [7]Pediatrics, Healthcare agency of the Aosta Valley, Beauregard Hospital, Aosta, Italy. [8]Center for Human Technologies, Non-coding RNAs and RNA-based therapeutics, Italian Institute of Technology, Genova, Italy. [9]Immunogenetics and Transplant Biology Service, Città Della Salute e Della Scienza di Torino, University Hospital, Turin, Italy. [10]Area of Neuroscience, International School for Advanced Studies (SISSA), Trieste, Italy. [11]Center for Human Technologies, Computational and Chemical Biology, Fondazione Istituto Italiano di Tecnologia, Genoa, Italy. [12]Centre Européen de Calcul Atomique et Moléculaire (CECAM), Ecole Polytechnique Fédérale de Lausanne, Lausanne, Switzerland. [13]These authors contributed equally: Giovanni Spirito, Sara Trova. ✉e-mail: manuela.vecchi@iit.it; lobino@ausl.vda.it; stefano.gustincich@iit.it

PNAS RESEARCH ARTICLE | CELL BIOLOGY OPEN ACCESS

p63 and ZNF148 cooperate to regulate head and neck squamous cell carcinoma

Rosalba Pecorari[a,1], Mara Mancini[a,b,1], Artem Smirnov[a,b,1], Giacomo Corleone[c], Flavia Novelli[b,d], Anna Maria Lena[b], Mariacristina Franzese Canonico[b], Manuela Montanaro[b], Angela Cappello[b], Andrea Sacconi[e], Gabriella Misso[f], Michela Falco[f,g], Chiara Tammaro[f], Fabiola Ciccosanti[h], Mauro Piacentini[h], Manuel Scimeca[b], Michele Caraglia[f,g], Giovanni Blandino[i], Alessandro Mauriello[b], Maurizio Fanciulli[c], Gerry Melino[b], and Eleonora Candi[a,b,2]

Affiliations are included on p. 10.

Edited by Tak Mak, University of Toronto, Toronto, ON, Canada; received January 13, 2025; accepted May 29, 2025

Head and neck squamous cell carcinoma (HNSCC) is a common and aggressive malignancy. While significant advances have been made in the management of low-grade cancer, treatment of advanced HNSCC remains challenging. Here, we used a proteomic approach to find binding partners of the oncogene p63, the most frequently amplified transcription factor in HNSCC. We identified a zinc finger protein, ZNF148, which is coexpressed and physically binds p63 in carcinoma cells. Genome occupancy analyses identified a functional transcribed enhancer-derived RNA (eRNA) upstream of the CCND1 gene occupied by both factors. Mechanistically, p63 and ZNF148 control transcription of this eRNA, leading to overexpression of cyclin D1 to reinforce tumor cell proliferation. Importantly, this axis is specific for cancer cells and remains inactive in normal epithelial cells. The expression levels of these factors and the eRNA are positively correlated in cancer and associated with advanced stage and metastasis. Collectively, our data reveal a molecular pathway controlling HNSCC progression and identify potential selective targets for cancer treatment.

p63 | ZNF148 | cancer | CCND1 | transcription

Significance

Head and neck tumors are common and can become aggressive in advanced stages, making treatment challenging. Understanding the molecular mechanisms underlying tumor development is crucial. Oncogenic transcription factors like p63 drive cancer progression, but whether they require additional cofactors remains unclear. Using proteomics, we identified ZNF148, a zinc-finger protein that cooperates with p63. In tumor cells, p63 and ZNF148 bind to each other and colocalize on DNA to regulate shared target genes. Notably, they transcribe an enhancer RNA that controls the expression of cyclin D1, a protein critical for tumor growth. Our findings reveal a p63/ZNF148/cyclin D1 axis driving cancer progression, offering insights into the molecular basis of head and neck tumors.

Squamous cell carcinoma (SCC) comprises a diverse group of aggressive tumors with limited therapeutic options. SCC develops in epithelia of different origins, including the epidermis, lung, and upper aerodigestive tract (esophagus, larynxes, pharynxes, and tongue); SCCs originating in the upper aerodigestive tract are also called head and neck squamous cell carcinoma (HNSCC) (1). Limited progress has been so far accomplished for improving SCC patients' treatment outcomes and survival due to the poor understanding of SCC pathogenesis. Approximately 60% of patients are diagnosed with advanced-stage disease, and more than 60% develop recurrent disease or metastatic disease, with a 5-y overall survival rate lower than 50% (2, 3). Treatment often requires a multidisciplinary approach based on radiation, chemotherapy, chemoradiotherapy, and more recently, targeted and immunological therapies (4). Despite these efforts, there is an urgent need to improve diagnostic strategies for predicting cancer survival rates. Cervical lymph nodes are early sites of laryngeal squamous cell carcinoma (LSCC) metastases which, as a crucial prognostic factor, often indicates a change in survival expectations (5). Unfortunately, the early detection of nodal micrometastases is not possible by standard imaging techniques, with consequent detrimental effects on the selection of the correct therapeutic strategies and on the clinical outcomes of the patients. In fact, the identification of crucial determinants for cancer progression and metastasis is mandatory (6, 7). Accordingly, genes affecting cell cycle progression are commonly mutated (e.g., *CDKN2A* and *CDKN2N*), amplified (*CCND1* and *MYC*), or overexpressed (*CCND1*) (8–10). In addition to mutations of driver genes (*TP53, CDKN2A, PTEN, PIK3CA,* and *HRAS*), ancillary aberrations of genes regulating proliferation and squamous differentiation, such as *TP63*, contribute to squamous cell carcinogenesis. Indeed, genomic amplification of the *TP63* gene is observed in circa 30% of tumors, with very frequent overexpression (8–12). The transcription factor p63 is a master regulator of ectodermal fate (13–20). Deletion of p63 or the N-terminally truncated ΔNp63 isoform (hereinafter referred to as "p63") during embryonic development results in perinatal lethality due to the absence of simple/stratified epithelia, glands, and limbs resulting from defects in regenerative proliferation and differentiation (13–17). p63 binds epithelial enhancers to regulate a gene expression program required for epidermal development and homeostasis (20–24). In tumors, which predominantly express ΔN isoform, p63 deletion induces cancer regression, while forced p63 expression in normal epithelial cells is sufficient to bypass senescence

Author contributions: M.P., M.S., M.C., G.B., A.M., M. Fanciulli, G.M., and E.C. designed research; R.P., M. Mancini, A. Smirnov, G.C., F.N., A.M.L., M.F.C., M. Montanaro, A.C., A. Sacconi, G.M., M. Falco, C.T., and F.C. performed research; R.P., M. Mancini, A. Smirnov, G.C., F.N., A.M.L., M.F.C., M. Montanaro, A.C., A. Sacconi, G.M., M. Falco, C.T., F.C., M.P., M.S., M.C., G.B., A.M., M. Fanciulli, and G.M. analyzed data; and E.C. wrote the paper.

The authors declare no competing interest.

This article is a PNAS Direct Submission.

[1]R.P., M.M., and A.S. contributed equally to this work.

[2]To whom correspondence may be addressed. Email: candi@uniroma2.it.

This article contains supporting information online at https://www.pnas.org/lookup/suppl/doi:10.1073/pnas.2500579122/-/DCSupplemental.

Published July 7, 2025.

and drive tumorigenesis and stem-like proliferation, an observation that confirms that epithelial tumors depend on high levels of p63 (25–31). In principle, this dependence indicates a quantitative and qualitative difference in the p63-dependent transcriptional program between cancer and normal cells. To delineate the mechanism underlying the oncogenic activity of p63, we identified key p63 proximity partners using the in vitro proximity-dependent labeling technique proximity-dependent biotin identification (BioID) (32, 33). We identified a number of p63 binding proteins belonging to different chromatin-interacting complexes. We focused on the transcription factor zinc finger protein 148 (ZNF148), a member of the Krüppel-type (Cys2-His2-type) zinc finger family with four zinc finger domains (34–36). p63 and ZNF148 proteins bind chromatin to control a transcriptional program that promotes tumor cell proliferation in vitro and in primary tumors in vivo. Concomitant binding of p63 and ZNF148 to a specific enhancer located upstream of CCND1 led to the action of an enhancer-derived RNA (eRNA3) contributing to CCND1 transcription. Analysis in primary HNSCCs, including LSCC, revealed that the p63/ZNF148, eRNA3, and cyclin D1 expression levels are highly correlated with tumor stage and lymph node involvement. These findings confirm the robust cooperation of the two transcription factors p63 and ZNF148 as oncogenic drivers in HNSCC. Taken together, these data, by delineating the molecular mechanism of p63 and ZNF148 cooperation and transcriptional regulation of CCND1, indicate a potential therapeutic approach to counteract high-stage and invasive HNSCC cases.

Results

ZNF148 Is a Cofactor of p63. We used a proximity-dependent labeling approach (BioID) (37) using a minimal biotin ligase (BirA*)-FLAG to detect cofactors of p63. Proximal proteins were covalently labeled with biotin, allowing a harsh lysis, followed by streptavidin pull-down and subsequent protein identification by mass spectrometry (Fig. 1*A*) (38). The p63-negative tet-inducible Flp-In T-REx HEK293 cells were transfected to express the fused empty vector (EV)-BirA-FLAG or ΔNp63α-BirA-FLAG proteins (*SI Appendix*, Fig. S1*A*). Induced ΔNp63α-BirA-FLAG was active on *BPAG1* luciferase reporter and correctly localized in the nucleus (*SI Appendix*, Fig. S1*A*). Mass spectrometry analysis was performed in triplicates and 89 high-confidence p63 proximity partners were identified (Fig. 1*B* and Dataset S1), most of which were coexpressed with *TP63* in HNSCC tumors (Fig. 1*B*) and involved chromatin remodeling and gene transcription pathways (Fig. 1*C*). Importantly, we detected several previously described p63 cofactors (e.g., KMT2D and p73) (Dataset S1) (39, 40). Among the most represented interacting proteins, the expression of *ZNF148* was significantly correlated and coamplified with *TP63* in normal skin (R = 0.48) and normal esophagus (R = 0.25) and different cancer types such as HNSCC (R = 0.44), LUSCC (R = 0.35), and CESCC (R = 0.31) (Fig. 1*D* and *SI Appendix*, Fig. S1 *B* and *C*). Similarly, *TP63* and *ZNF148* were coexpressed and coamplified in carcinoma cell lines (Fig. 1*E* and *SI Appendix*, Fig. S1*C* and Tables S1 and S2). Therefore, we focused on ZNF148 as a cofactor of p63. Semiendogenous coimmunoprecipitation of ZNF148 or overexpressed ΔNp63α-HA in HEK293T cells (Fig. 1 *F* and *G*) demonstrated a robust physical interaction between the two proteins. An interaction between p63 and ZNF148 was also shown at the endogenous level in FaDu (Fig. 1*H*) and A253 (*SI Appendix*, Fig. S1*D*) HNSCC cell lines, predominantly expressing ΔNp63α isoform of p63. These observations were further confirmed using proximity ligation assay (PLA) (Fig. 1*I* and *SI Appendix*, Fig. S1*D*) using specific anti-pan-p63 and anti-ZNF148 antibodies. The specificity of interaction was confirmed by p63 and ZNF148 knock-down as well as by using an irrelevant IgG antibody. p63 and ZNF148 were also colocalized in normal and tumor tissues as evaluated by immunofluorescence and confocal analysis (Fig. 1*J*). Exogenous coimmunoprecipitation in HEK293T overexpressing domains of ΔNp63α (*SI Appendix*, Fig. S1*E*) or ZNF148 (*SI Appendix*, Fig. S1*F*) revealed that p63/ZNF148 interaction is mediated by the C-terminus of p63 and the N terminus of ZNF148. Altogether, we identify ZNF148 as a cofactor of p63 in squamous epithelia and HNSCC.

p63 and ZNF148 Share Common Binding Regions on Chromatin. To establish the direct transcriptional regulatory mechanisms of p63 and ZNF148 in HNSCC, we assessed genome-wide p63 and ZNF148 binding by chromatin immunoprecipitation followed by high-throughput sequencing (ChIP-seq) analysis of endogenous p63 and ZNF148 in FaDu (Fig. 2 *A* and *B* and *SI Appendix*, Fig. S2*A*). As expected, the canonical p53 family DNA binding motif was the most highly enriched motif among the p63 ChIP-seq peaks (Fig. 2*A*). Motif analysis of ZNF148 showed that it binds mostly to G-rich DNA sequences (Fig. 2*B*). p63-enriched loci (peaks) were located mainly within intronic (46%) and intergenic (46%) chromatin regulatory regions, and only a few were located in promoters (4%) (Fig. 2*A*) in line with previous reports (24). In contrast, 19% of the ZNF148 peaks were located within promoters (Fig. 2*B*). Direct validation by ChIP-qPCR of selected p63 binding regions in tumor cells confirmed the accuracy of the p63 occupancy profiling results (*SI Appendix*, Fig. S2*B*) (41, 42). Interestingly, ZNF148 cobinding was detected in the same regions, confirming for these two genes the ChIP-seq results (*SI Appendix*, Fig. S2*B*). Analysis of the enriched loci detected in the p63 and ZNF148 ChIP data revealed 5,188 overlapping peaks concurrently bound by p63 and ZNF148 (Fig. 2*C* and Dataset S2) that were associated with 2,860 genes (Dataset S3). KEGG pathway enrichment analysis identified "*Pathways in cancer*" as the most enriched set of genes occupied by both factors (Fig. 2*D*). Analysis of p63/ZNF148 co-occupancy on chromatin/chromosome regions identified two main regions, on chromosomes 9 and 11 (Fig. 2*E*). Interestingly, the region of co-occupancy on chromosome 11 corresponds to an amplified region in HNSCC that contains several genes potentially involved in HNSCC pathogenesis, such as *FADD, Myeov,* and *CCND1* (8, 10) (Fig. 2*F*). To identify possible p63–ZNF148 coregulated targets within this region, we performed p63 or ZNF148 knock-down experiments in FaDu cells and checked the levels of expression of the 9 out of 13 from this locus which are highly expressed in the HNSCC tumors based on TCGA HNSC data (*SI Appendix*, Fig. S2*C*). Of note, we used two distinct siRNAs against ZNF148 to exclude possible off-target effects. Results obtained by RT-qPCR analysis showed that *CCND1* was the only gene sensitive to the loss of either p63 or ZNF148 proteins (*SI Appendix*, Fig. S2*C*). Furthermore, considering that p63 is crucial to control the proliferation of epithelial cells (43–45) and that *CCND1* is a relevant gene in HNSCC and in other cancer types (45), we decided to focus on p63/ZNF148-dependent regulation of CCND1 expression. Collectively, these data indicate that the p63–ZNF148 complex regulates a common transcriptional program in squamous cell carcinoma cells.

p63 and ZNF148 Promote the Expression of *CCND1*. We conducted a survey to investigate the occupancy of p63 and ZNF148 at the *CCND1* locus within a 400 kb genomic window. Our analysis identified three distal regions, named Peak1, Peak2, and Peak3,

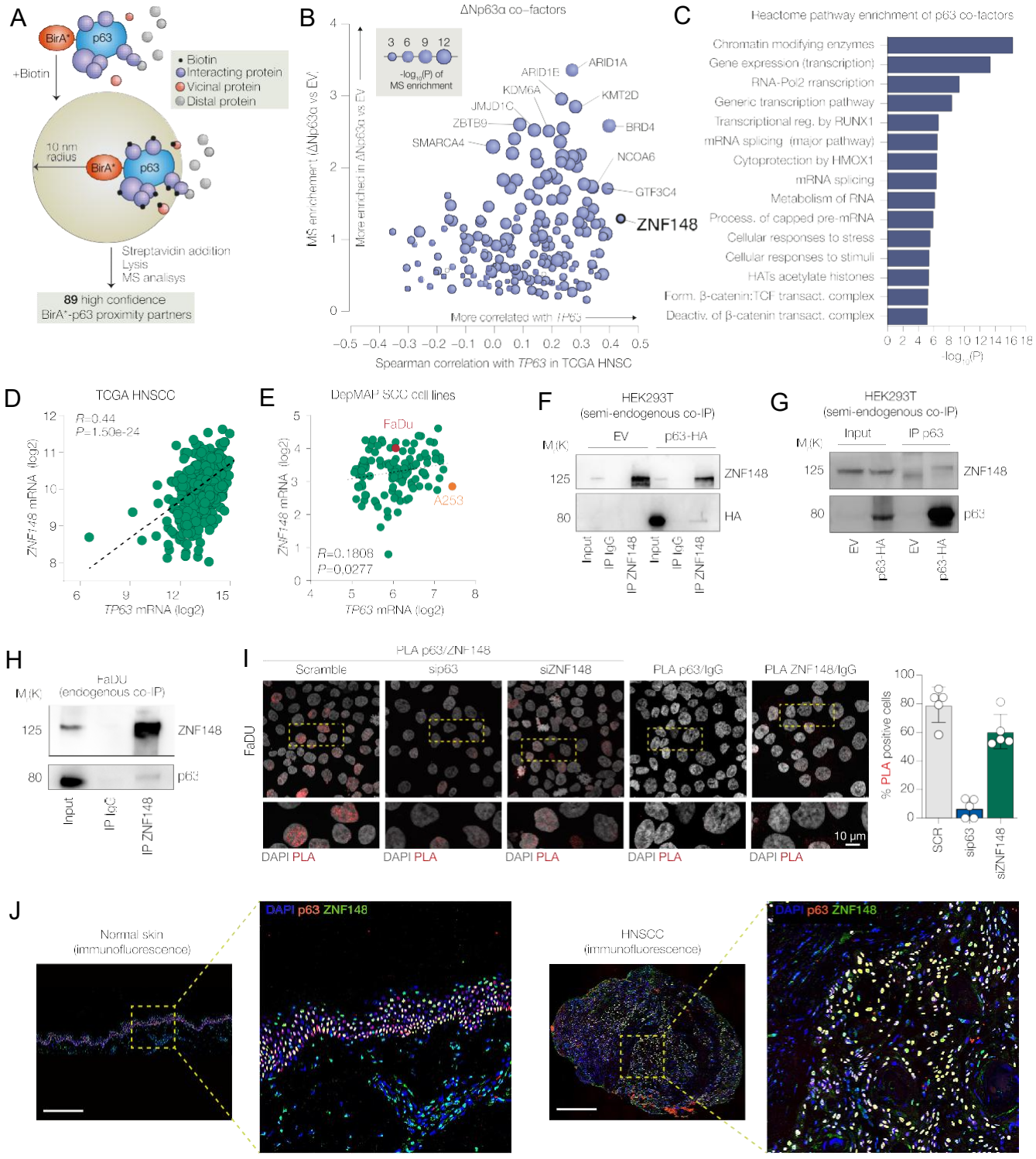

Fig. 1. ZNF148 is a cofactor of p63. (*A*) Schematic of the BioID-MS technique. (*B*) Volcano plot showing identified p63 proximity partners based on the MS enrichment (compared with EV) and *P* value as well as correlation of the mRNA expression with *TP63* levels in TCGA HNSC samples. (*C*) Bar plot showing Reactome pathway enrichment of identified cofactors of p63. (*D*) Scatter plots showing correlation between *TP63* and *ZNF148* expression in HNSCC samples (TCGA). (*E*) Scatter plots showing correlation between *TP63* and *ZNF148* mRNA expression in carcinoma cell lines (DepMAP). (*F*) Co-IP using anti-ZNF148 or anti-IgG antibodies in HEK293T cells transfected with either EV or ΔNp63α-HA. WB for ZNF148 and HA. (*G*) Co-IP using anti-p63 antibody in HEK293T cells transfected with either EV or ΔNp63α-HA. WB for ZNF148 and p63. (*H*) Co-IP using anti-ZNF148 antibody in FaDu cells. WB for p63 and ZNF148. (*I*) PLA between using p63 and ZNF148 or IgG antibodies in A253 knocked-down for p63 or ZNF148. Quantification of PLA-positive cells is shown on the *Right*. (*J*) Immunofluorescence of p63 and ZNF148 in normal skin (*Left*) or HNSCC tissue (*Right*). (Scale bar 200 μm.)

located upstream of the *CCND1* transcription start site (TSS). These regions showed a concomitant binding event of p63 and ZNF148 (Fig. 3*A*). To provide functional annotation for these regions, we used the Fantom 5 enhancer database. Interestingly, peaks 2 and 3 were classified as conserved enhancers (Fig. 3*A*). Furthermore, we observed a significant ZNF148 but not p63 binding on the *CCND1* promoter (Fig. 3*A*). Within the *CCND1* promoter, ZNF148 bound three proximal regions (Pr1, Pr2, and Pr3). ChIP–qPCR confirmed the presence of ZNF148 at the proximal sites (Fig. 3*B*). Of note, the same regions were

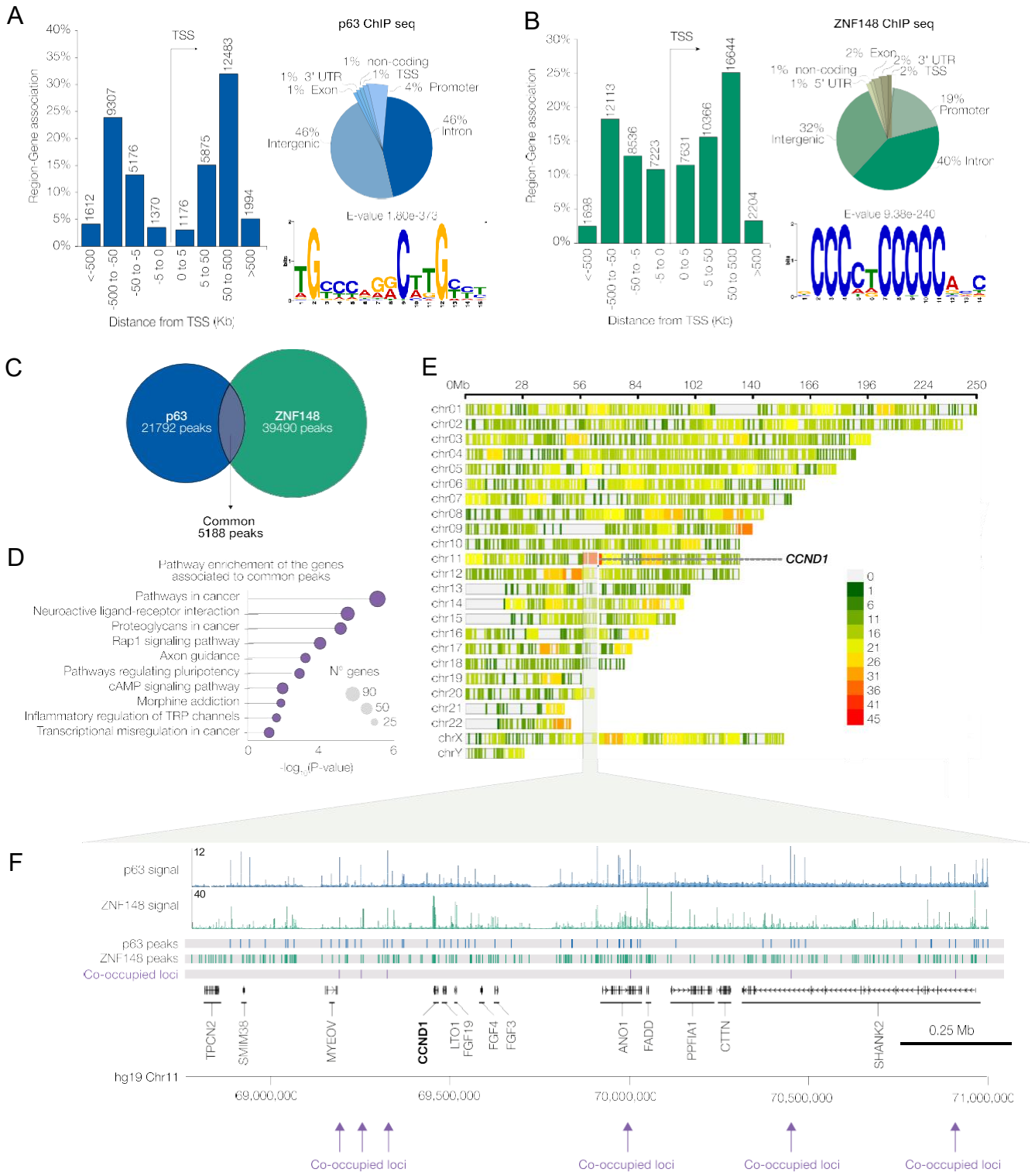

Fig. 2. p63 and ZNF148 share common binding regions on chromatin. (*A*) Bar plot (*Left*) and pie chart (*Right*) of the distribution of p63 ChIP seq peaks in FaDu cells. Identified binding motif is shown at the *Bottom*. (*B*) Bar plot (*Left*) and pie chart (*Right*) of the distribution of ZNF148 ChIP seq peaks in FaDu cells. Identified binding motif is shown at the *Bottom*. (*C*) Venn diagram showing the intersection of p63 and ZNF148 common peaks. (*D*) Pathway ontology of common p63 and ZNF148 peaks associated genes. (*E*) Co-occupancy analysis of p63 and ZNF148 peaks on chromatin in FaDu cells. (*F*) UCSC genome browser visualization of signal tracks of p63 and ZNF148 around CCND1 locus on chromosome 11. Single and shared peaks are shown. Co-occupied loci are shown by arrows.

enriched for H3K27ac active chromatin mark (Fig. 3*B*). The distal Peak1/2/3 regions were robustly bound by p63 and ZNF148 (Fig. 3*C*) confirming our ChIP seq data, and these regions were enriched for H3K27ac (Fig. 3*C*). However, ChIP-re-ChIP assay showed that only Peak3 was significantly bound by both p63 and ZNF148 simultaneously (Fig. 3*D*). Interestingly, FaDu and A253 cells knocked-down for p63 or ZNF148 (*SI Appendix*, Fig. S3*A*) exhibited reduced CCND1 mRNA and protein level (Fig. 3*E* and *SI Appendix*, Fig. S3*B*). Previous work has shown that p63 associates with Dnmt3a to activate target enhancers that affect epidermal stem cell functions (46). Therefore, we analyzed the role of the p63/ZNF148 complex at enhancer-derived RNAs (*eRNAs*). We then investigated whether the selected regions produced transcribed *eRNAs*, and by RT–qPCR, we found that

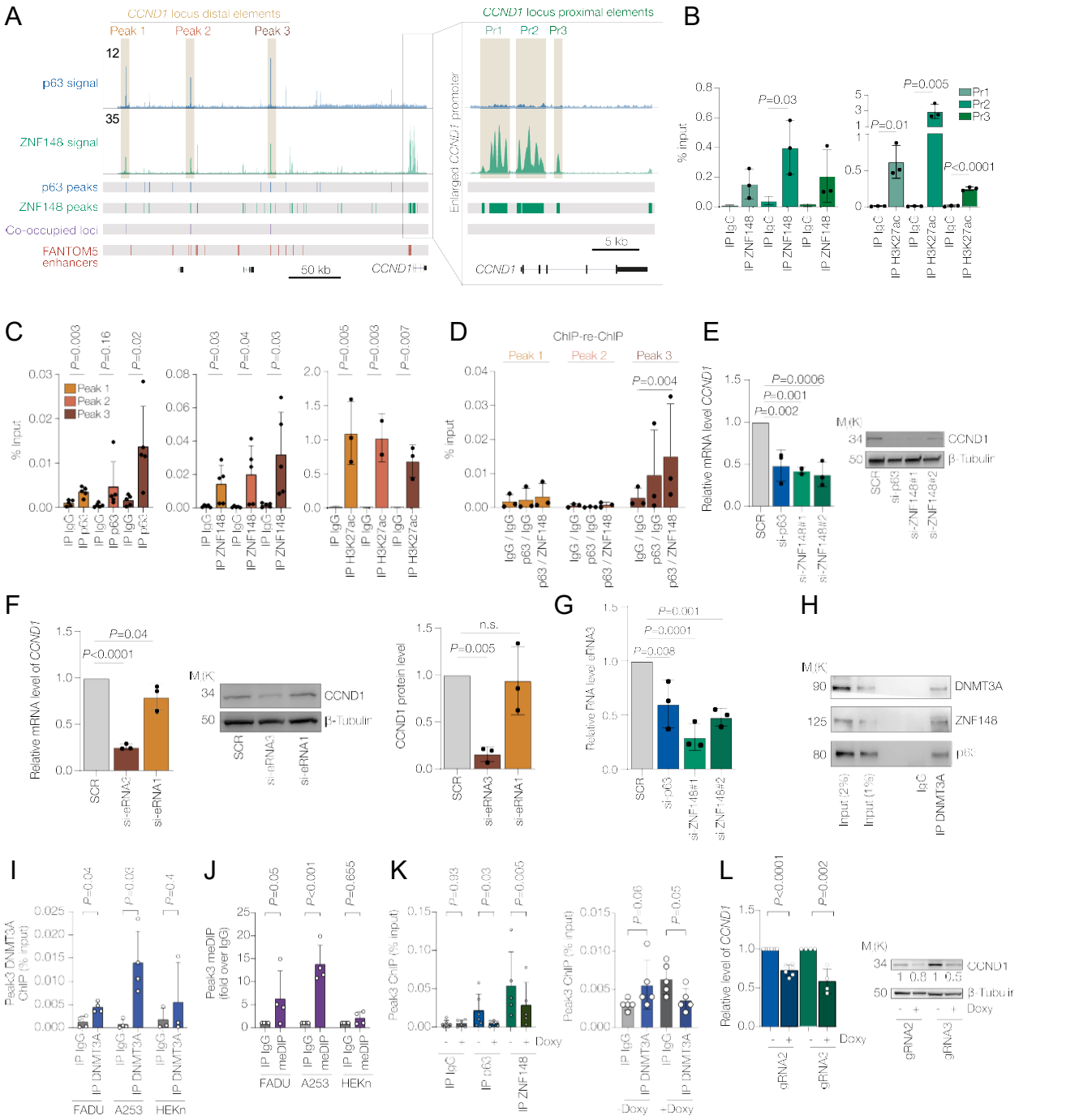

Fig. 3. p63 and ZNF148 promote the expression of CCND1. (*A*) UCSC genome browser visualization of signal tracks of p63 and ZNF148 around *CCND1* locus on chromosome 11. Single peaks, shared peaks, and FANTOM5 enhancers are shown. Enlarged *CCND1* promoter region is shown on the *Right*. Putative distal (Peak1/2/3) and proximal (Pr1/2/3) regulatory elements are highlighted by beige shading. (*B*) ChIP-qPCR analysis of ZNF148 and H3K27ac occupancy on proximal *CCND1* promoter regions Pr1/2/3. Data are shown as mean ± SD. $n = 3$ (biological replicates). *P* by Student's *t* test. (*C*) ChIP-qPCR analysis of p63, ZNF148, and H3K27ac occupancy on distal *CCND1* regions Peak1/2/3. Data are shown as mean ± SD. $n = 3$-4 (biological replicates). *P* by Student's *t* test. (*D*) ChIP-re-ChIP qPCR analysis of p63/ZNF148 co-occupancy on distal *CCND1* regions Peak1/2/3. Data are shown as mean ± SD. $n = 3$ (biological replicates). *P* by two-way ANOVA. (*E*) CCND1 mRNA and protein levels in FaDu cells transfected with p63 or ZNF148 (#1 and #2) siRNAs for 48 h. Data are shown as mean ± SD. $n = 3$ (biological replicates). *P* by one-way ANOVA. β-tubulin as a loading control. (*F*) CCND1 mRNA and protein levels in FaDu cells transfected with eRNA1 or eRNA3 siRNAs for 48 h. Data are shown as mean ± SD. $n = 3$ (biological replicates). *P* by one-way ANOVA. β-tubulin as a loading control. (*G*) eRNA3 levels in FaDu cells transfected with p63 or ZNF148 (#1 and #2) siRNAs for 48 h. Data are shown as mean ± SD. $n = 3$ (biological replicates). β-tubulin as a loading control. (*H*) Co-IP using anti-DNMT3A or anti-IgG antibodies in FaDu cells. WB for DNMT3A, ZNF148, and p63. (*I*) ChIP-qPCR analysis of DNMT3A occupancy on Peak3 in FaDu, A253, and HEKn cells. Data are shown as mean ± SD. $n = 4$ (biological replicates). *P* by Student's *t* test. (*J*) meDIP-qPCR analysis of methylated DNA within Peak3 region in FaDu, A253, and HEKn cells. Data are shown as mean ± SD. $n = 4$ (biological replicates). *P* by Student's *t* test. (*K*) (*Left*) ChIP-qPCR analysis of p63 and ZNF148 occupancy on Peak3 in CRISPR/Cas9 FaDu clones after 72 h induction with 2 μg/mL of doxycycline. Data are shown as mean ± SD of $n = 6$ individual clones. *P* by Student's *t* test. (*Right*) ChIP-qPCR analysis of DNMT3A occupancy on Peak3 in CRISPR/Cas9 FaDu clones after 72 h induction with 2 μg/mL of doxycycline. Data are shown as mean ± SD of $n = 5$ individual clones. *P* by Student's *t* test. (*L*) CCND1 mRNA and protein levels in CRISPR/Cas9 FaDu clones after 72 h induction with 2 μg/mL of doxycycline. Data are shown as mean ± SD of $n = 4$ to 6 individual clones per gRNA. *P* by Student's *t* test. β-tubulin as a loading control.

peak1 and peak3 corresponded to actively transcribed enhancers (named *eRNA1* and *eRNA3*, respectively) (*SI Appendix*, Fig. S3*C*). *eRNA1* and *eRNA3* knockdown (*SI Appendix*, Fig. S3*D*) revealed that only *eRNA3* regulates cyclin D1 expression at both the mRNA and protein levels (Fig. 3*F*). Of note, the Peak3 region is bound by p63 also in other cell types based on published ChIP

seq datasets (*SI Appendix*, Fig. S3*E*). Moreover, eRNA3 is directly regulated by p63 and ZNF148 binding to DNA, as p63 and ZNF148 knockdown significantly decreased *eRNA3* expression (Fig. 3*G*). As described for epidermal stem cells, we hypothesized that p63 and ZNF148 were components of a larger complex containing DNMT3A bound to chromatin at the Peak3 region. In fact, endogenous coimmunoprecipitation indicated physical interactions between p63, ZNF148, and DNMT3A (Fig. 3*H*). In addition, ChIP–qPCR experiments showed strong enrichment of DNMT3A in the region corresponding to Peak3. This enrichment was significant only on cancer cell lines FaDu and A253 but not in normal keratinocytes HEKn (Fig. 3*I*). Of note, p63 or ZNF148 silencing significantly reduced the binding of DNMT3A to the Peak3 region (*SI Appendix*, Fig. S3*F*). Furthermore, we saw an enrichment of methylated DNA within Peak3 region in FaDu and A253 cells but not in HEKn (Fig. 3*J*). In line with these observations, we did not see a significant enrichment of p63 or ZNF148 at the Peak3 in HEKn and *eRNA3* expression was undetectable in HEKn (*SI Appendix*, Fig. S3 *G* and *H*). In addition, low levels of DNMT3A expression was detected in HEKs as compared with FaDu and A253 cell lines and in normal tissues (NTs) compared with HSNCC from TCGA and GTEx databases (*SI Appendix*, Fig. S3*I*). These data underline the importance of epigenetic remodeling of this region in the regulation of *CCND1* expression in cancer cells. To prove this mechanism, we utilized two specific guides (gRNA2 and gRNA3, *SI Appendix*, Fig. S3 *I* and *J*) to perform CRISPR/Cas9-mediated deletion of the p63 and ZNF148 binding sites in peak3 (*SI Appendix*, Fig. S3*J*). The doxycycline-responsive inducible CRISPR/Cas9 system was employed to delete the p63/ZNF148 binding sites, resulting in a decrease in p63, ZNF148, and DNMT3A binding to the Peak3 region (Fig. 3*K*). This decrease in binding was accompanied by a decrease in *CCND1* mRNA and protein levels (Fig. 3*L*). Taken together, these data demonstrate the ability of the p63/ZNF148/DNMT3A complex to bind the Peak3 region in cancer cells, thus allowing the activation of eRNA3 to promote *CCND1* expression.

p63 and ZNF148 Control HNSCC Cell Proliferation. We then examined the effect of reducing cyclin D1 expression in HNSCC cells in the context of p63 or ZNF148 silencing. We examined downstream signaling by evaluating the expression of retinoblastoma protein (pRB) in three SCC cell lines (FaDu, A253, Fig. 4; HN30, *SI Appendix*, Fig. S4). In cells transfected with the scrambled siRNA sequence, cyclin D1 and retinoblastoma protein (pRB) were expressed at normal levels, and pRB was phosphorylated (S796, ppRB). However, in cells where p63 or ZNF148 was silenced, the levels of cyclin D1, pRB, and ppRB were significantly reduced or undetectable (Fig. 4 *A* and *B* and *SI Appendix*, Fig. S4 *A* and *B*). To further confirm these data, we analyzed the impact of p63 and ZNF148 knockdown in the three HNSCC cell lines and observed a significant impact on cell proliferation by a clonogenic assay (Fig. 4*C*), growth curve analysis (Fig. 4*D* and *SI Appendix*, Fig. S4*C*), and quantification of the number of cells in S phase (Fig. 4*D* and *SI Appendix*, Fig. S4*D*). An additional siRNA against p63 resulted in a similar phenotype in FaDu and A253 cells (*SI Appendix*, Fig. S4 *E* and *F*). Of note, we observed a variability in the effect of long-term knock-down in clonogenic assays, however, this is likely to be related to variable efficiency and stability of used siRNAs. Indeed, knock-down of with additional siRNAs against p63 or ZNF148 in FaDu and A253 cells led to a strong reduction of number of clones in most of siRNAs tested in FaDU and A253 cells (*SI Appendix*, Fig. S4*G*). Notably, the three cell lines examined (FaDu, A253, and HN30) have different p53 statuses (referring to whether the gene is mutated, null, or wild type), suggesting that the finding described is not influenced by p53 status (*SI Appendix*, Fig. S4*H*), even though p53 is a binding partner of ZNF148 in other cancer types (47).

We confirmed our findings also in doxycycline-inducible shZNF148 FaDu cells (Fig. 4*E*). Doxycycline treatment led to a reduction of the number of clones and proliferation rate (*SI Appendix*, Fig. S4*I*). We then injected Tet-On FaDu-shZNF148 cells in ultraimmunodeficient B-NDG mice and treated the animals with drinking water with or without doxycycline. Mice which received doxycycline had significantly smaller tumors (Fig. 4 *F* and *G*) and lower expression of ZNF148 and Ki67 (Fig. 4*H* and *SI Appendix*, Fig. S4*J*) compared to the control littermates. Furthermore, we observed a reduction of eRNA3 foci in nuclei of tumors from doxycycline-treated mice as assessed by FISH staining of samples (Fig. 4*I*). Importantly, CRISPR/Cas9-mediated modification of the peak3 region using gRNA2 and gRNA3 in FaDu cells led to modest yet significant reduction of the number EdU-positive cells (Fig. 4*J*). These data reveal that p63, along with its cobinding factor ZNF148 and the contribution of *eRNA3*, directly control the proliferation of HNSCC cells.

The p63/ZNF148/CCDN1 Axis Is Associated with HNSCC Aggressiveness. To assess the impact of the p63/ZNF148/*eRNA3*/CCND1 axis in tumors, we examined by RT-qPCR the expression of these genes in LSCC at different stages. Forty-eight samples of tumor tissue and the adjacent normal counterpart tissue were collected from patients diagnosed with LSCC and undergoing surgical resection. The clinical characteristics of the enrolled patients are shown in *SI Appendix*, Table S3. *eRNA3* showed higher values of RT-qPCR amplification compared with *eRNA1* and *eRNA2* (*SI Appendix*, Fig. S5*A*), furthermore, *eRNA1* and *eRNA2* amplification values were similar to negative controls, suggesting that these two *eRNAs* were not expressed in tumors (*SI Appendix*, Fig. S5*B*). At the transcriptional level, we observed a significant increase in *eRNA3* and *ZNF148* expression in stage III–IV tumor tissues compared to either NT or stage I–II tumor tissues. Moreover, a significant increase in *TP63* and *CCND1* expression was detected in stage III–IV tumor tissues compared to their normal adjacent counterparts (Fig. 5*A*). Interestingly, the expression of *eRNA3* was strongly correlated with that of *TP63*, *ZNF148*, and *CCND1* (Pearson R = 0.78, R = 0.91, and R = 0.87, respectively; Fig. 5*B*) in all tumor samples. The expression of *CCND1* was also strongly correlated with that of *TP63* and *ZNF148* (*SI Appendix*, Fig. S5 *C* and *D*). Notably, *eRNA3* expression was more strongly correlated with that of *TP63*, *ZNF148*, and *CCND1* in stage III–IV tumor tissue than in stage I–II tumor tissue (*SI Appendix*, Fig. S5*E*), confirming the relevance of the *eRNA3* transcript in aggressive LSCC. Lymph node-positive (LN+) laryngeal tumors showed a trend toward or significantly increased expression of *TP63*, *ZNF148*, *CCND1*, and *eRNA3* compared with lymph node-negative (LN−) tumors (Fig. 5*C*). Furthermore, in LN+ tumors, *TP63*, *ZNF148*, and *CCND1* expression was significantly correlated with *eRNA3* expression (Fig. 5*D*) and the correlation was stringer compared with LN- tumors (*SI Appendix*, Fig. S5*E*). Collectively, our data suggest that the most aggressive type of LSCC exhibits combined high mRNA levels of *TP63*, *ZNF148*, *CCND1*, and *eRNA3*.

To investigate whether the expression pattern at the translational level was consistent with the above-mentioned findings and to extend the results from LSCC to other HNSCC types, we analyzed the expression of p63, ZNF148, cyclin D1, and the proliferation marker Ki67 using a tissue microarray containing 70 HNSCC FFPE samples. The 70 samples were of different stages and from different anatomical sites (*SI Appendix*, *Methods*), with

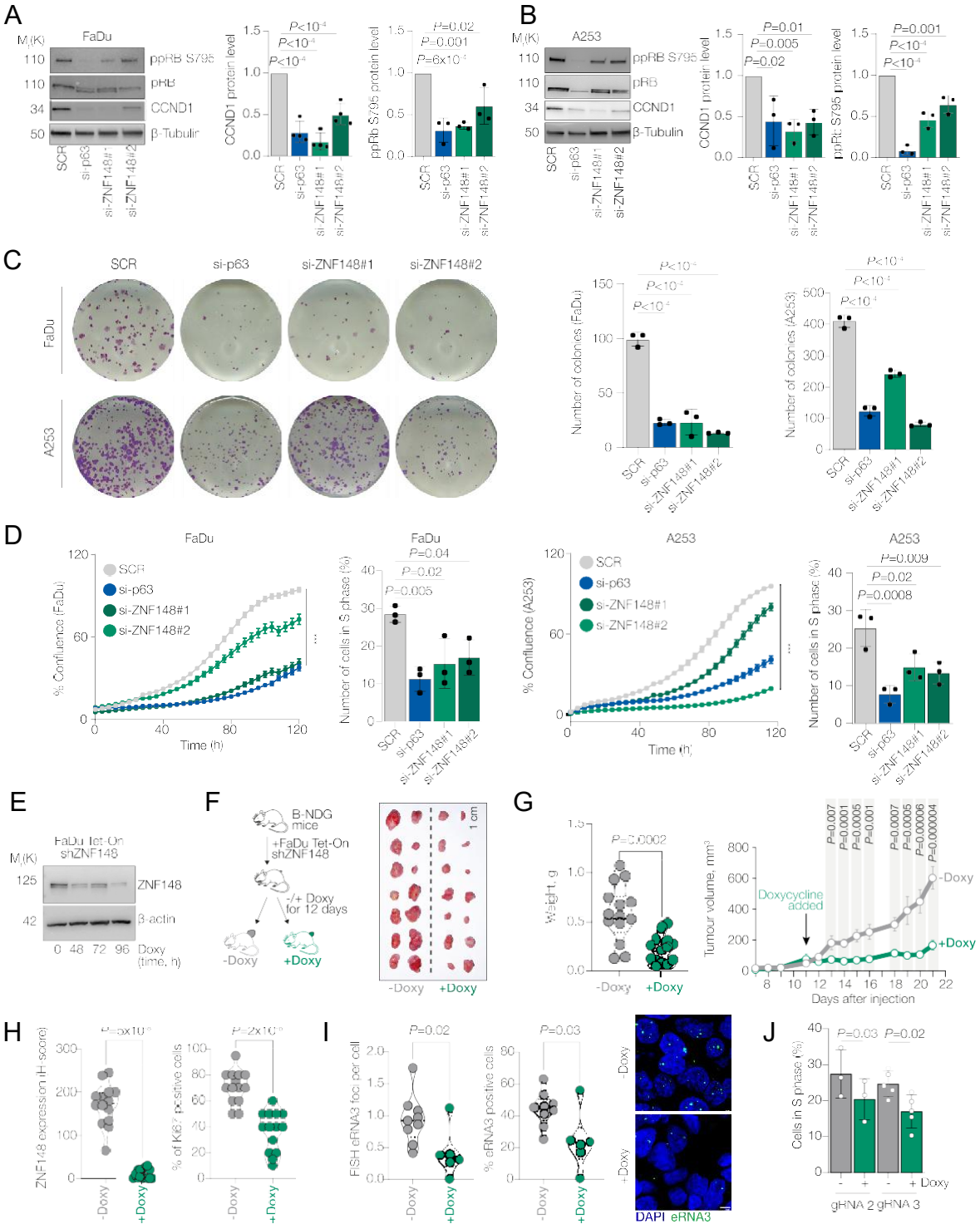

Fig. 4. p63 and ZNF148 control HNSCC cell proliferation. (*A*) CCND1, pRb, and ppRb S795 protein levels in FaDu cells transfected with p63 or ZNF148 (#1 and #2) siRNAs for 48 h. (*Right*) Densitometry of CCND1 and ppRb S795 protein levels in the same samples. Data are shown as mean ± SD. n = 3-4 (biological replicates). P by one-way ANOVA. β-tubulin as a loading control. (*B*) CCND1, pRb, and ppRb S795 protein levels in A253 cells transfected with p63 or ZNF148 (#1 and #2) siRNAs for 48 h. (*Right*) Densitometry of CCND1 and ppRb S795 protein levels in the same samples. Data are shown as mean ± SD. n = 3-4 (biological replicates). P by one-way ANOVA. β-tubulin as a loading control. (*C*) Clonogenic assay of FaDu or A253 cells transfected with p63 or ZNF148 (#1 and #2) siRNAs. Representative images (*Top*) and bar plots showing the number of clones (*Bottom*) are shown. Data are shown as mean ± SD. n = 3-4 (biological replicates). P by one-way ANOVA. (*D*) Growth curve and EdU incorporation assay in the FaDu (*Top*) or A253 (*Bottom*) cells transfected with p63 or ZNF148 (#1 and #2) siRNAs. Data are shown as mean ± SEM (growth curve) or SD (EdU incorporation assay). n = 3 (biological replicates). P by one-way ANOVA. (*E*) Western blot analysis of ZNF148 expression in FaDu Tet-On shZNF148 inducible cells. β-actin as a loading control. (*F*) Xenograft tumors of FaDu Tet-On shZNF148 inducible cells in immunodeficient B-NDG mice. Cartoon depicts workflow of experiment. Photograph shows harvested doxycycline-inducible FaDu-shZNF148 tumors. (Scale bar 1 mm.) n = 7 mice for each group. (*G*) (*Left*) Violin plot showing weight of harvested tumors. P by one-way ANOVA. (*Right*) Line plot showing tumor volume in time. P by one-way ANOVA compared with "no doxy." (*H*) Violin plots showing H-scores of ZNF148 expression (*Left*) or % of Ki67 positive cells (*Right*) in tumors from (*F*). (*I*) Violin plots showing mean number of FISH eRNA3 foci per cell (*Left*) or number of eRNA3 positive cells (>0 FISH foci) in samples from (*F*). n = 4 (no doxy) and n = 3 (doxy) mice. P by one-way ANOVA. Representative FISH images are shown on the *Right*. (*J*) EdU incorporation assay of CRISPR/Cas9 FaDu clones after 72 h induction with 2 μg/mL of doxycycline. Data are shown as mean ± SD of n = 3-5 individual clones. P by one-way ANOVA.

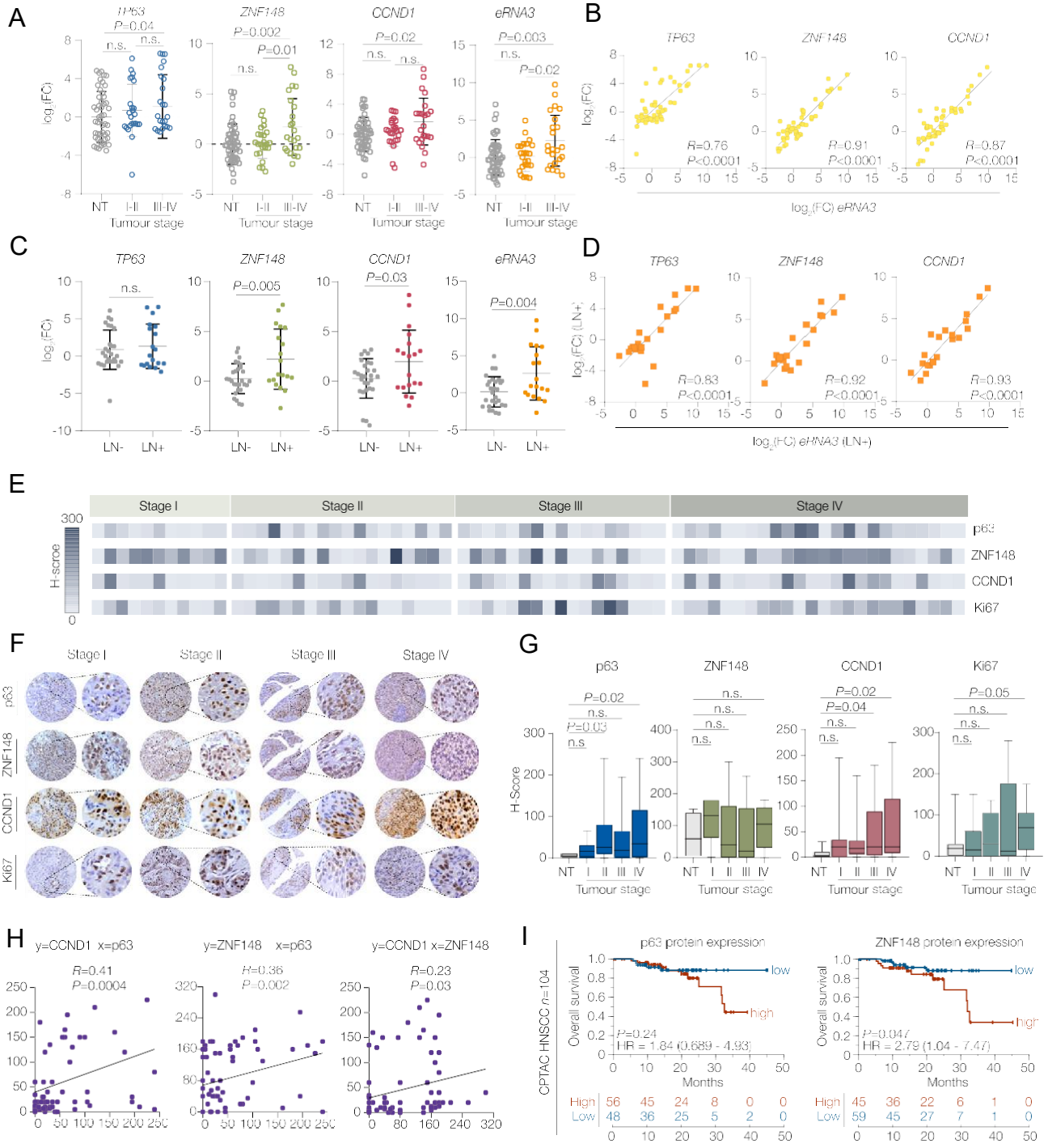

Fig. 5. The p63/ZNF148/CCND1 axis is associated with HNSCC aggressiveness. (*A*) *TP63*, *ZNF148*, *CCND1*, and *eRNA3* mRNA levels in clinical samples. NT, $n = 48$; I–II (tumor tissue stage I–II), $n = 24$; III–IV (tumor tissue stage III–IV), $n = 24$. *P* by Student's *t* test. (*B*) Correlation between *TP63*, *ZNF148*, *CCND1*, and *eRNA3* RNA levels in clinical samples. $n = 48$. (*C*) *TP63*, *ZNF148*, *CCND1*, and *eRNA3* mRNA levels in clinical samples. LN- (nonlymph nodes metastasis), $n = 30$; LN+ (lymph nodes metastasis), $n = 18$. *P* by Student's *t* test. (*D*) Correlation between *TP63*, *ZNF148*, *CCND1*, and *eRNA3* RNA levels in clinical samples. LN+ (lymph nodes metastasis), $n = 21$. (*E*) Heatmap of p63, ZNF148, CCND1, and Ki67 TMA (Tissue Micro Array) histological scores of expression (H-scores). (*F*) Representative TMA spots of p63, ZNF148, CCND1, and Ki67 at stage I, stage III, and stage IV (scale bar, 50 μm, scale bar, 10 μm). (*G*) Bar plot of p63, ZNF148, CCND1, and Ki67 H-score in NT or tumor samples based on stages. *P* by Student's *t* test. (*H*) Pearson correlation between p63, ZNF148, and CCND1 levels in samples from (*E*). (*I*) The Kaplan–Meier survival plots of HNSCC patients from the CPTAC study based on p63 or ZNF148 protein expression levels.

10 samples of NTs included as controls (*SI Appendix*, Fig. S5*F*). We observed significantly increased p63 and cyclin D1 protein expression in samples of advanced stages, accompanied by high Ki67 expression levels (Fig. 5 *E*–*G*). The ZNF148 protein level did not increase with increasing tumor stage. However, it was strongly positively correlated with both p63 and cyclin D1 expression in all the tumor samples analyzed (Fig. 5*H*). In addition, the strong correlation between the expression of p63, ZNF148, and CCND1 and that of the proliferation marker Ki67 (*SI Appendix*, Fig. S5*G*) confirmed the crucial role of these transcription factors in HNSCC proliferation. Finally, high ZNF148 protein levels were significantly associated with worse prognosis of HNSCC patients from the CPTAC study, moreover, p63 expression followed a similar trend although without reaching a statistical significance (Fig. 5*I*). Collectively, these data demonstrate that in human HNSCC, p63, acting together with ZNF148 through the

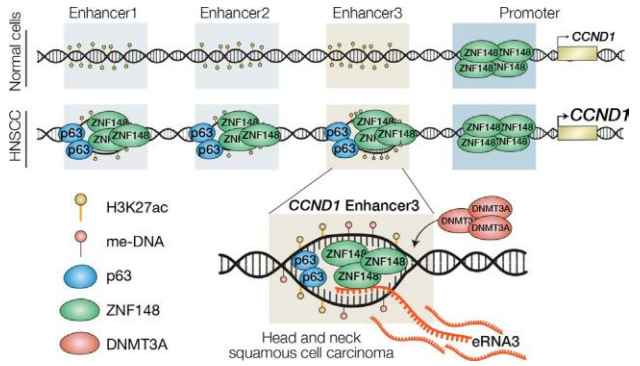

Fig. 6. p63–ZNF148 complex regulated CCND1 expression in HNSCC. Graphical representation of the enhancer regions upstream of the *CCND1* TSS. In HNSCC, p63–ZNF148–DNMT3A complex is recruited on the enhancer 3 region (peak 3) upstream of the *CCND1* TSS. ZNF148 also binds the *CCND1* promoter. p63/ZNF148 complex is important to drive uncontrolled proliferation in HNSCC.

regulation of eRNA3, sustains cyclin D1 expression to drive HNSCC proliferation associated with aggressive disease (Fig. 6).

Discussion

Here, we show that ZNF148 (also called Zfp148 and ZBP-89) is an important binding partner in p63-driven tumorigenesis. ZNF148 belongs to the Krüppel-type (Cys2-His2-type) zinc finger family, with four zinc finger domains and ubiquitous expression (48). It also has a bifunctional regulatory domain, indicating that it acts both as an activator and a repressor (49, 50). ZNF148 interacts directly with p53 through its zinc finger domain and indirectly with the histone acetyltransferase and transcriptional coactivator p300 through its amino terminus (51, 52), although its role in modulating p53 activity and in cancer is not fully defined. ZNF148 also contributes to IFNγ-mediated apoptosis (53). In cancer, ZNF148 seems to regulate the expression of proteins involved in invasion, epithelial–mesenchymal transition, and genomic instability (36, 54–57), and it is overexpressed in tumor tissues and cell lines of many cancers, including gastric cancer, colorectal cancer, melanoma, hepatocellular carcinoma, and oesophageal squamous cancer (51, 53, 58, 59). Nonetheless, its role as an oncogenic factor in humans has not been firmly established. Our experimental evidence defines a p53-independent oncogenic function of ZNF148 in HNSCC. ZNF148 is significantly coexpressed and coamplified with p63 in HNSCC, and ZNF148 and p63 physically associate and are highly coexpressed with cyclin D1. The ZNF148/p63 complex acquires an oncogenic function, strongly contributing to CCND1 overexpression through the transcriptional activity of an active enhancer and/or a transcribed enhancer RNA (*eRNA3*). CCND1 is commonly amplified (29 to 39%) or overexpressed (20 to 68%) in HNSCC (8, 10). HNSCCs exhibit mutually exclusive subsets of genomic aberrations, including amplicons on chromosome 11q, which contains the *CCND1* gene, or on chromosome arm 3q, which includes the *TP63* transcription factor. Interestingly, our findings led to the identification of a pathway based on p63/ZNF148 cooperative binding activity, which is responsible for cyclin D1 overexpression. More remarkably, concomitant binding of p63–ZNF148 and DNMT3a at *CCND1* enhancer regions followed by *eRNA3* transcription has not been identified in normal epithelial cells (i.e., HEKn), indicating that the epigenetic state of the *eRNA3* locus is different among cancer cells and normal epithelial cells. These observations, suggest that the transcription of *eRNA3* leads to a cancer-specific boost of CCND1 expression.

CCND1 is an established human oncogene, and the identification of two mechanisms leading to CCND1 transcription in cancer, namely, ZNF148 binding at the CCND1 promoter and p63/ZNF148/*eRNA3* binding at the enhancer, revealed a potentially interesting therapeutic approach. In fact, in addition to cyclin D1 protein turn-over and treatment with its associated CDK inhibitors, a possible alternative approach to target cyclin D1 in cancer involves the use of small molecules that can reduce CCND1 transcription (45), and the use of these small molecules in combination with therapies targeting multiple targets of cyclin D1 activity might provide therapeutic advantages in counteracting cancer formation and invasion. We validated our findings in an independent cohort of HNSCC patients, thus confirming that p63, ZNF148, and CCND1 exhibited significantly increased mRNA (48 patients analyzed) and protein (70 patients analyzed) expression levels and were coexpressed in stage III–IV tumors compared to stage I–II tumors, as well as in more aggressive lymph node-positive tumors. The *eRNA3* expression level paralleled those of p63, ZNF148, and cyclinD1 and was thus correlated with tumor aggressiveness and invasiveness.

In summary, we have identified a p63/ZNF148-driven oncogenic mechanism leading to the transcription of *CCND1* in HNSCC. The potential relevance of these findings is based not only on the role of cyclin D1 in controlling cell cycle progression, and thus the production of cells with uncontrolled proliferation, but also on the identification of distinct biomarkers (ZNF148 and *eRNA3*) and the stratification of tumors associated with specific adverse events. In conclusion, we demonstrate that ZNF148 is a component of the oncogenic machinery in HNSCCs and suggest that therapeutic interventions specifically targeting the ZNF148/p63 complex or *eRNA3* or at least suppressing ZNF148-mediated cyclin D1 transcription might lead to potentially innovative approaches for the treatment of these cancers.

Materials and Methods

Cell lines, Transfection, Proliferation, Growth Curve, and Clonogenic Assay. FaDu cells, a pharyngeal squamous cell carcinoma cell line, were obtained from ATCC and were cultured in Eagle's Minimum Essential Medium (EMEM, Corning 10-009-CV). A253 cells, a submaxillary salivary gland carcinoma cell line, were obtained from ATCC and were cultured in McCoy's 5A+ GLUTAmax (Thermo Fisher 36600088). HN30 cells, a pharyngeal squamous cell carcinoma cell line, were a gift and were cultured in Dulbecco's modified Eagle's medium (DMEM, Corning 10-102-CVR). HEK293T, an epithelial embryonal kidney cell line, was obtained from ATCC and cultured in Dulbecco's modified Eagle's medium (DMEM, Corning). The 293Flp-In TREx cells (Invitrogen) were grown in Dulbecco's Modified Eagle's Medium (DMEM, Corning) supplemented with 10% fetal bovine serum tet free (FBS-Tetracycline free, Thermo Fisher), human neonatal epidermal keratinocytes (HEKn) were purchased from Thermo Fisher (C0015C) and grown in EpiLife medium (Thermo Fisher, MEPI500CA). All cell lines were grown at 37 °C and 5% CO2 in a humidified atmosphere; a mix of penicillin, and streptomycin (100 U/mL) was added to the specific growth medium supplemented with 10% fetal bovine serum (FBS, Thermo Fisher). Specific siRNA (*SI Appendix*, Table S4, two specific siRNA sequences for p63, sip63-1 and sip63-2, and for ZNF148, siZNF148-1 and siZNF148-2, were used) transfections for silencing were performed with Lipofectamine RNAiMax Transfection Reagent (Invitrogen, Carlsbad, CA) according to the manufacturer's protocol. Cells were collected and analyzed 48 h after transfection. Plasmid DNA transfections were performed with both Lipofectamine® 2000 or 3000 (Invitrogen) according to the manufacturer's instructions. To measure proliferation rate, cells were labeled with 10 μM EdU and processed with a Click-iT EdU Alexa Fluor-488 flow cytometry assay kit (Invitrogen C10337). For EdU assay, the cell cycle was analyzed using a CytoFLEX cytometer (Beckman Coulter). A total of 12,000 events were evaluated. Cell growth was evaluated by seeding cells in 96 well-cell plates after 48 h of transfection with p63 (p63#1 and p63#2) and ZNF148 (ZNF148#1 and ZNF148#2) siRNAs. The cell growth was monitored every 3 h for 6 d using the Incucyte S3 live cells analysis system (Sartorius) and the related software was used to make growth curve.

Finally, the ability of FaDu and A253 cells to form colony after p63 or ZNF148 silencing was assayed by plating 100 cells per well in six-well cell plates. At the end of the assay, cells were washed with PBS and subjected to a mixture of 6.0% glutaraldehyde and 0.5% crystal violet for 15 min. The cells were washed with water, dried at room temperature, and the number of colonies was evaluated.

Human Biopsies Collection and Processing. Forty-eight LSCC patients enrolled for the study were new cases without other severe clinical disorders and before the onset of any therapy (See *SI Appendix*, Table S3 for clinical information). All patients were recruited from a series of Italian Hospitals agreeing to the program for LSCC samples collection. The study was approved by the University of Campania "L. Vanvitelli" Ethical Committee (Prot. 0025445/i). Informed consent was signed by each patient. Paired LSCC and non-tumor tissue samples were collected through surgical resection and tumor specimens were confirmed by histopathological analysis. Tissues were put into RNAlaterTM Stabilization solution (Invitrogen; catalogue AM7021) and stored at −80 °C until RNA extraction. Gene expression was assessed by RT-qPCR.

Other methods are included in *SI Appendix*.

Data, Materials, and Software Availability. All study data are included in the article and/or supporting information.

ACKNOWLEDGMENTS. We thank Prof. Massimiliano Agostini for discussion and support. This work was mainly supported by Ministry of Health PNRR-MAD-2022-12375755 project (to E.C.) and partially supported by IDI-IRCCS (R.C.), Grant RF-2019-12368888 (to E.C.), European Union Next Generation EU (M4C1 2022WW4J4B_001, CUP E53D23007320006), and Associazione Italiana Ricerca sul Cancro under (IG 2024-ID 31044) to E.C.

Author affiliations: [a]Istituto di Ricovero e Cura a Carattere Scientifico Istituto Dermopatico dell'Immacolata (IDI-IRCCS), Biochemistry Laboratory, Rome 00144, Italy; [b]Department of Experimental Medicine, University of Rome "Tor Vergata", Rome 00133, Italy; [c]Struttura di Area Funzionale di Ricerca Unit (SAFU), Department of Research, Advanced Diagnostics, and Technological Innovation, Translational Research Area, Istituto di Ricovero e Cura a Carattere Scientifico Regina Elena National Cancer Institute, Rome 00144, Italy; [d]Thoracic Oncology, University of Hawaii Cancer Center, Honolulu, HI 96816; [e]Biostatistics, Bioinformatics and Clinical Trial Center, Istituto di Ricovero e Cura a Carattere Scientifico Regina Elena National Cancer Institute, Rome 00144, Italy; [f]Department of Precision Medicine, University of Campania Luigi Vanvitelli, Naples 80138, Italy; [g]Laboratory of Precision and Molecular Oncology, Biogem Scarl, Institute of Genetic Research, Ariano Irpino 83031, Italy; [h]Department of Epidemiology, Preclinical Research and Advanced Diagnostics, National Institute for Infectious Diseases Istituto di Ricovero e Cura a Carattere Scientifico "L. Spallanzani", Rome 00149, Italy; and [i]Translational Oncology Research Unit, Department of Research, Diagnosis and Innovative Technologies, Istituto di Ricovero e Cura a Carattere Scientifico Regina Elena National Cancer Institute, Rome 00144, Italy

1. D. E. Johnson *et al.*, Head and neck squamous cell carcinoma. *Nat. Rev. Dis. Primers* **6**, 92 (2020).
2. E. Maghami *et al.*, Diagnosis and management of squamous cell carcinoma of unknown primary in the head and neck: ASCO guideline. *J. Clin. Oncol.* **38**, 2570–2596 (2020).
3. M. D. Mody, J. W. Rocco, S. S. Yom, R. I. Haddad, N. F. Saba, Head and neck cancer. *Lancet* **398**, 2289–2299 (2021).
4. C. Lo Nigro, N. Denaro, A. Merlotti, M. Merlano, Head and neck cancer: Improving outcomes with a multidisciplinary approach. *Cancer Manag. Res.* **9**, 363–371 (2017).
5. G. P. Gupta, J. Massagué, Cancer metastasis: Building a framework. *Cell* **127**, 679–95 (2006).
6. G. P. Dotto, A. K. Rustgi, Squamous cell cancers: A unified perspective on biology and genetics. *Cancer Cell* **29**, 622–637 (2016).
7. A. Sánchez-Danés, C. Blanpain, Deciphering the cells of origin of squamous cell carcinomas. *Nat. Rev. Cancer* **18**, 549–561 (2018).
8. N. Stransky *et al.*, The mutational landscape of head and neck squamous cell carcinoma. *Science* **333**, 1157–1160 (2011).
9. J. W. Rocco, C.-O. Leong, N. Kuperwasser, M. P. DeYoung, L. W. Ellisen, p63 mediates survival in squamous cell carcinoma by suppression of p73-dependent apoptosis. *Cancer Cell* **9**, 45–56 (2006).
10. Cancer Genome Atlas Network, Comprehensive genomic characterization of head and neck squamous cell carcinomas. *Nature* **517**, 576–582 (2015).
11. E. Alsahafi *et al.*, Clinical update on head and neck cancer: Molecular biology and ongoing challenges. *Cell Death Dis.* **10**, 540 (2019).
12. X. Yang *et al.*, ΔNp63 versatilely regulates a broad NF-κB gene program and promotes squamous epithelial proliferation, migration, and inflammation. *Cancer Res.* **71**, 3688–3700 (2011).
13. A. A. Mills *et al.*, P63 is a p53 homologue required for limb and epidermal morphogenesis. *Nature* **398**, 708–713 (1999).
14. A. Yang *et al.*, P63 is essential for regenerative proliferation in limb, craniofacial and epithelial development. *Nature* **398**, 714–718 (1999).
15. E. Candi *et al.*, Differential roles of p63 isoforms in epidermal development: Selective genetic complementation in p63 null mice. *Cell Death Differ.* **13**, 1037–1047 (2006).
16. R.-A. Romano *et al.*, ΔNp63 knockout mice reveal its indispensable role as a master regulator of epithelial development and differentiation. *Development* **139**, 772–782 (2012).
17. R. Pecorari, F. Bernassola, G. Melino, E. Candi, Distinct interactors define the p63 transcriptional signature in epithelial development or cancer. *Biochem. J.* **479**, 1375–1392 (2022).
18. G. Viticchiè *et al.*, P63 supports aerobic respiration through hexokinase II. *Proc. Natl. Acad. Sci. U.S.A.* **112**, 11577–11582 (2015).
19. A. M. Lena *et al.*, The p63 C-terminus is essential for murine oocyte integrity. *Nat. Commun.* **12**, 383 (2021).
20. E. Candi *et al.*, p63 in epithelial development. *Cell. Mol. Life Sci.* **65**, 3126–3133 (2008).
21. J. Qu *et al.*, Mutant p63 affects epidermal cell identity through rewiring the enhancer landscape. *Cell Rep.* **25**, 3490–3503.e4 (2018).
22. I. Sethi, C. Gluck, H. Zhou, M. J. Buck, S. Sinha, Evolutionary re-wiring of p63 and the epigenomic regulatory landscape in keratinocytes and its potential implications on species-specific gene expression and phenotypes. *Nucleic Acids Res.* **45**, 8208–8224 (2017).
23. R. Shalom-Feuerstein *et al.*, ΔNp63 is an ectodermal gatekeeper of epidermal morphogenesis. *Cell Death Differ.* **18**, 887–896 (2011).
24. E. N. Kouwenhoven *et al.*, Transcription factor p63 bookmarks and regulates dynamic enhancers during epidermal differentiation. *EMBO Rep.* **16**, 863–878 (2015).
25. M. R. Ramsey *et al.*, FGFR2 signaling underlies p63 oncogenic function in squamous cell carcinoma. *J. Clin. Invest.* **123**, 3525–3538 (2013).
26. V. Gatti *et al.*, ΔNp63-Senataxin circuit controls keratinocyte differentiation by promoting the transcriptional termination of epidermal genes. *Proc. Natl. Acad. Sci. U.S.A.* **119**, e2104718119 (2022).
27. W. M. Keyes *et al.*, P63 deficiency activates a program of cellular senescence and leads to accelerated aging. *Genes Dev.* **19**, 1986–1999 (2005).
28. S. V. Saladi *et al.*, ACTL6A is co-amplified with p63 in squamous cell carcinoma to drive YAP activation, regenerative proliferation, and poor prognosis. *Cancer Cell* **31**, 35–49 (2017).
29. L. Ha, R. M. Ponnamperuma, S. Jay, M. S. Ricci, W. C. Weinberg, Dysregulated ΔNp63α inhibits expression of Ink4a/arf, blocks senescence, and promotes malignant conversion of keratinocytes. *PLoS One* **6**, e21877 (2011).
30. W. M. Keyes *et al.*, ΔNp63α is an oncogene that targets chromatin remodeler Lsh to drive skin stem cell proliferation and tumorigenesis. *Cell Stem Cell* **8**, 164–176 (2011).
31. A. Smirnov *et al.*, ZNF185 is a p63 target gene critical for epidermal differentiation and squamous cell carcinoma development. *Oncogene* **38**, 1625–1638 (2019).
32. D. I. Kim, K. J. Roux, Filling the void: Proximity-based labeling of proteins in living cells. *Trends Cell Biol.* **26**, 804–817 (2016).
33. K. J. Roux, D. I. Kim, B. Burke, D. G. May, BioID: A screen for protein-protein interactions. *Curr. Protoc. Protein Sci.* **91**, 19.23.1–19.23.15 (2018).
34. S. Feo *et al.*, Conserved structure and promoter sequence similarity in the mouse and human genes encoding the zinc finger factor BERF-1/BFCOL1/ZBP-89. *Biochem. Biophys. Res. Commun.* **283**, 209–218 (2001).
35. Z. V. Zou *et al.*, Genomic profiling of the transcription factor Zfp148 and its impact on the p53 pathway. *Sci. Rep.* **10**, 14156 (2020).
36. J. Fang *et al.*, Functional characterization of a multi-cancer risk locus on chr5p15.33 reveals regulation of TERT by ZNF148. *Nat. Commun.* **8**, 15034 (2017).
37. K. J. Roux, D. I. Kim, M. Raida, B. Burke, A promiscuous biotin ligase fusion protein identifies proximal and interacting proteins in mammalian cells. *J. Cell Biol.* **196**, 801–810 (2012).
38. J. Gault *et al.*, High-resolution mass spectrometry of small molecules bound to membrane proteins. *Nat. Methods* **13**, 333–336 (2016).
39. J. M. Rozenberg, O. S. Rogovaya, G. Melino, N. A. Barlev, A. Kagansky, Distinct p63 and p73 protein interactions predict specific functions in mRNA splicing and polyploidy control in epithelia. *Cells* **10**, 25 (2020).
40. E. Lin-Shiao *et al.*, KMT2D regulates p63 target enhancers to coordinate epithelial homeostasis. *Genes Dev.* **32**, 181–193 (2018).
41. E. M. Memmi *et al.*, p63 sustains self-renewal of mammary cancer stem cells through regulation of Sonic Hedgehog signaling. *Proc. Natl. Acad. Sci. U.S.A.* **112**, 3499–3504 (2015).
42. T. M. Caserta *et al.*, P63 overexpression induces the expression of Sonic Hedgehog. *Mol. Cancer Res.* **4**, 759–768 (2006).
43. A. B. Truong, M. Kretz, T. W. Ridky, R. Kimmel, P. A. Khavari, P63 regulates proliferation and differentiation of developmentally mature keratinocytes. *Genes Dev.* **20**, 3185–3197 (2006).
44. M. Senoo, F. Pinto, C. P. Crum, F. McKeon, p63 is essential for the proliferative potential of stem cells in stratified epithelia. *Cell* **129**, 523–536 (2007).
45. E. A. Musgrove, C. E. Caldon, J. Barraclough, A. Stone, R. L. Sutherland, Cyclin D as a therapeutic target in cancer. *Nat. Rev. Cancer* **11**, 558–572 (2011).
46. L. Rinaldi *et al.*, Dnmt3a and Dnmt3b associate with enhancers to regulate human epidermal stem cell homeostasis. *Cell Stem Cell* **19**, 491–501 (2016).
47. C. Z. Y. Zhang, G. G. Chen, J. L. Merchant, P. B. S. Lai, Interaction between ZBP-89 and p53 mutants and its contribution to effects of HDACi on hepatocellular carcinoma. *Cell Cycle* **11**, 322–334 (2012).
48. M. C. Remington, S. A. Tarlé, B. Simon, J. L. Merchant, ZBP-89, a Krüppel-type zinc finger protein, inhibits cell proliferation. *Biochem. Biophys. Res. Commun.* **237**, 230–234 (1997).
49. L. Bai, J. L. Merchant, Transcription factor ZBP-89 cooperates with histone acetyltransferase p300 during butyrate activation of p21waf1 transcription in human cells. *J. Biol. Chem.* **275**, 30725–30733 (2000).
50. E. Wieczorek *et al.*, The zinc finger repressor, ZBP-89, binds to the silencer element of the human vimentin gene and complexes with the transcriptional activator, Sp1. *J. Biol. Chem.* **275**, 12879–12888 (2000).
51. L. Bai, J. L. Merchant, ZBP-89 promotes growth arrest through stabilization of p53. *Mol. Cell Biol.* **21**, 4670–4683 (2001).
52. G. G. Chen *et al.*, Mutation of p53 in recurrent hepatocellular carcinoma and its association with the expression of ZBP-89. *Am. J. Pathol.* **162**, 1823–1829 (2003).
53. L. Bai, J. L. Merchant, Transcription factor ZBP-89 is required for STAT1 constitutive expression. *Nucleic Acids Res.* **31**, 7264–7270 (2003).

54. R. C. Borghaei *et al.*, Zinc-binding protein-89 (ZBP-89) cooperates with NF-κB to regulate expression of matrix metalloproteinases (MMPs) in response to inflammatory cytokines. *Biochem. Biophys. Res. Commun.* **471**, 503–509 (2016).
55. J. L. Merchant, L. Bai, M. Okada, ZBP-89 mediates butyrate regulation of gene expression. *J. Nutr.* **133**, 2456S–2460S (2003).
56. X. Zhang, I. H. Diab, Z. E. Zehner, ZBP-89 represses vimentin gene transcription by interacting with the transcriptional activator, Sp1. *Nucleic Acids Res.* **31**, 2900–2914 (2003).
57. Y. Wu, I. Diab, X. Zhang, E. S. Izmailova, Z. E. Zehner, Stat3 enhances vimentin gene expression by binding to the antisilencer element and interacting with the repressor protein, ZBP-89. *Oncogene* **23**, 168–178 (2004).
58. C. Z. Y. Zhang, G. G. Chen, P. B. S. Lai, Transcription factor ZBP-89 in cancer growth and apoptosis. *Biochim. Biophys. Acta* **1806**, 36–41 (2010).
59. L. Bai, S. O. Yoon, P. D. King, J. L. Merchant, ZBP-89-induced apoptosis is p53-independent and requires JNK. *Cell Death Differ.* **11**, 663–673 (2004).

CDDpress

www.nature.com/cddiscovery

ARTICLE OPEN

Check for updates

LEADR, a p63 target, dampens interferon signalling in bladder cancer

Damiano Barnaba[1,5], Mariacristina Franzese Canonico[1,5], Manuela Helmer-Citterich[2], Paolo Gandellini[3], Gerry Melino[1], Artem Smirnov[1,4] ✉ and Eleonora Candi[1,4] ✉

Bladder cancer affects over half a million people worldwide each year. Recent advances in early detection allowed a successful management of non-aggressive cancers, yet the recurrence rate remains high. Aggressive muscle-invasive bladder tumours are life-threatening and challenging to cure. Therefore, understanding of key molecular pathways involved in cancer progression is critical for developing of new personalised targeted therapies. Recently, non-coding RNAs (ncRNAs) have emerged as key regulators orchestrating complex biological processes in cancer, yet their function is not fully understood. Here, we compare non-muscle invasive and muscle invasive cell lines and identify a ncRNA gene *MIR205HG* and its transcript *LEADR* among the top ncRNAs downregulated in muscle invasive urothelial tumours. We show that *LEADR* expression is epigenetically regulated by master transcription factor p63. *LEADR* is localised in the nuclei of non-muscle invasive bladder cancer cells where it dampens hyperactivation of interferon stimulated genes possibly increasing sensitivity of bladder cancer cells to interferon signalling. These findings uncover an anti-tumoral role of non-coding RNA *LEADR* in mediating immune response in bladder cancer.

Cell Death Discovery (2025) 11:264 ; https://doi.org/10.1038/s41420-025-02546-1

INTRODUCTION

Based on the latest GLOBOCAN data [1], bladder cancer (BLCA) is the ninth most common cancer worldwide, it ranks thirteenth in mortality rate and affects men more than women. The majority of bladder cancers originate from the urothelium, giving rise to urothelial carcinomas that can be either non-muscle invasive (NMIBC) or muscle invasive (MIBC) tumours. In approximately 75% of the patients diagnosed with bladder cancer, the tumour is confined to the bladder mucosa or to the lamina propria, while the remaining 25% of the tumours are invasive into the muscularis propria [2]. If diagnosed at early stages, transurethral resection (TUR or TURBT, transurethral resection of bladder tumour) allows a correct tumour staging and determines eventual adjuvant therapies, such as mitomycin C, gemcitabine or the immune adjuvant Bacillus Calmette–Guerin (BCG) [3, 4]. MIBC treatment includes radiotherapy [5, 6], neoadjuvant or adjuvant chemotherapy to lower the risk of recurrence, yet radical cystectomy with pelvic lymph node dissection (PLND) remains a standard surgical approach. Despite the available treatment options, the recurrence rate of MIBC is substantial, highlighting the need for deeper understanding the molecular basis underlying MIBC to improve patients survival.

In recent years, non-coding RNAs (ncRNAs) have emerged as key regulators of numerous biological processes, including cell differentiation, proliferation, and metabolism [7–13]. Over 120.000 ncRNAs have been annotated but the complex network of ncRNAs is still under intensive investigation. ncRNAs can be localised both in cytoplasm and nucleus and can regulate a variety of cellular pathways including chromatin remodelling and gene expression [14].

Alterations in expression of various ncRNAs can lead to cell transformation and tumorigenesis as well to cancer progression [15–19]. Several ncRNAs involved in bladder cancer progression have been identified, for instance urothelial carcinoma associated 1 (UCA1) [20] and ZEB2-AS1 [21] which are up-regulated in bladder tumours. Non-coding RNAs (ncRNAs) have been suggested as promising diagnostic biomarkers for the early detection of urothelial carcinoma and as valuable tools for assessing bladder cancer stage and prognosis [22]. Yet, it is not clear which ncRNAs are involved in the progression from NMIBC to MBIC cancers.

Here, we identify *MIR205HG* and its transcript *LEADR* as one of the most enriched ncRNAs in non-muscle invasive bladder cancer. The *MIR205HG* transcript gives rise to a micro-RNA *miR-205* and a Long Epithelial Alu-interacting Differentiation-related RNA (*LEADR*) lncRNA. While the role of miR-205 is well established [23], the function of *LEADR* remains poorly understood. Our findings demonstrate that in non-muscle invasive bladder cancer, LEADR is epigenetically regulated by p63 and functions as a negative regulator of the interferon pathway.

RESULTS

LEADR is highly expressed in non-invasive bladder cancer

To identify differentially expressed ncRNAs in low stage vs high stages bladder tumours, we chose two non-muscle invasive (RT4

[1]Department of Experimental Medicine, University of Rome Tor Vergata, Rome, Italy. [2]Biology Department, University of Rome Tor Vergata, Rome, Italy. [3]Department of Biosciences, University of Milan, Milan, Italy. [4]Istituto Dermopatico Immacolata (IDI-IRCCS), Rome, Italy. [5]These authors contributed equally: Damiano Barnaba, Mariacristina Franzese Canonico. ✉email: artem.smirnov@uniroma2.it; candi@uniroma2.it

Received: 16 April 2025 Revised: 29 April 2025 Accepted: 23 May 2025
Published online: 03 June 2025

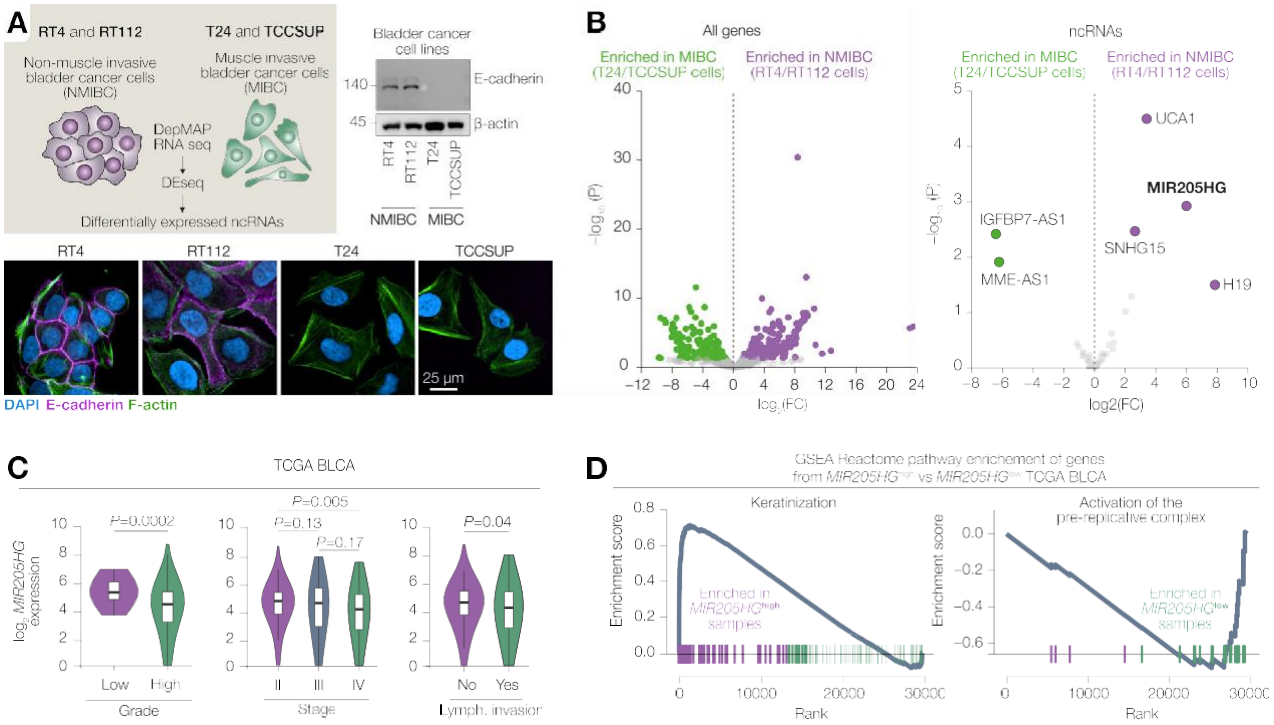

Fig. 1 *LEADR* is highly expressed in non-invasive bladder cancer. A (Top) Schematic showing the in vitro model to identify differentially expressed non-coding RNAs in non-muscle invasive vs muscle invasive bladder cancer. (Right) Western blot of e-cadherin expression in the panel of BLCA cell lines. β-actin as loading control. (Bottom) Immunofluorescence analysis by confocal microscopy of e-cadherin and F-actin expression in the same cell lines. B Volcano plots showing differential expression of either all genes or ncRNAs only in NMIBC vs MIBC cell lines. Genes with abs(log_2FC)>1 and $P < 0.05$ were considered significantly modulated. C *MIR205HG* log_2 RNA expression in TCGA BLCA samples based on the grade, stage or lymphovascular invasion positivity. *P* by Kolmogorov-Smirnov ("grade" and "invasion") or one-way ANOVA ("stage") tests. D GSEA Reactome pathway enrichment of genes differentially expressed in *MIR205HG*-high vs *MIR205HG*-low TCGA BLCA tumours. The top up- and down-regulated pathways are shown.

and RT112) and two muscle-invasive (T24 and TCCSUP) bladder cancer cell lines. Non-muscle invasive cells in vitro resembled epithelial phenotype and expressed high levels of junctional e-cadherin while muscle-invasive cells had mesenchymal appearance and were negative for e-cadherin (Fig. 1A). We then interrogated total RNA seq of these cell lines from Cancer Cell Line Encyclopaedia. By applying DEseq2, we identified differentially expressed ncRNAs. Four ncRNAs, including *H19*, *UCA1*, *MIR205HG*, and *SNHG15* were strongly expressed in non-muscle invasive cells (Fig. 1B). Of note, *H19* [24], *UCA1* [25] and *SNHG15* [26] have been recently studied in bladder cancer. *MIR205HG* is a host gene for microRNA *miR-205*. Of note, *miR-205* has been demonstrated to inhibit EMT by repressing ZEB1 in bladder cancer [27]. Yet, the function of the host gene itself in bladder cancer remains unknown. Therefore, we decided to investigate the role of the *miR-205*-independent spliced transcript of *MIR205HG* hereinafter referred to as *LEADR*. By interrogating TCGA bladder cancer cohort, we observed that *MIR205HG* expression was decreased in high grade and high stage tumours, as well as in patients with lymphovascular invasion (Fig. 1C). We then divided TCGA BLCA patients based on *MIR205HG* expression and performed differential expression analysis. *MIR205HG*^{high} tumours were enriched for genes related to epithelial pathways including keratinization, ECM interactions and collagen formation. On the contrary, genes from *MIR205HG*^{low} tumours were associated with replication, unfolded protein response and nuclear receptor transcription (Fig. 1D and Supplementary Fig. S1A). Altogether, *MIR205HG/LEADR* gene is one of the top ncRNAs downregulated during bladder cancer progression.

p63 regulates *LEADR* expression in bladder cancer

To understand the transcriptional regulation of *LEADR*, we ranked all known human transcription factors based on their co-expression with *MIR205HG* in TCGA bladder cancer cohort and identified p63 as the top hit (Fig. 2A). Moreover, *MIR205HG* resulted to be the most co-expressed and the strongest potential ncRNA target of p63 based on the target score of TargetGeneReg algorithm [28] (Supplementary Fig. S2A). Indeed, *MIR205HG* expression was strongly correlated with *TP63* both in bladder cancer and across all TCGA cancer types (Fig. 2B and Supplementary Fig. S2B). These observations are in line with previous reports of p63 regulating miR-205 and *LEADR* in prostate cancer [29]. We then confirmed that p63 and *LEADR* transcript were co-expressed in our panel of bladder cancer cell lines by using *LEADR*-specific primers. Predominantly N-truncated 75 kDa ΔNp63 isoform was detected exclusively in the nuclei of non-muscle invasive RT4 and RT112 bladder cancer cell lines (Fig. 2C). Accordingly, high levels of *LEADR* were detected in RT4 and RT112, but not T24 or TCCSUP cell lines (Fig. 2D). Of note, *LEADR* was localised within nuclei of tumour cells as assessed by fluorescence in situ hybridization (FISH) using *MIR205HG* or control *ACTB* (β-actin) probes, whereas the nuclei of T24 and TCCSUP cells were negative for *MIR205HG* (Fig. 2E). To understand whether p63 regulated *LEADR* expression, we used a set of siRNAs either against all transcripts of *TP63* gene or specifically ΔNp63 isoforms (Fig. 2F). All the siRNA led to a dramatic decrease of *LEADR* expression in RT4 cells. We further confirmed these data also in RT112 and SW780 non-muscle invasive cells using a pan-p63 siRNA (Supplementary Fig. S2C). Collectively, we show that p63 controls *LEADR* expression in non-muscle invasive bladder cancer.

LEADR is epigenetically repressed in advanced bladder cancer

p63 is a well-established pioneer factor which recognises specific binding motifs and recruits epigenetic modellers to relax chromatin [30]. Since p63 was undetectable in muscle-invasive

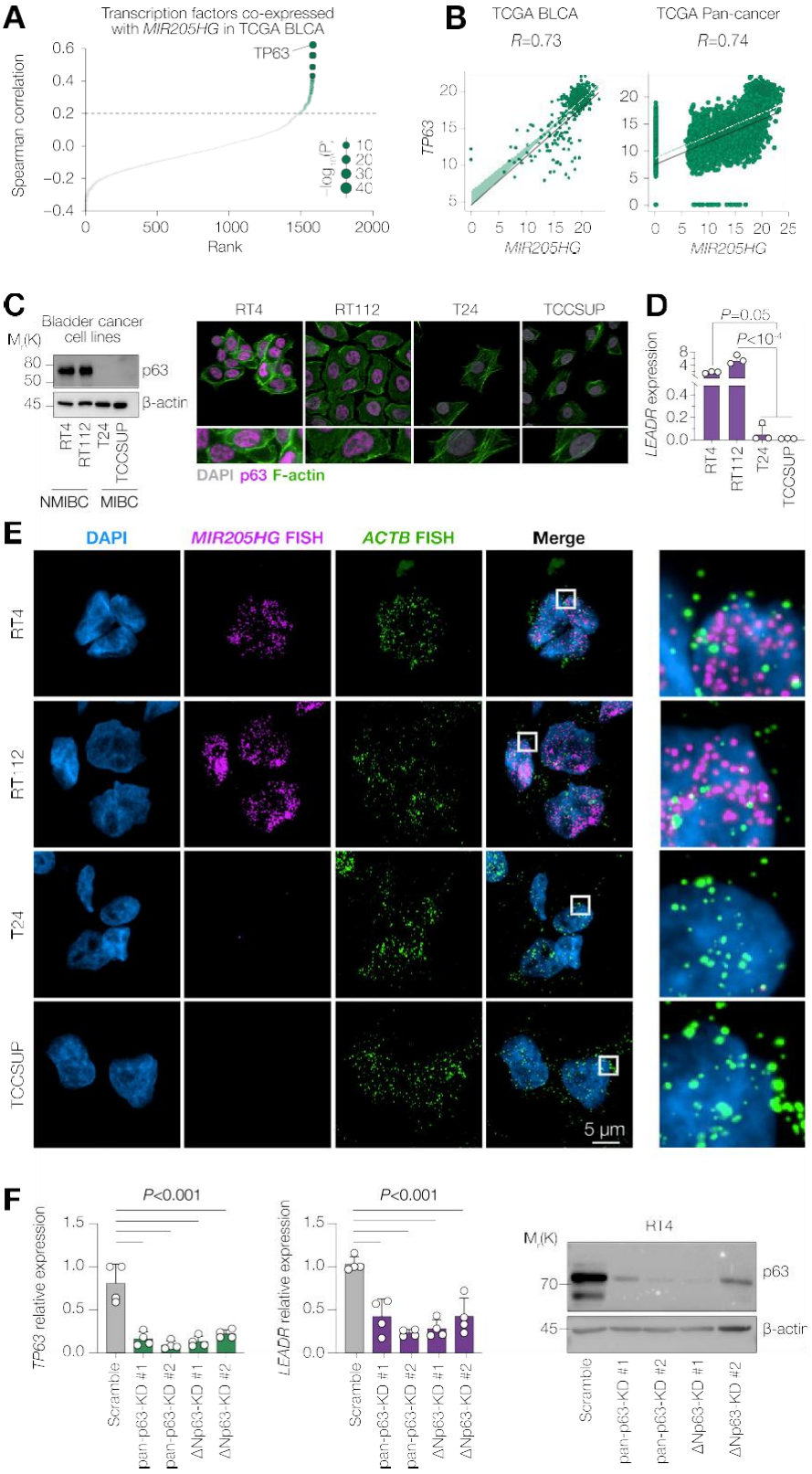

Fig. 2 p63 regulates *LEADR* expression in bladder cancer. A Dot plot showing Spearman correlation between *MIR205HG* RNA expression and expression of known human transcription factors in TCGA BLCA samples. B Dot plot showing expression of *MIR205HG* and *TP63* in either TCGA BLCA of TCGA Pan-cancer samples. C (Left) Western blot of p63 levels in the panel of BLCA cell lines. β-actin as loading control. (Right) Immunofluorescence analysis by confocal microscopy of p63 and F-actin expression in the same cell lines. D RT-qPCR analysis of *LEADR* expression in the same cell lines. $n = 3$ (biological replicates). *P* by one-way ANOVA. E RNA FISH analysis by confocal microscopy of *LEADR* in the cell lines from (D). ACTB as a positive control. F RT-qPCR analysis of p63 and *LEADR* expression in RT4 cell knocked-down for p63 using distinct siRNAs. $n = 4$ (biological replicates). *P* by one-way ANOVA. Western blot on the right confirms an efficient knock-down of p63. β-actin as loading control.

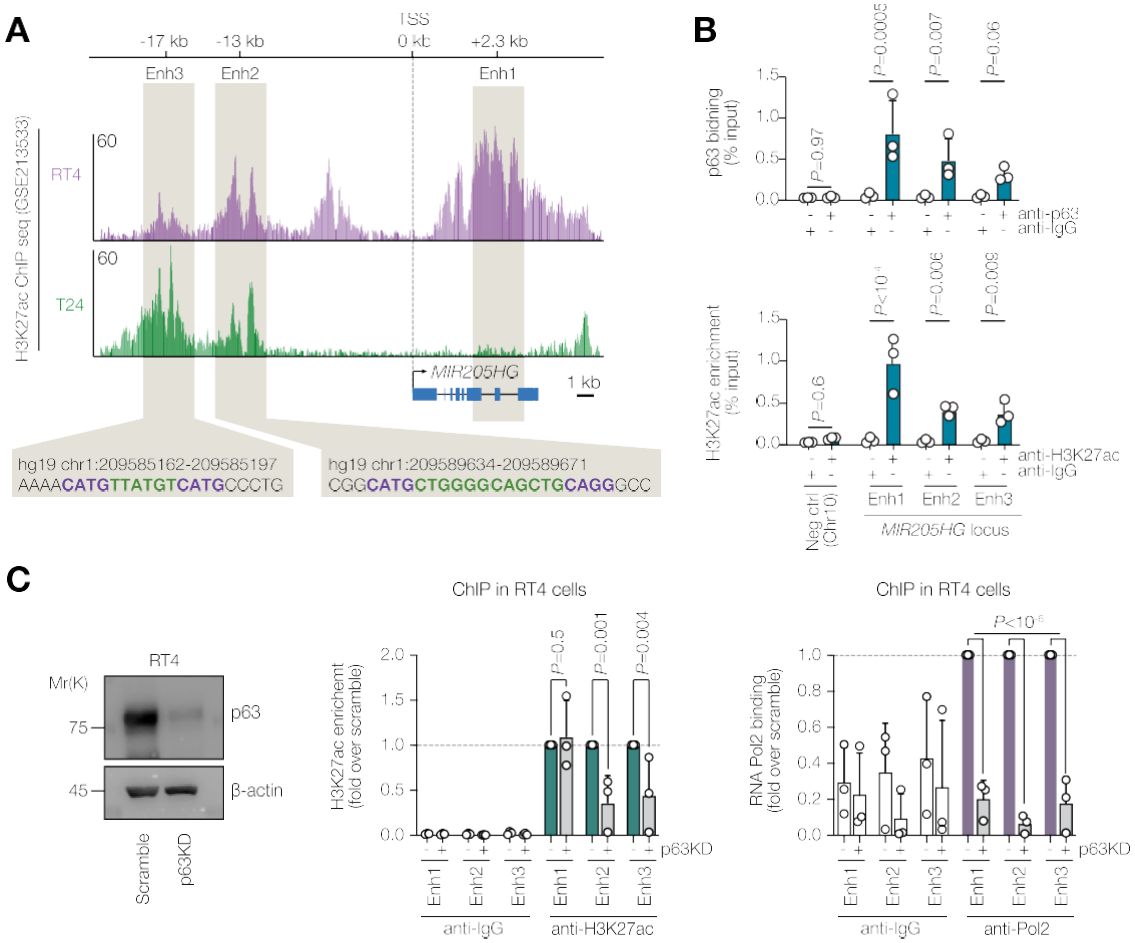

Fig. 3 *LEADR* is epigenetically repressed in advanced bladder cancer. A UCSC genome browser screenshot of H3K27ac ChIP seq signal tracks in RT4 and T24 from the GSE213533 study. The *MIR205HG* locus is shown. The three regions with putative p63 binding sites and enhancer activity are highlighted. The predicted p63 binding motifs are shown below. B ChIP-qPCR analysis of p63 binding and H3K27ac enrichment at the enhancers from (A) in RT4 cells. A gene desert region was used as negative control for p63 and H3K27ac occupancy. Isotype control IgG were used as negative control for the ChIP. $n = 3$ (biological replicates). *P* by two-way ANOVA. C ChIP-qPCR analysis of p63 binding and H3K27ac enrichment at the enhancers from (A) in RT4 cells transfected with either scramble or pan-p63 siRNAs. Isotype control IgG were used as negative control for the ChIP. Values shown are fold enrichment over scramble for each region analysed. $n = 3$ (biological replicates). *P* by two-way ANOVA.

cell lines, we questioned whether epigenetic state of the *MIR205HG* locus was altered by the transition from the low stage to high stage tumour. We interrogated two publicly available H3K27ac ChIP seq experiments carried out in RT4 and T24 cell lines (Fig. 3A). Several H3K27ac-rich regions were also bound by p63 in various ChIP seq experiments from non-urothelial cells (Supplementary Fig. S3A). The *MIR205HG* locus had three regions enriched for H3K27ac mark and potentially bound by p63, highlighted as enhancer 1 (intronic +2.3 kb region), enhancer 2 (intergenic -13 kb region), and enhancer 3 (intergenic −17 kb region). Of note, p63 binding to the enhancer region 1 was previously described [27]. RT4 showed high levels of histone acetylation within all the three enhancer sites. It was reduced at enhancer 1 and partially enhancer 2 regions whereas enhancer 3 retained acetylation in T24 cells. Both enhancer 2 and enhancer 3 had canonical p63 binding motifs. We performed ChIP using anti-pan-p63, anti-H3K27ac or isotype control IgG and confirmed that p63 physically bound the three regions in RT4 cells (Fig. 3B). The loss of p63 by RNA interference led to a reduction of histone acetylation at enhancers 2 and 3 (Fig. 3C). Since the epigenetic state can affect recruitment of RNA Pol 2, we checked Pol2 occupancy at the enhancer sites and observed a dramatic decrease at all the three regions (Fig. 3C). Altogether, we demonstrate that p63 controls the epigenetic state of the *MIR205HG* locus.

LEADR represses a subset of interferon stimulated genes

To understand the role of *LEADR* in non-muscle invasive cancer, we performed knock-down of *LEADR* spliced transcript using a specific siRNA which does not affect *MIR205*-generating unspliced RNA as described before [29] and carried out poly(A) RNA seq. We identified 312 *LEADR*-activated and 235 *LEADR*-repressed genes (Fig. 4A and Supplementary Fig. S4A, B). Reactome gene set enrichment analysis (GSEA) revealed that *LEADR*-activated genes belonged to several metabolic pathways however with low level of confidence. On contrary, *LEADR*-repressed genes were strongly associated with interferon signalling and homology directed repair and replication stress (Fig. 4B). We first checked whether the loss of *LEADR* altered cell proliferation by performing growth curve analysis and EdU incorporation assay, yet we did not observe any significant changes (Supplementary Fig. S4C). We then questioned whether interferon pathway was affected by *LEADR* knock-down. Among interferon-related genes (Fig. 4C), we saw key transcription factors from STAT and IRF families and downstream targets, for instance, IFITs (Fig. 4D). We assessed protein expression of several hits and observed a significant

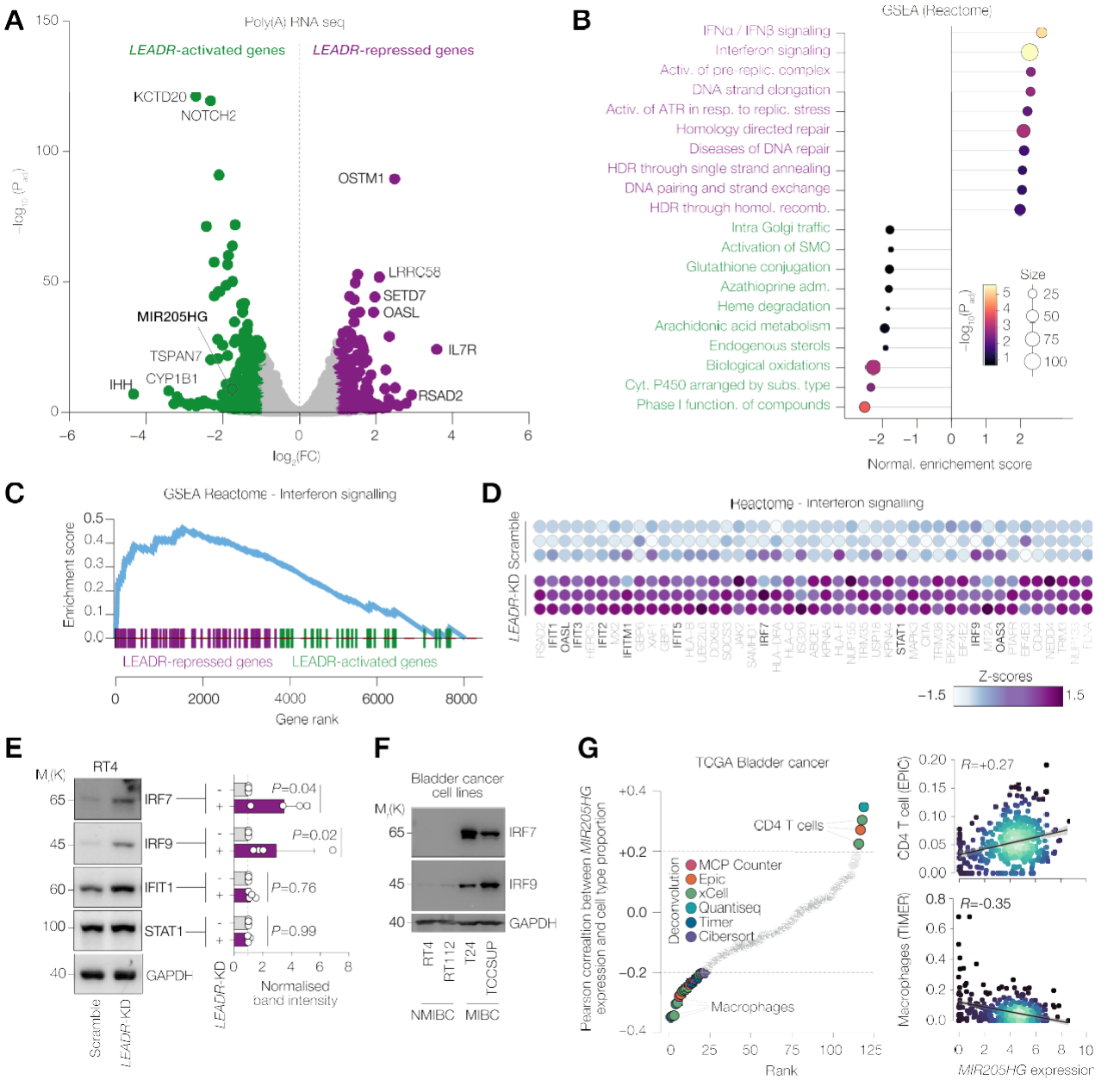

Fig. 4 *LEADR* represses a subset of interferon stimulated genes. A Volcano plots showing mRNA differential expression in RT4 cells transfected with either scramble or *LEADR* siRNAs. Genes with abs(log_2FC)>1 and $P < 0.05$ were considered significantly modulated. B GSEA Reactome pathway enrichment of modulated genes from (A). C GSEA Enrichment plot for the "Interferon signalling" pathway from (B). D Heatmap showing expression Z-scores of genes from the "Interferon signalling" pathway. E (Left) Western blot analysis of IRF7, IRF9, IFIT1, and STAT1 levels in RT4 cells transfected with either scramble or *LEADR* siRNAs. (Right) Band intensity analysis of the same samples. Values shown are fold enrichment over scramble normalised over GAPDH intensity for each protein. $n = 4$ (biological replicates). *P* by two-way ANOVA. GAPDH as loading control. F Western blot analysis of IRF7 and IRF9 levels in the panel of BLCA cell lines. GAPDH as loading control. G (Left) Dot plot showing Pearson correlation between *MIR205HG* expression and predicted proportion of infiltrating cells in TCGA BLCA samples based on publicly available deconvolution algorithms. (Right) Dot plots showing expression of *MIR205HG* and predicted proportion of either CD4 T cells or macrophages in TCGA BLCA.

increase in IRF7 and IRF9 protein levels in *LEADR*-depleted cells (Fig. 4E). Of note, IRF7 and IRF9 levels were dramatically increased in the two MIBC cell lines T24 and TCCSUP compared to non-invasive ones RT4 and RT112 (Fig. 4F). Since interferon pathway is a key signalling involved in immune response of tumours, we checked whether *MIR205HG* expression was correlated with any specific intratumoral cell types in bladder cancer by using distinct deconvolution methods. Tumours with high levels of *MIR205HG* were enriched for CD4 T cells and NK cells, on contrary *MIR205HG*^{low} tumours had a higher proportion of M2 macrophages (Fig. 4G). In summary, *LEADR* represses interferon-related genes and is associated with high CD4 T cells infiltration.

DISCUSSION

Here we identify a non-coding gene *MIR205HG* among the most enriched ncRNAs in non-muscle invasive bladder cancer. The primary transcript of *miR-205* host gene *MIR205HG* gives rise to a microRNA *miR-205* and a Long Epithelial Alu-interacting Differentiation-related RNA (*LEADR*). We and others described the role

of *miR-205* in various cancer types, including prostate [31–33], cervical [34], head and neck [35] cancer and melanoma [36], yet the role of the host gene remains understudied. Our data show that *MIR205HG* decreases during bladder cancer progression which is in line with a previous report [37, 38]. Indeed, *miR-205*, a product of *MIR205HG* gene, was shown to inhibit epithelial-mesenchymal transition through direct repression of ZEB1, ZEB2 and E-cadherin [38, 39].

Our screening of known transcription factors identified p63 as the most co-expressed with *MIR205HG* gene. p63, a member of the p53 transcription factor family, is essential for epithelial development and skin homeostasis [40–44]. In cancer, p63 exhibits context-dependent roles, acting as a tumor suppressor or oncogene depending on the isoform expressed [45–47]. In particular, the ΔNp63 isoform is crucial in bladder cancer, where it promotes epithelial identity and proliferation, and its dysregulation is linked to tumor progression and subtype specification.

Several reports showed p63 binding at the enhancer region (enhancer 1) within *MIR205HG* gene [29, 38] in prostate and bladder cancer. By assessing publicly available ChIP seq data and performing ChIP-qPCR assays, we showed that p63 bound additional −13 kb and −17 kb putative enhancers which harbour strong p63 motifs. p63 is a known pioneer factor able to recruit the chromatin remodellers to its binding sites to open chromatin. Contrary to a previous report [38], we did not see any changes of histone acetylation at the enhancer 1 after p63 knock-down, however, enhancer 2 and enhancer 3 H3K27ac levels were markedly reduced in absence of p63. Furthermore, all three regions lost RNA Pol2 binding in p63-depleted cells. It is plausible that the enhancer regions interact and form a loop allowing recruitment of Pol2 and active transcription of the gene. Since we observed p63 biding across the *MIR205HG* locus in the ChIP seq data from other tissues, it is likely that p63/*LEADR* regulatory axis is common for all epithelial tissues.

While the function of miR-205 has been thoroughly described, the role of the ncRNA transcript *LEADR* remains poorly understood. *LEADR* has been shown to affect cell proliferation in various cancers [48, 49] however we did not see any changes in cell growth or cell cycle upon *LEADR* knock-down in our model.

Of note, ZEB1/2, the miR205 targets in bladder cancer, were not affected by *LEADR* loss. Indeed, it was demonstrated that *LEADR* exerts a distinct miR-205-independent role in human prostate. By interacting with chromatin, *LEADR* binds to Alu sequences of *IL33* [50] and interferon stimulated genes (ISGs) [29, 51]. In this study, we performed an RNA sequencing of RT4 cells silenced for *LEADR* and observed a similar increase in expression of interferon α and β pathway genes. In fact, two key transcription factors IRF7 and IRF9 were significantly up-regulated also at protein level in *LEADR*-depleted cells.

Our analyses also indicate that the loss of *LEADR* may be associated with replicative stress and DNA damage response (DDR) which can stimulate activation of interferon pathway [52]. However, the enrichment of the DDR across *LEADR*-repressed genes was not strongly significant and we did not see any changes in cell proliferation. Therefore, it is plausible that *LEADR* directly represses interferon stimulated genes via the mechanism described previously [51]. Nonetheless, further investigation is needed to determine whether the loss of *LEADR* in bladder cancer cells can induce replicative stress and DNA damage, for instance, by analysing levels of phosphorylated histone H2AX and key proteins involved in DDR.

Interferon signalling is multifaceted, exhibiting both anti-tumour and pro-tumour activities [53]. A recent paper has shown that low grade bladder cancer cell lines are sensitive to IFNα treatment which induces expression of interferon stimulated genes and promotes tumour cell death [54]. On contrary, high grade cell lines are resistant to IFNα due to a constitutive activation of ISGs. This observation aligns with our findings, as we detected elevated levels of IRF7 and IRF9 in the muscle-invasive T24 and TCCSUP cell lines, but not in the non-muscle-invasive RT4 or RT112 cells. It is plausible that *LEADR* acts as an inhibitor of interferon response by preventing pro-tumoral chronic activation of ISGs [55]. Loss of *LEADR* in muscle-invasive tumours may be in part responsible for uncontrolled activation of the pathway and therefore development of resistance to immunotherapy. Since interferon response is a key signalling of the anti-tumoral immunity, we assessed the correlation between *MIR205HG* expression and immune infiltrate. In support of our hypothesis, deconvolution analyses revealed that tumours with high *LEADR* expression were enriched in CD4 T cells. Overall, our findings indicate that the non-coding RNA *LEADR* suppresses interferon signalling, thereby preserving tumour cell sensitivity to interferon and enhancing the anti-tumour immune response in bladder cancer.

MATERIALS AND METHODS

Cell lines

Established human bladder cancer cell lines were purchased from American Type Culture Collection or Cytion. RT4 cells (ATCC; HTB-2) and T24 (ATCC; HTB-4) were cultured in McCoy's medium (Gibco), RT112 cells (CLS; 300324) were cultured in RPMI medium (Gibco), TCCSUP (ATCC; HTB-5) cells were grown in Minimum essential medium (Eagle), and SW780 cells (ATCC CRL-2169) were cultured in Leibovitz's L-15 Medium (Invitrogen). All the media were supplemented with heat-inactivated 10% Fetal Bovine Serum (Invitrogen) and penicillin/streptomycin (100 µg/mL, Gibco). Cells were maintained at 37 °C and 5% CO_2 humidified atmosphere. Cells were routinely checked for possible mycoplasma contamination through MycoAlert Mycoplasma Detection Kit (Lonza).

RNA interference

For transfection experiments, cells were seeded at density of 150.000 cells per well in a 6 well plate 24 h prior transfection. Then the culture medium was removed, and cells were transfected with specific siRNAs for 48 h, using Optimem medium (Thermo Fisher Scientific) and Lipofectamine-RNAiMAX reagent (Thermo Fisher Scientific) according to the manufacturer's protocol. A control siRNA (scr, mission siRNA universal negative control #1 SIC001, Sigma) with no homology to any known human mRNA was used as a negative control. The siRNA used in the study are listed in the Supplementary Table S1.

RNA isolation, reverse transcription and RT-qPCR

Total RNA was isolated from cells by using RNeasy Mini Kit (QIAGEN, Hilden, Germany) with DNase I digestion (QIAGEN, Hilden, Germany) according to the manufacturer's protocol. RNA yield and A260/280 ratio were monitored with a NanoDrop 1000 spectrophotometer (Thermo Fisher Scientific Inc., Waltham, MA, USA). cDNA was synthesized using SensiFast cDNA Syntesis Kit with oligo-dT and random hexamer primers (Bioline). Real-time PCR was performed using the PowerUp SYBR Green Master Mix (AppliedBiosystems), in an QuantStudio™ 5 Real-Time PCR System (Applied Biosystems) with an amplification programme as follows: one cycle of 95 °C for 20 s and 40 cycles of 95 °C for 3 s and 60 °C for 20 s. GAPDH was used as housekeeping gene for data normalization. Relative expression was calculated by using the $2^{-\Delta\Delta Ct}$ method. The primers used in the study are listed in the Supplementary Table S1.

Immunoblotting analysis

For total protein extraction, cells were lysed in RIPA lysis buffer (50 mM Tris-HCl pH 8.0, 150 mM NaCl, 1% NP40, 0.5% Na-deoxycholate, 0.1% SDS + protease and phosphatase inhibitors) for 10 min on ice and then centrifuged for 10 min to remove any debris. Proteins were denatured and negatively charged with Laemmli buffer and then boiled at 95 °C for 5 min. Proteins were loaded onto SDS-PAGE for separation and transferred onto polyvinylidendifluoride membranes. Membranes were blocked for 1 h in 5% milk and incubated overnight with shaking at +4 °C with primary antibodies: anti-p63 (Sant Cruz Cat# sc-25268, RRID:AB_628092, 1:500), anti-E-cadherin (Cell Signaling Cat#14472, RRID: AB2728770, 1:1000), anti-IRF7 (Cell Signaling Cat#13014, RRID:AB_2737060,1:1000), anti-IRF9 (Cell Signaling Cat#76684, RRID:AB_2799885,1:1000), anti-IFIT1 (Cell Signaling

Cat#14769, RRID:AB_2783869,1:1000), anti-STAT1 (Cell Signaling Cat#14994, RRID:AB_2737027,1:1000), anti-GAPDH (Sigma-Aldrich Cat# G8795, RRID: AB1078991, 1:15000), and anti-β-actin (BioRad Cat#M-CA5775GA, RRID:AB_2571580, 1:15000). After three washes with 1× PBS-Tween 20, membranes were incubated with the secondary antibodies conjugated to horseradish peroxidase (anti-mouse or anti-rabbit 1:10000) (Biorad Cat# 170-6515 RRID:AB_11125142 and Cat# 170-5047 RRID:AB_11125142) for 1 h at room temperature. Immunoreactivity was detected by immunodetection system (Alliance Q9 Advanced; Uvitec) with Luminol Reagent (Western Lightning Plus, Revity). The band intensity was measured using ImageJ software. The uncropped western blots are shown in the Supplementary Fig. S5.

Immunofluorescence

Cells were grown in flat bottom 96 well PhenoPlates (Revvity) and then fixed in 10% formalin in 1X PBS for 10 min. Samples were washed twice for 5 min in 1X PBS. Cells were permeabilized in 0.25% Triton X-100 for 10 min. Five percent goat serum in PBS was used to block the samples for 1 h. Cells were incubated with primary antibodies diluted in 5% goat serum overnight at 4 °C. The wells were washed 3 times for 5 min in 1X PBS and DAPI (Sigma Cat# 11190301) and secondary antibodies were added to cells and incubated for 1 h. The plate was washed 3 times for 5 min in PBS. The samples were counterstained with 1 µg/mL DAPI (Sigma). The images were acquired on Operetta high content imaging system (Revvity) in confocal mode. The following antibodies were used: anti-p63 (Cell Signaling Cat# 39692S, RRID:AB_2799159, 1:200), anti-E-cadherin (Cell Signaling Cat#14472, RRID: AB2728770, 1:200), anti-mouse Alexa Fluor 647 (Invitrogen Cat #A-21235, RRID:AB_2535804), anti-rabbit Alexa Fluor 488 (Invitrogen Cat#A-11034, RRID:AB_2576217), phalloidin (Invitrogen Cat # A-12380).

Chromatin immunoprecipitation (ChIP) analysis

To perform ChIP assay, cells were cross-linked with methanol-free 1% formaldehyde (ThermoFisher) for 10 min at room temperature. The formaldehyde was quenched by addition of freshly prepared 125 mM glycine (Sigma). After washing three times with PBS, cell pellet was resuspended in 0.5% SDS sonication Buffer (10 mM Tris pH8.0, 0.5% SDS, 2 mM EDTA) with protease inhibitor and incubated for 30 min on ice and fragmented (Covaris M220) by sonication. Size of the sheared chromatin was determined by agarose gel electrophoresis. Chromatin was diluted 1:10 in RIPA-LS buffer (Tris−HCl 10 mM pH8, NaCl 140 mM, EDTA 1 mM pH8, SDS 0.1%, Na Deoxycholate 0.1%) buffer. One percent of chromatin was preserved as input. The antibodies were added to the chromatin and placed in a shaker at 4 °C overnight. The following antibodies were used: anti-p63 (Cell Signalling Cat# 13109, RRID:AB_2637091), anti-H3K27ac (Abcam Cat# ab4729, RRID: AB_2118291), anti-Pol2 (ActiveMotif Cat# 39097, RRID:AB_2732926), mouse Gamma Globulins (31878) (Invitrogen Cat# 31878, RRID:AB_2532170). The day after, the Dynalbeads Protein G or Protein A (Invitrogen Cat# 10004D and 10001D) were added to the complex for immunoprecipitation for 2 h at 4 °C. The beads were washed twice in RIPA-LS buffer, twice in RIPA-HS buffer (Tris−Cl 10 mM pH8, EDTA 1 mM pH 8, Na-Cl 500 mM, Triton x-100 1%, SDS 0.1%, Na Deoxycholate 0.1%), twice in RIPA-LiCl buffer (Tris HCl 10 mM pH8, EDTA 1 mM, LiCl 250 mM, NP-40 0,5%, Na Deoxycholate 0.5%), and then in 10 mM Tris pH8.0. The immunoprecipitated chromatin was eluted in elution buffer (Tris-HCl pH8 10 mM, EDTA pH 8 5 mM, NaCl 300 mM, SDS 0.4%) with proteinase K for de-crosslinking and incubated at 55 °C for 1 h and then at 65 °C for 1 h. DNA was purified by QIAquick PCR purification kit (Qiagen), resuspended in nuclease free water and used for Real-Time PCR quantification (QuantStudio™ 5 Real-Time PCR System; Applied Biosystems). The genomic quantification was normalized to the input sample. The primers used in the study are listed in the Supplementary Table S1.

RNA-FISH on cell lines

RNA-FISH was carried out as described in the protocol ViewRNA Tissue Fluorescence Assay (Invitrogen). Cells were fixed in 4% formaldehyde for 10 min and permeabilised in 70% ethanol for 1 h at 4 °C. RNA FISH probe was diluted in hybridization buffer 1:40, added to cells and then incubated for 2 h at 40 °C. Cells were washed twice for 10 min in Wash Buffer. RNA probes (diluted 1:25) were labelled with specific fluorophores (AlexaFluor-546 for *ACTB*; AlexaFluor-647 for *MIR205HG*) and incubated at 40 °C for 30 min. Finally, a counterstain was performed with 1 µg/mL DAPI (Sigma). Cells were washed two times with PBS and analysed on a high content imaging system Operetta (Revvity).

Cell proliferation

Five thousand cells were seeded onto 96 well plates 48 h after knock-down and allowed to attach. The cell growth was assessed in an automated cell counter IncuCyte (Sartorius) using 10x objective and acquiring 5 fields per well every 4 h for 3 days. The proportion of the cells in S phase was estimated by fluorescence-based Click-it EdU incorporation assay (ThermoFisher) with AlexaFluor488 azide. The cells were incubated with 10 µM EdU for 1 h and then stained as per manufacturer's protocol. The images were taken on the high content imaging system Operetta and quantified using Harmony software (Revvity).

RNA-sequencing and analysis

Total RNA was isolated as described before. The amount and integrity of the extracted RNA were assessed by Agilent TapeStation instrument (Agilent Technologies, CA). RNA sequencing was performed in paired-end mode with a read length of 150nt using the Illumina NovaSeq 6000 (Illumina, CA) in paired-end mode (2 × 100 bp) with a coverage of 100 M reads. Reads were mapped onto a reference genome (human genome build hg19). The abundance of the transcripts was quantified using the Salmon algorithm. The differential gene expression was analysed with DESeq2 package [56]. The reproducibility of biological replicates was assessed by Principal component analysis (PCA). Differentially expressed genes are shown in Supplementary Table S2.

Bioinformatic analyses

Cell line transcriptome data and TCGA data were downloaded from UCSC Xena Browser [57]and analysed using DESeq2 [56] and ggplot2 packages. The proportion of infiltrating cells were obtained from TIMER 2.0 [58]. Pathway enrichment was performed using fgsea package [59] and Reactome library. The list of known human TFs was downloaded from The Human Transcription Factors database. Volcano plots and correlation density plots were generated using ggplot2 package. Published ChIP seq data on H3K27ac were obtained from GSE213533 [60], while p63 ChIP seq data from ReMAP [61]. ChIP-seq signal tracks and peaks were visualised in UCSC Genome Browser. PCA plot was generated within DESeq2 package, while heatmaps were generated with pHeatmap package.

Statistical analyses

All the statistical analyses were performed in GraphPad Prism 10. For the RT-qPCR and densitometry analyses, the significance of the differences between the groups were determined by the Student's *t*-test or one-way ANOVA without adjustments. For the differential gene expression analysis, adjusted P values were calculated using DEseq2 package in R.

DATA AVAILABILITY

The RNA seq data have been deposited to NCBI GEO (accession: GSE293534).

REFERENCES

1. Bray F, Laversanne M, Sung H, Ferlay J, Siegel RL, Soerjomataram I, et al. Global cancer statistics 2022: GLOBOCAN estimates of incidence and mortality worldwide for 36 cancers in 185 countries. CA Cancer J Clin. 2024;74:229–63.
2. Siegel RL, Miller KD, Wagle NS, Jemal A. Cancer statistics, 2023. CA Cancer J Clin. 2023;73:17–48.
3. Zargar H, Aning J, Ischia J, So A, Black P. Optimizing intravesical mitomycin C therapy in non-muscle-invasive bladder cancer. Nat Rev Urol. 2014;11:220–30.
4. Han MA, Maisch P, Jung JH, Hwang JE, Narayan V, Cleves A, et al. Intravesical gemcitabine for non-muscle invasive bladder cancer. Cochrane Database Syst Rev. 2021;6:CD009294.
5. James ND, Hussain SA, Hall E, Jenkins P, Tremlett J, Rawlings C, et al. Radiotherapy with or without chemotherapy in muscle-invasive bladder cancer. N Engl J Med. 2012;366:1477–88.
6. Cahn DB, Handorf EA, Ghiraldi EM, Ristau BT, Geynisman DM, Churilla TM, et al. Contemporary use trends and survival outcomes in patients undergoing radical cystectomy or bladder-preservation therapy for muscle-invasive bladder cancer. Cancer. 2017;123:4337–45.

7. Lopez-Pajares V, Qu K, Zhang J, Webster DE, Barajas BC, Siprashvili Z, et al. A LncRNA-MAF:MAFB Transcription Factor Network Regulates Epidermal Differentiation. Dev Cell. 2015;32:693–706.
8. Kretz M, Siprashvili Z, Chu C, Webster DE, Zehnder A, Qu K, et al. Control of somatic tissue differentiation by the long non-coding RNA TINCR. Nature. 2013;493:231–5.
9. Panatta E, Lena AM, Mancini M, Smirnov A, Marini A, Delli Ponti R, et al. Long non-coding RNA uc.291 controls epithelial differentiation by interfering with the ACTL6A/BAF complex. EMBO Rep. 2020;21:e46734.
10. Mancini M, Sergio S, Cappello A, Farkas T, Bernassola F, Scarponi C, et al. Involvement of transcribed lncRNA uc.291 in hyperproliferative skin disorders. Biol Direct. 2023;18:82.
11. Li D, Kular L, Vij M, Herter EK, Li X, Wang A, et al. Human skin long noncoding RNA WAKMAR1 regulates wound healing by enhancing keratinocyte migration. Proc Natl Acad Sci. 2019;116:9443–52.
12. Rey F, Zuccotti GV, Carelli S. Long non-coding RNAs in metabolic diseases: from bench to bedside. Trends Endocrinol Metab. 2021;32:747–9.
13. Agostini M, Mancini M, Candi E. Long non-coding RNAs affecting cell metabolism in cancer. Biol Direct. 2022;17:26.
14. Nemeth K, Bayraktar R, Ferracin M, Calin GA. Non-coding RNAs in disease: from mechanisms to therapeutics. Nat Rev Genet. 2024;25:211–32.
15. Ji P, Diederichs S, Wang W, Böing S, Metzger R, Schneider PM, et al. MALAT-1, a novel noncoding RNA, and thymosin β4 predict metastasis and survival in early-stage non-small cell lung cancer. Oncogene. 2003;22:8031–41.
16. Gupta RA, Shah N, Wang KC, Kim J, Horlings HM, Wong DJ, et al. Long non-coding RNA HOTAIR reprograms chromatin state to promote cancer metastasis. Nature. 2010;464:1071–6.
17. Zhu N, Ahmed M, Li Y, Liao JC, Wong PK. Long noncoding RNA MALAT1 is dynamically regulated in leader cells during collective cancer invasion. Proc Natl Acad Sci. 2023;120:e2305410120.
18. Agostini M, Ganini C, Candi E, Melino G. The role of noncoding RNAs in epithelial cancer. Cell Death Discov. 2020;6:13.
19. Marini A, Lena AM, Panatta E, Ivan C, Han L, Liang H, et al. Ultraconserved long non-coding RNA uc.63 in breast cancer. Oncotarget. 2017;8:35669–80.
20. Wang XS, Zhang Z, Wang HC, Cai JL, Xu QW, Li MQ, et al. Rapid identification of UCA1 as a very sensitive and specific unique marker for human bladder carcinoma. Clin Cancer Res. 2006;12:4851–8.
21. Wu X, Yan T, Wang Z, Wu X, Cao G, Zhang C. LncRNA ZEB2-AS1 promotes bladder cancer cell proliferation and inhibits apoptosis by regulating miR-27b. Biomed Pharmacother. 2017;96:299–304.
22. Li HJ, Gong X, Li ZK, Qin W, He CX, Xing L, et al. Role of Long Non-coding RNAs on Bladder Cancer. Front Cell Dev Biol. 2021;9:672679.
23. Ferrari E, Gandellini P. Unveiling the ups and downs of miR-205 in physiology and cancer: transcriptional and post-transcriptional mechanisms. Cell Death Dis. 2020;11:980.
24. Elkin M, Shevelev A, Schulze E, Tykocinsky M, Cooper M, Ariel I, et al. The expression of the imprinted H19 and IGF-2 genes in human bladder carcinoma. FEBS Lett. 1995;374:57–61.
25. Fan Y, Shen B, Tan M, Mu X, Qin Y, Zhang F, et al. Long non-coding RNA UCA1 increases chemoresistance of bladder cancer cells by regulating Wnt signaling. FEBS J. 2014;281:1750–8.
26. Mokhtar A, Kong C, Zhang Z, Du Y. Down-regulation LncRNA-SNHG15 contributes to proliferation and invasion of bladder cancer cells. BMC Urol. 2021;21:83.
27. Tran MN, Choi W, Wszolek MF, Navai N, Lee ILC, Nitti G, et al. The p63 Protein Isoform ΔNp63α Inhibits Epithelial-Mesenchymal Transition in Human Bladder Cancer Cells. J Biol Chem. 2013;288:3275–88.
28. Fischer M, Schwarz R, Riege K, DeCaprio JA, Hoffmann S. TargetGeneReg 2.0: a comprehensive web-atlas for p53, p63, and cell cycle-dependent gene regulation. NAR Cancer. 2022;4:zcac009.
29. Profumo V, Forte B, Percio S, Rotundo F, Doldi V, Ferrari E, et al. LEADeR role of miR-205 host gene as long noncoding RNA in prostate basal cell differentiation. Nat Commun. 2019;10:307.
30. Lin-Shiao E, Lan Y, Welzenbach J, Alexander KA, Zhang Z, Knapp M, et al. p63 establishes epithelial enhancers at critical craniofacial development genes. Sci Adv. 2019;5:eaaw0946.
31. Tucci P, Agostini M, Grespi F, Markert EK, Terrinoni A, Vousden KH, et al. Loss of p63 and its microRNA-205 target results in enhanced cell migration and metastasis in prostate cancer. Proc Natl Acad Sci USA. 2012;109:15312–7.
32. Gandellini P, Profumo V, Casamichele A, Fenderico N, Borrelli S, Petrovich G, et al. miR-205 regulates basement membrane deposition in human prostate: implications for cancer development. Cell Death Differ. 2012;19:1750–60.
33. Gandellini P, Folini M, Longoni N, Pennati M, Binda M, Colecchia M, et al. miR-205 Exerts tumor-suppressive functions in human prostate through down-regulation of protein kinase Ce. psilon Cancer Res. 2009;69:2287–95.
34. Xie H, Zhao Y, Caramuta S, Larsson C, Lui WO. miR-205 expression promotes cell proliferation and migration of human cervical cancer cells. PLoS One. 2012;7:e46990.
35. Qu C, Liang Z, Huang J, Zhao R, Su C, Wang S, et al. MiR-205 determines the radioresistance of human nasopharyngeal carcinoma by directly targeting PTEN. Cell Cycle. 2012;11:785–96.
36. Dar AA, Majid S, de Semir D, Nosrati M, Bezrookove V, Kashani-Sabet M. miRNA-205 suppresses melanoma cell proliferation and induces senescence via regulation of E2F1 protein. J Biol Chem. 2011;286:16606–14.
37. Setti Boubaker N, Gurtner A, Trabelsi N, Manni I, Ayed H, Saadi A, et al. Uncovering the expression patterns and the clinical significance of miR-182, miR-205, miR-27a and miR-369 in patients with urinary bladder cancer. Mol Biol Rep. 2020;47:8819–30.
38. Tran MN, Choi W, Wszolek MF, Navai N, Lee ILC, Nitti G, et al. The p63 protein isoform ΔNp63α inhibits epithelial-mesenchymal transition in human bladder cancer cells: role of MIR-205. J Biol Chem. 2013;288:3275–88.
39. Gregory PA, Bert AG, Paterson EL, Barry SC, Tsykin A, Farshid G, et al. The miR-200 family and miR-205 regulate epithelial to mesenchymal transition by targeting ZEB1 and SIP1. Nat Cell Biol. 2008;10:593–601.
40. Yang A, Kaghad M, Wang Y, Gillett E, Fleming MD, Dötsch V, et al. p63, a p53 homolog at 3q27-29, encodes multiple products with transactivating, death-inducing, and dominant-negative activities. Mol Cell. 1998;2:305–16.
41. Romano RA, Smalley K, Magraw C, Serna VA, Kurita T, Raghavan S, et al. Δ *Np63* knockout mice reveal its indispensable role as a master regulator of epithelial development and differentiation. Development. 2012;139:772–82.
42. Smirnov A, Lena AM, Tosetti G, Yang X, Cappello A, Citterich MH, et al. Epigenetic priming of an epithelial enhancer by p63 and CTCF controls expression of a skin-restricted gene XP33. Cell Death Discov. 2023;9:446.
43. Li Y, Giovannini S, Wang T, Fang J, Li P, Shao C, et al. p63: a crucial player in epithelial stemness regulation. Oncogene. 2023;42:3371–84.
44. Rivetti di Val Cervo P, Lena AM, Nicoloso M, Rossi S, Mancini M, Zhou H, et al. p63–microRNA feedback in keratinocyte senescence. Proc Natl Acad Sci. 2012;109:1133–8.
45. Saladi SV, Ross K, Karaayvaz M, Tata PR, Mou H, Rajagopal J, et al. ACTL6A Is Co-Amplified with p63 in Squamous Cell Carcinoma to Drive YAP Activation, Regenerative Proliferation, and Poor Prognosis. Cancer Cell. 2017;31:35–49.
46. Pecorari R, Bernassola F, Melino G, Candi E. Distinct interactors define the p63 transcriptional signature in epithelial development or cancer. Biochemical J. 2022;479:1375–92.
47. Smirnov A, Lena AM, Cappello A, Panatta E, Anemona L, Bischetti S, et al. ZNF185 is a p63 target gene critical for epidermal differentiation and squamous cell carcinoma development. Oncogene. 2019;38:1625–38.
48. Zhang W, Liang F, Li Q, Sun H, Li F, Jiao Z, et al. LncRNA MIR205HG accelerates cell proliferation, migration and invasion in hepatoblastoma through the activation of MAPK signaling pathway and PI3K/AKT signaling pathway. Biol Direct. 2022;17:2.
49. Liu Y, Wang S, Wei S, Qiu X, Mei Y, Yan L. The promotive role of lncRNA MIR205HG in proliferation, invasion, and migration of melanoma cells via the JMJD2C/ALKBH5 axis. PLoS One. 2024;19:e0290986.
50. Takashima T, Zeng C, Murakami E, Fujiwara N, Kohara M, Nagata H, et al. Involvement of lncRNA MIR205HG in idiopathic pulmonary fibrosis and IL-33 regulation via Alu elements. JCI Insight. 2025;10:e187172.
51. Bezzecchi E, Pagani G, Forte B, Percio S, Zaffaroni N, Dolfini D, et al. MIR205HG/LEADR Long Noncoding RNA Binds to Primed Proximal Regulatory Regions in Prostate Basal Cells Through a Triplex- and Alu-Mediated Mechanism. Front Cell Dev Biol. 2022;10:909097.
52. Brzostek-Racine S, Gordon C, Van Scoy S, Reich NC. The DNA Damage Response Induces IFN. J Immunol. 2011;187:5336–45.
53. Holicek P, Guilbaud E, Klapp V, Truxova I, Spisek R, Galluzzi L, et al. Type I interferon and cancer. Immunol Rev. 2024;321:115–27.
54. Green JL, Osterhout RE, Klova AL, Merkwirth C, McDonnell SRP, Zavareh RB, et al. Molecular characterization of type I IFN-induced cytotoxicity in bladder cancer cells reveals biomarkers of resistance. Mol Ther Oncolytics. 2021;23:547–59.
55. Chhipa AS, Boscaro V, Gallicchio M, Patel S. The curious case of type I interferon signaling in cancer. Biochim Biophys Acta Rev Cancer. 2024;1879:189204.
56. Love MI, Huber W, Anders S. Moderated estimation of fold change and dispersion for RNA-seq data with DESeq2. Genome Biol. 2014;15:550.
57. Goldman MJ, Craft B, Hastie M, Repečka K, McDade F, Kamath A, et al. Visualizing and interpreting cancer genomics data via the Xena platform. Nat Biotechnol. 2020;38:675–8.
58. Li T, Fu J, Zeng Z, Cohen D, Li J, Chen Q, et al. TIMER2.0 for analysis of tumor-infiltrating immune cells. Nucleic Acids Res. 2020;48:W509–14.
59. Korotkevich G, Sukhov V, Budin N, Shpak B, Artyomov MN, Sergushichev A. Fast gene set enrichment analysis. 2016.

60. Guneri-Sozeri PY, Özden-Yılmaz G, Kisim A, Cakiroglu E, Eray A, Uzuner H, et al. FLI1 and FRA1 transcription factors drive the transcriptional regulatory networks characterizing muscle invasive bladder cancer. Commun Biol. 2023;6:199.
61. Hammal F, de Langen P, Bergon A, Lopez F, Ballester B. ReMap 2022: a database of Human, Mouse, Drosophila and Arabidopsis regulatory regions from an integrative analysis of DNA-binding sequencing experiments. Nucleic Acids Res. 2022;50:D316–25.

ACKNOWLEDGEMENTS

This work was supported by the Italian Ministry of University and Research under PNRR-CN3 (CN_00000041, CUPE83C22003200001 to EC and MH) and by European Union Next Generation EU (M4C1 2022WW4J4B_001, CUP E53D23007320006 to EC).

AUTHOR CONTRIBUTIONS

AS and EC conceived and designed the study. AS carried out bioinformatic analyses and prepared figures. DB and MFC performed all experiments in vitro. AS wrote the manuscript in consultation with MHC, GM, PG and EC. All authors discussed the results and contributed to the final manuscript preparation.

COMPETING INTERESTS

The author declares no competing interests.

ETHICAL APPROVAL AND CONSENT TO PARTICIPATE

All methods were performed in accordance with the relevant guidelines and regulations.

ADDITIONAL INFORMATION

Supplementary information The online version contains supplementary material available at https://doi.org/10.1038/s41420-025-02546-1.

Correspondence and requests for materials should be addressed to Artem Smirnov or Eleonora Candi.